

Volatile species generation

and its application in Analytical Chemistry

by

Alicia Mollo Firpo

Submitted in Partial Fulfilment of the Requirements for the
Degree

Doctor in Chemistry

Supervised by Professor Dr. Moisés Knochen

Facultad de Química
Universidad de la República
Montevideo
2019



ACTA DEFENSA DE TESIS

FECHA	14 de octubre de 2019		
CARRERA	DOCTORADO		
PLAN	2004		
	LUGAR	FECHA	HORA
EXAMEN			
DIRECTORES DE TESIS:			
Dr. Moisés Krochen 			
TRIBUNAL:			
Prof. Jiri Dedina Prof. Julia Torres Dra. Nely Manfay   			
ESTUDIANTE		CALIFICACIÓN	
APELLIDO Y NOMBRE	Cédula de Identidad	NUMERO	SIMBOLO
MOLLO FIRPO, ALICIA	2756870 - 2	12	EXCELENTE
NOMBRE DE TESIS: ' Volatile species generation and its application in Analytical Chemistry '			

ACIA. En Montevideo a los catorce días del mes de octubre de 2019, se reúne en la Facultad de Química el Tribunal que entendió en la defensa de tesis de Doctorado en Química que postula la Q. F. Alicia Molle, cuyo título es "Volatile species generation and its application in Analytical Chemistry".

Asisten todos sus integrantes: RNDr. Jiri Dédina, CSc. DSc., Dra. Nelly Mañay, Dra. Julia Torres, Dr. Moisés Knochen (Director de tesis).

El Tribunal, habiendo analizado la tesis en profundidad, considera:

El trabajo de tesis presenta una novedosa experiencia en Química Analítica en términos de desarrollo de metodologías alternativas para la determinación de elementos traza mediante generación de especies volátiles. Incorpora técnicas no convencionales hasta el momento no exploradas para estas determinaciones. En las diferentes metodologías desarrolladas se aprecia un trabajo sistemático de evaluación y optimización considerando interferencias y otras características de desempeño relevantes.

La presentación oral fue realizada empleando medios audiovisuales adecuados, destacándose la claridad y calidad de la exposición. Se deja constancia que esta presentación, así como la redacción de la tesis fueron realizadas en idioma inglés para facilitar la participación del Dr. Dédina.

Por lo anterior, el tribunal le otorga la calificación de EXCELENTE.



Dr. Jiri Dédina



Dra. Nelly Mañay



Dra. Julia Torres



Dr. Moisés Knochen



PROGRAMA DE DESARROLLO DE LAS CIENCIAS BÁSICAS
Ministerio de Educación y Cultura - Universidad de la República

Área Química

ACTA. En Montevideo a los catorce días del mes de octubre de 2019, se reúne en la Facultad de Química el Tribunal que entendió en la defensa de tesis de Doctorado en Química que postula la Q. F. Alicia Mollo, cuyo título es "Volatile species generation and its application in Analytical Chemistry".

Asisten todos sus integrantes: RNDr. Jifí Dédina, CSc. DSc., Dra. Nelly Mañay, Dra. Julia Torres, Dr. Moisés Knochen (Director de tesis).

El Tribunal, habiendo analizado la tesis en profundidad, considera:

El trabajo de tesis presenta una novedosa experiencia en Química Analítica en términos de desarrollo de metodologías alternativas para la determinación de elementos traza mediante generación de especies volátiles. Incorpora técnicas no convencionales hasta el momento no exploradas para estas determinaciones. En las diferentes metodologías desarrolladas se aprecia un trabajo sistemático de evaluación y optimización considerando interferencias y otras características de desempeño relevantes.

La presentación oral fue realizada empleando medios audiovisuales adecuados, destacándose la claridad y calidad de la exposición. Se deja constancia que esta presentación, así como la redacción de la tesis fueron realizadas en idioma inglés para facilitar la participación del Dr. Dédina.

Por lo anterior, el tribunal le otorga la calificación de EXCELENTE.

Dr. Jifí Dédina

Dra. Nelly Mañay

Dra. Julia Torres

Dr. Moisés Knochen

ÁREA QUÍMICA

Facultad de Química, Av. General Flores 2124, Montevideo 11800, URUGUAY
Teléfonos: (+598) 29242338 Fax: (+598) 29241906.
Página web: www.pedeciba.edu.uy/quimica
Correo electrónico: isegredo@fq.edu.uy - gabig@fq.edu.uy

Acknowledgements

Programa de Desarrollo de las Ciencias Básicas – PEDECIBA Química and Comisión Sectorial de Investigación Científica – CSIC for financial support.

Evaluating committee: Prof. Dr. Jiri Dedina for coming from so far and evaluate my work and Prof. Dr. Nelly Mañay and Prof. Dr. Julia Torres for accepting performing the evaluation in a foreign language.

Mariela Pistón for introducing me Prof. Dedina.

Mariana Da Luz Potes for refer the UV commercial reactor.

Dr. Erna Frins and Dr. José A. Ferrari for their kind assistance in performing the emission profile of the in-house reactor.

Gabriel González for mounting the UV reactor.

Gustavo Pignalosa for awaking my interest in volatile species.

Ricardo Mosquera for his will in the construction and the teaching related to the electrically heated atomiser.

My workmates.

My friends.

My family: the one where I was born and raised and the one I made.

Abstract

The generation of volatile species consists on the transference of an element (ion or organo-compound), from the condensed phase (typically liquid) to the gaseous by means of a reduction reaction which yields a derivative that leaves the solution and is transported by an inert gas towards an atomization cell where it is determined by atomic spectrometry. Inherently the analyte is preconcentrated improving the limits of detection and quantification. As it is separated from the matrix, their interaction is minimised and so the interferences. Since not every species of the elements are able of being volatilized, chemical speciation is possible.

The formation of volatile derivatives can be carried out chemically, photochemically and electrochemically. The first is the most used in the laboratories of Analytical Chemistry; volatiles hydrides are generated by sodium tetrahydroborate and determined by atomic absorption spectrometry.

The present work proposes the use of photons and electrons as a clean alternative to tetrahydroborate, which is an eco-toxic reagent, of a high price given the high purity in which it should be used, unstable in aqueous solution and nowadays increasingly difficult to import it. This strategy represents both an analytical and operational challenge since there is no experience of its use in our laboratory, also requiring the design and construction of suitable reactors.

Among the experimental procedures implemented, stands out for the chemical generation, the development of a flow system for the determination of selenium by atomic absorption spectrometry through sequential injection hydride generation and the determination of lead with atomic emission spectrometry in microwave induced plasma as a detection system.

Although an electrochemical cell was designed and built, the results obtained were not as expected.

Related to the photochemical generation, an in-house reactor was built and a commercial one was used, the latter being the one achieving the best performance. The methodologies for the respective determination of mercury and selenium at trace level were developed, also implementing a strategy for nitrate removal, one of the main limiting concomitant when using this technique.

In all cases, the variables of influence affecting the generation of the volatile derivative were evaluated and an interference study was carried out. The methodologies were optimized and characterized, assessing their applicability with Certified Reference Materials or spiked samples.

The results obtained brought new knowledge to our area, initiating a new line of research.

Resumen

La generación de especies volátiles consiste en la transferencia de un elemento en forma de ion o compuesto orgánico, desde la fase condensada (líquida generalmente) a la gaseosa mediante una reacción de reducción que resulta en la formación de un derivado que se desprende de la solución y se transporta mediante un gas inerte a una celda de atomización para determinarse por espectrometría atómica. Inherentemente el analito es preconcentrado, por lo que se mejoran los límites de detección y de cuantificación. Al separarse de la matriz, la interacción con la misma se limita disminuyendo y controlando las potenciales interferencias. Como no todas las especies de los elementos son capaces de ser volatilizadas, posibilita la especiación química.

La formación de derivados volátiles puede realizarse química, fotoquímica y electroquímicamente. La primera es la más utilizada en los laboratorios de Química Analítica; emplea tetrahidrobórato de sodio como agente reductor, genera hidruros volátiles y la determinación se realiza por espectrometría de absorción atómica.

El presente trabajo propone el uso de fotones y electrones como alternativa limpia al tetrahidrobórato, que es un reactivo ecotóxico, de elevado precio dada la elevada pureza en la que debe emplearse, inestable en solución acuosa y hoy por hoy cada vez más difícil de conseguir su importación. Esta estrategia representa un desafío tanto analítico como operativo ya que no hay experiencia de su uso en nuestro laboratorio, requiriéndose además el diseño y construcción de reactores adecuados.

Dentro de los procedimientos experimentales implementados destaca en lo referente a la generación química, el desarrollo de un sistema en flujo para la determinación de selenio por espectrometría de absorción atómica mediante generación de hidruros por inyección secuencial y la determinación de plomo con espectrometría de emisión atómica en plasma inducido por microondas como sistema de detección.

Si bien se diseñó y construyó una celda electroquímica los resultados obtenidos no fueron los esperados.

Para la generación fotoquímica se construyó un reactor "in-house" y se empleó uno comercial, siendo el último el de mejor desempeño. Se desarrollaron metodologías para la determinación de mercurio y de selenio a niveles traza, elaborándose también una estrategia para la eliminación de nitrato que es uno de los principales limitantes al empleo de la técnica.

En todos los casos se evaluaron las variables de influencia que afectan la formación del derivado volátil y se realizó un estudio de los principales interferentes. Las metodologías fueron optimizadas y caracterizadas, corroborándose su aplicabilidad con materiales de referencia certificados o muestras aditivadas.

Los resultados obtenidos aportaron nuevos conocimientos a nuestra área, iniciando una línea de investigación en la que se va a continuar trabajando.

General Index

Acknowledgements	5
Abstract	6
Resumen	7
General Index	8
Figure Index	17
Table Index	23
1 Volatile species generation	28
1.1 Background	28
1.2 Motivation	29
1.3 Work strategy	29
1.4 Monograph organisation	30
Chapter 2: Abbreviations	33
2 Chemical vapour generation (CVG)	34
2.1 Introduction	34
2.2 Selenium Determination by Sequential Injection Hydride Generation Atomic Absorption Spectrometry	40
2.2.1 Introduction	40
2.2.2 Part I – Working conditions optimisation	41
2.2.2.1 Instrumentation	41
2.2.2.2 Reagents and solutions	42
2.2.2.3 Procedure	42
2.2.2.4 Results and discussion	43
2.2.2.4.1 Size of the reaction coil	43
2.2.2.4.2 Sample volume	44
2.2.2.4.3 Nitrogen flow rate	45
2.2.2.4.4 Reductant concentration	45
2.2.2.4.5 Acidity of the sample	45
2.2.2.4.6 Salting-out effect	46
2.2.2.4.7 Addition of 0,1 mol L ⁻¹ KI	46
2.2.2.4.8 Summary of the optimum working conditions	47

2.2.3	Part I – Method characterisation	47
2.2.3.1	Instrumentation	47
2.2.3.2	Reagents and solutions	47
2.2.3.3	Procedure	48
2.2.3.3.1	Linear range	48
2.2.3.3.2	Limits of detection and quantification	48
2.2.3.3.3	Precision of repeatability.....	48
2.2.3.3.4	Trueness	48
2.2.3.4	Results and discussion.....	49
2.2.3.4.1	Linear range.....	49
2.2.3.4.2	Limits of detection and quantification	49
2.2.3.4.3	Precision of repeatability.....	50
2.2.3.4.4	Trueness	50
2.2.3.4.4.1	Spike / recovery.....	50
2.2.3.4.4.2	Comparison of the methodologies (SI-HG-AAS vs Reference Method).	51
2.2.4	Part II – Working conditions optimisation.....	53
2.2.4.1	Introduction.....	53
2.2.4.2	Instrumentation	54
2.2.4.3	Reagents and solutions	54
2.2.4.4	Procedure	54
2.2.4.5	Results and discussion.....	56
2.2.4.6	Conclusions.....	59
2.2.5	<i>Part II</i> – Method characterisation	59
2.2.5.1	Instrumentation	59
2.2.5.2	Reagents and solutions	59
2.2.5.3	Procedure	60
2.2.5.3.1	Linear range	60
2.2.5.3.2	Limits of detection and quantification	60
2.2.5.3.3	Precision of repeatability.....	60
2.2.5.3.4	Trueness	61
2.2.5.4	Results and discussion.....	62
2.2.5.4.1	Linear range.....	62

2.2.5.4.2	Limits of detection and quantification and precision of repeatability	62
2.2.5.4.3	Trueness	63
2.2.5.4.3.1	Normal distribution of the data	63
2.2.5.4.3.2	Spike / recovery	64
2.2.5.4.3.3	Comparison of the results obtained with the SI-HG-AAS method and the Reference Method	65
2.2.5.5	Conclusions	65
2.2.6	<i>Part II</i> – Interference analysis	66
2.2.6.1	Introduction	66
2.2.6.2	Instrumentation	67
2.2.6.3	Reagents and solutions	67
2.2.6.4	Procedure	68
2.2.6.5	Results and discussion	69
2.2.6.5.1	Arsenic	69
A calibration plot was drawn up to 30 $\mu\text{g L}^{-1}$, and the same was constructed with 150 $\mu\text{g L}^{-1}$ As and 50 $\mu\text{g L}^{-1}$ As.		69
2.2.6.5.2	Cobalt, mercury and zinc	70
2.2.6.5.3	Copper (II), iron (II), iron (III), and nickel (II)	70
2.2.6.5.4	Nitrate	73
2.2.6.6	Conclusions	74
2.2.7	General conclusions for the SI-HG-AAS method	75
2.3	Lead determination by microwave induced plasma emission atomic spectrometry	86
2.3.1	Introduction	86
2.3.2	Working conditions optimisation	88
2.3.2.1	Instrumentation	88
2.3.2.2	Reagents and solutions	88
2.3.2.3	Procedure	89
2.3.2.4	Results and discussions	89
2.3.3	Working conditions optimisation using $\text{K}_3\text{Fe}(\text{CN})_6$ as additive for hydride generation	89
2.3.3.1	Instrumentation	89
2.3.3.2	Reagents and solutions	90
2.3.3.3	Procedure	90

2.3.3.4	Results and discussion.....	90
2.3.3.5	Conclusions.....	91
2.3.4	Evaluation of the incidence of acidity and nitrate in lead's response	91
2.3.4.1	Evaluation of the incidence of the acidity of the medium in lead's response	92
2.3.4.2	Evaluation of the incidence of nitrate concentration in lead's response	93
2.3.4.3	Evaluation of the incidence of the reagent interaction in lead's response	95
2.3.5	Method characterisation.....	97
2.3.5.1	Experimental section.....	97
2.3.5.2	Instrumentation	97
2.3.5.3	Reagents and solutions	97
2.3.5.4	Procedure	98
2.3.5.5	Results and discussion.....	99
2.3.5.5.1	Evaluation of the linear range and calibration function	99
2.3.5.5.2	Some figures of merit.....	99
2.3.6	Conclusions.....	102
Chapter 3: Abbreviations.....		109
3	Electrochemical vapour generation (ECVG)	110
3.1	Introduction.....	110
3.2	Experimental section.....	112
3.3	Instrumentation	112
3.3.1	Electrolytic cell.....	112
3.3.2	Electrical assembly	114
3.3.3	Continuous flow electrochemical manifold	114
3.4	Reagents and solutions	115
3.5	Procedure	115
3.6	Results and discussion.....	116
3.7	Conclusions.....	118
Chapter 4: Abbreviations.....		121
4	Photochemical Vapour Generation.....	122
4.1	Introduction.....	122
4.2	Experiences achieved with the "in-house" reactor.....	132
4.2.1	Continuous flow UV reactor	132

4.2.2	First attempts in PVG with the “in-house” reactor	134
4.2.3	Photochemical Vapour Generation - Head Space - Single Drop Micro Extraction -Electro Thermal Atomic Absorption Spectrometry (PVG-HS-SDME-ETAAS)	139
4.3	Experiences achieved with the commercial reactor	156
4.3.1	Reactor description	156
4.3.2	Continuous flow manifold	159
4.3.3	Flow injection manifold	160
4.3.4	Atomic absorption cells	160
4.3.4.1	Absorption cell (mercury)	160
4.3.4.2	Atomisation cell	161
4.3.5	Peristaltic pumps	162
4.3.6	Gas-liquid separator	164
4.3.7	Data acquisition software	165
4.3.8	First attempts in photochemical vapour generation	166
4.3.8.1	Experimental section	166
4.3.8.2	Instrumentation	166
4.3.8.3	Reagents and solutions	166
4.3.8.4	Procedure	166
4.3.8.5	Results and discussion	167
4.3.8.6	Conclusions	167
4.4	Photochemical generation of mercury	170
4.4.1	Introduction	170
4.4.2	Continuous flow photochemical cold vapour generation (CF-PCVG)	172
4.4.2.1	Experimental section	172
4.4.2.2	Instrumentation	172
4.4.2.3	Reagents and solutions	172
4.4.2.4	Procedure	172
4.4.2.5	Results and discussion	173
4.4.2.6	Conclusions	173
4.4.3	Flow injection photochemical cold vapour generation (FI-PCVG)	174
4.4.3.1	Experimental section	174
4.4.3.2	Instrumentation	174

4.4.3.3	Reagents and solutions	174
4.4.3.4	Procedure	174
4.4.3.5	Results and discussions	175
4.4.3.5.1	Low molecular weight organic compound and LMWOC's concentration:	175
4.4.3.5.2	Carrier composition of the FI system	177
4.4.3.5.3	Irradiation time.....	178
4.4.3.5.4	Argon : hydrogen (92:8) flow	179
4.4.3.5.5	Sample volume	180
4.4.3.5.6	Efficiency	181
4.4.3.5.7	Some parameters for characterising the method for each LMWOC.	181
4.4.3.5.7.1	Evaluation of the linear range and calibration function	182
4.4.3.5.7.1.1	1,0 % w/w ethyl alcohol:	182
4.4.3.5.7.1.2	0,5 % w/w formic acid:.....	183
4.4.3.5.7.1.3	0,5 % w/w acetic acid:.....	184
4.4.3.5.7.2	Signal dispersion between replicates.....	185
4.4.3.5.7.2.1	1,0 % w/w ethyl alcohol:	185
4.4.3.5.7.2.2	0,5 % w/w formic acid:.....	185
4.4.3.5.7.2.3	0,5 % w/w acetic acid:.....	186
4.4.3.5.7.3	Limit of detection and quantification.....	187
4.4.3.5.7.3.1	1,0 % w/w ethyl alcohol:	187
4.4.3.5.7.3.2	0,5 % w/w formic acid:.....	188
4.4.3.5.7.3.3	0,5 % w/w acetic acid:.....	188
4.4.3.5.7.4	Summary of the working conditions and performance of the photochemical vapour generation of mercury.....	189
4.4.3.5.7.5	Attempt to method application	189
4.4.3.6	Conclusions.....	191
4.5	Photochemical generation of volatile selenium compounds.....	198
4.5.1	Introduction.....	198
4.5.2	PVG working conditions optimisation	200
4.5.2.1	<i>Experimental section</i>	200
4.5.2.1.1	Instrumentation.....	200
4.5.2.1.2	Reagents and solutions	200

4.5.2.1.3	Procedure	200
4.5.2.2	<i>Results and discussion</i>	201
4.5.2.2.1	Low molecular weight organic compound and LMWOC's concentration:	201
4.5.2.2.2	Carrier composition of the FIA system	204
4.5.2.2.3	Irradiation time.....	206
4.5.2.2.4	Argon : hydrogen (92:8) flow rate	207
4.5.2.2.5	Sample volume	208
4.5.2.2.6	Efficiency	208
4.5.2.2.7	Summary of the working conditions for the photochemical vapour generation of selenium derivatives.....	208
4.5.2.2.8	Influence of HCOOH in the atomisation cell.....	208
4.5.3	Nitric acid interference abatement study	210
4.5.3.1	Introduction.....	210
4.5.3.2	Experimental section.....	212
4.5.3.2.1	Instrumentation.....	212
4.5.3.2.2	Reagents and solutions	212
4.5.3.2.3	Procedure	213
4.5.3.2.3.1	On-line interference abatement	213
4.5.3.2.3.2	Off-line interference abatement.....	213
4.5.3.2.3.2.1	Se(VI) reduction to Se(IV).....	213
4.5.3.2.3.2.2	Simultaneous elimination of nitrate and reduction of Se(VI)	213
4.5.3.2.3.2.3	Nitrate elimination under stronger conditions	214
4.5.3.4	Results and discussion.....	214
4.5.3.4.1	On-line interference abatement	214
4.5.3.4.1.1	Formic acid:	214
.....	214
4.5.3.4.1.2	Sulfamic acid:	215
4.5.3.4.1.3	Ascorbic acid	216
4.5.3.4.2	Off-line interference abatement	217
4.5.3.4.2.1	Simultaneous reduction of Se(VI) to Se(IV) and nitrate elimination:.....	217
4.5.3.4.2.2	Nitrate elimination in stronger reductant conditions.....	217
4.5.4	Method characterization/method evaluation	219

4.5.4.1	<i>Experimental section</i>	219
4.5.4.2	<i>Instrumentation</i>	219
4.5.4.3	<i>Reagents and solutions</i>	220
4.5.4.4	<i>Procedure</i>	220
4.5.4.5	<i>Results and discussion</i>	221
4.5.4.5.1	Evaluation of the linear range and calibration function	221
4.5.4.5.2	Signal dispersion between replicates	221
4.5.4.5.3	Summary of the performance of the photochemical vapour generation of selenium derivatives in 1,5 % w/w HCOOH.	223
4.5.5	Elucidation of the lack of signal after nitrate elimination	225
4.5.5.1	<i>Nitrate was not eliminated</i>	225
4.5.5.2	<i>Increased levels of formic acid</i>	225
4.5.5.3	<i>Formaldehyde treatment causes selenium losses</i>	230
4.5.5.4	<i>Reduction step was not properly accomplished</i>	230
4.5.3.4.1	Se(IV) determination by CVG	230
4.5.6	Conclusions	232
Chapter 5: Abbreviations		239
5	Construction of an electrically heated volatile species atomiser	240
5.1	Background	240
5.2	Atomiser evolution	241
5.2.1	Nichrome wire and ceramic fibre tape	241
5.2.1.1	Atomiser performance	245
5.2.1.1.1	Instrumentation	245
5.2.1.1.2	Reagents and solutions	246
5.2.1.1.3	Procedure	246
5.2.1.1.4	Results and discussion	247
5.2.1.1.5	Conclusions	250
5.2.2	Proportional – Integral – Derivative (PID) temperature controller	250
5.2.2.1	Introduction	250
5.2.2.2	Instrumentation	251
5.2.2.3	Procedure	251
5.2.2.4	Results and discussions	252

5.2.3	Nichrome tape.....	254
5.3	Final version of the atomiser.....	255
5.4	Conclusions.....	257
6	General conclusions and perspectives	264
7	Bibliography.....	268

Figure Index

Figure 1: a) Mechanism of the hydrolysis of THB b) Mechanism of selenium hydride generation; B-H: symbolises all the hydridoboron intermediates.	34
Figure 2: SIA manifold. SV: selection valve; HC: holding coil; P: propulsion system; R: reagents; W: waste. Extracted from R.B.R. Mesquita, A.O.S.S. Rangel / <i>Analytica Chimica Acta</i> 648 (2009) 7–22	40
Figure 3: Sequential Injection system used for selenium determination (<i>Part I</i>). PE5000: atomic absorption spectrometer; A/D: analogue to digital interface; C: carrier (water); HC: holding coil (2 m); HS: hydrostatic gas-liquid separator; MV: multiposition valve; N ₂ : nitrogen input; P: syringe pump; PC: personal computer with the software control; QC: quartz atomisation cell; R: reagent (NaBH ₄); RC: reaction coil (0,2 m); S: pre-reduced sample; W: waste.	41
Figure 4: Photograph of the system used. HS: hydrostatic gas-liquid separator; MV: multiposition valve; P: syringe pump; QC: quartz atomisation cell; W: waste.	42
Figure 5: Sequential loading of sample and reagent in the holding coil (<i>Part I</i>).....	43
Figure 6: Selenium calibration curves for a sample volume of 250 µL and 333 µL respectively. A _{int} : integrated absorbance (s); C: concentration of selenium in µg L ⁻¹	44
Figure 7: Flow-meter calibration with nitrogen. FR: nitrogen flow rate (mL min ⁻¹); I: indication.....	45
Figure 8: Evaluation of the salting-out effect for the SI-HG-AAS Part I system. Calibration curve for selenium with (blue) and without (red) sodium chloride. A ₅₀ : absorbance of the solutions with NaCl; A: absorbance of the solutions without NaCl; C: selenium concentration in µg L ⁻¹	46
Figure 9: Evaluation of the linear range. Left, selenium calibration curve. Right, dispersion of the residuals for the SI-HG-AAS system Part I.	49
Figure 10: Recovery of the spiked samples analysed by SI-HG-AAS system <i>Part I</i>	51
Figure 11: Correlation of the results of selenium determination in spiked tap water by the SI-HG-AAS method and the Reference Method. c Se SI-HG-AAS: concentration of selenium in µg L ⁻¹ determined by SI-HG-AAS method; c Se HG-AAS: concentration of selenium in µg L ⁻¹ determined by the Reference Method.....	52
Figure 12: Sequential Injection system used for selenium determination (<i>Part II</i>). AAS: atomic absorption spectrometer; A/D: analogue to digital interface; C: carrier (water); HC: holding coil (2 m); HRC: heated reactor coil (1 m); HS: hydrostatic gas-liquid separator; MV: multiposition valve; N ₂ : nitrogen input; P: syringe pump; PC: personal computer with the software control; QC: quartz atomisation cell; R: reagent (NaBH ₄); RC: reaction coil (0,2 m); W: waste.	54
Figure 13: Sequential loading of sample and reagent in the holding coil.....	55
Figure 14: Doehlert design for two factors and its sequentiality in space.....	57
Figure 15: Different levels tried without reaching optimum working conditions.....	57
Figure 16: Doehlert experimental design; optimum working conditions.	58
Figure 17: Evaluation of the salting-out effect for SI-HG-AAS system Part II. % Reponse: percentage ratio of the signal when NaCl is added over the signal of the solution without the addition.....	58
Figure 18: Evaluation of the linear range. Left, selenium calibration curve. Right, dispersion of the residuals for the SI-HG-AAS system Part II.	62
Figure 19: Relative and cumulative relative frequency distribution of SI-HG-AAS system <i>Part II</i> data.	63
Figure 20: Trueness assessment by spike / recovery study of spiked samples.....	64

Figure 21: Variation in Se signal at increasing As concentration by Si-HG-AAS and the Reference Method. Left: From 100 to 500 $\mu\text{g L}^{-1}$ As added; Right: From 100 to 5000 $\mu\text{g L}^{-1}$ As added.	69
Figure 22: Variation in Se signal at increasing Cu concentration by Si-HG-AAS and the Reference Method. Left: From 0,1 to 1,0 $\mu\text{g L}^{-1}$ Cu added; Right: From 0,1 to 100 $\mu\text{g L}^{-1}$ Cu added.	71
Figure 23: Variation in Se signal at increasing Fe (II) concentration by Si-HG-AAS and the Reference Method.	72
Figure 24: Variation in Se signal at increasing Fe (III) concentration by Si-HG-AAS and the Reference Method.	72
Figure 25: Variation in Se signal at increasing Ni concentration by Si-HG-AAS and the Reference Method.	73
Figure 26: Variation in Se signal at increasing NO_3^- concentration by Si-HG-AAS and the Reference Method.	74
Figure 27: Scheme and photograph of the cyclonic spray chamber. Adapted from Anal Bional Chem (2007) 388:735-741 and https://www.agilent.com/cs/library/applications/5991-72828EN_MP-eBook.pdf respectively.	88
Figure 28: Comparison of lead response in hydrochloric and nitric acid at 283,305 nm and 405,781 nm by HG-MIP OES. I: emission signal; C: lead concentration in $\mu\text{g L}^{-1}$	91
Figure 29: Variation of lead response for different hydrogen ion concentration.	93
Figure 30: Variation of lead response for different nitrate concentration.	94
Figure 31: Combination of different reagents used for evaluating the interaction between them. Adapted from https://www.agilent.com/cs/library/applications/5991-72828EN_MP-eBook.pdf	95
Figure 32: Evaluation of the linear range for lead determination at 283,305 nm and 405,781 nm by HG-MIP OES. I: emission signal at the corresponding wavelength; C: lead concentration in $\mu\text{g L}^{-1}$	99
Figure 33: Lateral view of both compartments of the cell. The sizes are in mm.	112
Figure 34: Upper view of the half cell.	113
Figure 35: Thin layer electrolytic cell.	113
Figure 36: Electrical assembly of the electrochemical cell.	114
Figure 37: Continuous flow electrochemical system manifold. EC: electrolytic cell; GLS: gas-liquid separator; AAS: quartz cell in the atomic absorption spectrometer; W: waste; N_2 : nitrogen. In blue: electrical assembly previously shown.	114
Figure 38: Electrolytic cell with new electrical connector.	117
Figure 39: Left: cathode half-cell. Right: Ion exchange membrane after electrolysis.	117
Figure 40: Viability of different products formation according to the starting electronic state of the reagents. R: molecule in the ground state; R^* : molecule in the excited state.	123
Figure 41: Absorption spectra of a) formic acid and b) acetic acid. Adapted from J. Anal. At. Spectrom., 2012, 27, 222-231.	124
Figure 42: Some reactions taking place when a formic acid aqueous solution is irradiated by UV irradiation.	125
Figure 43: Example of a flow through UV reactor, extracted from D. Qin et al. / Spectrochimica Acta Part B 88 (2013) 10–14. L: low pressure mercury lamp; IP: tubing inside the lamp; OP: tubing wrapped around the lamp	127
Figure 44: In-house reactor. Germicidal tube with PFA tube around it.	132

Figure 45: Rear and front view of the reactor once mounted in the shell for operator's protection	132
Figure 46: Characteristic spectra of germicidal lamps (extracted from http://www.eurosep.com/fichiers-joints/web-hgg20t10.pdf)	133
Figure 47: Measurement of the emission lines of the reactor's lamp	133
Figure 48: Efficiency of the photo generation of selenium at different formic acid concentrations	140
Figure 49: Photo generation efficiency as a function of irradiation time for $20 \mu\text{g L}^{-1} \text{Se} - 1,7 \text{ mol L}^{-1} \text{HCOOH}$	141
Figure 50: Scheme of the SDME device, extracted from V. Colombini et al. / Talanta 63 (2004) 555–560	143
Figure 51: a) HD – SDME device b) without stirring c) with stirring.....	144
Figure 52: Calibration curves for Se determination by PVG-HS-SDME-ETAAS at low and high concentration ranges. A_{int} : integrated absorbance, C: Se concentration ($\mu\text{g L}^{-1}$)	146
Figure 53: Diagram of the UV reactor 1: low pressure mercury lamp; 2: sample quartz tube; 3: lamp quartz tube; 4: tungsten electrodes; 5: power source; 6: sealed gas chamber between inner lamp tube and outer sample quartz tube; 7: sample inlet; 8: sample outlet; 9: straight line section of the sample quartz tube; 10: bending section of the sample quartz tube that communicate both parallel straight sections of the sample quartz tube.....	156
Figure 54: Spectrum of the UV reactor's lamp.....	157
Figure 55: UV reactor holder. Internal view.....	157
Figure 56: Lateral external view of the reactor from the fan side outlet Figure 57: Lateral external view of the reactor from the airing outlet.....	158
Figure 58: Continuous flow manifold. LMWOC: low molecular weight organic compound; GLS: forced outlet gas liquid separator; AAS: atomic absorption quartz detection cell; W: waste	159
Figure 59: Flow injection manifold: LMWOC: low molecular weight organic compound; FI carrier: flow injection carrier; IV: injection valve; GLS: gas-liquid separator; AAS: atomic absorption quartz detection cell; W: waste	160
Figure 60: Mercury absorption cell.	161
Figure 61: Mercury absorption cell: inlet connected from the gas-liquid separator, outlet connected to the waste flask.....	161
Figure 62: Atomisation cell and atomisation cell in heating device.....	161
Figure 63: Correlation between pump speed instrument indication and irradiation time (s) for the Rainin, Dynamax RP-1 peristaltic pump fitted with a 1,52 mm inner diameter Tygon tube. t_{UV} : irradiation time (s); In: indication.....	162
Figure 64: Correlation between pump speed instrument indication and irradiation time (s) for the Thermo Scientific VP100 peristaltic pump fitted with a 3,16 mm inner diameter Tygon tube. t_{UV} : irradiation time; Ind: indication.....	163
Figure 65: Correlation between pump speed instrument indication and irradiation time (s) for the Thermo Scientific VP100 peristaltic pump fitted with a 1,52 mm inner diameter Tygon tube. t_{UV} : irradiation time; Ind: indication.....	163
Figure 66: Forced outlet gas-liquid separator	164
Figure 67: Selenium signal using the gas liquid separator empty or filled with glass beads.	165

Figure 68: Pb ($130 \mu\text{g L}^{-1}$), in 0,01% w/wHCl, 0.8% w/w CH_3COOH ; irradiation time 14 s; Ar:H ₂ 200 mL min ⁻¹ ; atomisation temperature: 900°C. The decrease in the signal corresponds to the replacement of the lead solution by water (*)	167
Figure 69: Hg ($15 \mu\text{g L}^{-1}$) in $\text{CH}_3\text{CH}_2\text{OH}$ 10%; irradiation time: 14 s, Ar:H ₂ : 200 mL min ⁻¹ . The decrease of the signal corresponds to the replacement of the mercury solution by water (*)	167
Figure 70: Se ($150 \mu\text{g L}^{-1}$), in 0.01% w/wHCl, 0.8% w/w CH_3COOH ; irradiation time 14 s; Ar:H ₂ 100 mL min ⁻¹ ; atomisation temperature: 900°C. The decrease in the signal corresponds to the replacement of the selenium solution by water. (*)	167
Figure 71: Mercury calibration curve in the continuous flow mode. A: absorbance; C: mercury concentration in $\mu\text{g L}^{-1}$	173
Figure 72: Variation of mercury signal (Absorbance) with ethanol concentration. $50 \mu\text{g L}^{-1}\text{Hg}$; sample volume: 0,15 mL; irradiation time: 6 s; Ar:H ₂ flow rate: 200 mL min ⁻¹	175
Figure 73: Variation of the mercury signal (Absorbance) with formic acid concentration. $50 \mu\text{g L}^{-1}\text{Hg}$; sample volume: 0,15 mL; irradiation time: 6 s; Ar:H ₂ flow rate: 200 mL min ⁻¹	176
Figure 74: Variation of the mercury signal (Absorbance) with acetic acid concentration. $50 \mu\text{g L}^{-1}\text{Hg}$; sample volume: 1,0 mL; irradiation time: 3,5 s; Ar:H ₂ flow rate: 500 mL min ⁻¹	176
Figure 75: Mercury signal for air, water and 1,0% $\text{CH}_3\text{CH}_2\text{OH}$ as FI carriers. $50 \mu\text{g L}^{-1}\text{Hg}$; 1,0% $\text{CH}_3\text{CH}_2\text{OH}$; Sample volume: 0,15 mL; irradiation time: 6 s; Ar:H ₂ flow rate: 200 mL min ⁻¹	177
Figure 76: FI system using air as the carrier	177
Figure 77: Variation of mercury signal (peak height) for different irradiation times for formic acid, acetic acid and ethylic alcohol respectively.	178
Figure 78: Mercury signal for different irradiation times $60 \mu\text{g Kg}^{-1}\text{Hg}^{+2}$; 1,0% $\text{CH}_3\text{CH}_2\text{OH}$; 0,6 mL sample; Ar:H ₂ 500 mL min ⁻¹	178
Figure 79: Mercury signal for different irradiation times $60 \mu\text{g Kg}^{-1}\text{Hg}^{+2}$; 0,5% HCOOH; 0,6 mL sample; Ar:H ₂ 500 mL min ⁻¹	178
Figure 80: Mercury signal for different Ar : H ₂ flow $60 \mu\text{g kg}^{-1}\text{Hg}^{+2}$; 1,0% $\text{CH}_3\text{CH}_2\text{OH}$; 0,6 mL sample	179
Figure 81: Mercury signal for different Ar : H ₂ flow $60 \mu\text{g kg}^{-1}\text{Hg}^{+2}$; 0,5% HCOOH; 0,6 mL sample.....	179
Figure 82: Mercury signal using the mixture Ar:H ₂ (92:8) and Ar as the carrier gas in the gas liquid separator	180
Figure 83: Mercury signal for different amount of sample (different loops). $60 \mu\text{g kg}^{-1}\text{Hg}^{+2}$; 1,0% $\text{CH}_3\text{CH}_2\text{OH}$; Ar : H ₂ 500 mL min ⁻¹	180
Figure 84: Evaluation of the calibration function for mercury in 1,0 % w/w $\text{CH}_3\text{CH}_2\text{OH}$	182
Figure 85: Peak height as a function of the concentration	Figure 86: Peak area as a function of the Concentration.
Figure 87: Peak height as a function of the concentration.	Figure 88: Peak area as a function of the concentration.
Figure 89: Peak height as a function of the concentration.	Figure 90: Peak area as a function of the concentration.
Figure 91: Signal replicates for blank, $5 \mu\text{g kg}^{-1} - \text{Hg}$ and $50 \mu\text{g kg}^{-1} - \text{Hg}$ respectively.....	185
Figure 92: Signal replicates for blank, $5 \mu\text{g kg}^{-1} - \text{Hg}$ and $50 \mu\text{g kg}^{-1} - \text{Hg}$ respectively.....	185
Figure 93: Signal replicates for blank and $50 \mu\text{g kg}^{-1} - \text{Hg}$ respectively	186

Figure 94: Variation of selenium signal (peak absorbance) for acetic and formic acid at different concentration levels ($C_{Se} = 30 \mu\text{g L}^{-1}$).....	202
Figure 95: Selenium signal ratio for different acidic concentration in 5 % and 10 % formic acid. Light blue column corresponds to the reference.....	202
Figure 96: Variation of selenium signal with the addition of formic acid according to the acidic media.	203
Figure 97: Selenium signal variation according to the variation of chloride given either by HCl or NaCl.	204
Figure 98: Selenium signal for 5 % sodium chloride, water and nitrogen as carriers of the flow injection system.	205
Figure 99: Selenium signal using nitrogen and air as carriers.....	206
Figure 100: FI system when using air as a carrier. Figure 101: FI system when nitrogen used as a carrier.	206
Figure 102: Variation of the peak height of selenium signal according to the carrier flow rate variation of the FIA system.	207
Figure 103: Selenium signal for different Ar:H ₇ flows in the gas liquid separator	207
Figure 104: Flow injection manifold for the chemical hydride generation of dihydrogenselenide. GLS: gas-liquid separator; W: waste; AAS: electrically heated quartz cell for AAS.	209
Figure 105: Selenium signal for a 0.5% w/w HNO ₃ – 1,0 % w/w HCl – 5,0 % w/w HCOOH - 25 $\mu\text{g kg}^{-1}$ Se solution added with 10 % w/w HCOOH.	214
Figure 106: Selenium signal in 0,5 % w/w HNO ₃ solution after the addition of sulfamic acid and formic acid.....	215
Figure 107: Selenium signal for solutions containing different amounts of formic and sulfamic acid.....	216
Figure 108: Elimination of nitric acid's interference in the selenium (VI) reduction step. Nitric acid concentration refers to % w/w of 65% HNO ₃	217
Figure 109: Signal ratio for the elimination of different amounts of nitrate with different reductant (H ₂ CO) concentrations.....	218
Figure 110: Elimination of nitric acid interference by 40% w/w H ₂ CO. Nitric acid concentration refers to % w/w of 65% HNO ₃	219
Figure 111: Calibration function: Peak area as a function of the concentration.....	221
Figure 112: Signal replicates for a) blank; b) 10 $\mu\text{g kg}^{-1}$ – Se; c) 100 $\mu\text{g kg}^{-1}$ – Se.....	221
Figure 113: Titration curves and its first and second derivative. a) titration of formic acid added, b) titration of total formic/formate, c) titration of HCl.	228
Figure 114: EHQTA cell heated by nichrome wire.....	241
Figure 115: Calcination of the tape.	241
Figure 116: Electrical assembly of the EHQTA.	242
Figure 117: Temperature at the surface of the cell at increasing times for different constant currents supplied.	242
Figure 118: Temperature rise according to the voltage supplied for different resistances.	243
Figure 119: Type K inner and outer thermocouples for monitoring temperature as voltage increases. .	244
Figure 120: Internal and external cell temperature at increasing voltages	244
Figure 121: Manifold for the atomisation of antimony in the electrically heated EHQTA. MHS 15: hydride generation system; EHQTA: externally heated quartz tube atomiser; AAS: atomic absorption spectrometer; VM: voltmeter; AM: ammeter; TM: thermocouple multimeter; PS: power supply.	246

Figure 122: Relative standard deviation of antimony integrated absorbance (blue) and ratio signal to noise (red) at different atomisation temperatures.....	247
Figure 123: Signal variation (integrated absorbance, A_{int} , s) for increasing amounts of antimony (m, ng), for the electrically heated EHQTA (left) and the flame heated EHTQA (right).	248
Figure 124: Comparison of the response for different amounts of antimony of the flame EHQTA and the electrically heated EHQTA.....	248
Figure 125: Antimony peak shape in the electrically heated atomiser.....	249
Figure 126: Atomiser electrical assembly. TC: temperature controller; SSR: solid state relay; PS: power supply.	251
Figure 127: Temperature variation without PID control. Set temperature: 1050 °C.....	252
Figure 128: Temperature variation with PID control. Setpoints: 600 and 950°C. Pb: proportional band; Ir: integral rate; Dt: derivative time.....	253
Figure 129: Temperature variation setting a Ir value. Pb: proportional band; Ir: integral rate; Dt: derivative time	254
Figure 130: Nichrome tape as heating element (interwoven in the ceramic tape).....	255
Figure 131: Nichrome tape as heating element (wrapped around the cell).....	255
Figure 132: Resistance (Fe Cr Al) as heating device.	255
Figure 133: Electrical connection. TC: PID temperature controller; I1: 10A bipolar thermomagnetic switch; In: bipolar switch; C1: 220 V coil contactor; SSR: solid state relay; T: 220/24 V single phase transformer; F: Indicator light; 25A bipolar thermomagnetic switch (Device and diagram constructed by R. Mosquera).	256
Figure 134: Left: internal view of the electrical control of the atomiser. Right: external view.	256

Table Index

Table 1: Performance for the different reactors. s_r (%): relative standard deviation of five instrumental replicates of the $50 \mu\text{g L}^{-1}$ Se solution.	44
Table 2: Limits of detection (LOD) and quantification (LOQ) for the SI-HG-AAS <i>Part I</i> and the Reference Method.	49
Table 3: Precision of repeatability for the SI-HG-AAS system at different concentration levels.	50
Table 4: Two level factor experimental design. + : factor in the higher level; - : factor in the lower level; c HCl: concentration of HCl, mol L^{-1} ; V NaBH ₄ : volume of NaBH ₄ , mL; c NaBH ₄ : concentration of NaBH ₄ , % w/v.	56
Table 5: Values for the + higher and – lower levels of the factors of Table 1.	56
Table 6: Limits of detection (LOD) and quantification (LOQ), precision of repeatability for the SI-HG-AAS system <i>Part II</i> . s_r (%): relative standard deviation.	62
Table 7: Results for the Chi-square test performed for the SI-HG-AAS data.	63
Table 8: t-test for the spiked solutions at different concentration levels.	64
Table 9: Homoscedasticity and t-test of the results found by both methods	65
Table 10: Slopes of the calibration function of Se at different arsenic levels.	69
Table 11: Slopes of the calibration function of Se at different copper levels.	70
Table 12: Slopes of the calibration function of Se at different iron (II) levels.	71
Table 13: $100 \mu\text{g L}^{-1}$ Pb solutions at different additive and acid concentration evaluated for the different reductant concentrations.	91
Table 14: Instrumental parameters for lead determination at 283,305 nm and 405,781 nm. (*) dissolved in 1% w/v NaOH.	91
Table 15: Influence of reagent interaction in lead's response at 283,305 nm	96
Table 16: Influence of reagent interaction in lead's response at 405,781 nm	96
Table 17: Figures of merit for determinations at 283,305 nm. I: emission signal; C: lead concentration in $\mu\text{g L}^{-1}$; s_r : relative standard deviation.	100
Table 18: Figures of merit for determinations at 405,781 nm. I: emission signal; C: lead concentration in $\mu\text{g L}^{-1}$; s_r : relative standard deviation.	100
Table 19: Photochemical generation working conditions for the different analytes specified. LMWOC: low molecular weight organic compound; t_{UV} : irradiation time.	136
Table 20: ETAAS working conditions. Sample volume: 20 μL . T_p : pyrolysis temperature; T_a : atomisation temperature.	137
Table 21: Photochemical working conditions in which volatile species generation is suspected. LMWOC: low molecular weight organic compound; t_{UV} : irradiation time.	137
Table 22: Efficiency of the photo generation of selenium derivatives for different LMWOC. Preliminary results.	139
Table 23: Efficiency of the photo generation of volatile species of selenium at different formic acid concentrations.	140
Table 24: Generation efficiency for low and high levels of selenium in 1,7 and 4,6 mol L^{-1} HCOOH.	141

Table 25: Temperature programme of the graphite furnace for Se in 1,7 mol L ⁻¹ and 4,6 mol L ⁻¹ HCOOH	142
Table 26: Graphite furnace temperature program for selenium determination after HS – SDME.	145
Table 27: Graphite furnace working conditions for the different analytes. Except for Pb in Ce(IV)/KI, sorbent acted as chemical modifier. T _p : pyrolysis temperature (°C); T _a : atomisation temperature (°C)..	147
Table 28: Analytical signal for different concentrations of Pb by PVG-HS-SDME-AAS.	148
Table 29: Analytical signal for different replicates of Ni in 5 % HCOOH by PVG-HS-SDME-AAS and their corresponding blank signals using 75 mg L ⁻¹ Pd as absorbent solution. A _{int} : integrated absorbance (s)..	149
Table 30: Concentration of the analytes assayed at different media. The signal found for the working conditions marked with (*) are shown in Figure 68, Figure 69, and Figure 70.....	166
Table 31: Photochemical mercury vapour generation efficiency in 0,5 % w/w CH ₃ COOH, 1 % w/w CH ₃ CH ₂ OH and 0,5 % w/w HCOOH.....	181
Table 32: Instrumental precision at different concentration levels of mercury in 1,0 % w/w ethyl alcohol.	185
Table 33: Instrumental precision at different concentration levels of mercury in 0,5 % w/w formic acid.	186
Table 34: Instrumental precision at different concentration levels of mercury in 0,5 % w/w acetic acid.	186
Table 35: Calibration function and limit of detection (LOD) and limit of quantification (LOQ) for the photochemical generation of mercury in 1,0 % w/w ethyl alcohol. A: absorbance; A _{int} : integrated absorbance (s); C: mercury concentration (µg kg ⁻¹).....	187
Table 36: Calibration function and limit of detection (LOD) and limit of quantification (LOQ) for the photochemical generation of mercury in 0,5 % w/w formic acid. A: absorbance; A _{int} : integrated absorbance (s); C: mercury concentration (µg kg ⁻¹).....	188
Table 37: Calibration function and limit of detection (LOD) and limit of quantification (LOQ) for the photochemical generation of mercury in 0,5 % w/w acetic acid. A: absorbance; A _{int} : integrated absorbance (s); C: mercury concentration (µg kg ⁻¹).....	188
Table 38: Summary of the variables affecting mercury signal studied and the optimum conditions found. For every experience, the flow rate of the Ar: H ₂ mixture was 500 mL min ⁻¹	189
Table 39: Selection of type and concentration of the LMWOC.	201
Table 40: Volume of sample injected to the UV reactor.....	208
Table 41: Summary of the working conditions	208
Table 42: Instrumental precision at different concentration levels of selenium in 1,5 % w/w formic acid.	222
Table 43: Method characterisation. A _{int} : integrated absorbance (s); C: concentration (µg kg ⁻¹); LOD: limit of detection; LOQ: limit of quantification; s _r (%): relative standard deviation; n: number of replicates. Trace Element in Water CRM: 24,3 µg L ⁻¹ - Se; Spiked rice flour digest: 103,1 µg L ⁻¹ - Se.	223
Table 44: Relative standard deviation (sr, %, n = 10) for peak height and peak area for both atomisation devices.....	249

Chapter I

Volatile species generation

This chapter compiles a brief approach of the advantages of the volatile species generation as well as a general overview of the different ways of achieving it. The motivation, working strategies and the organisation of the present work are also presented.

1 Volatile species generation

1.1 Background

Volatile species generation is a sample introduction technique used, among others, in optic atomic spectrometry.

The volatile species is generated from the element ion or its organo-element compound and transferred to the gaseous phase. An inert gas transports it to an atomisation cell for its determination at the most suitable wavelength according to the technique employed.

As all the analyte is separated from the sample solution and driven altogether to the atomisation cell, this technique inherently preconcentrates the analyte, allowing low limits of detection and quantification. Selectivity is enhanced also as, by a careful modification of the working conditions, only the analyte can produce volatile species.

Moreover, as the analyte gets out of the sample, its interaction with the matrix is minimised and consequently, there is an improved interference control.

This technique enables the speciation study as volatile generation is not achieved with all the elements oxidation states or organo-element compounds.

Among the volatile species, hydrides of the Group 14 (Ge, Sn, Pb), Group 15 (As, Sb, Bi), Group 16 (Se, Te) and Group 12 (Zn, Cd) are the most studied; several compendia analytical methods use hydride generation for determining elements at trace and ultratrace concentration levels. Other species of analytical interest are carbonyls ($\text{Ni}(\text{CO})_4$), oxides (OsO_4 , RuO_2), alkyls ($\text{Pb}(\text{CH}_3\text{CH}_2)_2$) and some halides.

In regards to the methods for hydride generation Dedina & Tsalev (Dedina & Tsalev, Hydride Generation Atomic Absorption Spectrometry, 1995) divide the hydride generation in direct transference mode where the hydride is generated and transferred to the atomiser or collection mode where the hydride is first trapped and then transferred to the atomiser.

Among the direct mode, the generation can be accomplished in batch, where the reactor acts as well as gas-liquid separator, or either in continuous or injection flow. Both last incorporate a gas-liquid separator on-line between the reactor and the atomisation cell.

The generation itself can be accomplished also by different means:

Chemical volatile species generation: sodium tetrahydroborate is the reagent most used for this purpose and hydrides the reaction products.

Electrochemical volatile species generation: the reaction is driven in an electrolytic cell; the analyte is reduced in the cathode as well as hydrogen is formed both reacting to generate the hydride as the volatile species.

Photochemical volatile species generation: the reaction is driven in a UV reactor where UV irradiation excites a low molecular weight organic compound (mostly a carboxylic acid) leading to the element volatile alkyl derivatives.

Once generated, the gaseous compounds are transferred to the gaseous phase by an inert gas stream and transported towards the atomisation cell. According to the atomiser device will be the atomisation process. (Dedina & Tsalev, Hydride Generation Atomic Absorption Spectrometry, 1995) (Smichowski & Farías, 2000) (Laborda, Bolea, & Castillo, 2007)

1.2 Motivation

This work was motivated by:

The search for specificity in analytical determinations; in view of the advantages of the technique, it is worthwhile the study of different working conditions in order to develop methodologies able to determine the analytes despite concomitants achieving limits of detection and quantification suitable for trace concentration levels.

The eagerness to work with “non-chemical reagents” like electrons and photons.

The challenge that implied the above mentioned; there was no background of these activities in the area of my performance, thus a new field of knowledge had to be settled with the consequent adaptation and creation of devices able to accomplish it.

1.3 Work strategy

A reduced number of elements were selected in order to allow greater depth in the investigation: lead, mercury and selenium.

Chemical hydride generation was first applied for selenium generation in order to get familiar with the work with volatile species and then was assayed for electrochemical generation. Then, in the different reactors constructed for photochemical generation attempts were made with several elements at a time until finding evidence of generation success.

In all cases, the influence of the different variables affecting the formation of the volatile derivative for every specific technique was studied.

The systems and methods developed were optimised from the point of view of volatile derivative production using mostly univariate experimental designs and characterised by the determination of linear working range, limits of detection and quantification, precision of repeatability and trueness. The

last was assessed using Certified Reference Materials whenever possible and when not, spike/recovery analysis and comparison with the Reference Method. Interference analyses were carried out with the major interferences expected.

Sample introduction was achieved by flow techniques as sequential injection, continuous flow and flow injection analysis. Atomic absorption and atomic emission spectrometry were used as detection techniques.

1.4 Monograph organisation

In Chapter I, (Volatile species generation, **28**) there is a brief introduction to the main topic of the thesis. Afterwards in each chapter a theoretical approach specifically related to the thematic under consideration will be done.

From Chapter II onwards, each chapter refers to the different ways the generation has been accomplished along the work. At a time, they are divided in sections considering the different analytes determined or the different manifolds used:

Chapter II (2 Chemical vapour generation (CVG), 34): Selenium determination as dihydrogenselenide by batch, flow injection and continuous flow systems. In the three methods the determination was achieved by atomic absorption spectrometry. The methodology was applied to tap and lake water samples.

Lead determination using a continuous flow system and atomic emission spectrometry determination. The method was applied to water, soil and sewage sludge reference materials.

Chapter III (3 Electrochemical vapour generation (ECVG), 110): Attempts to selenium determination generating dihydrogenselenide in a continuous flow system are presented.

Chapter IV (4 Photochemical Vapour Generation, 122): Mercury determination in a flow injection system. The methodology was attempted to be used in dogfish liver Certified Reference Material.

Carbonylselenide and dihydrogenselenide determination in a flow injection system. The methodology was applied to water Certified Reference Material and selenium free rice flour digests.

Both mercury and selenium were detected by atomic absorption spectrometry.

Chapter V (**5 Construction of an electrically heated volatile species atomiser, 240**) involves a different aspect of the thesis, by the time there was a need of an electrically heated atomiser instead of the flame heated available. An "in-house" electrically heated atomiser was constructed in different stages. Many performance tests have been carried out along its construction; the most relevant, using antimony as the analyte and trihydroantimony as the volatile species generated in batch mode is presented.

Finally, even if each chapter have its conclusions, Chapter VI (General conclusions and perspectives, 264) contains general comments about the work done and to be done, and Chapter VII (Bibliography, **268**) a list of the literature consulted.

Chapter II

Chemical Vapour Generation

This chapter first summarises theoretically the mechanisms involved in the chemical generation of volatile species by sodium tetrahydroborate. Chemical vapour generation was applied to selenium and lead hydride generation. Selenium was determined by sequential injection atomic absorption spectrometry and lead by continuous flow microwave induced plasma atomic emission spectrometry.

Chapter 2: Abbreviations

AAS: Atomic Absorption Spectrometry

CRM: Certified Reference Material

CVG: Chemical Vapour Generation

EHQTA: Externally Heated Quartz Tube Atomiser

MIP OES: Microwave Induced Plasma Atomic Emission Spectrometry

SIA: Sequential Injection Analysis

SI-HG-AAS: Sequential Injection Hydride Generation Atomic Absorption Spectrometry

THB: Tetrahydroborate

2 Chemical vapour generation (CVG)

2.1 Introduction

Hydrides are ones of the most extended volatile species used for analytical purposes in trace and ultratrace analysis. There are several regulatory analytical methods which use mainly sodium tetrahydroborate (THB) as the derivatisation reagent. The mechanism of hydride generation is dependent on the acidic concentration of the reaction medium as it determines the prevailing reagent and analyte species in solution and thus their mutual reactivity as well as the stability of the hydride formed.

In analytical reaction conditions, that means, $2,0 \times 10^{-4} < \frac{\text{mol L}^{-1} \text{ analyte}}{\text{mol L}^{-1} \text{ THB}} < 2,0 \times 10^{-5}$, mechanisms of THB hydrolysis and hydride generation can be represented as:

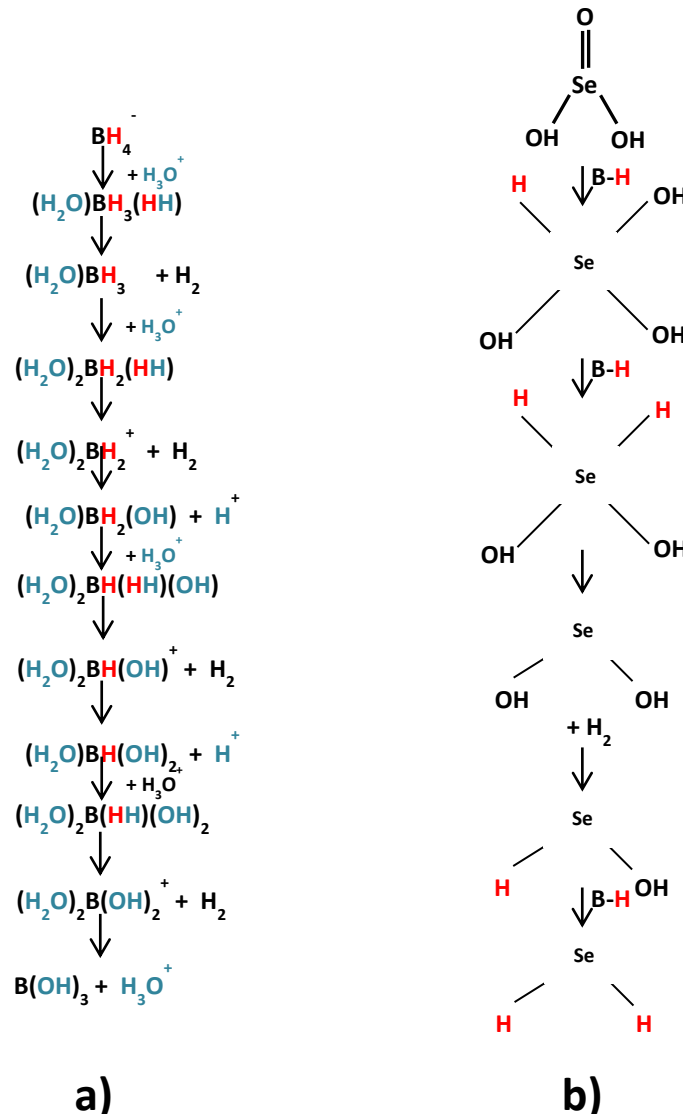


Figure 1: a) Mechanism of the hydrolysis of THB b) Mechanism of selenium hydride generation; B-H: symbolises all the hydridoboron intermediates.

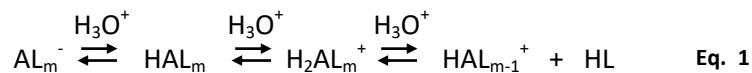
Figure 1 evidences that both are stepwise reactions. Figure 1 a) shows the decomposition of THB in acidic media. Different colours were used for the sake of exemplifying the interaction of the reagent with the solvent.

Hydron reacts with the hydride anion in a disproportionation reaction yielding hydrogen. The solvating water molecules participate in an acid-base reaction and the remaining OH substitutes the leaving hydride; the overall reaction is a sequential exchange of the hydride with the solvent leading, in addition to hydrogen, hydridoboron intermediates and boric acid as the final reaction product.

Every hydridoboron intermediate are, at different extent, able to react with the analyte generating intermediate hydrido-metal complexes in an also stepwise reaction which final product is the analyte's volatile hydride (Figure 1 b) shows an example for Selenium).

The aforementioned equilibria are affected also by ligand properties towards hydridoboron or analyte intermediates from the counter ion of the acid.

In turn, the analyte participates also in acid base equilibria; it can be considered as a weak acid HAL_m (A: analyte, L: O or OH, and m: number of ligands).



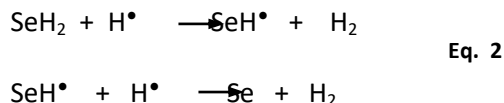
Each intermediate (Eq. 1) interacts different with the hydridoboron intermediates as the substrate can be more accessible or the central atom activated towards the hydride attack.

The hydride formed can participate also in acid-base reactions generating ionic species which fix the analyte to solution preventing the hydride release.

Therein lies the importance of a strict control of the working conditions in terms of media acidity, type of acid, reactor design and reaction time to promote the generation and preserve the integrity of the volatile species. (D'Ulivo, Onor, & Pitzalis, Role of Hydroboron Intermediates in the Mechanism of Chemical Vapor Generation in strongly acidic media, 2004) (D'Ulivo, Baiocchi, Pitzalis, Onor, & Zamboni, 2004) (D'Ulivo, Chemical vapor generation by tetrahydroborate(III) and other borane complexes in aqueous media A critical discussion of fundamental processes and mechanisms involved in reagent decomposition and hydride formation, 2004) (D'Ulivo, Mechanism of generation of volatile species by aqueous boranes Towards the clarification of most controversial aspects, 2010) (D'Ulivo, Mechanisms of chemical vapor generation by aqueous tetrahydridoborate. Recent developments toward the definition of a more general reaction model, 2016) (D'Ulivo, The contribution of chemical vapor generation coupled with atomic or mass spectrometry to the comprehension of the chemistry of aqueous boranes, 2019).

The atomisation process depends on the atomisation device. At this stage only atomisation in externally heated quartz tube atomisers (EHQTA) was considered at that time as the sole available in this work for atomic absorption spectrometry.

EHQTA are T-shaped tubes which horizontal arm is the optical path and the central arm the inlet of the gaseous phase (gas stream and hydride). They can be heated electrically or by an acetylene-air flame. The mechanism of atomisation is due to the collisions between the hydride molecule and hydrogen radicals formed in the atomiser (Eq. 2):



In the atomiser, hydrogen (evolved from THB hydrolysis) and oxygen (at very low concentration, dissolved in reagent solutions, diffusing from the atmosphere or as contaminant of the carrier gas) react generating a hydrogen radical cloud; heating of the cell is necessary for accomplishing and maintaining this reaction. The hydride decomposition is not thermal but by radical collisions. The location of the cloud depends on the temperature profile of the tube, its design and the gas flow rate. The efficiency of the atomisation process depends on the hydrogen cloud sectional density; thus, the oxygen requirement is determined by the diameter of the tube and the temperature. Higher tube's temperature needs lower amounts of oxygen.

Analyte atoms must be transported to the optical path in order to be determined; their stability is conditioned by the radical cloud, once they leave it they react with the tube surface and decay, the worse the surface integrity of greater relevance the attrition. Convection due to the gas stream also contributes to decrease the response. (Dedina & Rubeska, Hydride atomization in a cool hydrogen-oxygen flame burning in quartz tube atomizer, 1980) (Dedina & Tsalev, Hydride Generation Atomic Absorption Spectrometry, 1995) (Welz & Sperling, 1999) (Dedina J. , 2007) (Dvořák, Talába, Kratzer, & Dědina, 2019)

Chapter II

Selenium determination by Sequential Injection – Hydride Generation - Atomic Absorption Spectrometry

This section describes the sequential injection chemical generation of dihydrogenselenide and its determination by atomic absorption spectrometry. According to the pre-reduction of Se(VI) to Se(IV) it is divided in Part I (off-line pre-reduction) and Part II (on-line pre-reduction). For both the system was characterised and applied to tap and local lake water samples respectively.

2.2 Selenium Determination by Sequential Injection Hydride Generation Atomic Absorption Spectrometry

This work was the first accomplished within the thesis studies. It can be divided in two parts, first, the assembly of the system, its optimisation and application to the determination of selenium in water samples with the pre-reduction stage (the volatile species is formed from Se(IV) exclusively) performed off line. It is presented as Part I.

For the second part, the system was modified by the incorporation of an on line pre-reduction stage. A complete chemical interferences study was also performed. This work is presented as Part II.

2.2.1 Introduction

Sequential Injection Analysis (SIA) is a flow technique in which sample and reagents are sequentially taken and dispensed to a holding coil where, by a back and forth movement they are first high efficiently mixed and then sent to the detection system. The main advantage of this technique is the low reagent consumption as they are aspirated at a time, not continuously as other flow techniques.

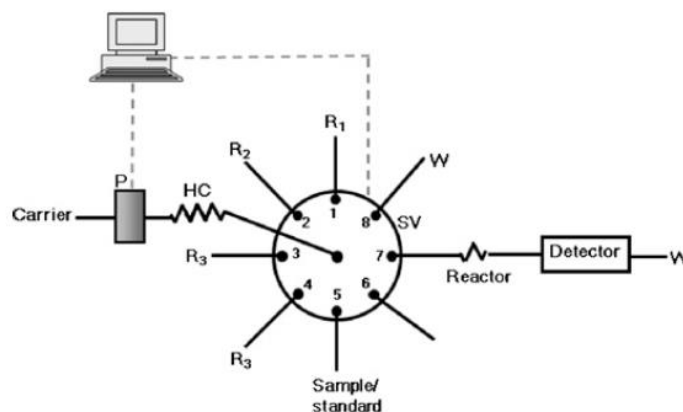


Figure 2: SIA manifold. SV: selection valve; HC: holding coil; P: propulsion system; R: reagents; W: waste. Extracted from R.B.R. Mesquita, A.O.S.S. Rangel / *Analytica Chimica Acta* 648 (2009) 7–22

A scheme of a SIA system is depicted in Figure 2. The propulsion system aspirates sample and reagents through the selection valve to the holding coil, a reverse flow let them mix and then, the carrier pushes them to the detector. A syringe pump can serve as the propeller. All the system is controlled by software, with a high repeatability in the volume dispensing (Ruzicka & Marshall, 1990) (Mesquita & Rangel, 2009).

2.2.2 Part I – Working conditions optimisation

2.2.2.1 Instrumentation

The manifold was constructed with a Tecan Cavro (Männedorf, Switzerland) XP-3000 5-mL syringe pump, and a Valco (Houston, TX, USA) EMHMA-CE multiposition motorised valve.

Holding and reactors coils were constructed of Teflon FEP tubing (0,8-mm internal diameter).

The hydride was separated in a lab-built glass hydrostatic separator. For the atomisation of the hydride, an externally heated quartz tube atomiser (EHQTA), T-shaped cell (Precision Glassblowing, Centennial, CO, USA) was used. The optical tube was 18-cm long and 1-cm internal diameter fitted with graphite cooling rings at its ends in order to prevent hydrogen ignition. The inlet arm had a 0,5 cm inner diameter. The cell was heated by an air-acetylene flame on a 10-cm burner installed in a Perkin Elmer (Norwalk, CT, USA) model 5000 atomic absorption spectrometer fitted with a Photron (Narre Warren, Australia) Superlamp intensified emission selenium hollow-cathode lamp.

The analytical wavelength was 196,0 nm. All other operating conditions were set as established by the manufacturer.

Nitrogen flow was regulated by a Cole Parmer variable area flow meter with valve.

The system was controlled from a personal computer (PC) by means of software compiled in Visual Basic 6.0. Analogue signals from the spectrometer were digitised with a USB-1408FS 14-bit analogue-to-digital interface (Measurement Computing, Norton, MA, USA) connected to the PC via a USB port and operated at a 1-Hz sampling rate. The program performed data acquisition, on-screen visual presentation and storage of the data in ASCII format. It also controlled the syringe pump and the multiposition valve via RS-232 serial communications ports. Data was processed post-run by means of the Peak Simple 3.29 program (SRI Inc., Torrance, CA, USA).

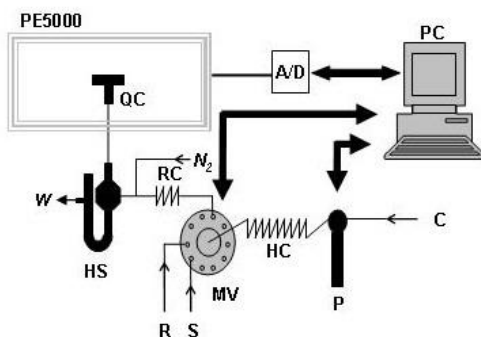


Figure 3: Sequential Injection system used for selenium determination (*Part I*). PE5000: atomic absorption spectrometer; A/D: analogue to digital interface; C: carrier (water); HC: holding coil (2 m); HS: hydrostatic gas-liquid separator; MV: multiposition valve; N₂: nitrogen input; P: syringe pump; PC: personal computer with the software control; QC: quartz atomisation cell; R: reagent (NaBH₄); RC: reaction coil (0,2 m); S: pre-reduced sample; W: waste.



Figure 4: Photograph of the system used. HS: hydrostatic gas-liquid separator; MV: multiposition valve; P: syringe pump; QC: quartz atomisation cell; W: waste.

The scheme of the system used is presented in Figure 3 and the photograph in Figure 4.

2.2.2.2 Reagents and solutions

De-ionised water (ASTM type I) was obtained from a Millipore (São Paulo, Brazil) Direct-Q 5 water purifier. Selenium stock standard solution was prepared from Se powder (Aldrich, 100 mesh, 99.99%) dissolved in concentrated HNO_3 . The solution was evaporated to dryness and then dissolved in 10 % v/v HCl and diluted to 1 L with 10 % v/v HCl. Working standard solutions were prepared daily by dilution of the stock solution with deionised water.

Sodium tetrahydroborate solution (0,20 % w/v in sodium hydroxide $0,05 \text{ mol L}^{-1}$) was prepared from sodium tetrahydroborate (Hydride-Generation grade, Fluka).

All reagents used were of analytical reagent grade unless otherwise specified. Standard nitrogen and acetylene were supplied by Linde Uruguay.

2.2.2.3 Procedure

Before the introduction to the SIA system, 20 mL of sample (sample or calibration solution) was added by 10 mL of 37 % w/w HCl and gently boiled in a hot plate for 40 min. After the evaporation, sample was taken anew to 20 mL with water.

In the SIA system, an air bubble was aspirated into the holding coil followed by 500 μL of reductant (NaBH_4) solution, 250 μL of pre-reduced sample and further reductant solution (500 μL). The scheme can be seen in Figure 5:

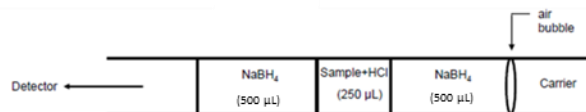


Figure 5: Sequential loading of sample and reagent in the holding coil (*Part I*).

A flow reversal motion step was performed for achieving an effective mixing of the sample with the reductant. The carrier (deionised water, 3,0 mL) pushed the mixture and transported it to the gas-liquid separator. There, a stream of nitrogen helped release the hydride from the solution and reach the atomisation cell. The air bubble introduced avoided the contact between the water used as carrier and the reagent preventing the early decomposition of the tetrahydroborate when the bolus is transported by the carrier to the detector.

The aforementioned procedure was optimised in terms of reaction coil size, sample volume, nitrogen flow rate, reductant concentration and evaluation of the benefits of the addition of additives as sodium chloride (salting out effect) and potassium iodide (catalytic effect) for hydride release.

2.2.2.4 Results and discussion

Variables affecting the hydride generation are: hydrochloric acid concentration in the sample (the remaining after Se (VI) reduction which determined the amount of reductant needed for a suitable hydride generation efficiency), volume and concentration of the reductant, carrier gas flow rate in the gas-liquid separator (along with the evolving hydrogen removed the hydride from the solution and transported it to the atomisation cell), sample volume (both amount of Se (IV) and hydrogen ion that reacted with the reductant) and size of the reaction coil (determined reaction time).

2.2.2.4.1 Size of the reaction coil

A five point calibration curve (up to 100 µg L⁻¹) was constructed and measured using the different reactors. Five instrumental replicates of the 50 µg L⁻¹ Se solution were measure in order to assess the instrumental repeatability. Results are presented in Table 1.

reactor size (m)	peak height		peak area	
	slope (L µg ⁻¹)	s _r (%)	slope (sL µg ⁻¹)	s _r (%)
0,2	0,0012	3,2	0,0029	5,3
0,5	0,0011	7,8	0,0029	3,5
1	0,0014	8,2	0,0023	9,4

Table 1: Performance for the different reactors. s_r (%): relative standard deviation of five instrumental replicates of the $50 \mu\text{g L}^{-1}$ Se solution.

The 1 m reactor was discarded as it had the poorest sensitivity and was more disperse than the others. 20 cm and 50 cm long gave similar results in terms of sensibility and dispersion, but considering the peak shape, 20 cm length lead to well defined peaks, better in appearance than that of 50 cm.

2.2.2.4.2 Sample volume

The volume of the solutions taken to the holding coil depends on the incremental movement of the syringe plunger, the pump resolution and the syringe size. Different volumes were tried: 83, 167, 250 and 333 μL . As volume increased, so did the sensitivity.

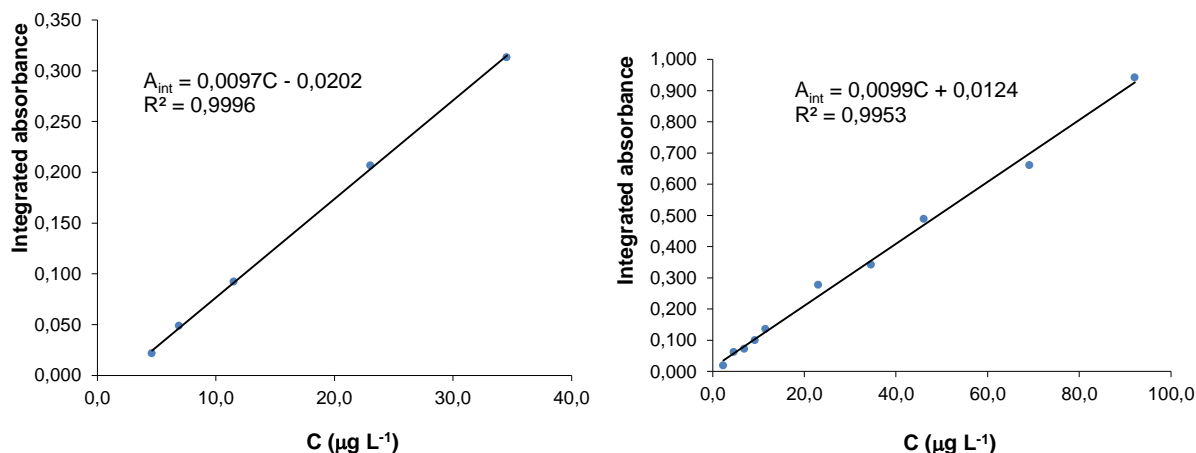


Figure 6: Selenium calibration curves for a sample volume of 250 μL and 333 μL respectively. A_{int} : integrated absorbance (s); C : concentration of selenium in $\mu\text{g L}^{-1}$.

As can be seen in Figure 6, sensitivity expressed as peak area related to analyte concentration is the same for volumes 250 and 333 μL . The latter involves higher amount of analyte (same concentration and higher volume, higher analyte mass in the atomiser), hence, 33% lower.

Atomisation for taking place needs beside hydrogen, the presence of oxygen so as to generate free radicals. The amount of oxygen for both sample volumes is expected to be the same as is the one dissolved in the reagent solutions, or diffusing across the tubes or as impurity of the nitrogen. The temperature is high enough as the quartz tube is heated by the flame. As it was observed that for 333 μL sample volume, there was more hydrogen evolution, increasing the gas flow rate. It is probable that the ratio O_2/H_2 is decreased and so the radical density, and so the atomisation efficiency, explaining the

decrease in sensitivity. This hypothesis could have been confirmed by adding a supply of oxygen to the nitrogen line and evaluating the variation of sensitivity.

250 μL sample volume was chosen as when using 333 μL , there was a significant hydrogen evolution causing overpressure; the gas-liquid separator got overflowed and the peaks distorted.

2.2.2.4.3 Nitrogen flow rate

The flow meter was first calibrated with nitrogen for each indication, measuring the time elapsed while a soap bubble crossed the mark for 100,0 mL volume.

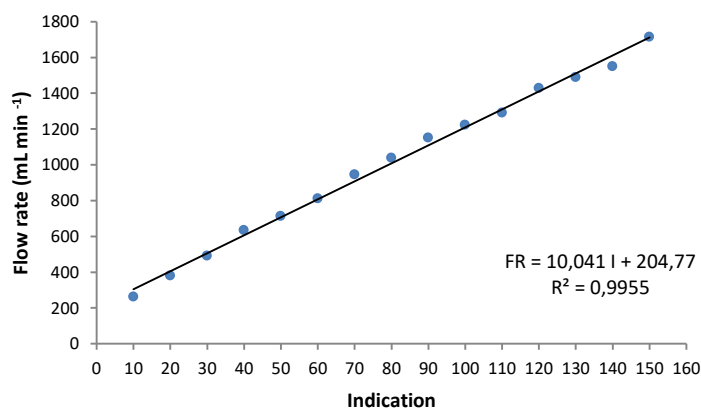


Figure 7: Flow-meter calibration with nitrogen. FR: nitrogen flow rate (mL min^{-1}); I: indication

Carrier gas flow rate was varied along the different flows until a well-defined transient signal was obtained. It was set at 760 mL min^{-1} .

2.2.2.4.4 Reductant concentration

Reductant was tried at 0,2 % w/v and 1,0 % w/v; the last caused high hydrogen evolution thus discarded.

2.2.2.4.5 Acidity of the sample

Samples were gently boiled with concentrate hydrochloric acid for about 40 min on a hot plate (sample: HCl – 2:1). Once partially evaporated they were retaken up to its original volume with deionised water. Conditions were optimised so as to obtain reproducible results. The resulting solution was directly measured.

2.2.2.4.6 Salting-out effect

In order to decrease dihydrogenselenide solubility, NaCl was added to the calibration standards for the salting out effect evaluation.

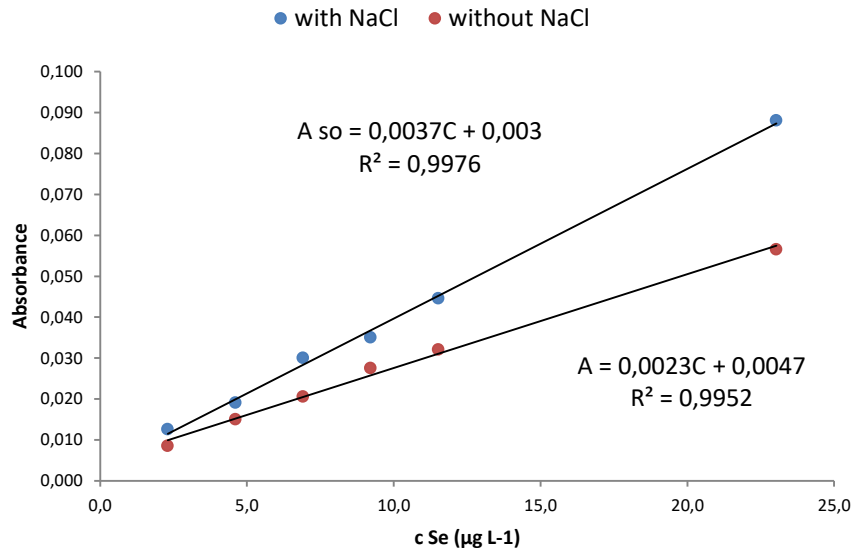


Figure 8: Evaluation of the salting-out effect for the SI-HG-AAS Part I system. Calibration curve for selenium with (blue) and without (red) sodium chloride. A_{SO} : absorbance of the solutions with NaCl; A : absorbance of the solutions without NaCl; C : selenium concentration in $\mu\text{g L}^{-1}$.

At each concentration level the solutions were measured with and without the addition of NaCl. Figure 8 shows an increment in the slope of selenium calibration curve close to 40 % when NaCl is added; solutions were then saturated with NaCl.

2.2.2.4.7 Addition of 0,1 mol L⁻¹ KI

The eventual catalytic effect of potassium iodide was also evaluated. Iodide reduces Se(IV) to Se(0) in a stepwise reaction whose intermediates are more reactive towards boranes than selenite; furthermore, there are also formed hydridoboron species that might collaborate in selenium signal enhancement. The reaction is pH-dependant as at high acidities selenium complete reduction prevails against dihydrogenselenide formation (Dedina & Tsalev, Hydride Generation Atomic Absorption Spectrometry, 1995) (D'Ulivo, The contribution of chemical vapor generation coupled with atomic or mass spectrometry to the comprehension of the chemistry of aqueous boranes, 2019).

0,1 mol L⁻¹ KI was used as a catalyst trying to decrease the amount of tetrahydroborate used but was not successful. For the concentration of additive tried, selenium signal remained unchanged.

2.2.2.4.8 Summary of the optimum working conditions

Reaction coil (cm)	Sample volume (μL)	Reductant volume (μL)	N_2 flow rate (L min^{-1})	c NaBH_4 (% w/v)
20	250	500 per segment	0,76	0,2

2.2.3 Part I – Method characterisation

2.2.3.1 Instrumentation

The SIA system described in **2.2.2.1 Instrumentation** was used.

For assessing trueness and comparing the methodologies, APHA Method 3114B “Manual Hydride Generation/Atomic Absorption Spectrometric Method” (Clesceri, Greenberg , & Eaton, 1998) was performed, it will be addressed in this section as the Reference Method.

For performing it, a manually operated Mercury Hydride System Perkin Elmer MHS 15 was used: sample is introduced in the reaction flask and the reductant in the reservoir; by manually activating a pneumatic valve the nitrogen stream transport the THB to the reactor and the hydride formed is transferred to the atomiser. The atomiser is an EHQTA on the spectrometer burner as described previously.

2.2.3.2 Reagents and solutions

De-ionised water (ASTM type I) was obtained from a Millipore (São Paulo, Brazil) Direct-Q 5 water purifier. Selenium stock standard solution was prepared from Se powder (Aldrich, 100 mesh, 99.99%) dissolved in concentrated HNO_3 . The solution was evaporated to dryness and then dissolved and diluted to 1 L with 10 % v/v HCl. Working standard solutions were prepared daily by dilution of the stock solution with deionised water. Sodium tetrahydroborate solution, 0.20 % w/v in sodium hydroxide 0,05 mol L^{-1} was prepared from sodium tetrahydroborate (Hydride-Generation grade, Fluka).

For the Reference Method, sodium tetrahydroborate solution (3,0 % w/v in 1% w/v NaOH) was prepared from sodium tetrahydroborate (Hydride-Generation grade, Fluka).

Standard nitrogen and acetylene were supplied by Linde Uruguay.

All reagents used were of analytical reagent grade unless otherwise specified. Water samples were obtained from different locations in the country.

2.2.3.3 Procedure

The procedure mentioned in **2.2.2.3 Procedure** was performed for calibration solutions and samples.

For the Reference Method, 10 mL of sample (spiked samples or calibration standards solutions) were introduced in the MHS 15 and added with the reductant until the maximum signal was attained. Samples were measured by triplicate.

2.2.3.3.1 Linear range

Nine calibration solutions were prepared and measured by the SI-HG-AAS system developed; integrated absorbance was plotted against concentration of selenium. The linear range was evaluated by visual inspection and the study of the dispersion of the residuals.

2.2.3.3.2 Limits of detection and quantification

Blank signal does not differ significantly from the baseline, so, for estimating the limits of detection and quantification the blank was spiked at a low concentration of selenium.

Limits of detection and quantification were calculated as follows: $LOD = \frac{3s}{m}$ and $LOQ = \frac{10s}{m}$ where s is the standard deviation of ten signal replicates (integrated absorbance) of the spiked blank and m the slope of the calibration function.

2.2.3.3.3 Precision of repeatability

Selenium free, tap water samples were added with Se (VI) at different concentration levels. Precision of repeatability was estimated as the relative standard deviation of five replicates of them.

2.2.3.3.4 Trueness

20 samples of selenium free tap water for different locations of the country were spiked in the range of $10 - 40 \mu\text{g L}^{-1}$. Samples were analysed both by the SI-HG-AAS and the Reference Method. Trueness was assessed by means of recovery of the spike value and by comparison of the results from both methodologies.

2.2.3.4 Results and discussion

2.2.3.4.1 Linear range

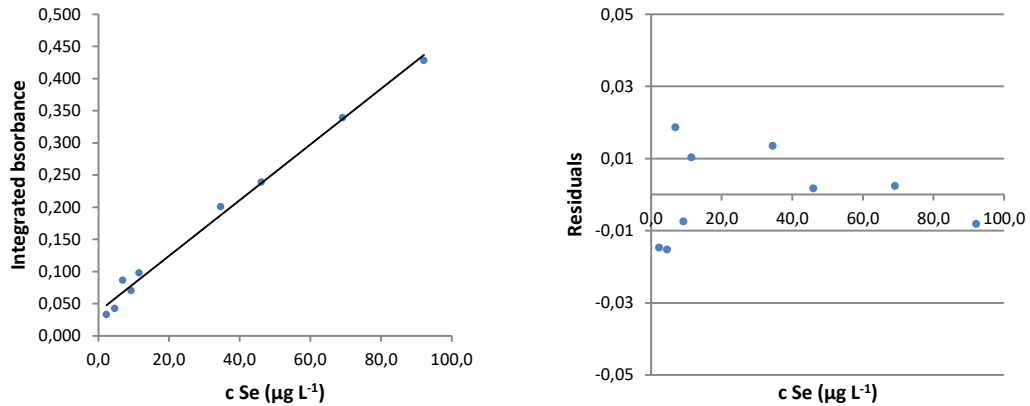


Figure 9: Evaluation of the linear range. Left, selenium calibration curve. Right, dispersion of the residuals for the SI-HG-AAS system Part I.

As can be seen in Figure 9, after the visual inspection of the calibration function and the dispersion found in the residual study, the calibration function can be considered linear within the whole range tried (up to 100 µg L⁻¹ Se).

2.2.3.4.2 Limits of detection and quantification

	SI – HG – AAS	Reference Method
LOD (µg L ⁻¹)	0,34	0,31
LOQ (µg L ⁻¹)	1,13	1,01

Table 2: Limits of detection (LOD) and quantification (LOQ) for the SI-HG-AAS Part I and the Reference Method.

Table 2 shows the limits of detection and quantification for both methods; there is no significant difference between the limits attained.

2.2.3.4.3 Precision of repeatability

Concentration level ($\mu\text{g L}^{-1}$)	s_r (%)
5	2,4
10	1,8
20	4,2
30	1,1
40	4,5

Table 3: Precision of repeatability for the SI-HG-AAS system at different concentration levels.

s_r (%): relative standard deviation for five replicates.

Table 3 shows the precision of repeatability for spiked samples at different levels for the SI-HG-AAS method.

2.2.3.4.4 Trueness

2.2.3.4.4.1 Spike / recovery

Selenium was determined in the spiked selenium-free samples and thus the recovery calculated as:

$$\text{Recovery (\%)} = \frac{C_{\text{sample}}}{C_{\text{spiked}}} \times 100$$

C_{sample} is the concentration of selenium found after the analysis of the spiked sample by the SI-HG-AAS method and C_{spiked} is the concentration of the spike in the sample.

Recovery was plotted against the concentration of the spike.

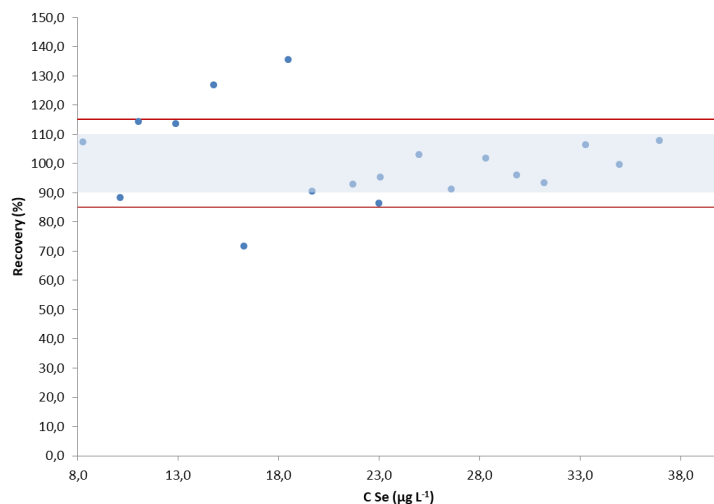


Figure 10: Recovery of the spiked samples analysed by SI-HG-AAS system *Part I*.

As can be seen in Figure 10, most of the samples had a recovery between 85 – 115 % (red lines in the figure); among them 75 % have a recovery between 90 – 110 % (shaded band). Spiked sample at 5 µg L⁻¹ Se had a recovery close to 200 % and was intentionally left aside.

2.2.3.4.4.2 Comparison of the methodologies (SI-HG-AAS vs Reference Method).

Spiked samples were also analysed by the Reference Method. Results from the SI-HG-AAS method were plotted against the results from the Reference Method. In the absence of systematic error, the regression line relating the results obtained with each of them would have ideally a slope (m) of 1 and a zero intercept (b) (Miller & Miller, 2010). The hypothesis was confirmed by joint confidence ellipse for slope and intercept (Mandel & Lining, 1957).

The correlation between the results obtained by the SI-HG-AAS method and the Reference Method are presented in Figure 11:

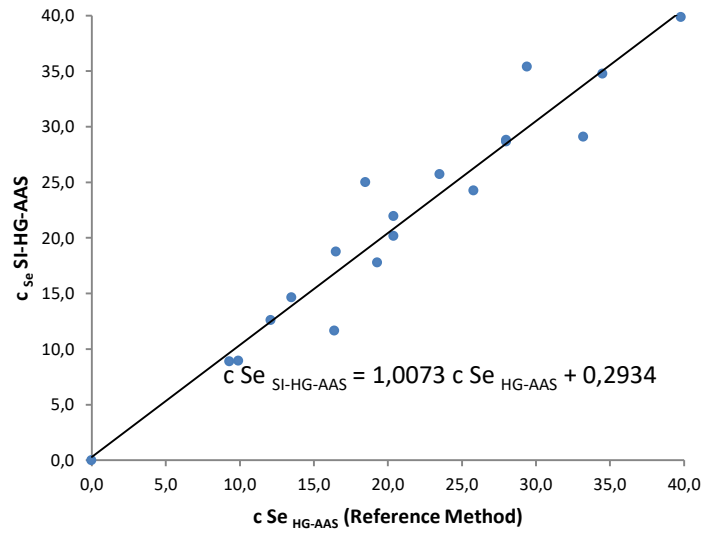


Figure 11: Correlation of the results of selenium determination in spiked tap water by the SI-HG-AAS method and the Reference Method. c Se SI-HG-AAS: concentration of selenium in $\mu\text{g L}^{-1}$ determined by SI-HG-AAS method; c Se HG-AAS: concentration of selenium in $\mu\text{g L}^{-1}$ determined by the Reference Method.

As $F_{\text{experimental}} = 0,246 < F_{(1-b)(2,n-2)} = 3,592$ the null hypothesis can be accepted hence no significant differences between the value of the slope and 1, and the value of the intercept and 0 were found. The absence of systematic error when determining selenium by SI-HG-AAS was confirmed.

2.2.4 Part II – Working conditions optimisation

2.2.4.1 Introduction

Generally the reduction of Se(VI) to Se(IV) takes place heating with hot hydrochloric acid for a few minutes. The time needed for Se(VI) to get reduced decreases as more concentrated is the acidic media and elevated the temperature. The aim of the work at this stage was to cover the whole analysis on-line in the same system (Stripeikis, Costa, Tudino, & Troccoli, 2000).

The reduction step was achieved on-line heating the acidified sample in a boiling water bath just before being introduced to the holding coil.

As the hydrochloric acid concentration changed, tetrahydroborate concentration and volume needed optimisation anew; all three were chosen as factors to optimise using an experimental design. First a preliminary study was run using a two-level factorial experimental design in order to identify between them, which of the variables had an actual impact in the response. The levels were defined by the higher and lower value assigned to the variable. Thus, the number of experiments was set by the number of factors ($k = 3$) and the number of levels for each factor (2) as $2^k = 2^3$ in this case, 8 experiments.

After screening the factors (Results are presented and discussed in **2.2.4.5** and **Table 4**), only hydrochloric and tetrahydroborate concentration were of relevance; in that way, a deeper study was carried out increasing the number of levels per factor. With more levels a response surface can be drawn evidencing more precisely the optimum working conditions. For that purpose a Doehlert matrix design was used attaining with few experiments useful information.

Doehlert design foresees different number of levels for both variables: the one of most impact (hydrochloric acid concentration in this case) was studied at five levels, and tetrahydroborate concentration at three levels. Whenever the combinations of the levels are framed between values away from the optimum, the surface response has the shape of a saddle. The frame can be moved until the surface delimited by the parameters is mound shaped; best working conditions can be calculated as those for each factor from which arises the maximum response (Massart, Vandeginste, Buydens, De Jong, Lewi, & Smeyers-Verbeke, 1997) (C. Ferreira, dos Santo, Quintella, Neto, & Bosque-Sendra, 2004).

2.2.4.2 Instrumentation

The manifold used was the same as previously described in **2.2.2.1 Instrumentation** incorporating in the sample connector a reaction coil immersed in a boiling water bath where sample already acidified with HCl was held during 60s for the reduction of Se(VI) to Se(IV) (Figure 12).

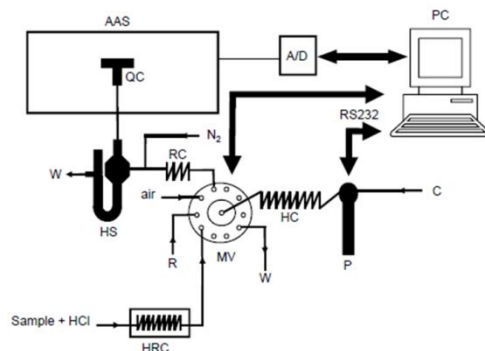


Figure 12: Sequential Injection system used for selenium determination (*Part II*). AAS: atomic absorption spectrometer; A/D: analogue to digital interface; C: carrier (water); HC: holding coil (2 m); HRC: heated reactor coil (1 m); HS: hydrostatic gas-liquid separator; MV: multiposition valve; N₂: nitrogen input; P: syringe pump; PC: personal computer with the software control; QC: quartz atomisation cell; R: reagent (NaBH₄); RC: reaction coil (0,2 m); W: waste.

2.2.4.3 Reagents and solutions

De-ionised water (ASTM type I) was obtained from a Millipore (São Paulo, Brazil) Direct-Q 5 water purifier. Selenium stock standard solution was prepared from Se powder (Aldrich, 100 mesh, 99.99%) dissolved in concentrated HNO₃. The solution was evaporated to dryness and then dissolved and diluted to 1 L with 10 % v/v HCl. Working standard solutions were prepared daily by dilution of the stock solution with deionised water. Sodium tetrahydroborate solutions in sodium hydroxide 0,05 mol L⁻¹ were prepared from sodium tetrahydroborate (Hydride-Generation grade, Fluka).

All reagents used were of analytical reagent grade unless otherwise specified.

Standard nitrogen and acetylene were supplied by Linde Uruguay.

2.2.4.4 Procedure

Before the introduction to the SIA system, 10 mL of sample (sample or calibration standard solution) was mixed with 13,3 mL of HCl and taken to 25 mL with water. When sample (or calibration standard solution) was to be measured an excess volume was aspirated into the heated reactor coil immersed in the boiling water bath and thermostated for 60 s. Afterwards, 420 µL of sample was aspirated and

discarded to waste. This volume corresponds to the one which, when loading the sample remains out of the boiling bath and so was not reduced. When merely repeating the injection of the same sample it was not necessary to wait.

An air bubble was aspirated into the holding coil followed by 420 μL of reductant (NaBH_4) solution, 250 μL of acidified sample (corresponding to the portion inside the water bath, and thus, already reduced) and again reductant solution (420 μL). The scheme can be seen in Figure 13:

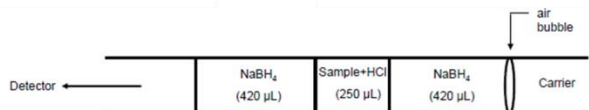


Figure 13: Sequential loading of sample and reagent in the holding coil.

A flow reversal motion step was performed for achieving an effective mixing of the sample with the reductant. The carrier solution (3,3 mL deionised water) transported the mixture to the gas-liquid separator. A stream of nitrogen helped release the hydride from the solution and reach the atomisation cell. The air bubble introduced avoids the contact between the water used as carrier and the reagent preventing the early decomposition of the tetrahydroborate when the bolus is transported by the carrier to the detector.

2.2.4.5 Results and discussion

Hydrochloric concentration is the variable that makes the difference with respect to the system developed in *Part I*. It must be enough for Se(VI) reduction in a short time, but its amount determines the rate of decomposition of the tetrahydroborate. Thus, hydrochloric acid concentration and volume and concentration of tetrahydroborate needed optimisation in this new system design.

Sample volume, size of the reaction coil and carrier gas flow rate in the gas-liquid separator remained as optimised in *Part I*.

For the optimisation of hydrochloric acid concentration in the sample and, volume and concentration of reductant a two factorial experimental design was performed:

Experiment	c HCl	V NaBH ₄	c NaBH ₄	Absorbance
1	+	+	+	0,081
2	+	+	-	0,064
3	+	-	+	0,077
4	+	-	-	0,074
5	-	+	+	0,058
6	-	+	-	0,051
7	-	-	+	0,061
8	-	-	-	0,050

Table 4: Two level factor experimental design. + : factor in the higher level; - : factor in the lower level; c HCl: concentration of HCl, mol L⁻¹; V NaBH₄: volume of NaBH₄, mL; c NaBH₄: concentration of NaBH₄, % w/v.

Levels	+	-
c HCl	6,0 mol L ⁻¹	3,0 mol L ⁻¹
V NaBH ₄	0,8 mL	0,5 mL
c NaBH ₄	1,0 % w/v	0,2 % w/v

Table 5: Values for the + higher and – lower levels of the factors of Table 1.

For evaluating the relevance of the three factors, eight solutions were prepared as detailed in Table 4. Results show that volume of the reductant does not impact in the response. Further optimisation was carried on with the concentration of hydrochloric acid and sodium tetrahydroborate.

Doehlert experimental design for two factors describes a hexagon and its central point.

Experiment	Factor 1	Factor 2
	c HCl	c NaBH ₄
1	1	0
2	-1	0
3	0,5	0,866
4	-0,5	0,866
5	0,5	-0,866
6	-0,5	-0,866
7	0	0

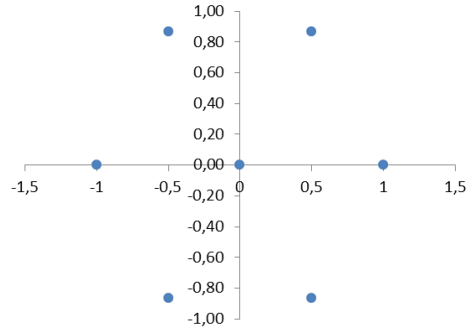


Figure 14: Doehlert design for two factors and its sequentiality in space.

Different values were assigned for the levels until a well-shaped surface was attained (Figure 15). The central point was prepared by triplicate.

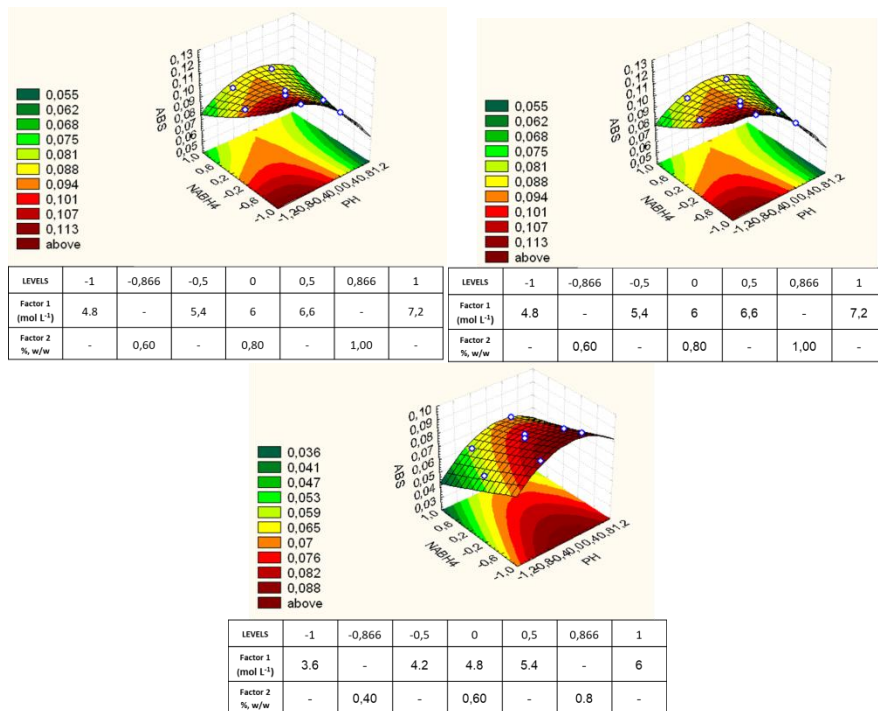


Figure 15: Different levels tried without reaching optimum working conditions

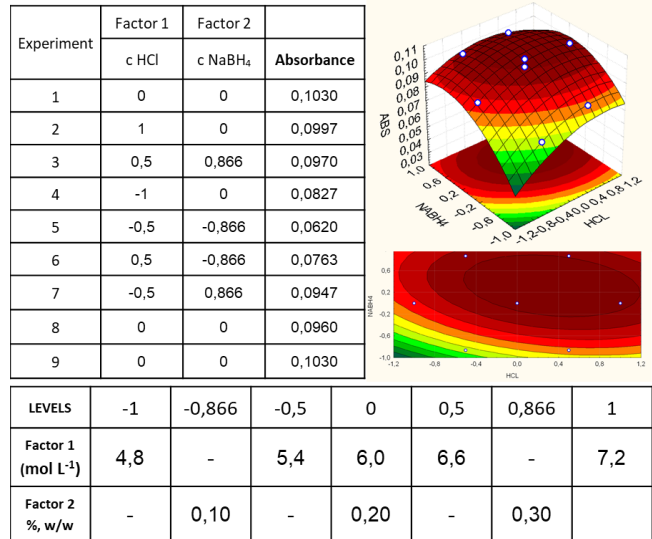


Figure 16: Doehlert experimental design; optimum working conditions.

Figure 16 shows the Doehlert experimental design leading to a mound shaped surface; optimum working conditions can be drawn. According to the critical values, optimal conditions can be calculated from the coded values: 6,4 mol L⁻¹ HCl and 0,24 % w/v NaBH₄.

Summarising, working conditions for the SI – HG – AAS system *Part II*:

Reaction coil (cm)	Sample volume (μL)	Reductant volume (μL)	N ₂ flow rate (L min ⁻¹)	c HCl (mol L ⁻¹)	c NaBH ₄ % w/v
20	250	420 per segment	0,76	6,4	0,24

The salting-out effect was also evaluated in SI-HG-AAS system *Part II* adding NaCl to the solutions.

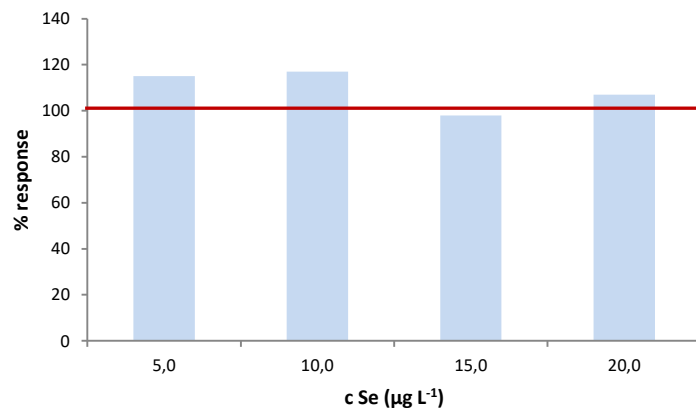


Figure 17: Evaluation of the salting-out effect for SI-HG-AAS system *Part II*. % Reponse: percentage ratio of the signal when NaCl is added over the signal of the solution without the addition.

Figure 17 shows the % Response against the concentration levels:

$$\% \text{ Response} = \frac{S_{\text{salting out}}}{S} \times 100$$

where $S_{\text{salting out}}$ is the signal of the solution with NaCl and S the signal of the same solution without addition.

It can be seen that there is no signal improvement; probably the temperature compensated already the salting out effect. As solution is heated while reduction of Se(VI) takes place, the drop in the solubility caused by the increment of the temperature probably already makes a signal improvement and the salting out effect in these conditions is of no significance.

2.2.4.6 Conclusions

By combining chemometric tools and qualitative aspects of the response, optimum working conditions were found for selenium determination by SI-HG-AAS.

2.2.5 *Part II* – Method characterisation

2.2.5.1 Instrumentation

The SIA system described in **2.2.4.2 Instrumentation** was used.

For assessing trueness manual hydride-generation was performed using a Perkin Elmer MHS 15 batch system.

2.2.5.2 Reagents and solutions

De-ionised water (ASTM type I) was obtained from a Millipore (São Paulo, Brazil) Direct-Q 5 water purifier. Selenium stock standard solution was prepared from Se powder (Aldrich, 100 mesh, 99.99%) dissolved in concentrated HNO₃. The solution was evaporated to dryness and then dissolved and diluted to 1 L with 10 % v/v HCl. Working standard solutions were prepared daily by dilution of the stock solution with deionised water. Sodium tetrahydroborate solution 0,24 % w/v in sodium hydroxide 0,05 mol L⁻¹ was prepared from sodium tetrahydroborate (Hydride-Generation grade, Fluka).

For the Reference Method, sodium tetrahydroborate solution (3,0 % w/v in 1% w/v NaOH) was prepared from sodium tetrahydroborate (Hydride-Generation grade, Fluka).

All reagents used were of analytical reagent grade unless otherwise specified.

Standard nitrogen and acetylene were supplied by Linde Uruguay.

Water samples were obtained from a local lake.

2.2.5.3 Procedure

The procedure mentioned in **2.2.4.4 Procedure** was performed for calibration solutions and samples. For the Reference Method, 10 mL of sample (spiked samples or calibration standards solutions already reduced to Se(IV) in hydrochloric acid) were introduced in the MHS 15 and added with the reductant until the maximum signal was attained. Samples were measured by triplicate. Water samples were first analysed by the Reference Method; in view of the results, they could be considered selenium-free.

2.2.5.3.1 Linear range

Six calibration solutions were prepared and measured by the SI-HG-AAS system developed; absorbance was plotted against concentration of selenium. The linear range was evaluated by visual inspection and the study of the dispersion of the residuals.

2.2.5.3.2 Limits of detection and quantification

Blank signals did not differ from the baseline, so, for estimating the limits of detection and quantification the blank was spiked at a low concentration of selenium.

Limits of detection and quantification were calculated as follows: $LOD = \frac{3s}{m}$ and $LOQ = \frac{10s}{m}$ were s is the standard deviation of ten signal replicates (absorbance) of the spiked blank and m the slope of the calibration function.

2.2.5.3.3 Precision of repeatability

Selenium free water samples were added with selenium at different concentration levels (5 – 10 – 15 and 20 $\mu\text{g L}^{-1}$). Precision of repeatability was estimated as the relative standard deviation of five replicates of the measured values.

2.2.5.3.4 Trueness

Water samples, free of selenium were spiked at 5 – 10 – 20 – 30 – 40 and 50 $\mu\text{g L}^{-1}$. Trueness was assessed by means of recovery of the spike value and by comparison with the results of the analysis using the Reference Method. In both cases a Student's t-test was performed; as this test assumes results are drawn from a normal population, previously, the hypothesis of normal distribution of the data had to be supported.

For verifying the normal distribution a Chi-square test was performed which needs at least 50 data, so 51 determinations were done in a 30 $\mu\text{g L}^{-1}$ Se solution.

2.2.5.4 Results and discussion

2.2.5.4.1 Linear range

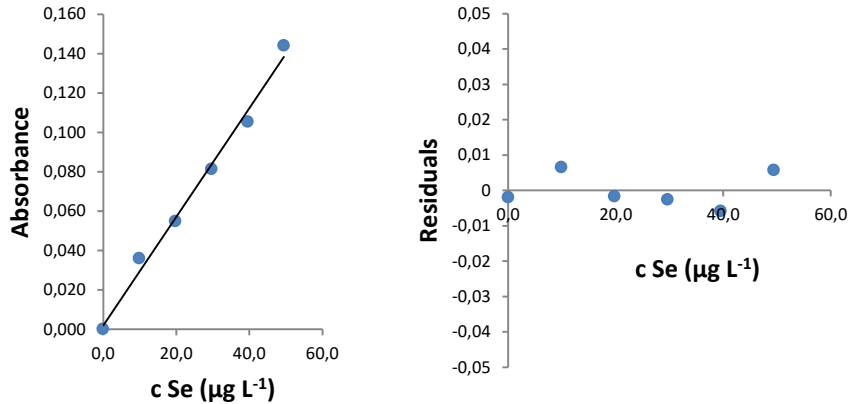


Figure 18: Evaluation of the linear range. Left, selenium calibration curve. Right, dispersion of the residuals for the SI-HG-AAS system Part II.

The linear range was assessed up to $50 \mu\text{g L}^{-1}$ Se; as shown in Figure 18, upon a visual inspection and the dispersion of the residuals, the response can be considered linear in all the concentration range.

2.2.5.4.2 Limits of detection and quantification and precision of repeatability

Results are presented in Table 6:

LOD ($\mu\text{g L}^{-1}$)	LOQ ($\mu\text{g L}^{-1}$)
0,6	2,0
Precision of repeatability, s_r (%) ($n = 10$)	
5	3,6
10	2,2
15	2,5
20	2,4

Table 6: Limits of detection (LOD) and quantification (LOQ), precision of repeatability for the SI-HG-AAS system *Part II*. s_r (%): relative standard deviation.

2.2.5.4.3 Trueness

2.2.5.4.3.1 Normal distribution of the data.

In order to perform the Chi-square test, each data value was separated according to number of times of appearance. Nine classes were assigned according to their frequency.

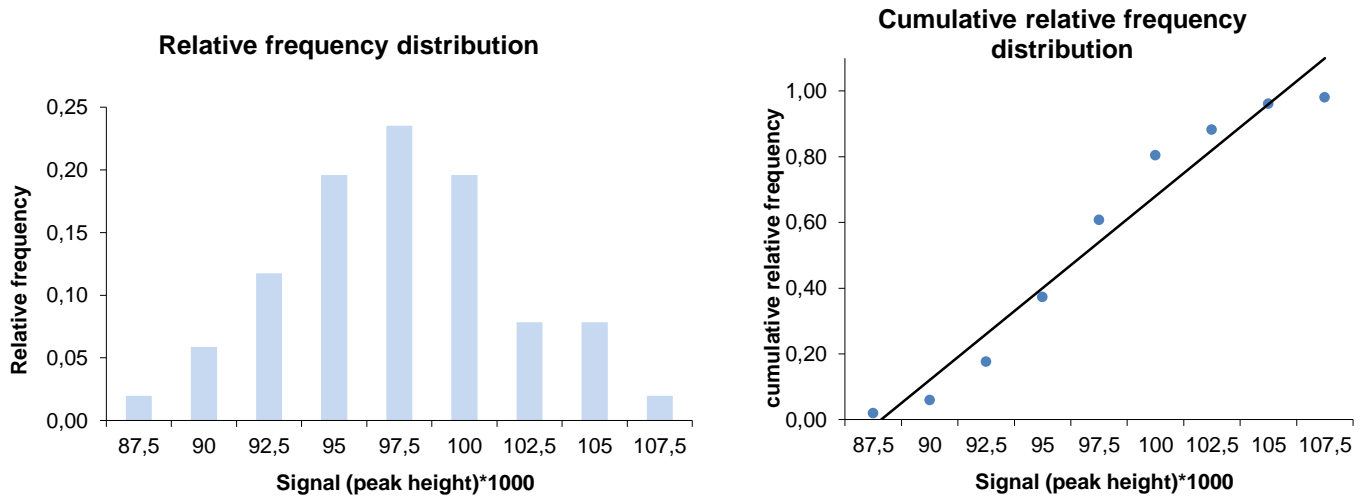


Figure 19: Relative and cumulative relative frequency distribution of SI-HG-AAS system *Part II* data.

Each class represented an interval of responses (the responses were multiplied by 1000 in order to facilitate the visualisation in the graph). Figure 19 shows the plot of the relative frequency and cumulative relative frequency against the central value of the classes of data.

The χ^2 was calculated and compared with the critical value χ^2 for 2 degree of freedom at a 95% significance level.

χ^2	0.0076
χ^2	5.99
Asymmetry coefficient (± 0.5)	0.08
Kurtosis coefficient (± 0.5)	-0.34

Table 7: Results for the Chi-square test performed for the SI-HG-AAS data.

From the results in Table 7, since χ^2 is lesser than χ^2 it can be accepted that data obtained by SI-HG-AAS were drawn from a normal population.

2.2.5.4.3.2 Spike / recovery

Selenium was determined in the spiked selenium-free samples and thus the recovery calculated as:

$$Recovery (\%) = \frac{C_{sample}}{C_{spike}} \times 100$$

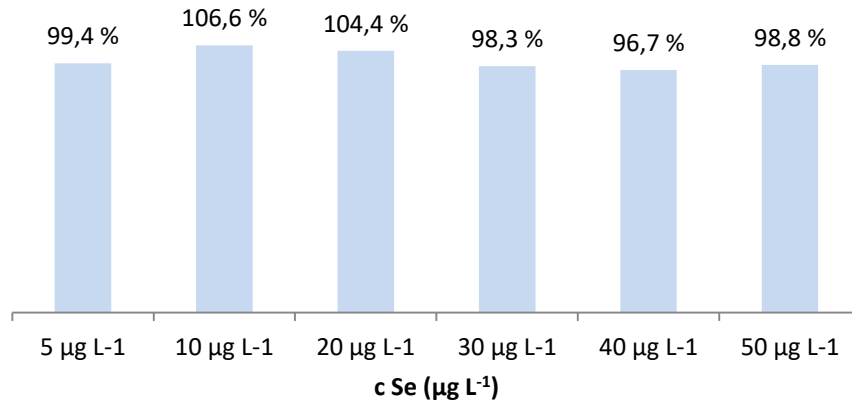


Figure 20: Trueness assessment by spike / recovery study of spiked samples.

As shown in Figure 20 for all the concentration levels the recoveries were very close to 100 %.

Nevertheless, a t-test comparing the mean obtained with the known amount added was performed for each concentration level. Analyses were achieved by quintuplicate. For each concentration level $|t|_{\text{experimental}}$ was calculated and compared against the critical value. Results are presented in Table 8:

Level (µg L ⁻¹)	5,0	10,0	20,0	30,0	40,0	50,0
$ t _{\text{experimental}}$	1,83	2,35	2,26	1,03	2,37	1,10
$t_{0,05, 4}$	2,78					

Table 8: t-test for the spiked solutions at different concentration levels.

At every concentration level, every $|t|_{\text{experimental}}$ found is below the critical value hence the null hypothesis that the method is not subject to systematic errors is accepted. There is no evidence of differences between the value found and the spiked amount for the range of concentrations studied.

2.2.5.4.3.3 Comparison of the results obtained with the SI-HG-AAS method and the Reference Method

The mean values obtained by the SI-HG-AAS method and the Reference Method were compared by means of a t-test. First, a comparison of their standard deviation was performed using a F-test.

Homoscedasticity test						
Level ($\mu\text{g L}^{-1}$)	5,0	10,0	20,0	30,0	40,0	50,0
$F_{\text{experimental}}$	2,7	1,4	1,0	1,4	1,3	1,3
$F_{0,05,4,4}$	9,605					
t-test: Comparison of mean values						
Level ($\mu\text{g L}^{-1}$)	5,0	10,0	20,0	30,0	40,0	50,0
$ t _{\text{experimental}}$	2,14	1,51	0,85	0,58	1,59	2,17
$t_{0,05;8}$	2,31					

Table 9: Homoscedasticity and t-test of the results found by both methods

As can be seen in Table 11, $F_{\text{experimental}} < F_{0,05,4,4}$ for every concentration level, so the null hypothesis that the standard deviation of the methods do not differ significantly can be accepted.

As homoscedasticity was accepted, the t-test was performed. From the last, the null hypothesis that results obtained by both methods do not differ significantly can be accepted.

There is no evidence of difference between the results obtain by the SI-HG-AAS method and the Reference Method.

2.2.5.5 Conclusions

The figures of merit found make the SI-HG-AAS method suitable as an alternative to the Reference Method as precision of repeatability is better than 5,0 % for all the levels of concentration tried, and evidence of bias was not found. Limits of detection and quantification are of the same order (limits for the Reference Method were presented in Table 2), low enough to be used in trace analyse.

2.2.6 Part II – Interference analysis

2.2.6.1 Introduction

Along the process of hydride generation, interferences can arise during each of stages involved: generation, transport and atomisation. Its extent depends on the generating system.

The detection technique related to this work is AAS, thus, spectral and nonspectral interferences could be expected. However, spectral interferences are not of main relevance as the hydride generation technique inherently causes a matrix separation limiting the compounds reaching the atomisation cell. Certainly, other hydride forming elements or even volatile organic compounds present in the sample could reach the cell; the spectral interference occasioned is dependent on their relative concentration and the temperature in which the cell is operating.

The type of interferences that becomes more important is the nonspectral caused by concomitants. Their interaction may occur either in the liquid phase affecting the rate and/or the efficiency of the hydride generation, or in the gaseous phase, affecting the rate and/or the efficiency during the transport towards the atomiser or also in the gaseous phase, and affecting the process in the atomiser itself.

Considering the liquid phase, compound interference is of relevance; whenever the form of the analyte in the solution is other than the one used for the calibration standards, or, whether the analyte is in a different oxidation state or bonded to an organic compound, its behaviour with the reductant would be different and so the hydride release. In the particular case of selenium, as only Se(IV) generates the hydride, the signal would directly be suppressed if it is not previously transformed to that species.

In the liquid phase also, concomitants, depending on their concentration, can be able to interact with the analyte conditioning the generation or hydride release efficiency. In flow systems as the reductant and sample are mixed and go afterwards to the gas-liquid separator, the separation may occur before the interfering interaction takes place, thus minimising or eliminating its effect. As the slow reaction is left unachieved, it is called kinetic discrimination.

In flow systems, kinetic release interference and kinetic transport interference have no incidence in the supply function that depends on the sample flow rate, the analyte concentration and the hydride transport efficiency. The transient signal of the flow injection system is independent of the hydride release rate; if it was so slow that sample run to waste before the release is fulfilled, the kinetic release interference would turn into release efficiency interference. When kinetic transport interference is present, the peak will be delayed in its appearance and its height decreased, but the peak area will remain unchanged.

Changes in peak area are a result of a decreased amount of analyte in the atomisation cell as a consequence of decrease of release efficiency (as already mentioned) or transport efficiency interference due to losses of the hydride in its way towards the atomiser (adsorption to the tubes walls or decomposition in condensed water along the tubes) or interferences in the atomiser.

A certain hydrogen radical population with a cross section density in accordance with the atomiser dimensions is required to achieve the atomisation. Out from the hydrogen radical cloud, free atoms are unstable and its population starts to decay leading to products in the inner surface of the atomiser tube that accelerate the attrition of the still remaining atoms. Thus, interferences in the atomiser can arise if the interferent reduces the hydrogen radical cloud population (incomplete analyte's hydride atomisation) or if it shortens the lifetime of the analyte atoms by changing the inlet arm or optical tube surface next to the hydrogen cloud.

As in general interferent exceeds in amount the analyte the aforementioned situations can occur depending on:

- i. Oxygen supply and temperature of the atomisation cell: both parameters are related as in EHQA the oxygen available is the one coming from solutions and gases, so the lack of oxygen may be compensated with a higher atomisation temperature
- ii. The EHQA dimensions and surface: optical and inlet tube diameter and surface state
- iii. Working conditions in the hydride generation: determines the amount of hydrogen, analyte and gas flow rate

(Dedina & Tsalev, Hydride Generation Atomic Absorption Spectrometry, 1995) (Welz & Sperling, 1999)
(Dedina J. , 2007)

The interferents studied in this work were: arsenic, cobalt, copper, ferric, ferrous, mercury, nickel and zinc ions and nitrate. Inorganic selenium is only considered and the reduction step always accomplished thus, compound interferences (due to selenium bonded to an organic compound or in other oxidation state) are not considered. The expected type of interference due to each of them will be discussed altogether with the results found.

2.2.6.2 Instrumentation

The SI-HG-AAS manifold and the equipment for the Reference Method described in **2.2.4.2 Instrumentation** were used.

2.2.6.3 Reagents and solutions

De-ionised water (ASTM type I) was obtained from a Millipore (São Paulo, Brazil) Direct-Q 5 water purifier. Selenium stock standard solution was prepared from Se powder (Aldrich, 100 mesh, 99.99%) dissolved in concentrated HNO₃. The solution was evaporated to dryness and then dissolved and diluted to 1 L with 10 % v/v HCl. Working standard solutions were prepared daily by dilution of the stock solution with deionised water.

Sodium tetrahydroborate solution 0,24 % w/v in sodium hydroxide 0,05 mol L⁻¹ was prepared from sodium tetrahydroborate (Hydride-Generation grade, Fluka).

Standard nitrogen and acetylene were supplied by Linde Uruguay.

For the Reference Method, sodium tetrahydroborate solution (3,0 % w/v in 1% w/v NaOH) was prepared from sodium tetrahydroborate (Hydride-Generation grade, Fluka).

As(III), Co(II), Cu(II), Fe (III), Hg(II) and Ni(II) atomic standard solutions and reagent grade (NH₄)₂Fe(SO₄)₂·6H₂O and KNO₃ were used for the interference analyses.

2.2.6.4 Procedure

The procedure mentioned in **2.2.4.4 Procedure** was performed for calibration solutions and samples of the SI-HG-AAS method.

For the Reference Method, 10 mL of sample (spiked samples or calibration standards solutions already reduced to Se(IV) in hydrochloric acid) were introduced in the MHS 15 and added with the reductant until the maximum signal was attained. Samples were measured by triplicate.

Calibration plots at low and high concentration levels of interferent were constructed for As, Co, Cu, Fe (II), Hg and Ni. The difference between the resulting slopes was evaluated. Peak area was taken as the analytical signal as it reflexes the amount of hydride in the atomiser. A peak area decrease denotes a loss of efficiency in the process.

For As(III), Cu(II), Fe(II), Fe(III), Ni(II) and NO₃⁻, 30 µg L⁻¹ Se solutions were added by increments of interferent and analysed both by SI-HG-AAS and the Reference Method so as to compare if there was difference between both technique's response. Some interferent showed clear selenium signal decay at increasing interferent concentrations; peak height was considered at this time and the % Response plotted against the concentration of the interferent. % Response was calculated as follows:

$$\% \text{ Response} = \frac{S_{\text{with interferent}}}{S_{\text{without interferent}}} \times 100$$

*S*_{with interferent} is selenium peak height in the solution with interferent added and *S*_{without interferent} is selenium peak height in a solution of the same concentration of selenium but without interferent added.

2.2.6.5 Results and discussion

2.2.6.5.1 Arsenic

A calibration plot was drawn up to $30 \mu\text{g L}^{-1}$, and the same was constructed with $150 \mu\text{g L}^{-1}$ As and $50 \mu\text{g L}^{-1}$ As.

c As ($\mu\text{g L}^{-1}$)	0	50	150
Slope of Se calibration function ($\text{s L } \mu\text{g}^{-1}$)	0,0060	0,0064	0,0064

Table 10: Slopes of the calibration function of Se at different arsenic levels.

Upon results found (Table 10), the differences in the slope are less than 5 %, so it can be considered that As does not interfere on selenium determination by SI-HG-AAS up to $150 \mu\text{g L}^{-1}$ As.

When increasing the amount of arsenic for a given concentration of selenium, selenium signal decay could be observed for both methodologies. Results can be seen in Figure 21:

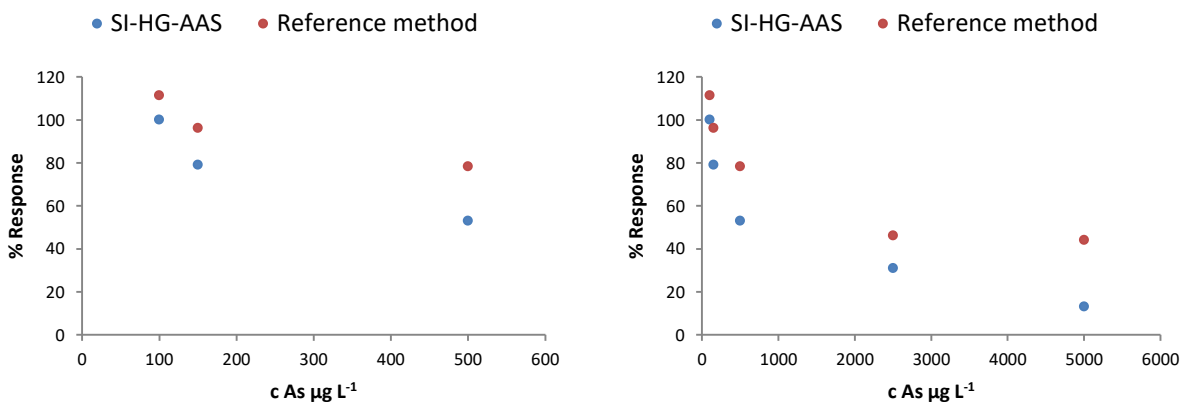


Figure 21: Variation in Se signal at increasing As concentration by SI-HG-AAS and the Reference Method. Left: From 100 to $500 \mu\text{g L}^{-1}$ As added; Right: From 100 to $5000 \mu\text{g L}^{-1}$ As added.

As (III) in the reaction media generates volatile hydrides which are transported and atomised altogether with dihydrogenselenide; they can interact in the gaseous phase. At low arsenic concentration, peak height decreased but peak area was not influenced for the SI-HG-AAS system. This probably evidenced transport interference, being the peak delayed in its appearance but the amount of hydride reaching the atomiser remaining unaltered.

When arsenic concentration exceeded $500 \mu\text{g L}^{-1}$, both methodologies were interfered, the SI-HG-AAS in a higher extent than the Reference Method. The faster decay could be explained by the lower availability of hydrogen radicals in the atomiser for the SI-HG-AAS system: hydrogen radicals come from the reaction in the quartz cell of the hydrogen released by the tetrahydroborate decomposition and the oxygen present in the system. As the same solution is measured by both methods, the analyte/interferent rate is the same for both methods. Sodium tetrahydroborate concentration and volume is lower thus, as the same atomisation cell is used for both determination, hydrogen radical population is decreased. Even if the amount of hydrides reaching the cell is less also (shorter sample volume), it is possible that arsine demand of radicals in the working conditions, prevent the complete atomisation of dihydrogenselenide. This can be a possible explanation of the behaviour but the experiment carried out cannot confirm it (Dedina & Tsalev, Hydride Generation Atomic Absorption Spectrometry, 1995) (Welz & Sperling, 1999) (Dedina J. , 2007).

2.2.6.5.2 Cobalt, mercury and zinc.

Calibration curves of selenium were added by 2 and 10 mg L^{-1} Co and 10 mg L^{-1} Zn with no difference between each slope and the slope of the interferent-free selenium calibration plot. Mercury was tried at 1 and $3 \mu\text{g L}^{-1}$ with the same results.

2.2.6.5.3 Copper (II), iron (II), iron (III), and nickel (II).

c Cu (mg L^{-1})	0	2	10
Slope of Se calibration function (s L mg^{-1})	0,0049	0,0030	0,0028

Table 11: Slopes of the calibration function of Se at different copper levels.

As can be seen in Table 11 copper reduces selenium signal almost in a 50%. The mechanism reported for the interference of copper in dihydrogenselenide generation is hydride – ion type: once formed the hydride, reacts with the interference in its ionic species forming insoluble copper selenide (Dedina & Tsalev, Hydride Generation Atomic Absorption Spectrometry, 1995). Even though, no precipitate was appreciated.

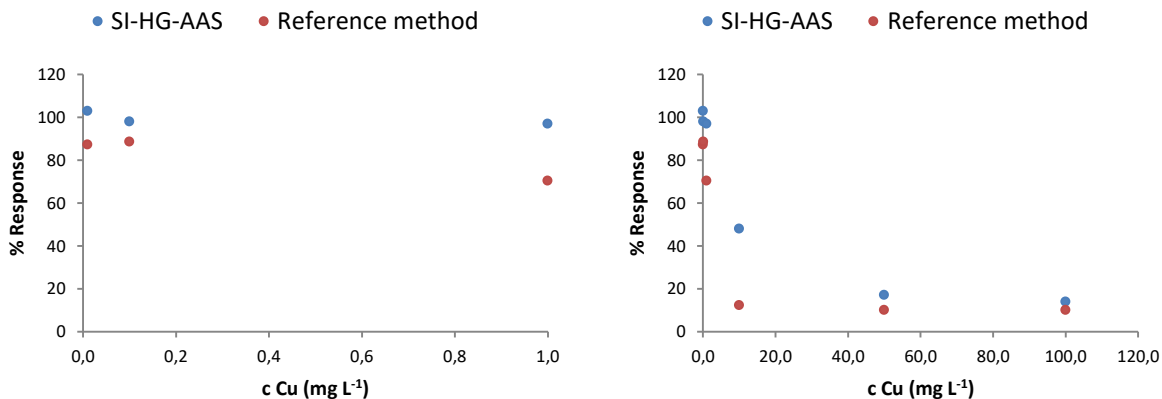


Figure 22: Variation in Se signal at increasing Cu concentration by SI-HG-AAS and the Reference Method. Left: From 0,1 to 1,0 $\mu\text{g L}^{-1}$ Cu added; Right: From 0,1 to 100 $\mu\text{g L}^{-1}$ Cu added.

Figure 22 shows that for copper concentrations up to 1 mg L^{-1} the SI-HG-AAS system does not evidence an interaction between dihydrogenselenide and copper, as recoveries are close to 100%. The batch Reference Method behaves as well up to 0,1 mg L^{-1} Cu; with the proposed method there is a tenfold increase in the tolerable copper concentration at those levels. Up to 50 mg L^{-1} Cu, the SI-HG-AAS presents more tolerance to the interference, probably due to the increased acidity of the media or perhaps due to kinetical discrimination of the flow system (Dedina & Tsalev, Hydride Generation Atomic Absorption Spectrometry, 1995) (Welz & Sperling, 1999).

In the case of iron (II), the slope of the calibration curve of Se was decreased almost a 50% for a 200 mg L^{-1} Fe(II) concentration (Table 12). A 1000 mg L^{-1} Fe selenium curve was also constructed but signal almost disappeared.

c Fe(II) (mg L^{-1})	0	200	1000
Slope of Se calibration function ($\text{s L } \mu\text{g}^{-1}$)	0,0049	0,0028	-----

Table 12: Slopes of the calibration function of Se at different iron (II) levels.

Nevertheless, the SI-HG-AAS showed to be influenced by Fe(II) at higher concentrations than the Reference Method (Figure 23).

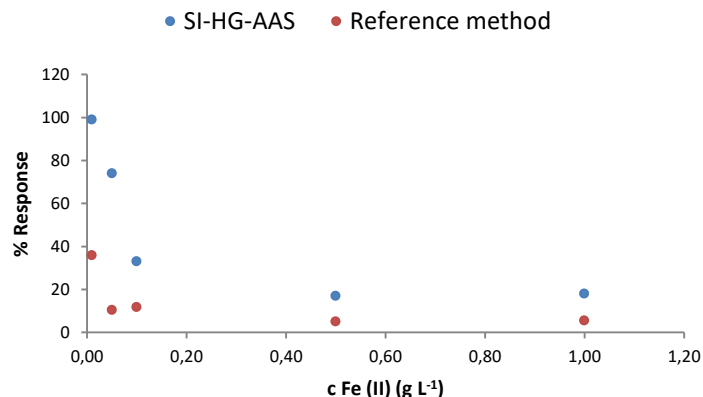


Figure 23: Variation in Se signal at increasing Fe (II) concentration by Si-HG-AAS and the Reference Method.

Up to 10 mg L⁻¹, selenium signal in the SI-HG-AAS system remained unaltered while the Reference Method suffered a significant decay. The possible interference is a hydride – product interference, in which the hydride generated, is absorbed by the solid concomitantly formed by reduction to the elemental species of the interferent caused by the tetrahydrobrat.

Figure 24 shows that both methods have the same behaviour for the determination of selenium in the presence of Fe(III); up to around 3 – 5 g L⁻¹, Fe(III) does not influence selenium response in none. For the sake of simplifying the visualisation of the wide range of concentrations tried, % Response was plotted against logarithm of the concentration.

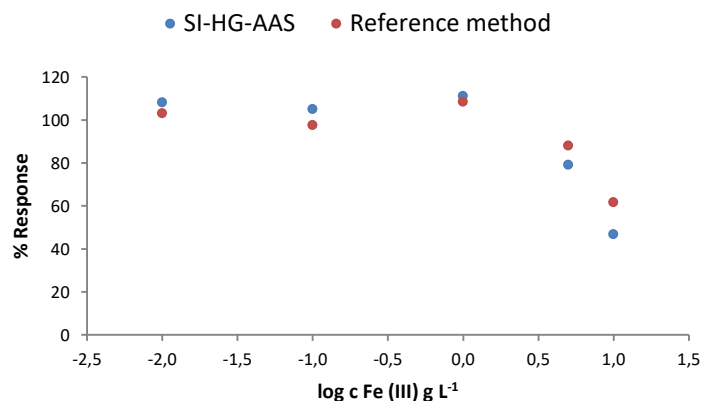


Figure 24: Variation in Se signal at increasing Fe (III) concentration by Si-HG-AAS and the Reference Method.

Nickel showed no effect on the slope of the calibration plot of selenium when added at 2 and 10 mg L⁻¹ Ni. As it is described as a relevant interferent of hydride generation, Ni-spiked solutions were analysed

by both methods. Results are presented in Figure 25; SI-HG-AAS method allows selenium determination in the presence of nickel at least up to 1000 mg L⁻¹ (recoveries are between 90 – 110 %). However, at 10 mg L⁻¹ Ni, the Reference Method decays 30 %, and selenium signal is completely depleted at 1000 mg L⁻¹.

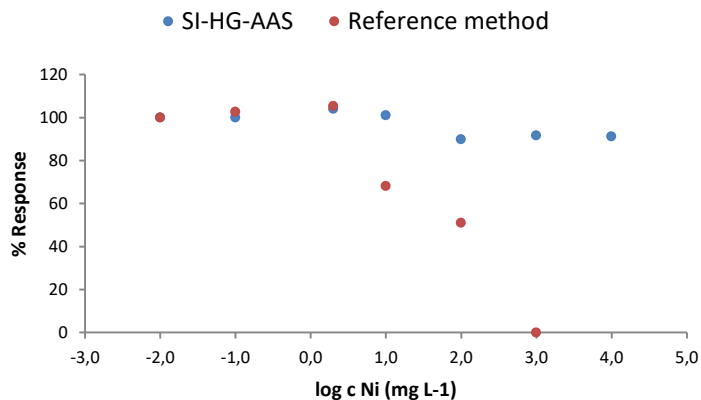


Figure 25: Variation in Se signal at increasing Ni concentration by Si-HG-AAS and the Reference Method.

Ni expected interaction is of the type hydride – product interference; probably both the increased acid and reduced tetrahydroborate concentration prevented the formation of the fine dispersed elemental Ni that would absorb and decompose the hydride. A kinetic discrimination in the SI-HG-AAS method may also take place and the hydride evolved before nickel reduction.

2.2.6.5.4 Nitrate

Nitrite (nitrate reduction product) rather than nitrate turns dihydrogenselenide into elemental selenium in what could be considered a hydride – ion interference (considering nitrite as the species remaining after a nitric digestion of the sample) or a hydride – product interference if media conditions allow tetrahydroborate reaction with nitrate. Notwithstanding the foregoing, the interaction leads to the formation of selenium species that is not able to generate the hydride, thus the final process is a compound interference.

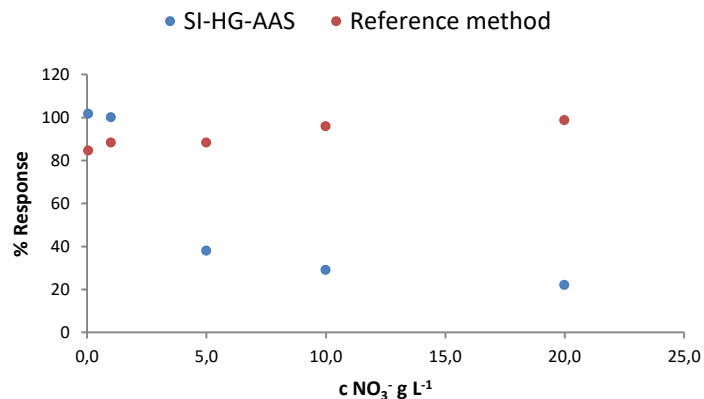


Figure 26: Variation in Se signal at increasing NO₃⁻ concentration by SI-HG-AAS and the Reference Method.

Figure 26 shows that, while selenium response using the Reference Method is not affected by nitrate at any concentration tried, there is a sharp signal decline for nitrate concentration higher than 1 g L⁻¹ in the SI-HG-AAS method. In terms of nitrate coming from an acid digestion, the media should be around 0,15 % v/v HNO₃ to behave as interference free, too low for sample treatment purposes.

A possible explanation of the chemistry operating the SI-HG-AAS system is that nitrate gets reduced with hydrochloric acid at high concentration, when sample is heated for Se(VI) reduction. As solution is confined within the reaction coil, there is no chance of the intermediates products of nitrate reduction to be removed from solution, thus, nitrate reduction intermediates are present when the hydride is generated and the interaction takes place decomposing the volatile species.

The reduction step of Se(VI) in the Reference Method takes place in open vessels at lower hydrochloric acid concentration during a longer time. Thus, nitric intermediates, if formed, can be drawn out of the solution before the hydride generation.

2.2.6.6 Conclusions

The interference study revealed no incidence in selenium signal when cobalt and zinc are present in a concentration up to 10 mg L⁻¹ and mercury up to 3 µg L⁻¹.

When nitrate is present, SI-HG-AAS method behaved worse than the Reference Method as even at low concentration of nitrate selenium signal was completely abated. The problem probably arose in the step of the on-line Se(VI) reduction. As the Reference Method was not affected it could be an alternative for those samples presenting up to 20 g L⁻¹ NO₃⁻, to make the reduction stage off line, or evaluate the addition of a reductant before the on-line reduction so as to eliminate nitrate at the time Se(VI) is reduced as well.

In the case of the presence of arsenic and ferric ions, differences between the results found by both methodologies were not of concern; both were interfered almost in the same extent for the same concentration of interferent.

Copper, ferrous and nickel ions showed an interference free range extension in comparison with the Reference Method.

2.2.7 General conclusions for the SI-HG-AAS method

Both the SI-HG-AAS and the Reference Method were found to behave similarly. From the point of view of the levels of selenium that could be attained, the limits of detection and quantification have no difference and thus, the scope of sample concentration is the same for both.

Nitrate is a concomitant of concern that needs to be previously eliminated when using the SI-HG-AAS method but it can operate in an extended interference-free concentration range in the presence of copper, ferrous and nickel ions.

The actual reason for selecting the SI-HG-AAS method instead of the Reference Method is the reduced sample and reagent amount that can be used: sample consumption can be reduced a tenfold and sodium tetrahydroborate at least 30 times (considering 2,0 mL approximately of 3,0 % NaBH₄ per determination in the Reference Method). One third of the amount of waste are generated which pH is not as low as the generated using the Reference Method.

Furthermore, while the Reference Method spends 40 minutes for sample reduction and has a performance of 25 samples per hour, the SI-HG-AAS method can analyse 45 samples per hour including the reduction step.

For the aforementioned the SI-HG-AAS method can be considered a promising alternative for selenium determination in water samples.

Chapter II

Selenium determination by SI – HG – AAS

Scientific production

This section presents the diffusion of the results.

ESTUDIO COMPARATIVO PARA LA DETERMINACIÓN DE SELENIO POR HG-AAS (BATCH) Y SIA-HG-AAS

Delmonte, D.; Mollo, A.; Knochen, M.

Universidad de la República - Facultad de Química

Av. Gral. Flores 2124 - 11800 Montevideo – Uruguay – Tel. 9241808

amolloy@fq.edu.uy

El selenio se encuentra en el grupo de los metaloides. Es esencial para la salud de los humanos en cantidades traza; tiene un rango muy estrecho entre la deficiencia dietaria (menor de 40 µg diarios) y los niveles tóxicos (mayor de 400 µg diarios).

En la Unidad de Análisis de Agua (UAA) de la Facultad de Química (UdelaR) se determina selenio en agua potable como análisis de rutina por espectrometría de absorción atómica con generación de hidruros (método *batch*).

A fin de aumentar la productividad analítica se propone como método alternativo la generación del hidruro a través de un sistema de análisis por inyección secuencial (SIA) de modo de realizar un ensayo más rápido de confiabilidad comparable.

Se usó un espectrómetro AA Perkin Elmer 5000 con llama aire acetileno y lámpara Photron Superlamp®. Se empleó un sistema *batch* PerkinElmer MHS-15. El sistema SIA se construyó empleando una bomba de jeringa (Cavro XP-3000) y una válvula selectora de 10 puertos (Valco). La adquisición de datos y el control del sistema se hicieron desde un PC mediante un programa escrito en Visual BASIC.

Los resultados obtenidos para ambos métodos se indican en la tabla:

Cifras de mérito	Método batch	Método SIA
Linealidad	1.02 a 15.0 µgL ⁻¹	0.82 a 20.0 µgL ⁻¹
Límite de detección	0.31 µgL ⁻¹ (3s, n=5)	0.25 µgL ⁻¹ (3s, n=10)
Límite de cuantificación	1.02 µgL ⁻¹ (10s, n=5)	0.82 µgL ⁻¹ (10s, n=10)
Precisión de repetibilidad s _r (%)= (s/m)*100 s: desviación estándar m: promedio de las réplicas	8 (3 µgL ⁻¹ , n=3)	2 (5 µgL ⁻¹ , n=10)
	5 (6 µgL ⁻¹ , n=3)	4 (10 µgL ⁻¹ , n=10)
	2 (11 µgL ⁻¹ , n=3)	4 (20 µgL ⁻¹ , n=10)
Recuperación (%)	108 (8 µgL ⁻¹)	100 (5 µgL ⁻¹)
	103 (11 µgL ⁻¹)	104 (20 µgL ⁻¹)
Frecuencia muestreo	25 muestras/hora	60 muestras/hora
Consumo NaBH ₄ (mg/muestra)	1.7	150

Se concluye que el sistema SIA es más rápido y económico que el *batch* y comparable en precisión y exactitud.

Alicia Mollo, Diego Delmonte, Moisés Knochen

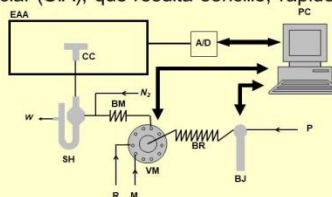
UdelaR, Facultad de Química, DEC. Av. Gral. Flores 2124, 11800 Montevideo, Uruguay
amollo@fq.edu.uy

INTRODUCCIÓN

El selenio es un micronutriente esencial para la salud humana. La cantidad ingerida es crítica ya que presenta toxicidad a niveles ligeramente superiores a los requeridos por el organismo.

La determinación de selenio en muestras de agua se realiza frecuentemente por espectrometría de absorción atómica con generación de hidruros (HG-AAS). Se presenta una nueva metodología para la generación del hidruro por un método automatizado de análisis por inyección secuencial (SIA), que resulta sencillo, rápido y con resultados comparables a los del método oficial.

BJ: Bomba de jeringa Cavro XP-3000 (5 mL)
VM: Válvula multiposición motorizada Valco modelo EMHMA-CE
BR: Bobina de retención en FEP de 0.8 mm (DI) y 2.0 m de largo
BM: Bobina de mezclador en FEP de 0.8 mm (DI) y 0.2 m de largo
P: agua destilada (portador)
R: NaBH₄ 0.2 % (m/v) en hidróxido de sodio 0.05 % (m/v)
M: muestras y disoluciones patrón en HCl (2:1) calentadas durante 1 h a ebullición suave y saturadas con NaCl
SH: separador de fases hidrostático
N₂: nitrógeno 0.76 L min⁻¹ (gas portador)
CC: celda de cuarzo
EAA: espectrómetro de absorción atómica de llama Perkin Elmer 5000
A/D: interfase analógico/digital de 14 bits
PC: sistema de control y de adquisición de datos compilado en Visual Basic 6.0
W: descarte



CIFRAS DE MÉRITO

Linealidad (n = 8)	0.82 a 20.0 µg L ⁻¹
Límite de detección (3s, n = 10)	0.25 µg L ⁻¹
Límite de cuantificación (10s, n = 10)	0.82 µg L ⁻¹
Precisión de repetibilidad Sr (%) = (s/m) * 100 s = desviación estándar m = promedio de réplicas	2.1 (5µg L ⁻¹ , n = 10)
	3.6 (10µg L ⁻¹ , n = 10)
	4.5 (20µg L ⁻¹ , n = 10)



DISCUSIÓN DE LOS RESULTADOS

Durante la etapa de optimización del método los parámetros ensayados fueron: largo de reactor, tamaño de muestra y concentración del reductor. Se comprobó también que se favorecía la liberación del hidruro saturando las soluciones de estándares y muestras con cloruro de sodio. Una vez halladas las condiciones óptimas de trabajo se validó la metodología. Los parámetros de validación seleccionados fueron: límites de detección y cuantificación, linealidad, precisión y exactitud. Dado que el método se aplica para el análisis de muestras de agua, la linealidad se estudió hasta 20 µg L⁻¹. Los límites se estimaron empleando una solución de selenio de baja concentración (2.5 µg L⁻¹). Para la precisión de repetibilidad se emplearon muestras libres de selenio fortificadas a tres niveles de concentración. Para la exactitud se emplearon veinte muestras de distintos puntos del país libres de selenio y fortificadas en el rango de 10 a 40 µg L⁻¹. Se evaluaron comparando con el método APHA mediante pruebas estadísticas, sin encontrarse evidencia significativa de que los resultados provistos por el método propuesto difieran a los encontrados por el método oficial.

Evaluación del impacto ambiental del método SIA-HG-AAS respecto al método oficial (HG-AAS)		
Los valores presentados corresponden a consumos de muestra y reactivos, y residuos generados por determinación	HG-AAS	SIA-HG-AAS
Volumen de muestra	10 mL	250 µL
Consumo de NaBH ₄	150	1.7
Volumen de descarte	15 mL	3.8 mL
Acidez del descarte	pH = 0	pH = 1
Manipulación de muestras	mayor	menor
Frecuencia de muestreo (determinaciones / hora)	25	60

CONCLUSIÓN

El método SIA-HG-AAS desarrollado aumenta notoriamente la eficiencia de las determinaciones, minimiza el consumo de muestras y reactivos, y el volumen de residuos generados, armonizando así con las nuevas tendencias al desarrollo de metodologías que disminuyan el impacto ambiental.

AGRADECIMIENTOS

Programa de Desarrollo de las Ciencias Básicas (PEDECIBA Química), Comisión Sectorial de Investigación Científica (UdelaR-CSIC), Prof. Isabel Dol



UNIVERSIDAD
DE LA REPUBLICA
URUGUAY

DETERMINACIÓN DE SELENIO TOTAL EN AGUA MEDIANTE ANÁLISIS POR INYECCIÓN SECUENCIAL (SIA) Y DETECCIÓN POR HG-AAS

Alicia Mollo*(PG), Mariela Pistón (PG), Moisés Knochen (PQ)

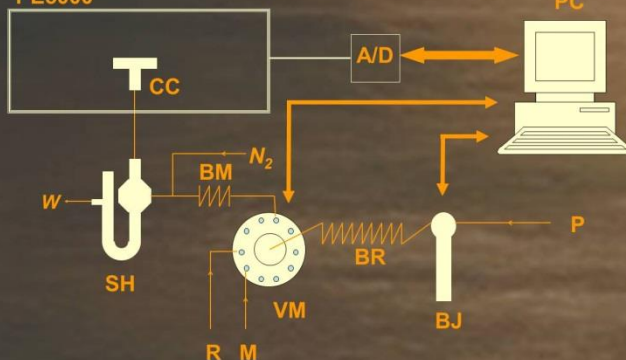
Universidad de la República (UdelaR), Facultad de Química. Av. Gral Flores 2124 Montevideo – Uruguay
amolloy@fq.edu.uy

INTRODUCCIÓN

Frecuentemente la determinación de selenio en muestras de agua se realiza empleando la técnica de espectrometría de absorción atómica con generación de hidruros (HG-AAS). Se propone un método automatizado de análisis de inyección secuencial (SIA) basado también en la generación de hidruros pero que agiliza el análisis, requiere menos muestra y genera menos volumen de residuos.

MATERIALES

PE5000



BJ: Bomba de jeringa Cavro XP-3000 (5 mL)

VM: Válvula multiposición motorizada Valco modelo EMHMA-CE

BR: Bobina de retención en FEP de 0.8 mm (DI) y 2.0 m de largo

BM: Bobina de mezclado en FEP de 0.8 mm (DI) y 0.2 m de largo

P: agua destilada (portador)

R: NaBH_4 0.2 % (m/v) en hidróxido de sodio 0.05 % (m/v)

M: muestras y disoluciones patrón en HCl (2:1) calentadas durante 1 h a ebullición suave y saturadas con NaCl

SH: separador de fases hidrostático

N_2 : nitrógeno 0

PE5000: espectrómetro de absorción atómica de llama Perkin Elmer 5000

A/D: interfase analógico/digital de 14 bits

PC: sistema de control y de adquisición de datos compilado en Visual Basic 6.0

W: descarte RESULTADOS

Linealidad (n = 8)	0.82 a 20 $\mu\text{g L}^{-1}$
Límite de detección (3s, n=10)	0.25 $\mu\text{g L}^{-1}$
Límite de cuantificación (10s, n=10)	0.82 $\mu\text{g L}^{-1}$
PRECISIÓN (S_r, n=10)	
Nivel 1: 5 $\mu\text{g L}^{-1}$	2 %
Nivel 2: 10 $\mu\text{g L}^{-1}$	4 %
Nivel 3: 20 $\mu\text{g L}^{-1}$	4 %
RECUPERACIÓN (% , n=10)	
Nivel 1: 5 $\mu\text{g L}^{-1}$	100
Nivel 2: 10 $\mu\text{g L}^{-1}$	90
Nivel 3: 20 $\mu\text{g L}^{-1}$	104
Frecuencia de muestreo	60 hora ⁻¹

VALORACIÓN DEL IMPACTO AMBIENTAL (1)

NaBH_4	1.7 mg
muestra	250 μL
Volumen del descarte	3.75 mL
Acidez del descarte	pH = 1



(1) Los valores presentados corresponden a consumos de muestra y reactivos y residuos generados por determinación

CONCLUSIONES

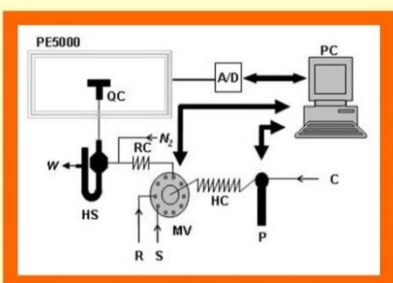
El método SIA aumenta la eficiencia de las determinaciones y minimiza el consumo de muestras y reactivos. Los residuos generados además de ser de poco volumen tienen una concentración hidrogeniónica definida que facilita la neutralización a diferencia de los residuos habituales de generación de hidruros cuyo pH es cero. Por ser un método automatizado disminuye la exposición del operador. Las cifras de mérito que logra son adecuadas para el límite de 10 $\mu\text{g L}^{-1}$ que establece la norma local vigente para el análisis de muestras de agua.

Por lo tanto el método SIA-HG-AAS desarrollado es una alternativa rápida, precisa, eficiente y segura para la determinación de selenio en muestras de agua que brinda su aporte en el cuidado del medio ambiente.

AGRADECIMIENTOS

Comisión Sectorial de Investigación Científica (UdelaR-CSIC) y Programa de Desarrollo de las Ciencias Básicas (PEDECIBA-QUÍMICA) por el financiamiento específico

The interference of other hydride forming elements and transition metals in the determination of selenium by HG-AAS has been largely studied and its mechanism is well known. Nevertheless, when a new method of hydride generation is developed, it is imperative to make an exhaustive analysis of the conditions where the method can be applied without significant interference or the extent of it when it becomes significant.



An investigation was carried out using an experimental design to evaluate the effect of several potential interferents. The method studied involves hydride generation by sequential injection analysis (HG-SIA) where the selenium hydride is formed by the addition of NaBH₄ in NaOH solution, separated in a hydrostatic glass separator with a nitrogen flow and determined by AAS at 196.0 nm in an externally heated quartz cell.

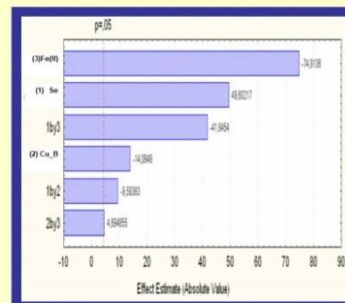
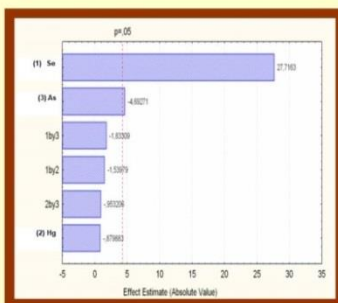
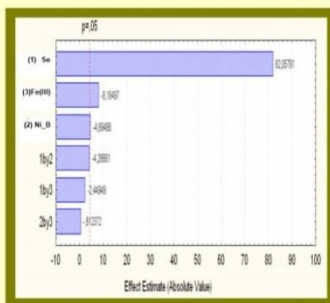
A two level factorial design was carried out for three factors at a time. Every experiment had selenium concentration as a factor, the other two were, As and Hg, Cu and Fe (II), Ni and Fe (III), and Co and Ni. The experimental design evaluated the effect of the individual factor and their interaction in the magnitude of selenium signal (absorbance).

MV: multiposition valve; P: syringe pump; HC: holding coil; RC: reaction coil; PE5000: Perkin Elmer 5000; A/D: analogue/digital interface; HS: hydrostatic separator; N₂: nitrogen stream; QC: quartz cell; S: samples or standard solutions; R: sodium tetrahydroborate; W: waste

EXPERIENCE	Se	NI	Fe (III)
1	+	+	+
2	+	+	-
3	+	-	+
4	+	-	-
5	-	+	+
6	-	+	-
7	-	-	+
8	-	-	-
central point	0	0	0
central point	0	0	0
central point	0	0	0
Concentration (mg L ⁻¹)	+	central point	-
Se	0.030	0.020	0.010
Ni	2	6	10
Fe (III)	50	100	150

EXPERIENCE	Se	Hg	As
1	+	+	+
2	+	+	-
3	+	-	+
4	+	-	-
5	-	+	+
6	-	+	-
7	-	-	+
8	-	-	-
central point	0	0	0
central point	0	0	0
central point	0	0	0
Concentration (µg L ⁻¹)	+	central point	-
Se	30	20	10
Hg	3	2	1
As	150	100	50

EXPERIENCE	Se	Cu	Fe (II)
1	+	+	+
2	+	+	-
3	+	-	+
4	+	-	-
5	-	+	+
6	-	+	-
7	-	-	+
8	-	-	-
central point	0	0	0
central point	0	0	0
central point	0	0	0
Concentration (mg L ⁻¹)	+	central point	-
Se	0.030	0.020	0.010
Cu	2	6	10
Fe (II)	200	600	1000



The experience with Co and Ni is not showed but there was no influence on selenium signal up to a concentration of the interferents of 10 mg L⁻¹. At the chosen levels, no influence of mercury, cobalt or nickel was evidenced and an interference of Fe(II), Cu, As and Fe(III) was found.

ACKNOWLEDGEMENTS: UdelaR-CSIC (Universidad de la República – Comisión Sectorial de Investigación Científica), PEDECIBA (Programa de Desarrollo de Ciencias Básicas), and Isabel Dol.

Sequential Injection Analysis in Selenium Determination by HG-AAS: Optimisation and Interference Study

Alicia Mollo*¹, Sergio Luis Costa Ferreira² and Moisés Knochen*¹

¹*Cátedra de Química Analítica, Universidad de la República (UdelAR), Facultad de Química, Av. Gral. Flores 2124, 11800 Montevideo, Uruguay*

²*Grupo de Pesquisa em Química e Quimiometria, Universidade Federal da Bahia, Campus Ondina, Instituto de Química, CEP: 41.195.001 Salvador, Bahia, Brazil*

Abstract: A sequential-injection hydride-generation atomic absorption spectrometry (SIA-HG-AAS) system for the determination of trace levels of selenium was designed and characterised. The system included on-line pre-reduction from Se(VI) to Se(IV) and used NaBH₄ as reagent for the generation of the hydride. The operation of the system was optimised regarding the main operating variables by means of appropriate experimental designs. The analytical response was linear in the range 2.0 - 20 µg L⁻¹ ($A_{\text{max}} = 0.0048 C$, with $C = \text{concentration in } \mu\text{g L}^{-1}$, $r^2 = 0.9973$). Detection (3 s) and quantification (10 s) limits were 0.6 and 2.0 µg L⁻¹ respectively with precision (repeatability, $s_r(\%)$, $n = 10$) from 2.2% to 3.6% for concentrations between 5 and 20 µg L⁻¹. Sampling frequency was 60 hour⁻¹. An interference study was carried out comparing the performance of both the proposed system and an HG-AAS reference system involving batch generation of the hydride. As, Co, Cu, Fe(II), Fe(III), Hg, Ni, nitrate and Zn were chosen as potential interferents. Interference from As and nitrate was shown to be more severe in the proposed system than in the batch one. Co, Hg and Zn did not present any significant interference in either system. The presence of Fe(III) at the concentrations tried showed the same behaviour in the response for both systems. The range of concentrations of Cu, Fe(II) and Ni allowing an interference-free selenium determination was wider in the SIA-HG-AAS system than in the reference HG-AAS system.

Keywords: Hydride generation, interference analysis, multivariate factorial design, SIA.

INTRODUCTION

Selenium determination is often accomplished by hydride generation coupled with atomic absorption spectrometry (HG-AAS). Selenium hydride is released in acidic solution when the sample reacts with a chemical reductant, NaBH₄, being used almost exclusively for this purpose. In order to achieve the reaction, selenium must be in the Se(IV) oxidation state. A pre reduction step is then necessary. For this purpose, some reference methods propose the use of hydrochloric acid digestion heating in a water bath for at least 20 minutes [1-3].

Aiming at the various advantages of flow-based techniques, a number of research papers have been published showing different flow systems designed to carry out the generation of selenium hydride with detection by atomic absorption [4-6], atomic fluorescence [7, 8], and atomic emission [9] spectrometry. Some of these systems [4,9] include an online pre-reduction step. Atomic Fluorescence Spectrometry (AFS) is the preferred detection technique because of its extremely low detection limits. However, Atomic Absorption Spectrometry (AAS) is more widely

available and is thus preferable as long as detection and quantification limits obtained with a given method are fit for the purpose.

Atomic spectrometric techniques such as AAS and AFS benefit from hyphenation with flow techniques such as Flow Injection Analysis (FIA) [10]. In this way they become amenable to automation and the goals involved in the concept of Green Analytical Chemistry [11] can be accomplished and thus lower amounts of hazardous chemicals are employed and the volume of harmful wastes is decreased.

Sequential injection analysis (SIA) [12, 13] is a flow technique featuring low consumption of reagents and samples. However the use of this technique for the determination of selenium by hydride generation atomic spectrometry is not widely reflected in the literature [14, 15]. Since a number of interferences may arise during the hydride generation step, and they depend heavily on the technique used for sample and reagent introduction, further research is necessary in order to determine the main interferences occurring when SIA is hyphenated with hydride generation spectrometric techniques.

This work presents the development and optimisation of a system for the determination of total selenium based on sequential injection hydride-generation atomic absorption spectrometry (SIA-HG-AAS) attempting to low sample con-

*Address correspondence to these authors at the Cátedra de Química Analítica, Universidad de la República (UdelAR), Facultad de Química, Av. Gral. Flores 2124, 11800 Montevideo, Uruguay; Tel: +598 29241808; Fax +598 29241906; E-mail: amolloy@fq.edu.uy, miknochen@fq.edu.uy

Chapter II

Lead determination by Microwave Induced Plasma –Atomic Emission Spectrometry

This section describes the chemical generation of lead tetrahydride and its determination by microwave induced plasma atomic emission spectrometry.

2.3 Lead determination by microwave induced plasma emission atomic spectrometry

The study of lead was selected because among the frequent analytes of analytical interest it is one whose volatile derivative generating conditions raised controversy as additives presence are mandatory. For the determination microwave induced plasma atomic emission spectrometry was chosen as it remains still not very used for this analyte.

2.3.1 Introduction

The efficiency of the direct reaction between Pb(II) and NaBH₄ yielding lead tetrahydride (PbH₄) is very low (Dedina & Tsalev, Hydride Generation Atomic Absorption Spectrometry, 1995); its generation needs the presence of an additive, species with ligand/donor and/or redox properties which interact with the analyte and/or the tetrahydroborate producing and analytical useful reactivity modification.

There is a general consensus about the need of media modification in order lead tetrahydride is generated in an appreciable amount, but, there is no agreement about the role played of some of the additives used in this particular case.

Castillo et al. studied the recovery of lead on sample solution after the hydride generation in the presence of potassium dichromate, potassium permanganate, cerium (IV) sulphate, hydrogen peroxide and ammonium persulphate. Except for dichromate, all of them are thermodynamically able of oxidising Pb(II) to Pb(IV). Recoveries increase in the order they are presented, less than 5 % the three first, close to 40 % for H₂O₂ and reaching almost 100 % for (NH₄)₂S₂O₈. He found a linear relationship between the logarithm of the absorbance and the normal potential of the oxidant involved (Castillo, Mir, Martínez, Val, & Colón, 1985).

On the opposite, Nerin *et al.* used H₂O₂ as additive and found the production of lead tetrahydride was not limited to the valence state of lead as the oxidant needs to be present whichever ionic lead species is present; they concluded it facilitates the formation of lead tetrahydride by an intermediate with catalytic effect but not by the oxidation of Pb(II) (Nerin, Olavide, Cacho, & Garnica, 1989).

Potassium dichromate is not thermodynamically able to oxidise Pb(II) unless halides or organic acids (malic, lactic tartaric) are added, maybe stabilising Pb(IV) by complexation (producing a shift in the redox potentials) or modifying the structure of the ligand.

D'Ulivo *et al.* largely studied the role of hexacyanoferrate (III) in the generation of lead tetrahydride as is one of the most frequent additives used. Like dichromate, it is not thermodynamically able to oxidise Pb(II).

They postulated that hexacyanoferrate (III) formed a hydridoboron intermediate that reacts with Pb(II) enhancing the formation of lead tetrahydride. For that purpose they designed an experience in which

they alterned the order of mixing the reactivs (acidic lead solution (A), acidic hexacyanoferrate (III) (B) and basic tetrahydroborate (C)):

1. (A+B) + C
2. A + B + C
3. A + (B+C)

For experiences 1. and 2. they found the same results and a signal enhancement for experience 3., evidencing the formation of the hydridoboron intermediate which is not formed in the absence of hexacyanoferrate (III) (D'Ulivo , Onor, Spiniello, & Pitzalis, 2008) (D'Ulivo, The contribution of chemical vapor generation coupled with atomic or mass spectrometry to the comprehension of the chemistry of aqueous boranes, 2019).

Barnet reported in 1987 the first (to his knowledge) evidence of lead tetrahydride detection by MIP AES using helium plasma (Barnett, 1987) after hydride generation with sodium persulphate.

Matsumoto A. and Nakahara T. used nitrogen MIP AES for the detection of several hydride forming elements, lead among them in their work “High power nitrogen microwave induced plasma atomic emission spectrometry coupled with hydride generation technique for the determination of several elements”, but only the abstract was accessible. No other work coupling lead hydride generation with nitrogen microwave induced plasma atomic emission spectrometry was found in the literature consulted.

The nitrogen microwave induced plasma used runs with air reducing considerable the cost in comparison to inductively coupled plasma optical emission spectrometry (ICP-OES) that used argon instead. The plasma is created by excitation of nitrogen by a magnetic field. The combination of an axial magnetic field and a transverse electric one allow a good interaction of the plasma and the sample, as well as higher temperatures inside the plasma. It reaches temperatures around 5000 K depending on the nitrogen flow selected in the chamber and the position of the plasma viewed (Hammer, 2008) (Goncalves, McSweeney , & Donati, 2016).

2.3.2 Working conditions optimisation

2.3.2.1 Instrumentation

A nitrogen microwave induced plasma atomic emission spectrometer (Agilent 4210 MIP-OES) equipped with a standard torch was used. Nitrogen (99,5 %) was supplied by a nitrogen generator (Agilent 4107) coupled with an air compressor. Determinations were performed at 405,781 nm and 283,305 nm with automatic background correction. Viewing position was set at the recommended by the manufacturer.

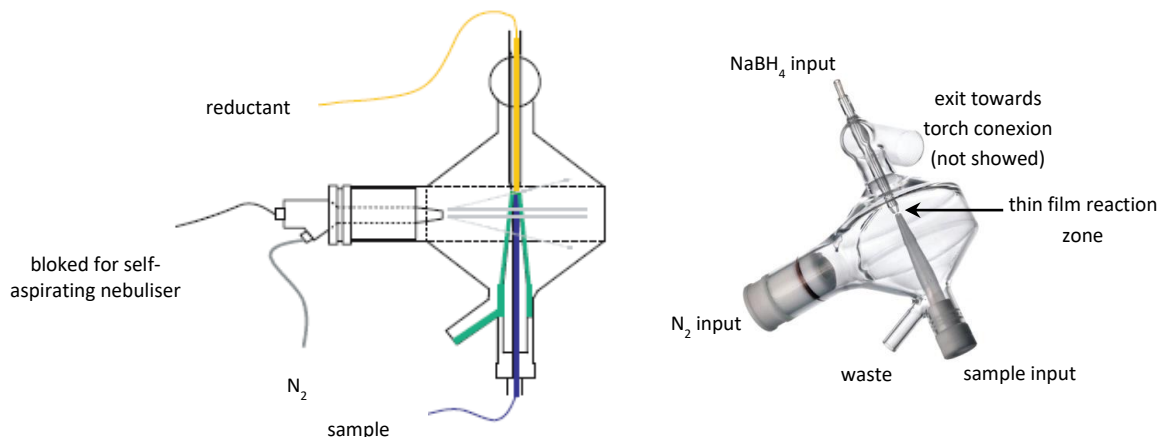


Figure 27: Scheme and photograph of the cyclonic spray chamber. Adapted from Anal Bional Chem (2007) 388:735-741 and https://www.agilent.com/cs/library/applications/5991-72828EN_MP-eBook.pdf respectively.

For the hydride generation the peristaltic pump fitted altogether with the spectrometer pushes sample and reductant towards a multimode spray chamber for hydride generation (MSIS, Agilent). The last consists in a glass cyclonic chamber (Figure 27) where sample and reductant flows converge between the vertically opposed conical tubes mixing in a thin film; hydrides once generated are stripped towards the plasma by a nitrogen flow. For preliminary studies the nitrogen flow in the nebuliser was the one recommended by the manufacturer.

2.3.2.2 Reagents and solutions

Diluted solutions were prepared with deionised water (ASTM type I) obtained from a Millipore (São Paulo, Brazil) Direct-Q 5 water purifier. Lead working solutions were prepared daily by dilution of their corresponding 1000 mg L⁻¹ atomic absorption standard solution.

Potassium dichromate, 100 vol hydrogen peroxide, cerium and ammonium nitrate, potassium hexacyanoferrate (III), 37 % w/w hydrochloric and lactic acid were of analytical reagent grade.

Sodium tetrahydroborate solution (2 % w/v in 1% w/v NaOH) was prepared from sodium tetrahydroborate (hydride generation grade, Fluka)

2.3.2.3 Procedure

100 $\mu\text{g L}^{-1}$ Pb solutions containing different commons additives for lead determination were prepared and measured against 0,4% - 1,5% - 3,4% w/v NaBH_4 in 1% w/v NaOH. For all samples with each reductant different pump speed were tried.

2.3.2.4 Results and discussions

Test solutions were 100 $\mu\text{g L}^{-1}$ Pb(II) and:

- i. 0,5 % w/v $\text{K}_2\text{Cr}_2\text{O}_7$ – 4% w/v lactic
- ii. 1 % v/v H_2O_2 – 4% v/v HCl
- iii. 10 % v/v H_2O_2 – 2% v/v HNO_3
- iv. 20 % v/v H_2O_2 – 2% v/v HNO_3
- v. 40 % v/v H_2O_2 – 2% v/v HNO_3
- vi. 10 % v/v H_2O_2 – 10% v/v HNO_3
- vii. 20 % v/v H_2O_2 – 10% v/v HNO_3
- viii. 20 % v/v H_2O_2 – 10% v/v HNO_3
- ix. 40 % v/v H_2O_2 – 10% v/v HNO_3
- x. 0,8% w/v $\text{Ce}(\text{NH}_4)_2(\text{NO}_3)_6$ – 4% v/v HCl
- xi. 0,5 % w/v $\text{K}_2\text{S}_2\text{O}_8$ – 4% v/v HCl
- xii. 1 % w/v $\text{K}_3\text{Fe}(\text{CN})_6$ – 0,1 mol L^{-1} HCl

The soles solutions giving signals were i. and xii. at both wavelength with higher signals for the 3,4% w/v NaBH_4 in 1% w/v NaOH solution.

As dichromate solutions have hazardous connotations, they were no longer tried and only hexacyanoferrate (III) was considered for further optimisation.

2.3.3 Working conditions optimisation using $\text{K}_3\text{Fe}(\text{CN})_6$ as additive for hydride generation

2.3.3.1 Instrumentation

Determinations were performed at 405,781 nm and 283,305 nm with automatic background correction. Viewing position, nitrogen flow in the chamber and pump speed (leading to the corresponding sample/reductant ratio) were optimised for each working solution.

2.3.3.2 Reagents and solutions

Solutions of $100 \mu\text{g L}^{-1}$ Pb containing 0,5 – 1,0 and 1,5 % w/v $\text{K}_3\text{Fe}(\text{CN})_6$ were prepared both in 0,12 and $1,0 \text{ mol L}^{-1}$.

Potassium hexacyanoferrate (III) and 37 % w/w HCl were of Analytical grade.

Sodium tetrahydroborate solutions 0,5 – 1,0 and 2,0 % w/v in 1% w/v NaOH were prepared from sodium tetrahydroborate (hydride generation grade, Fluka). Even if the preliminary studies 3,4 % gave the best results, it is too high the concentration for routine analysis; the reagent is very expensive and no longer imported to our country in that grade.

2.3.3.3 Procedure

Acid lead solutions containing hexacyanoferrate (III) were measured against tetrahydroborate solutions at different flow rates and different nitrogen flows. The viewing position and the stabilisation time (time elapsed since sample and reductant start to mix and the signal is read) were also varied for each measurement until finding the highest signals.

2.3.3.4 Results and discussion

Table 13 shows the different reagent concentrations tried for $100 \mu\text{g L}^{-1}$ Pb solutions; in bold appears the concentration giving the higher signals.

$\text{K}_3\text{Fe}(\text{CN})_6$	HCl	NaBH_4
0,5 % w/v	0,12 mol L ⁻¹	0,5 % w/v
		1,0 % w/v
		2,0 % w/v
	1,0 mol L ⁻¹	0,5 % w/v
		1,0 % w/v
		2,0 % w/v
1,0 % w/v	0,12 mol L ⁻¹	0,5 % w/v
		1,0 % w/v
		2,0 % w/v
	1,0 mol L ⁻¹	0,5 % w/v
		1,0 % w/v
		2,0 % w/v
1,5 % w/v	0,12 mol L⁻¹	0,5 % w/v
		1,0 % w/v
		2,0 % w/v
	1,0 mol L ⁻¹	0,5 % w/v
		1,0 % w/v
		2,0 % w/v

Table 13: 100 µg L⁻¹ Pb solutions at different additive and acid concentration evaluated for the different reductant concentrations.

Optimum working conditions are summarised in Table 14:

Instrumental parameters		
Pump speed:	30 rpm	
Nitrogen flow (L min ⁻¹)	0,5 at 283,305 nm – 0,75 at 405,781 nm	
Reading time	5 s	
Viewing position	0 at 283,305 nm – 0 at 405,781 nm	
Stabilisation time	20 s	
Working conditions		
K ₃ Fe(CN) ₆	HCl	NaBH ₄ ^(*)
1,5 % w/v	0,12 mol L ⁻¹	2,0 % w/v

Table 14: Instrumental parameters for lead determination at 283,305 nm and 405,781 nm. (*) dissolved in 1% w/v NaOH.

2.3.3.5 Conclusions

Once having determined the optimum conditions, application for samples analysis will be evaluated.

2.3.4 Evaluation of the incidence of acidity and nitrate in lead's response

Working solutions for lead determination usually come from a wet digestion, thus, it is expected they have nitric acid added. Envisaging the applicability of the methodology, the influence of nitric acid concentration in the response was evaluated. Six point calibration curve was prepared in 2 % v/v HNO₃ and compared towards one prepared in 0,12 mol L⁻¹ HCl.

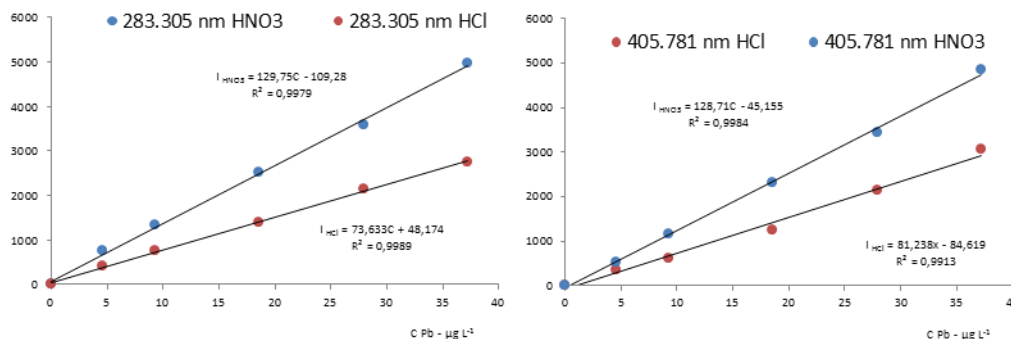


Figure 28: Comparison of lead response in hydrochloric and nitric acid at 283,305 nm and 405,781 nm by HG-MIP OES. I: emission signal; C: lead concentration in µg L⁻¹.

As can be seen in Figure 28, there is about a 76% at 283,305nm and about 58% at 405,781 nm of signal's increment when using HNO₃ instead of HCl; thus, in order to assess if signal enhancement is due to sample acidity and/or nitrate presence, both situations will be studied separately.

2.3.4.1 Evaluation of the incidence of the acidity of the medium in lead's response

Solutions with the same concentration of lead and increasing concentration of hydrochloric acid and 1,5% w/w K₃Fe(CN)₆ were prepared and measured at 283,305 nm and 405,781 nm.

The 50 µg kg⁻¹ Pb solutions were prepared by gravimetric dilution from the 1000 mg kg⁻¹ Pb atomic standard solution. In order to be able to compare the signals, as the concentration is within the linear range of the response, the signal given by an exactly 50 µg kg⁻¹ Pb solution was calculated from the measured signal (normalised signal for now on).

$$S_{normalised} = 50 \times \frac{S_{measured}}{C_{solution}}$$

$S_{normalised}$ is the calculated signal of a solution containing exactly 50 µg kg⁻¹ Pb; $S_{measured}$ is the signal of the prepared (and measured) solution and $C_{solution}$ is the real concentration of the measured solution (obtained by gravimetric dilution). The net signal of the 50 µg kg⁻¹ Pb – 0,12 mol L⁻¹ HCl – 1,5 % w/w K₃Fe(CN)₆ was taken as the reference, comparing towards it the signal of all the solutions of different acid concentration.

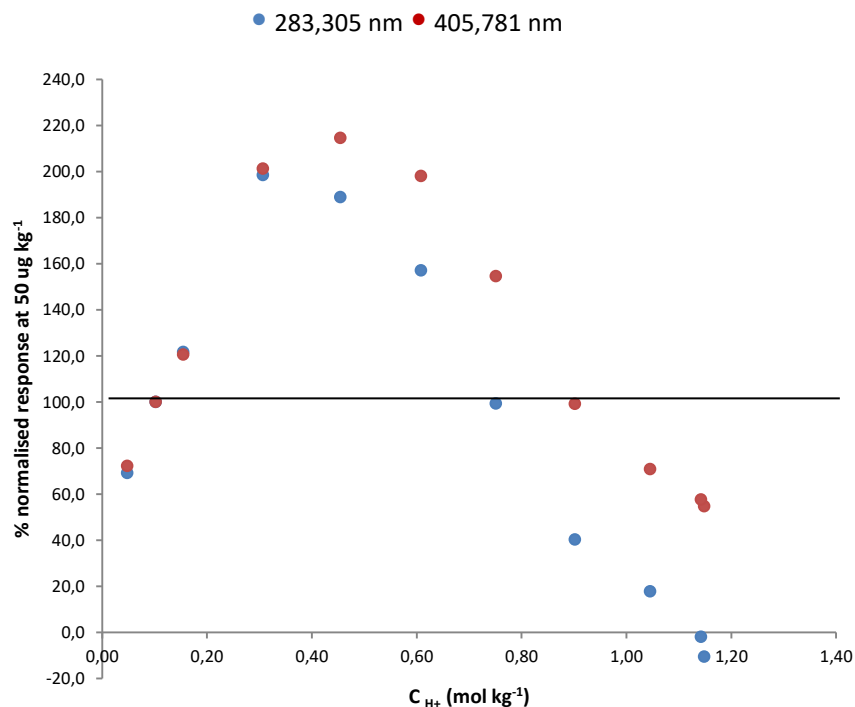


Figure 29: Variation of lead response for different hydrogen ion concentration.

Figure 29 show how the signal of lead varies upon the different hydrogen ion concentration of the media. As can be seen, signal increases reaching a maximum for 0,30 mol L⁻¹ H⁺ at 283,305 nm and 0,55 mol L⁻¹ H⁺ at 405,781 nm. From then on it decreases almost disappearing close to 1,20 mol L⁻¹ H⁺. Between 0,30 and 0,90 mol L⁻¹ H⁺ 405 nm line is more sensitive also.

Consequently, whenever aiming to determine Pb by HG – MIP OES samples should have a hydrogen ion concentration between 0,12 and 0,8 mol L⁻¹ H⁺, which, in terms of acids usually added to the samples is as saying between (1,0 – 6,7)% v/v HCl or (0,8 – 5,5)% v/v HNO₃. Signal variation is wide in a quite narrow range of concentration, thus calibration standards require also a careful pH control. Difference in hydrogen ion concentration between samples and calibration solution certainly ensure biased results. Probably, a neutralisation stage and a subsequent acidity adjustment is the best way to face the determination to minimise this risk.

2.3.4.2 Evaluation of the incidence of nitrate concentration in lead's response

50 µg kg⁻¹ Pb – 0,12 mol L⁻¹ HCl (1% w/w approx.) – 1,5 % w/w K₃Fe(CN)₆ solutions with increasing concentration of nitrate (added as KNO₃) were prepared and measured at 283,305 nm and 405,781 nm.

As previously mentioned, signals were normalised, and the net signal of $50 \mu\text{g kg}^{-1}$ Pb – 1% w/w HCl – 1,5 % w/w $\text{K}_3\text{Fe}(\text{CN})_6$ (without nitrate) solution was taken as the reference.

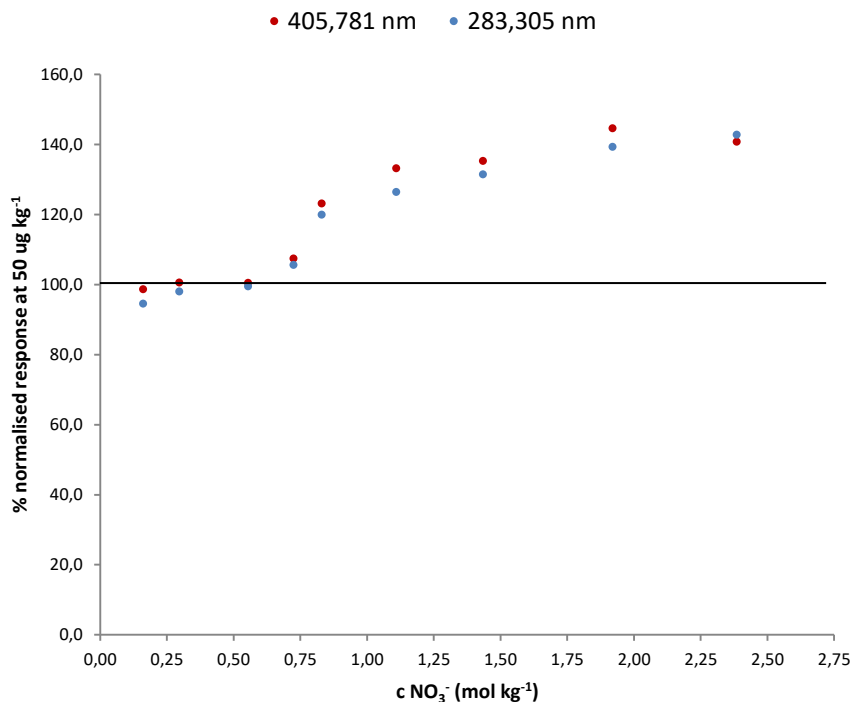


Figure 30: Variation of lead response for different nitrate concentration.

It can be seen in Figure 30 that nitrate enhances lead signal for nitrate concentration above about $0,6 \text{ mol kg}^{-1}$. Considering nitric acid used for the digestion of the sample as the source of nitrate ions, it corresponds to a concentration of 4,2 % v/v HNO_3 approximately in the measuring solution. Thus, for samples with higher nitrate concentration, besides the pH adjustment, an addition of nitrate is necessary in the calibration standards as well. Signal enhancement is quite constant in the upper range. Concentrations above the ones showed are limited by potassium nitrate's solubility. Nitrate amount adjustment is not as critical as the one of the hydrogen ion; ensuring a nitrate concentration within $1,5 - 2,5 \text{ mol kg}^{-1} \text{NO}_3^-$ is enough; if nitric acid is the main source of nitrates, 10,5 – 17,0 % v/v HNO_3 (calculations have been done considering 65 % w/w HNO_3 , $d = 1,39 \text{ g mL}^{-1}$).

2.3.4.3 Evaluation of the incidence of the reagent interaction in lead's response

As remarked previously in **2.3.1 Introduction**, it is expected an interaction between tetrahydroborate and hexacyanoferrate (III) which facilitates the generation of lead tetrahydride, thus, a signal enhancement would be expected when comparing to the situation where there is no previous contact between the reagents.

Up to now, all the additives, namely, HCl, $K_3Fe(CN)_6$, KNO_3 have been added altogether with Pb(II); reductant solution has been $NaBH_4$ dissolved in NaOH solution.

In this stage, additives will be transferred sequentially to the reductant solution in order to evaluate their potential effect in the response.

Different combinations in the mixing of sample, additives and reductant were achieved by changing the composition of the reductant and sample solution (Figure 31).

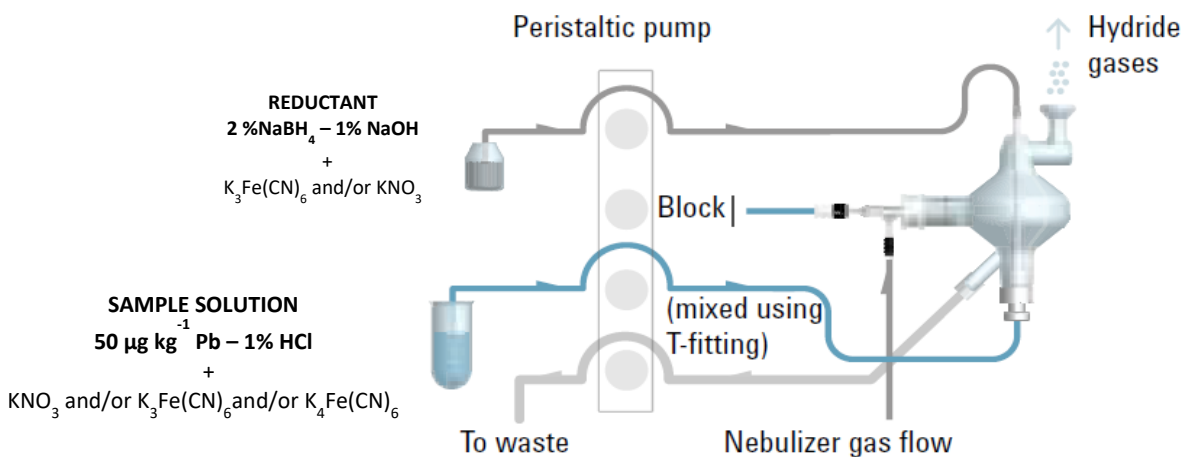


Figure 31: Combination of different reagents used for evaluating the interaction between them. Adapted from https://www.agilent.com/cs/library/applications/5991-72828EN_MP-eBook.pdf

Normalised net signal of $50 \mu g \text{ kg}^{-1} \text{ Pb} - 1\% \text{ w/w HCl} - 1,5\% \text{ w/w } K_3Fe(CN)_6$ solution measured against $2\% \text{ w/w } NaBH_4 - 1\% \text{ NaOH}$ was taken as the reference. After measuring each run, the normalised signal was calculated according to lead concentration in the sample solution and compared with that of the reference.

Results for each one at 283,305nm are presented in Table 15 and at 405,781 nm in Table 16.

REDUCTANT	SAMPLE SOLUTION (50 $\mu\text{g kg}^{-1}$ Pb)	% normalised response
1,5 % $\text{K}_3\text{Fe}(\text{CN})_6$ – 2 % NaBH_4	a) 1% w/w HCl	114
	b) 1% w/w HCl – 2 mol kg^{-1} NO_3^-	179
	c) 1% w/w HCl – 0,2% $\text{K}_4\text{Fe}(\text{CN})_6$	98
1,5 % $\text{K}_3\text{Fe}(\text{CN})_6$ – 2 % NaBH_4 – 2 mol kg^{-1} NO_3^-	d) 1% w/w HCl	95
	e) 1% w/w HCl – 0,2% $\text{K}_4\text{Fe}(\text{CN})_6$	83
2 % NaBH_4 – 2 mol kg^{-1} NO_3^-	f) 1% w/w HCl – 1,5% $\text{K}_3\text{Fe}(\text{CN})_6$	108
	g) 1% w/w HCl – 1,5% $\text{K}_3\text{Fe}(\text{CN})_6$ – 2 mol kg^{-1} NO_3^-	159

Table 15: Influence of reagent interaction in lead's response at 283,305 nm

Reductant reagent composition	Measured solution (50 $\mu\text{g kg}^{-1}$ Pb)	% normalised response
1,5 % $\text{K}_3\text{Fe}(\text{CN})_6$ – 2 % NaBH_4	a) 1% w/w HCl	109
	b) 1% w/w HCl – 2 mol kg^{-1} NO_3^-	147
	c) 1% w/w HCl – 0,2% $\text{K}_4\text{Fe}(\text{CN})_6$	102
1,5 % $\text{K}_3\text{Fe}(\text{CN})_6$ – 2 % NaBH_4 – 2 mol kg^{-1} NO_3^-	d) 1% w/w HCl	93
	e) 1% w/w HCl – 0,2% $\text{K}_4\text{Fe}(\text{CN})_6$	85
2 % NaBH_4 – 2 mol kg^{-1} NO_3^-	f) 1% w/w HCl – 1,5% $\text{K}_3\text{Fe}(\text{CN})_6$	98
	g) 1% w/w HCl – 1,5% $\text{K}_3\text{Fe}(\text{CN})_6$ – 2 mol kg^{-1} NO_3^-	130

Table 16: Influence of reagent interaction in lead's response at 405,781 nm

The results obtained show no evidence of signal improvement by the addition of $\text{K}_3\text{Fe}(\text{CN})_6$ to the reductant instead of to the lead's solution (experience a). Neither was with the addition of $\text{K}_4\text{Fe}(\text{CN})_6$ (experience c).

An interesting remark is that nitrate only causes enhancement when it is added to lead's solution (experiences b and g), but not when added to the reductant (experience d,e and f). Perhaps the time contact during the formation of the thin film of reaction in the cyclonic chamber is not enough for nitrate interaction.

Results found in these experiences do not differ significantly from those found in **2.3.4.2 Evaluation of the incidence of nitrate concentration in lead's response**.

2.3.5 Method characterisation

2.3.5.1 Experimental section

Aiming to evaluate the applicability of the method, different matrixes were chosen. With the results found in **2.3.4.2 Evaluation of the incidence of nitrate concentration in lead's response**, the first purpose was to find matrixes with different nitrate amount; samples requiring high nitric acid concentration for its digestion would be perfectly suitable to exemplify the need of adding a high amount of nitrate to standards to avoid the bias.

The laboratory in which this work was carried out has lead additivated potato and sweet potatoes digest: $10 \mu\text{g kg}^{-1} \text{Pb} - 16 \% \text{ v/v HNO}_3$. They were intended to be used as high nitrate concentration samples but, as their hydrogen ion is within the range of signal inhibition the neutralising stage is necessary. Neutralisation causes nitrate dilution to a concentration out of the enhancement range.

The other materials available with a known lead content are water CRM, soil CRM and sewage sludge CRM.

Water CRM is $2\% \text{ v/v HNO}_3$, so nitrate amount has no impact in lead signal ($0,29 \text{ mol kg}^{-1} \text{NO}_3^-$ approx.); nevertheless, hydrogen ion ($0,29 \text{ mol kg}^{-1} \text{H}^+$ approx.) is the enhancement zone. Matrix matching of the calibration solutions is needed.

Sewage sludge CRM and soil CRM were digested with microwave assistance in nitric acid; the high level lead content (300 mg kg^{-1} approx.) make necessary a one hundred times dilution previous HG-MIP OES analysis; remaining nitric acid concentration is no longer relevant neither for the nitrate nor the hydrogen ion amount. The dilution was made in $2\% \text{ v/v HNO}_3$, in order to interpolate its signal in the same calibration curve as the water CRM.

2.3.5.2 Instrumentation

Instrumental parameters used are presented in Table 14. Measures were performed at 283,305 nm and 405,781 nm using the auto background corrector provided by the spectrometer.

2.3.5.3 Reagents and solutions

Diluted solutions were prepared with deionised water (ASTM type I) obtained from a Millipore (São Paulo, Brazil) Direct-Q 5 water purifier. Lead working solutions were prepared daily by gravimetric dilution of their corresponding 1000 mg L^{-1} atomic absorption standard solution.

Sodium tetrahydroborate solution (2 % w/v in 1% w/v NaOH) was prepared from sodium tetrahydroborate (hydride generation grade, Fluka).

Calibration solutions were prepared in 2 % HNO₃ - 1,5 % w/v K₃Fe(CN)₆ and 0,12 mol L⁻¹ HCl - 1,5 % w/v K₃Fe(CN)₆.

Certified reference material, MRC.INO.101 Trace elements in water, was obtained from Laboratorio Tecnológico del Uruguay (LATU).

Trace Metals – Sewage Sludge 2, CRM029-50G ACLASS

Soil Certified Reference Material: RM-Agro E2002a

2.3.5.4 Procedure

For the interference study a six point calibration curve was constructed both in 0,12 mol L⁻¹ HCl and 2 % HNO₃.

The linear range was evaluated up to 100 µg L⁻¹ with a seven point external standards calibration curve. For evaluating the figures of merit of the methodology for lead determination in nitric samples, triplicates of six point calibration curves were prepared in 2% v/v HNO₃. The limit of detection and the limit of quantification were calculated from the standard deviation of five replicates of the blank (each replicate was measured three times and the average taken as the signal).

Precision of repeatability was assessed at 30 Pb - µg L⁻¹ level as the relative standard deviation of the results of the six replicates of water CRM.

2.3.5.5 Results and discussion

2.3.5.5.1 Evaluation of the linear range and calibration function

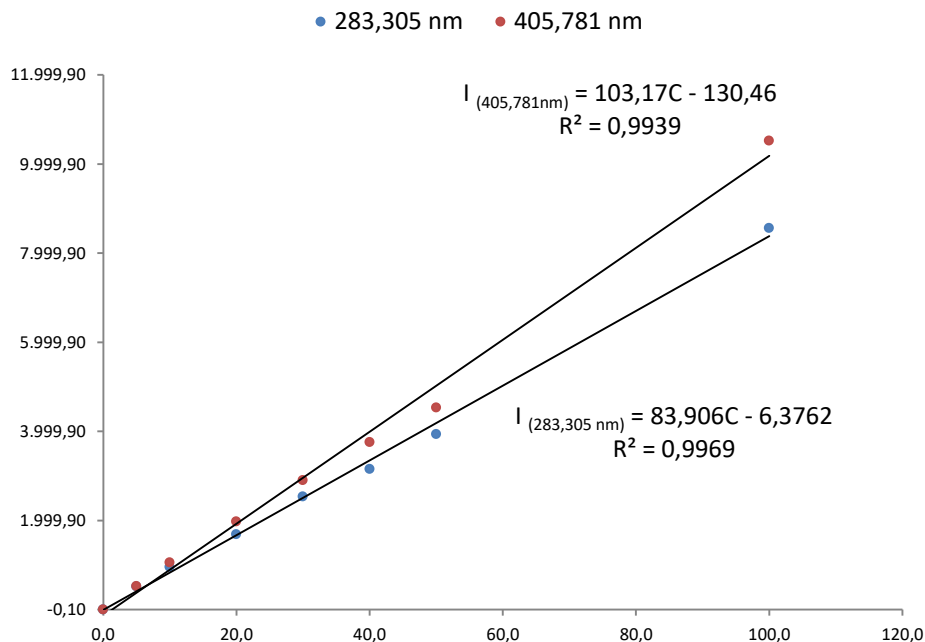


Figure 32: Evaluation of the linear range for lead determination at 283,305 nm and 405,781 nm by HG-MIP OES. I: emission signal at the corresponding wavelength; C: lead concentration in $\mu\text{g L}^{-1}$.

The calibration function was linear along all the range studied (Figure 32). The calibration standards used were prepared in $0,12\text{ mol L}^{-1}$ HCl.

2.3.5.5.2 Some figures of merit

In order to characterise the methodology for the determination of lead in nitric samples, all the parameters were evaluated in 2% HNO_3 solutions.

As blank solutions had an emission signal different from zero, its dispersion was used for calculating the limits of detection and quantification.

Limits were calculated as follows: $LOD = \frac{3s}{m}$ and $LOQ = \frac{10s}{m}$ where s is the standard deviation for the average of three measurements of five replicates of blank solution in nitric acid and m the slope of the corresponding calibration function.

Results are summarised in Table 17 and Table 18 :

Lead determination at 283,305 nm			
		Calibration function	
		$I = 133,3C + 138,6$	
		$R^2 = 0,9988$	
		LOD ($\mu\text{g kg}^{-1}$)	LOQ ($\mu\text{g kg}^{-1}$)
		0,37	1,2
Trace metal in water CRM (n = 6)			
Precision ($30 \mu\text{g L}^{-1}$)	s_r (%) : 3,4	Trueness, %	75
Other CRM assayed (trueness, %):			
Soil (n = 2)	82	Sewage sludge (n = 1)	59

Table 17: Figures of merit for determinations at 283,305 nm. I: emission signal; C: lead concentration in $\mu\text{g L}^{-1}$; s_r : relative standard deviation.

Lead determination at 405,781 nm			
		Calibration function	
		$I = 151,8C + 132,6$	
		$R^2 = 0,9995$	
		LOD ($\mu\text{g kg}^{-1}$)	LOQ ($\mu\text{g kg}^{-1}$)
		0,25	0,82
Trace metal in water CRM (n = 6)			
Precision ($30 \mu\text{g L}^{-1}$)	s_r (%) : 3,3	Trueness, %	90
Other CRM assayed (trueness, %):			
Soil (n = 2)	91	Sewage sludge (n = 1)	78

Table 18: Figures of merit for determinations at 405,781 nm. I: emission signal; C: lead concentration in $\mu\text{g L}^{-1}$; s_r : relative standard deviation.

Considering the emission lines of the spectra of lead, 405,781 nm is the most intense. 283,305 nm was chosen as one of the others with considerable intensity and determination were also performed at that wavelength also in order to have more information and eventually use it with quantification purposes if a good performance was found.

As can be seen in Table 17 and Table 18, even if limit of detection and quantification at 283,305 nm are acceptable, overall performance was better achieved at 405,781 nm in terms of limits of detection and quantification, precision of repeatability and trueness.

2.3.6 Conclusions

After the evaluation of different generating media, HCl – $\text{K}_3\text{Fe}(\text{CN})_6$ resulted the most suitable. The efficiency for lead tetrahydride generation is strongly dependent of the pH of the media, as in a narrow concentration range, hydrogen ion presence can turn from being a signal enhancer to an absolutely inhibitor probably due to the tetrahydroborate decomposition prevalence (Dedina & Tsalev, Hydride Generation Atomic Absorption Spectrometry, 1995). Nitrate on the contrary shows a positive impact on the signal when its concentration overcomes $0,6 \text{ mol kg}^{-1}$.

Bearing both considerations in mind, according to the sample, a neutralisation stage or a matrix match one can be faced. For example, when analysing the certified reference material of water, which is 2% HNO_3 , nitrate concentration ($0,29 \text{ mol L}^{-1}$ approx.) is not expected to modify the response but hydrogen ion ($0,29 \text{ mol L}^{-1}$ as well) do so. In this case, instead of neutralising, it is more convenient to prepare the calibration standards in 2% HNO_3 .

If it happens to ignore about the composition (nitrate content) of the sample, an addition of it (as KNO_3 for example) to both sample and calibration standards is advisable as it does no matter if there was already nitrate in the sample, the response keeps quite constant once in the enhancement range.

Literature often mentions the drawbacks lead hydride generation has, nevertheless, presence of acid and nitrate in the media have been evaluated and a methodology for its determination developed. With it, auspicious results have been achieved: absence of bias in the determination of lead in three references materials, wide linear range and low detection limit, comparable to those achievable with a graphite furnace, rendering this methodology very suitable for trace analysis. Using MIP OES as detection system after hydride generation is not extended in use, at least in the literature that is within my reach to consult.

Chapter II

Lead determination by HG – MIP OES

Scientific production



Rio Symposium on Atomic Spectrometry

6 – 11 October 2019 · Mendoza – Argentina

PLUMBANE DETERMINATION BY HG-MIP OES: STUDY OF THE VARIABLES AFFECTING ITS GENERATION, INTERFERENCE ANALYSES AND APPLICATION

Alicia Mollo,^{1*} Florencia Cora Jofré,² Alexandra Sixto,¹ Mariela Pistón,¹ Marianela Savio^{2*}

¹Grupo de Análisis de Elementos traza y desarrollo de estrategias simples para preparación de muestras (GATPREM). Analytical Chemistry. Faculty of Chemistry. Universidad de la República. Montevideo, Uruguay.

² Facultad Ciencias Exactas y Naturales, Universidad Nacional de La Pampa, Av. Uruguay 151, L6300XAI. Instituto de Ciencias de la Tierra y Ambientales de La Pampa (INCITAP), Mendoza 109, L6302EPA. Santa Rosa, La Pampa, Argentina

*marianelasavio@gmail.com - amollo@fq.edu.uy

Among the hydride forming elements, lead volatilization by plumbane generation is not very extended for its determination¹. Microwave induced plasma atomic emission spectrometry (MIP OES) uses nitrogen to fuel the plasma reducing dramatically the associated cost. The aim of this work was to study the variables affecting both the plumbane generation and its determination by HG-MIP OES. A new methodology for lead determination at trace levels was developed.

Different plumbane generation conditions were evaluated. Results showed that 0.1 mol L⁻¹ HCl - 1.5% w/w K₃Fe(CN)₆ - 2% w/w NaBH₄ was a suitable balance between the hexacyanoferrate (III) enhancement of plumbane generation² and the acidity of the generated wastes. Hydrogen ion was found to enhance the signal up to 0.3 mol kg⁻¹ and then inhibit it at larger amounts. For concentration above 1.0 mol kg⁻¹, signal was completely abated. Nitrate ion was found to have a positive impact on lead's signal for concentrations above 1.0 mol kg⁻¹ NO₃⁻ (10% w/w HNO₃) enhancing the signal about 50%. For the formerly said, acid and nitrate concentration (the last generally deliberately added for sample digestion) are of concern for quantification purposes, so neutralizing and buffering the nitrate amount was mandatory. Analytical determinations were performed at 405.781 nm optimizing stabilization time of the chamber (20s), nebulizer flow (0.75 L min⁻¹), pump speed (30 rpm), viewing position (0) and read time (5s). A linear response was found along the concentrations studied range (from LOQ (10s) 0.82 up to 100 µg L⁻¹). A limit of detection (LOD (3,3s)) of 0.27 µg L⁻¹ was achieved, 100-fold better than that attained with MIP OES without HG. Trueness was assessed using a certified reference material (CRM) of water for low lead concentrations, and a CRM of soil and also mud for high ones. Mean recoveries were of 89, 91 and 78 % respectively.

This study allowed evaluating the incidence of acid and nitrate concentration in plumbane generation. To the best of our knowledge, this is the first attempt that HG-MIP OES was performed for lead determination with a promising performance for trace analysis.

Acknowledgements

Comisión Sectorial de Investigación Científica (CSIC) and Programa de Desarrollo de las Ciencias Básicas (PEDECIBA - Química) for financial support. Consejo Nacional de Investigaciones Científicas y Técnicas (CONICET), Agencia Nacional de Promoción Científica y Tecnológica (ANPCYT), Universidad Nacional de La Pampa.

References

- [1] Huang K., Xia H., Li M., Gao Y., Zheng Ch. and Hou X., *Analytical Methods Anal. Methods* 4 (2012) 4058-4062.
- [2] D'Ulivo A., Onor M., Spiniello R., Pizzalis E., *Spectrochimica Acta Part B* 63 (2008) 835-842.

Chapter III

Electrochemical Vapour Generation

In this section the description of the construction of an electrolytic cell is presented and the attempts of using it for selenium determination. Results were not satisfactory.

Chapter 3: Abbreviations

CVG: Chemical Vapour Generation

ECVG: Electrochemical Vapour Generation

EHQTA: Externally Heated Quartz Tube Atomiser

GLS: Gas-liquid Separator

3 Electrochemical vapour generation (ECVG)

3.1 Introduction

ECVG use electrons as mediators for hydride generation. Reaction takes place in an electrolytic cell; analyte is reduced in the cathode together with hydron, and water oxidised in the anode; both half cells are separated by a semipermeable membrane.

According to Denkhaus et al. (Denkhaus , Beck , Bueschler , Gerhard , & Golloch, 2001) the mechanism of generation can be accomplished by electrocatalytic or electrochemical mechanism, upon hydrogen overvoltage of the cathode.

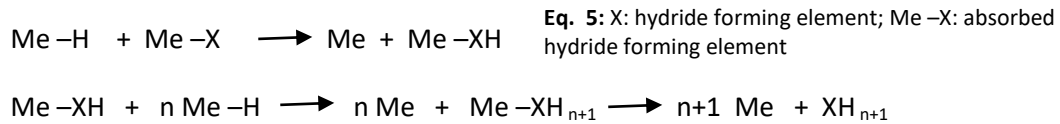
The first step is the electrodeposition of the hydride forming element on the electrode surface; analyte diffuses towards the electrode and gets reduced on its surface by a charge-transfer reaction from the electrode to the element (Eq. 3).



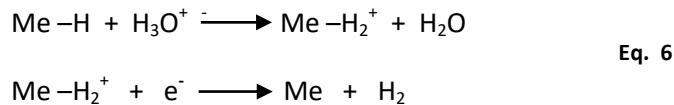
Palladium, platinum, silver and gold cathodes, whose hydrogen overvoltage is low, absorb high amounts of hydrogen in accordance with an electrocatalytic mechanism (Eq. 4) where adsorbed hydrogen recombines to form gaseous hydrogen and leaves the surface:



The analyte already bonded to the electrode surface reacts by a stepwise mechanism with the adsorbed hydrogen (Eq. 5) and the hydride gets desorbed. Adsorbed hydrogen competes with hydride generation as it remains bonded to the electrode's surface.



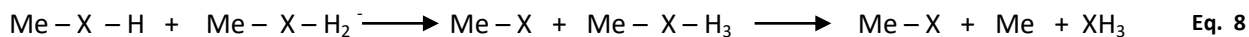
Conversely, cadmium, lead and mercury cathodes have high hydrogen overvoltage and absorb hydrogen in lesser amount in the surface. In the electrochemical mechanism, hydrogen evolves by the reaction between the already adsorbed hydrogen and hydronium followed by electron transference on the cathode surface (Eq. 6):



For the hydride generation there is a charge transfer between the cathode surface and the adsorbed analyte as well as a reaction of the adsorbed analyte and hydronium (Eq. 7).



According to Salzberg et al. (Salzberg & Goldschmidt, 1960) the hydride generation is achieved by a disproportionation reaction by neighbouring Me - X - H and Me - X - H₂ groups followed by the desorption of the hydride (Eq. 8):



Me - X - H is the hydride forming element - hydrogen group on the electrode (M) surface and Me - X - H₂ is the hydride forming element - dihydrogen group on the electrode (M) surface.

At first, analyte (X⁺³, for example) diffuses towards the cathode where a charge transfer reaction reduces it to its elemental form remaining absorbed at the cathode surface. Me - X - H is electrochemically formed by reaction of the reduced metal in the surface of the electrode and water.

Formation of Me - X - H₂ can result from the electrochemical reaction between water and Me - X - H or a disproportionation reaction between two close Me - X - H molecules.

The electrode material, the current density, catholyte type, concentration and flow rate, pH and temperature will affect the generation process.

Cathodes with higher hydrogen overvoltage leads to higher generation efficiency as higher negative potentials can be reached; ordered by decreasing reducing power: Pb > Hg-Ag > Cd > galssy carbon > Ag > Au > Pt. Consequently, for a given element, some of them are able to generate the hydride from the lowest oxidation state but not from the highest. Notwithstanding, this can be useful for speciation purposes.

Electrolytic cells most frequently used are continuous flow or flow injection devices. Diluted hydrochloric or sulphuric acid are usually used as catholyte (cathode solution) whereas sulphuric acid is generally used as anolyte (anode solution) as it can be recirculated after oxygen separation. Their flow rates are dependant of the cell design.

Laborda et al. (Laborda, Bolea, & Castillo, 2007) classified the cells according to the relative cathodic and anodic compartment arrangement; parallel when both compartment are adjacent (also called thin layer cells) and concentric when the cathodic or anodic space is sourrounder by the other. The first involves two dimensional cathodes (laminar or wire shaped electrodes) while the second uses three dimensional electrodes as packed particulate material.

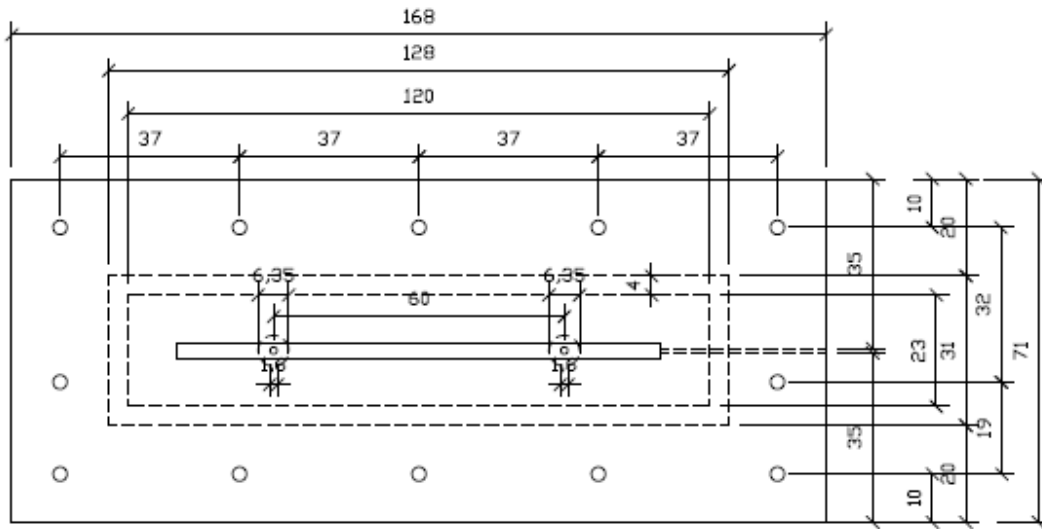


Figure 34: Upper view of the half cell.

A silicone rubber framed cathode and anode compartment preventing the leakage of solutions, besides, it was sealed by 12 screws (Figure 35).

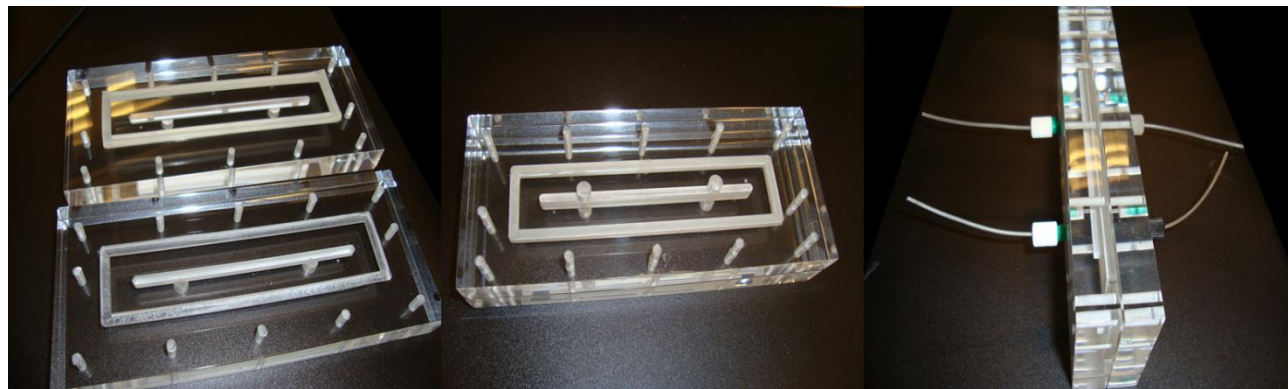


Figure 35: Thin layer electrolytic cell.

3.3.2 Electrical assembly

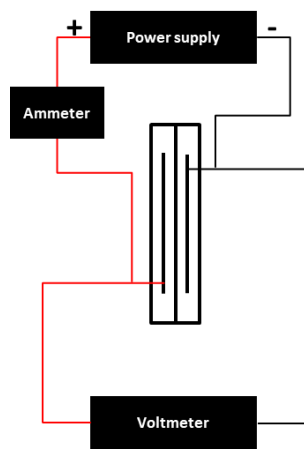


Figure 36: Electrical assembly of the electrochemical cell.

In Figure 36 is shown the electrical assembly of the cell. It consisted on a 0 - 30 V / 0 - 5 A power supply able to provide constant current. The common current used was around 100 mA. The voltmeter was placed in parallel (3 – 4 V) and the ammeter in serial in order to know the stability of the current supply ($\pm 0,3$ mA).

3.3.3 Continuous flow electrochemical manifold

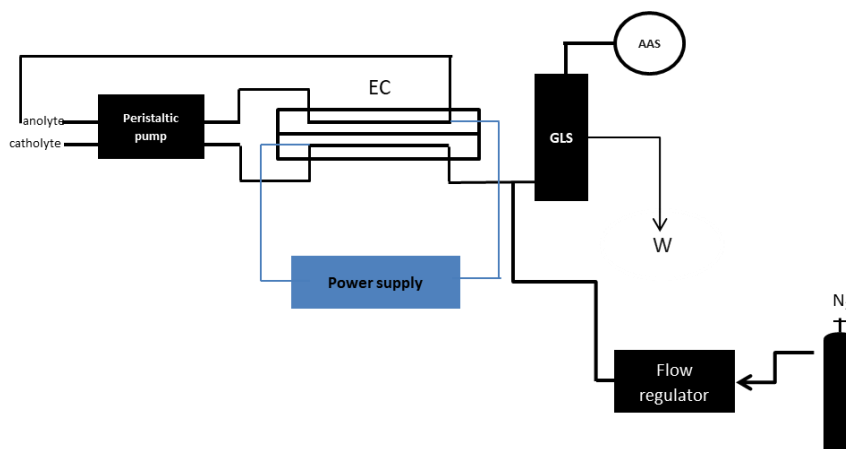


Figure 37: Continuous flow electrochemical system manifold. EC: electrolytic cell; GLS: gas-liquid separator; AAS: quartz cell in the atomic absorption spectrometer; W: waste; N₂: nitrogen. In blue: electrical assembly previously shown.

Figure 37 shows the continuous flow system for electrochemical volatile species generation. Solutions were pumped by means of a peristaltic pump (Rainin, Dynamax RP-1). A flow regulator (Cole Parmer) controlled the nitrogen flow before entering the hydrostatic gas-liquid separator. The atomisation device was a EHQTA heated by an air-acetylene flame on a 10-cm burner installed in a Perkin Elmer , AAnalyst 200 provided with a selenium electrodeless discharge lamp (196,0 nm) and deuterium background corrector.

For the CVG, a batch hydride generator, Perkin Elmer MHS15 was used with the same atomisation and detection system previously mentioned.

3.4 Reagents and solutions

De-ionised water (ASTM type I) was obtained from a Millipore (São Paulo, Brazil) Direct-Q 5 water purifier. Selenite solutions were prepared from sodium selenite (Aldrich, 99 %). Selenium working solutions were prepared daily by dilution of the Se(IV) 1000 mg L⁻¹ standard solution in 1 mol L⁻¹ HCl (catholyte solution).

Anolyte solution used was 2 mol L⁻¹ H₂SO₄.

All reagents used were of analytical reagent grade unless otherwise specified.

Lead wire 1,0 mm diameter (99,99%, Aldrich) was used as cathode and platinum wire 0,5 mm diameter (99,99 %, Kurt J. Lesker) as the anode. Both half cells maintained the electrical contact by an ion exchange membrane 0,007 inches (Nafion® 117, Aldrich).

For the CVG, sodium tetrahydroborate solution (3,0 % w/v in 1% w/v NaOH) was prepared from sodium tetrahydroborate (Hydride-Generation grade, Fluka).

Standard nitrogen and acetylene were supplied by Linde Uruguay.

3.5 Procedure

The cell was operated at different constant currents between 100 and 200 mA. The peristaltic pump propelled both catholyte and anolyte to the electrochemical cell; the anolyte recirculates and the catholyte was added by the anolyte. A nitrogen stream intercepted the catholyte after leaving the cell and before entering the gas-liquid separator; then it transferred the hydride to the atomisation cell for its detection.

The generation efficiency was determined by CVG analysing the solution before and after the ECVG.

3.6 Results and discussion

100 $\mu\text{g L}^{-1}$ Se – 1 mol L^{-1} HCl and 10 mg L^{-1} Se – 1 mol L^{-1} HCl were passed through the cell at different flow rates, constant current values between 100 and 200 mA and different nitrogen flow rates, however, no signal was appreciated.

The absence of signal not necessarily means there is no generation, as the hydride can be diluted in its way towards the detection system. Thus, selenium was determined in a 10 $\mu\text{g L}^{-1}$ Se – 1 mol L^{-1} HCl solution which is the maximum concentration within the linear range of the batch system; the solution was analysed by CVG, passed through the cell and analysed again in the waste from the GLS. Signal decay would confirm the generation.

The nitrogen flow rate was fixed at 760 mL min^{-1} that was found suitable in previous work for that GLS. Catholyte flow rate was 1,1 mL min^{-1} .

$$ECVG \text{ efficiency (\%)} = 100 - \frac{S_{\text{after ECVG}}}{S_{\text{before ECVG}}} \times 100$$

$S_{\text{after ECVG}}$ is the analytical signal (peak area) of the waste solution and $S_{\text{before ECVG}}$ is the analytical signal (peak area) of the solution before entering the electrolytic cell.

The ECVG efficiency found was about 20 %.

Sample flow (catholyte) was varied to 0,6 mL min^{-1} in order to increase the electrolysis time. The efficiency found was 28 %.

After few minutes of operation a whitish film appeared along the cathode. The electrode was rinsed every time with 1 mol L^{-1} HNO_3 until the film dissolved.

Apart from the low generation efficiency, the electrolytic cell had its drawbacks: after few minutes of operation leakages started to appear at the electrode connection or from the lateral of the cell throughout the screws. Silicone grease within the junctions helped to delay the leakage but it could never be avoided. Furthermore, the electrical connection of the electrodes with the power supply was very feeble and current passage was frequently interrupted. Cell design was not appropriate.

The cell was fixed by a local turnery in order to get the electrical contact by means of a banana plug as it is showed in Figure 38:



Figure 38: Electrolytic cell with new electrical connector.

It is not clear from the picture but the cell had the same type of connection for the other electrode also. The photograph on the right shows the cell mounted in the Thermo Scientific VP100 system. Despite the new connections, the leakage remains; the cell was operated up to 200 mA and a black deposit appears in the cathode half cell (Figure 39).



Figure 39: Left: cathode half-cell. Right: Ion exchange membrane after electrolysis.

Ion exchange membrane was deteriorated by a black solid that firmly adhered to its surface.

3.7 Conclusions

There was no direct evidence of dihydrogenselenide generation. The confirmation of ECVG occurrence was determined indirectly, by CVG of the solution before and after its passage through the electrolytic cell. The efficiency found showed there were still variables to adjust in order to improve the generation: different electrolysis currents, flow rates of the catholyte, and electrolyte type and concentration. Once the generation was optimised, the nitrogen flow rate could have been changed so as to get a suitable signal in the detector.

Beyond the aforementioned, the constructed cell could not be properly operated: neither the leakage nor the electrode deterioration could be controlled. Maybe setting up a cavity for the ion exchange membrane, despite its extreme thinness, could be helpful.

Moreover, lead wire resulted very ductile and got easily broken in the connection sites.

A new cell design should be faced as well as a new electrode material format, perhaps a thicker wire or a piece of sheet that render handling easier. Platinum wire, even if narrower was very friendly to handle and can be kept as the anode electrode.

Chapter IV

Photochemical Vapour Generation

This chapter describes the generation of volatile species using photons as mediators for chemical reactions to occur. First, a theoretical approach is given, and then a chronological report of the experience collected by the use of different reactors is presented.

Chapter 4: Abbreviations

AAS: Atomic Absorption Spectrometry

CF-HG-AAS: Continuous Flow Hydride Generation Atomic Absorption Spectrometry

CF-PCVG-AAS: Continuous flow Photochemical Cold Vapour Generation Atomic Absorption Spectrometry

CRM: Certified Reference Material

CVG: Chemical Vapour Generation

ETAAS: Electro Thermal Atomic Absorption Spectrometry

FI: Flow injection

FI-PCVG-AAS: Flow Injection Photochemical Cold Vapour Generation Atomic Absorption Spectrometry

FI-PVG-AAS: Flow Injection Photochemical Vapour Generation

GLS: Gas-liquid separator

HG – AAS: Hydride Generation Atomic Absorption Spectrometry

LMCT : ligand-to-metal charge transfer transition

LMWOC: Low molecular weight organic compound

PVG: Photochemical Vapour Generation

PVG-HS-SDME-ETAAS: Photochemical Vapour Generation Head Space Single Drop Micro Extraction
Electro Thermal Atomic Absorption Spectrometry

UV: Ultraviolet

4 Photochemical Vapour Generation

4.1 Introduction

Photochemical vapour generation (PVG) is an alternative to chemical vapour generation (CVG), which, instead of tetrahydroborate, uses the interaction of the photons with organic acids, alcohols and, in some cases aldehydes, to create the reducing environment which yields the volatile species. Ultraviolet (UV) irradiation excites the organic molecule yielding radicals which reduce the analyte ion to the corresponding hydrogenated, carboxylated or alkylated volatile compound.

Unlike chemical vapour generation, neither sodium tetrahydroborate nor high concentrated hydrochloric acid are needed, thus hydrogen evolution is dramatically decreased and, when using plasmas as atomisation devices its stability is improved. For the aforementioned and as the aliphatic carboxylic acids which employ are in low concentration (generally not above 10 %), there are not hazardous wastes generated.

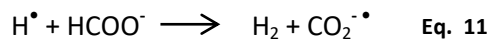
PVG can be applied for the already known elements amenable to hydride formation (elements of the groups IV, V and VI), but also to the transition and noble group elements; speciation analysis can also be achieved (Sturgeon & Grinberg, 2012) (Sturgeon R. , 2017) (Leonori & Sturgeon, 2019).

The interaction of the matter with visible or ultraviolet irradiation can result in chemical reactions and/or physical changes. Both the energy of matter and the energy of light are quantised: matter has different energy levels where electrons may be found and light can transfer the energy by means of photons. The energy of the photon follows the Planck's law:

$$E = h\nu$$

where E is the energy of the photon, h Planck's constant (6.63×10^{-34} Js) and ν the frequency at which the photon oscillates (s^{-1} , Hertz). The separation between the energy levels of the matter is of the same order as the energy of the visible and UV light. Thus, from the interaction of both, as light is absorbed by the matter, the photon transfers its energy enabling the promotion of the electron from the electronic ground state to the excited state, leading to an excited species. Once the excited species is formed, changes within the electronic configuration of the molecule, luminescence or heat transfer process, and energy or electron transfer with other ground state molecules can occur. The latter is the one of concern in photochemical vapour generation.

The photochemical reaction involves the excited species as reagent, thus, products that are thermodynamically non-viable from the ground state molecule can be formed from the excited one.



The carbonyl radical, a strong reductant, is formed, so the system has no longer oxidising OH^\bullet , turning more reducing the media. Furthermore, the acid itself also absorbs the UV irradiation (Eq. 13) yielding reducing species as well (Buxton & Sellers, 1977) (Thomsen, Madsen, Keiding, & Thogersen, 1997) (Reuther, Laubereau, & Nikogosyan, 1996) (Leonori & Sturgeon, 2019). As the energy of the UV irradiation is of the same magnitude as the energy of the covalent bond, the molecule suffers photolysis, the cleavage of the molecule in two species with unpaired electrons (radicals):

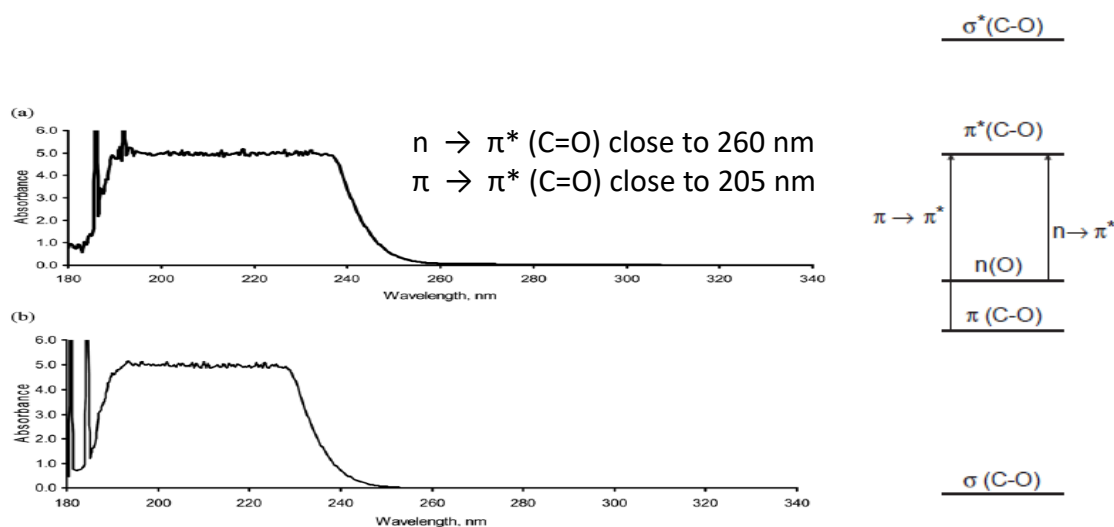
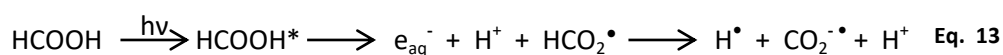


Figure 41: Absorption spectra of a) formic acid and b) acetic acid. Adapted from J. Anal. At. Spectrom., 2012, 27, 222-231

Figure 41 shows the absorbance spectra of formic and acetic acid due to the electronic transition caused by the UV irradiation; the absorption of photons of suitable energy, causes the electron promotion from the nonbonding (n) to the antibonding (π^*) orbital and from the bonding (π) to antibonding (π^*) orbital.

The interaction between the different products of photolysis of both water and carboxylic acid lead to different compounds. Figure 42 shows the example for formic acid (Zechner & Getoff, 1974) (Leonori & Sturgeon, 2019).

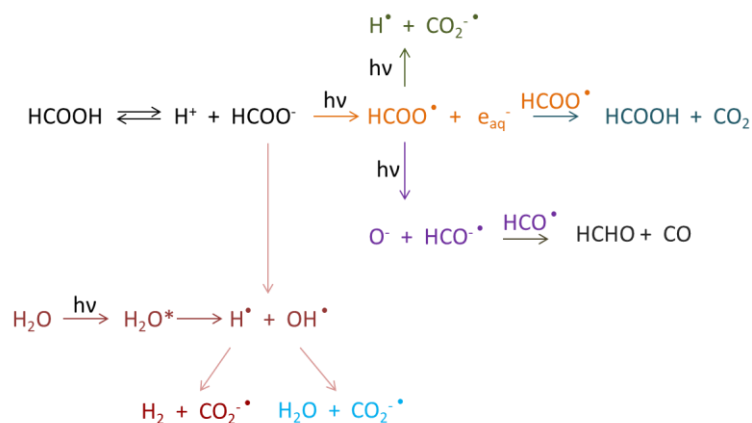
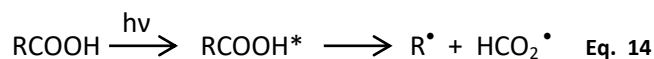


Figure 42: Some reactions taking place when a formic acid aqueous solution is irradiated by UV irradiation

In general, for short chain organic acids, RCOOH:



R is the aliphatic chain of the acid. When the UV irradiation is absorbed, only the C-COOH bond is broken (Eq. 14) (Mittal, Mittal, & Hayon); any further bond breakage proceeds. For a carboxylic acid of n carbons length, (n-1) carbons length radical are formed for the element ion derivatisation. The extent of this reaction depends on the pH of the solution as takes places in the non-dissociated acid. Afterwards, R^\bullet may undergo other radical – radical recombination reactions depending on its concentration. In water, HCO_2^\bullet also participates in an acid base reaction (Eq. 15).



From all above mentioned, reductant species like e_{aq}^- , H^\bullet , R^\bullet and $\text{CO}_2^{\bullet-}$ are formed. If the solution contains an ion of an element amenable to reduction, once the photon is absorbed, the electron is transferred from the bonding ligand-centred molecular orbital to the antibonding metal-centred molecular orbital in a ligand-to-metal charge transfer transition (LMCT); the electron of an occupied molecular orbital is transferred to a vacant molecular orbital, ligand oxidises and the metal is reduced.

As can be seen, many reactions can take place and, consequently, the chemical conformation of volatile species depends on the acid added to the solution; formic acid leads to H^\bullet and HCO^\bullet , so the species

formed, in the case of selenium are SeH_2 and SeCO ; when acetic acid (CH_3COOH) is used, $\text{CH}_3\text{Se}^\bullet$ is formed and so $\text{Se}(\text{CH}_3)_2$; when propionic acid ($\text{C}_2\text{H}_5\text{COOH}$) is used, $\text{C}_2\text{H}_5\text{Se}^\bullet$ is formed, and so $\text{Se}(\text{C}_2\text{H}_5)_2$, for example.

The use of irradiation as a mean of reducing ions has its origin in the study of the photo remediation of aquatic systems by sunlight and low molecular weight organic acids. Many bacterial and abiotic systems also lead to volatile compounds generation; reduction and alkylation of the oxyanions of selenium is a known detoxification process in natural systems, reduction and methylation of mercury ions by acetate and sunlight also. Sturgeon and Guo were the first to take account of such process and use them as sample introduction technique for analytical purposes (Guo, Sturgeon, Mester, & Gardner, Photochemical Alkylation of Inorganic Selenium in the Presence of Low Molecular Weight Organic Acids, 2003) (Yin, Liu, & Jiang, 2011).

The Commission Internationale de l'Éclairage, CIE S 17 – 1367/E: 2011 (Bureau, 2011) divides the UV region in three zones upon the wavelength involved: UV A for wavelength range between 315 and 400 nm, UV B from 280 to 315 nm and UV C from 100 to 280 nm. The latter is the range of interest in photochemistry. The irradiation at those wavelengths is drawn by mercury lamps, which, at a time can be classified in three categories depending on its mercury's inner pressure: low (0,1 – 1 Pa), medium (around 0,1 MPa) and high pressure (around 10 MPa). Apart from mercury, lamps have an inert gas inside the bulb under high pressure and tungsten electrodes at the extremes serves as the electrical connection to the power supply.

In medium pressure mercury lamps, pressure is determined by the amount of mercury as it evaporates completely during operation. In order to avoid mercury condensation they work at a temperature range of 600 to 900°C and are cooled by air. They have more emission lines than the low pressure one, a continuum in the UV C zone and are much brighter also. High pressure mercury lamps operate at elevated temperatures as well, using water as the cooling system. They have a broader continuum spectra with high intensity but, due to self-absorption, 253,7 nm line is absent.

Low pressure mercury lamps, in turn, operate at temperatures between 40 and 60°C. Liquid mercury is in equilibrium with vapour mercury during operation. They are less intense and present a line spectrum, which two prominent lines are related to the 6^3P_1 to 6^1S_0 transition at 253,7 nm and the 6^1P_1 to 6^1S_0 transition at 184,9 nm. For this kind of lamps, the efficiency of irradiation in the UV C range is about 40% whilst for the medium and high is about 16%. Low pressure mercury lamps are the ones preferred for PVG; medium and high pressure, even if more intense, emit a continuum, need refrigeration and overheat solutions. Besides the already mentioned wavelength of the UV C region, other mercury lines of quite high intensity in the UV B (313,2 nm), UV A (365,0 nm) and visible region (404,7, 435,8, 546,1, 577,0 and 579,1 nm) are also present (Golimowski & Golimowska, 1996) (Sturgeon R. , 2017) (Wardle, 2009).

The intensity and wavelength of irradiation that reach the samples depends on the intensity of the lamp, the distance from the solution and the transparency both of the lamp's bulb and the sample container. Oxygen has a high absorbance below 200 nm, so it must not be present in the way of the irradiation to

the sample. Consequently, the geometry of the reactor and the material that compose it are of upmost importance for the expected sample irradiance efficiency.

The high absorbance of the LMWOC (Figure 41) evidence the low penetrability of the irradiation to the samples, so flow systems yielding thin film sample solutions are in general more efficient than batch ones.

Two examples of flow reactors are taken from the literature as were the ones used in this work.

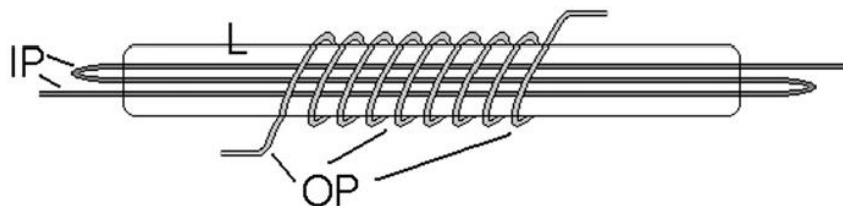


Figure 43: Example of a flow through UV reactor, extracted from D. Qin et al. / *Spectrochimica Acta Part B* 88 (2013) 10–14. L: low pressure mercury lamp; IP: tubing inside the lamp; OP: tubing wrapped around the lamp

Figure 43 shows in the same image two kind of reactor frequently used: a low mercury pressure lamp as radiation source, and two sample irradiation options; high efficient through the inner of the lamp (IP), or wrapped around it (OP).

Qin et al (Qin , et al., 2013) tried both kind of reactors for different tubing material: opaque, partly transparent and transparent quartz tubes and PTFE tubes. In the case of the IP model, the pipeline is inserted in the inner lamp, thus, when solution circulates inside it is irradiated in all directions mainly at 253,7 and 184,9 nm; the irradiance available for being absorbed depends only in the transparence of the tube. At 184,9 nm, due to its high energy besides the interaction with water and the LMWOC explained previously, the irradiation can induce other reaction or bond breakage with the concomitants of the matrix. As expected, the best efficiency found for the photoreactions was when using the synthetic quartz (high transmission at 184,0 nm).

The OP model, has the 184,9 nm line hindered as the envelope of the lamp (natural quartz, high transmission at 253,7 nm) suppresses it. In these conditions, only 253,7nm line belonging to the UV C range is available.

For both reactors, synthetic quartz tubes always showed an improved transparency for all the wavelengths, PTFE the worse, it was only partly transparent. Guo *et al* registered the spectra of a low pressure mercury lamp after passing through a PTFE tube 1,1 mm i.d. x 1,7 mm o.d. and they found the irradiation was attenuated a 95 % (Guo, Sturgeon, Mester, & Gardner, *Photochemical Alkylation of Inorganic Selenium in the Presence of Low Molecular Weight Organic Acids*, 2003).

Up to now, the physical part of the photo generation system was described: type of radiation source, design of the reactor and material of the pipelines; these parameters will determine the irradiation energy and its intensity towards the solution. From now on, the interaction of the irradiation with the

components of the solution will be considered starting by the influence of the identity and concentration of the LMWOC.

Of course the type of reactor, for a given media will determine the species found in solution, but is not the sole factor: as it might be expected, if the reactor allows 184,9 nm line to reach the solution, homolytical cleavage of water (Eq. 9) will occur and the concentration of carboxyl radicals (Eq. 11 and Eq. 12) will be raised creating a strong reducing media. However, the same effect can be attained in the absence of the 184,9 nm line if a transition metals is present in solution; iron for example yields hydrated electrons when irradiated with UV C lines (253,7 nm in this case) creating a strong reducing media as well. Thus, the final products of the photochemical process depend not only in the reactor design, tubing material and LMWOC but also in the composition of the samples.

Sturgeon & Grinberg studied the products evolving from the PVG in the gaseous phase by GC-MS after the irradiation of clean solutions of element ions and different LMWOC; for example, AsH_3 , SeH_2 and SeCO are found after irradiation of a formic solution. Acetic solution yealds $\text{As}(\text{CH}_3)_3$, and $\text{Se}(\text{CH}_3)_2$; propionic acid $\text{Se}(\text{C}_2\text{H}_5)_2$ and $\text{As}(\text{C}_2\text{H}_5)_3$ (Sturgeon & Grinberg, 2012).

Related to the amount of LMWOC in solution, its concentration needs to be high enough to ensure reagent availability to reduce and derivatise the analyte. However, if too elevated radical – radical recombination prevails against the generation process. The acidity of the media must be contolled; depending on the concentration, it can influence the accessibility of the ligand to the ion species or can suppress the volatile species generation; it was found for selenium that the last could be balanced by increasing irradiation times.

The derivatisation process starts by the photolysis of the organic compound that reduces the analyte and yields the derivatising radicals; then, the derivatisation itself is accomplished and if still irradiated, the volatile species can decompose. The time each stage last depends for every analyte, on the LMWOC and its concentration, so, the irradiation time and is another variable of paramount importance in PVG.

A carrier gas flow is also needed to remove the volatile species from solution in the gas-liquid separator and transport the gaseouos phase to the atomisation device. For atomic absorption spectrometry a quartz cell is usually used. Only formic acid photolysis yields hydrogen and in a scarce ratio, so it is ussualy added to the atomisation cell. The gas flow has to fulfil the following requirements: removal of the volatile species generated from the solution, its transport to the atomisation cell and a suitable supply of hydrogen to promote the radical atomisation process. (Guo, Sturgeon, Mester, & Gardner, UV Vapor Generation for Determination of Selenium by Heated Quartz Tube Atomic Absorption Spectrometry, 2003) (Guo, Sturgeon, Mester, & Gardner, Vapor Generation by UV Irradiation for Sample Introduction with Atomic Spectrometry, 2004) (Han, Zheng, Wang, Cheng, Lv, & Hou, 2007) (Zheng, Ma, Wu, Hou, & Sturgeon, 2010) (Sturgeon R. , 2017)

Chapter IV: Photochemical Vapour Generation

“In-house” reactor

This section contains a description of the first UV reactor used in the first exploits in photochemical vapour generation.

4.2 Experiences achieved with the “in-house” reactor

4.2.1 Continuous flow UV reactor

The first reactor used was an in-house made one, consisting on a 15 W germicidal tube (Phillips) with a 0,8x5400-mm perfluoroalcoxy tube (2,7 mL) wrapped around along the tube’s body (Figure 44). It was mounted vertically in a steel shell opened at the top and the bottom in order to ensure appropriate ventilation (Figure 45).

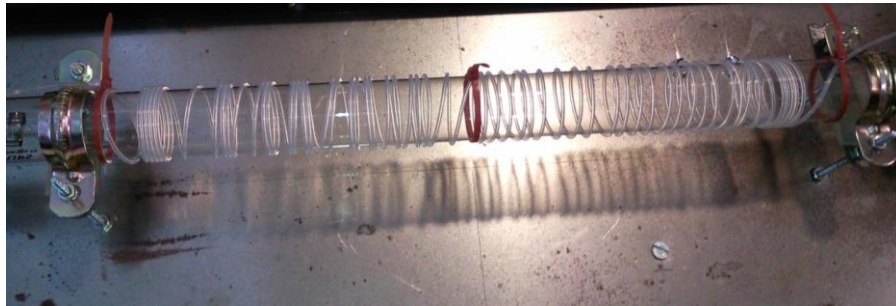


Figure 44: In-house reactor. Germicidal tube with PFA tube around it.



Figure 45: Rear and front view of the reactor once mounted in the shell for operator’s protection

A germicidal lamp's typical spectrum is shown in Figure 46; they are mercury lamps with a high emission near 254 nm.

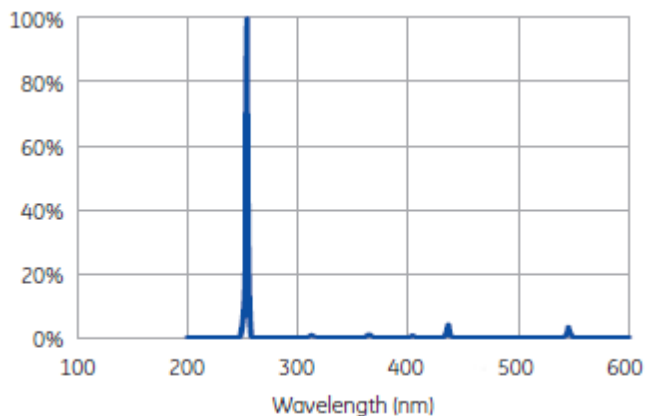


Figure 46: Characteristic spectra of germicidal lamps (extracted from <http://www.eurosep.com/fichiers-joints/web-hgg20t10.pdf>)

The emission lines of the used germicidal tube were confirmed at the Faculty of Engineering. Lamp spectrum was obtained and compared with one of a standard mercury lamp, finding an overlap of both spectra. The lamp employed is in accordance with the requirements for the photo generation. It was found that the intensity varies substantially in the first moments of operation, so it needs to be warmed up for an hour previous sample irradiation.

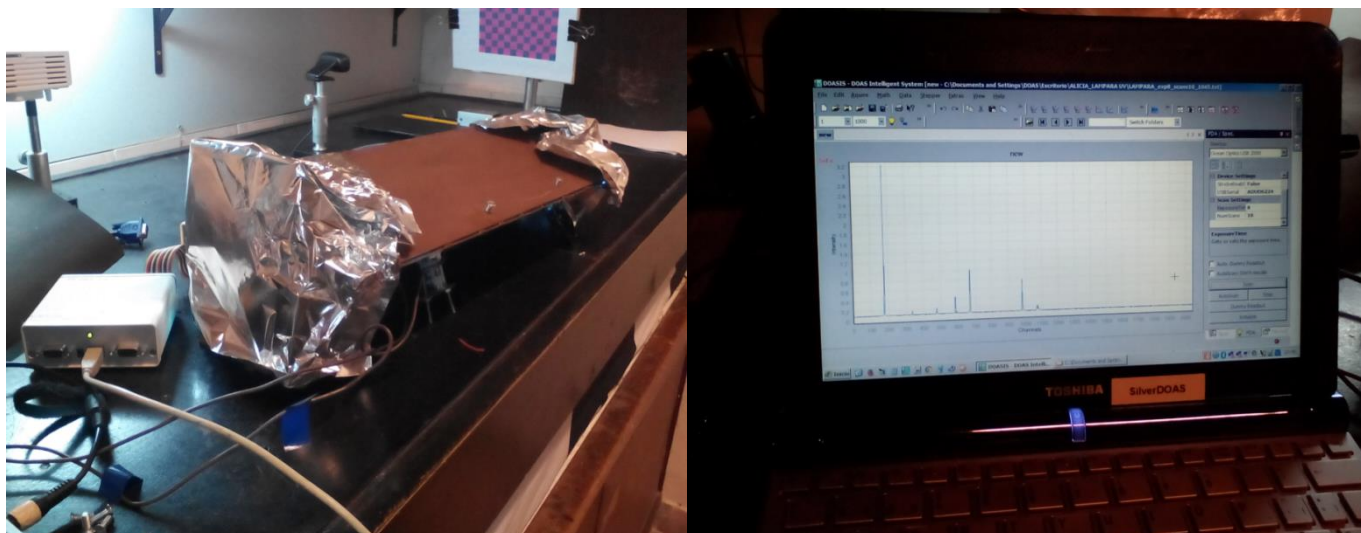


Figure 47: Measurement of the emission lines of the reactor's lamp.

Sample solution was introduced to the reactor by means of a peristaltic pump (Rainin, Dynamax RP-1).

4.2.2 First attempts in PVG with the “in-house” reactor

4.2.2.1 Preliminary considerations

The generation of volatile species and its determination by atomic absorption spectrometry implies different steps along the analysis which contribute to the overall performance of the methodology. As was previously mentioned, once the gaseous species is generated, it has to be transferred to the gaseous phase, transported to the atomisation cell and be atomised.

The species can be efficiently produced but can be very unstable in the generating media and thus never leave the solution, or be absorbed along the tubing or diluted while transported or non-efficiently atomised once in the atomisation cell. It must be kept in mind that the photo generation process does not evolve hydrogen in the most of the cases, so an extra supply has to be provided to the atomisation cell in a suitable ratio so as to reach the optimum number of radical species to ensure the atomisation; neither less for incomplete atomisation nor much to deplete the radical population. Whichever one or combinations of the aforementioned situations occur the result is a lack of signal in the detection device.

In order to circumvent these inconvenient the strategy of work was to ascertain whether the photo generation was achieved properly to be able to focus laterly in the others stages of the determination. For that purpose, the analyte was determined before and after accomplishing the photo generation process by a reliable technique in well-established conditions.

The alternatives techniques chosen were conventional chemical vapour generation, hydride generation atomic absorption spectrometry (HG-AAS) and electrothermal atomic absorption spectrometry (ETAAS). In both cases optimum working conditions were previously determined for each analyte at each generation media assayed.

For the photo generation, analyte concentration in the test solutions were selected within the linear range of the selected technique; in those conditions, the evidence of the photo generation could be assessed by comparing the magnitude of the signal of the solutions before and after the irradiation stage.

Tentative generation efficiency can be calculated as follows:

$$Efficiency (\%) = \left(1 - \frac{S_{irradiated}}{S_{non\ irradiated}} \right) \times 100$$

$S_{irradiated}$ refers to the analytical signal of the analyte in the irradiated solution and $S_{non\ irradiated}$ to the analytical signal of the analyte in the non-irradiated solution; as transient signals are obtained in both techniques, unless other stated, S correspond to peak area.

The determination of the analyte by the alternative technique has an inherent variability that must be considered before assuming the photo generation is being achieved; efficiencies below 20 % were

considered as a decrease in the signal due to the uncertainty in the determination, not because of an actual decline of the amount of analyte yielded by the volatile species generation.

In the first stages of the work the direct determination of the volatile species was sought by atomic absorption spectrometry using an externally heated quartz cell atomiser. The gas flow rate of the gas-liquid separator, gas flow rate and composition (nitrogen / hydrogen ratio) at the atomiser and type of gas-liquid separator were varied and changed for every analyte at each generation conditions without achieving a signal different from baseline. Determining the analyte that remains after the photo generation makes focusing the attention just in its generating conditions and removal from solution.

The above strategy mentioned is an indirect way of assessing the success of the photo generation; it has no quantitative purposes but is a dependable way of working in the safe side; from now on it will be referred as the indirect method.

4.2.2.2 Experimental section

Antimony, arsenic (III), cadmium, iron, lead, nickel, selenium (IV) and tin solutions in different concentrations of LMWOC were irradiated at different times.

Photochemical generation efficiency was indirectly determined by ETAAS and in the case of antimony, also by HG-AAS.

4.2.2.3 Instrumentation

The system described in **4.2.1 Continuous flow UV reactor** was used.

For HG-AAS, antimony hydride was generated in a manual hydride generator Perkin Elmer MHS 15 Mercury Hydride System. Hydrides were atomised in a T-shaped cell (Precision Glassblowing, Centennial, CO, USA). The optical tube was 18-cm long and 1-cm internal diameter fitted with graphite cooling rings at its ends in order to prevent hydrogen ignition. The inlet arm had a 0,5 cm inner diameter. It was mounted on an air-acetylene burner in a Perkin Elmer AAnalyst 200 Atomic Absorption Spectrometer (Singapore) fitted with an electrodeless discharge lamp. Deuterium background correction was achieved. Peak area was the analytical signal.

For ETAAS a Thermo Scientific (Waltham, MA, USA) iCE 3500 AAS Spectrometer with GFS35Z Graphite Furnace fitted with a the corresponding hollow cathode lamps (Thermo Scientific) and pyrolytic coated graphite tubes was used. Zeeman background correction was performed. Working conditions were optimised by means of atomisation and pyrolysis curves. Peak area was the analytical signal.

4.2.2.4 Reagents and solutions

Cadmium, iron, lead, nickel, selenium and tin working solutions were prepared daily by dilution of their corresponding 1000 mg L⁻¹ atomic absorption standard solution.

Antimony stock solution (1000 mg L⁻¹ Sb) was prepared dissolving K(SbO)C₄H₄O₆·½H₂O in water. Dilutions from the stock were prepared daily.

Arsenic (III) stock solution (1000 mg L⁻¹ As) was prepared dissolving As₂O₃ (Sigma – Aldrich, A.C.S. standard titrimetric reagent) in 0,4 % w/w NaOH. Dilutions from the stock were prepared daily.

For hydride generation, 3,0 % w/v sodium tetrahydroborate solution in 0,05 mol L⁻¹ sodium hydroxide was prepared from sodium tetrahydroborate (Hydride-Generation grade, Fluka).

Acetic, formic, propionic and oxalic acids and ethyl alcohol were of analytical reagent grade.

High purity argon, standard nitrogen and acetylene were supplied by Linde Uruguay.

4.2.2.5 Procedure

Several analytes were tested by the indirect method in different media and irradiation times as specified in Table 19; up to 35 s the irradiation time was controlled by the flow rate; larger times were performed by stopped-flow mode.

The irradiated sample was bubbled with nitrogen for up to 10 min in order to remove all the volatile species generated.

Analyte in the resulting solution was determined by ETASS; in particular antimony was also determined by HG-AAS.

Analyte	LMWOC	t _{UV}
Ni(II), Fe(III), As(III), Sb(III) (20 µg L ⁻¹)	5 % HCOOH	10 – 35 – 120 and 300s
	5 % CH ₃ CH ₂ COOH	
	5 % H ₂ C ₂ O ₄	
Sb(III) (100 µg L ⁻¹)	5 % CH ₃ COOH	10 – 20 – 35 – 360 – 720s
Cd (40 µg L ⁻¹)	25 % HCOOH	10 – 30 – 300 s
Pb (25 µg L ⁻¹)	5 % HCOOH	10 – 20 s
Pb (20 µg L ⁻¹)	2 – 5 – 10 – 15 – 25 – 50 – 75 % CH ₃ CH ₂ OH	15 – 30 – 60 – 180 – 300 – 600
Sn (150 µg L ⁻¹)	25 % HCOOH	60 – 120 – 180

Table 19: Photochemical generation working conditions for the different analytes specified. LMWOC: low molecular weight organic compound; t_{UV}: irradiation time.

Analyte	λ (nm)	Matrix modifier (μg per firing)	T_p ($^{\circ}\text{C}$)	T_a ($^{\circ}\text{C}$)
As	193,7	Pd (2,5), Mg (1,5)	1200	2600
		Pd (2,5), Mg (μg)	1300	2600
Cd	228,8	Pd (5)	800	1000
Fe	248,3	-----	1100	2100
Ni	232,0	-----	1000	2500
Pb	283,3	$\text{NH}_4\text{H}_2\text{PO}_4$ (50)	800	1200
		Pd (5)	1100	2200
Sb	217,6	Pd (2,5), Mg (1,5)	1200	2200
		Pd (5)	1200	2200
Sn	286,3	$\text{Mg}(\text{NO}_3)_2$ (50)	1200	1800

Table 20: ETAAS working conditions. Sample volume: 20 μL . T_p : pyrolysis temperature; T_a : atomisation temperature.

Operative conditions for ETAAS are presented in Table 20. HG-AAS was performed on 10 mL of sample.

4.2.2.6 Results and discussion

Results found, in general, were not consistent; for example in the case of antimony, a 30 % generation efficiency was obtained in 5 % HCOOH and 10s irradiation but these results could not be supported in time. This kind of behaviour was frequent when accomplishing PVG with the in-house reactor.

For cadmium and iron the lack of success in the photochemical generation is more certain. Tin was more studied than the previous and it can be finally concluded that there was no evidence of photochemical vapour generation in none of the working conditions tried.

Generation of volatile species of arsenic (III), lead and nickel turned out to be more uncertain. When repeating analyses some results fell close to the decision zone. For the generating conditions specified in Table 21 efficiencies attained in the most of the cases were between 20 – 30 %.

Analyte	LMWOC	t_{UV}
As(III)	5 % HCOOH	10 s
Pb	5 % HCOOH	10 s
	10 % $\text{CH}_3\text{CH}_2\text{OH}$	30 s
Ni	5 % HCOOH	300 s

Table 21: Photochemical working conditions in which volatile species generation is suspected. LMWOC: low molecular weight organic compound; t_{UV} : irradiation time.

Selenium (IV) behaviour was completely different. Even if results were variable the photochemical generation could be ascertained. As it was the sole which could be determined directly, the assays performed will be discussed separately in **4.2.3.1 Background: indirect evidence of photo generation of volatile selenium derivatives.**

4.2.2.7 Conclusions

Results obtained may suggest photochemical vapour generation of volatile species of arsenic, lead, and nickel in 5 % HCOOH and lead in 10 % CH₃CH₂OH. Direct determination of the volatile species must be performed to confirm.

4.2.3 Photochemical Vapour Generation - Head Space - Single Drop Micro Extraction -Electro Thermal Atomic Absorption Spectrometry (PVG-HS-SDME-ETAAS)

PVG-HS-SDME-ETAAS was developed for the direct determination of arsenic, lead, nickel and selenium: the volatile species were generated by photochemical vapour generation and pre concentrated in a palladium drop at the head space of the generating media after irradiation. Next, the drop was introduced into the graphite furnace and the analyte determined by electro thermal atomic absorption spectrometry.

Selenium was the only analyte that could be determined in this way, thus, this section is dedicated first to the evidence of its photochemical generation by the indirect method and to its direct determination using PVG-HS-SDME-ETAAS. At the end of the section, the results from the attempts to the direct determination of the other analytes are presented.

4.2.3.1 Background: indirect evidence of photo generation of volatile selenium derivatives

20 $\mu\text{g L}^{-1}$ Se - 5 % v/v solutions of formic, oxalic and propionic acid were irradiated during 36, 120 and 300 s. The first irradiation time was achieved introducing the sample at a flow rate of 4,6 mL min^{-1} . For the others a stopped flow mode was used: sample was introduced to the reactor with the lamp already stabilised but turned off and then turned on 2 and 5 minutes respectively.

Efficiency (%)	Irradiation time (s)		
	36	120	300
HCOOH	-----	30	10
CH ₃ CH ₂ COOH	0	10	12
H ₂ C ₂ O ₄	0	0	15

Table 22: Efficiency of the photo generation of selenium derivatives for different LMWOC. Preliminary results.

The determinations for the efficiency calculation were performed by ETAAS in the optimum conditions for each LMWOC. Results are presented in Table 22; apparently selenium derivatives are formed in formic acid. Further studies are now needed in order to ascertain the photo generation and find the best working conditions.

4.2.3.1.1 Formic acid concentration

Triplicates of 20 $\mu\text{g L}^{-1}$ Se solutions at different formic acid concentration were prepared, irradiated in the continuous flow mode and their photo generation efficiency calculated by ETAAS.

c_{HCOOH} (mol L^{-1})	Efficiency (%)
0,5	19
1,2	67
2,3	66
4,6	56
6,0	49
7,0	49

Table 23: Efficiency of the photo generation of volatile species of selenium at different formic acid concentrations

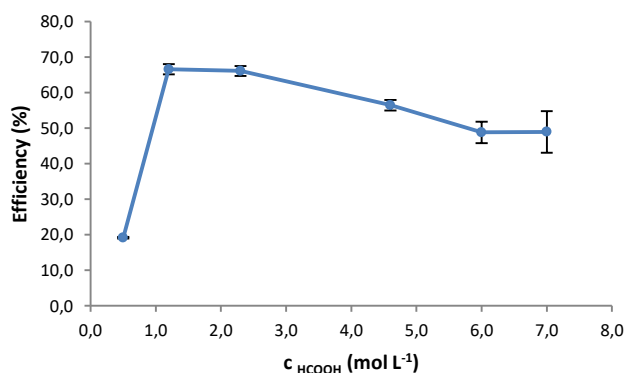


Figure 48: Efficiency of the photo generation of selenium at different formic acid concentrations

Results for the different concentrations of formic acid are presented in Table 23 and plotted in Figure 48 with the respective dispersion.

As can be seen, in the concentration range between 1,2 and 2,3 mol L^{-1} HCOOH there was not much difference in the generation efficiency and although there was a slight decrease up to 4,6 mol L^{-1} , this last acid concentration was also considered because the dispersion was low. From that concentration on, dispersion started to increase and the generation efficiency to diminish as the population of organic radical rises and so the radical – radical recombination.

4.2.3.1.2 Irradiation time

For 1,7 mol L⁻¹ HCOOH (the average of the low concentration range) and 4,6 mol L⁻¹ HCOOH, 20 µg L⁻¹ Se solution was irradiated during 15, 30, 45, 60 y 120 seconds (in triplicate for each time). Results are shown in Figure 49 for 1,7 mol L⁻¹ HCOOH media, similar results were found for 4,6 mol L⁻¹ HCOOH. The highest photo generation efficiency was within 15 and 45 s so irradiation time of 30 seconds was chosen.

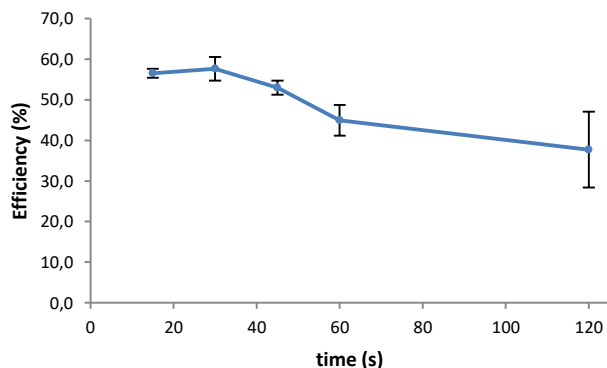


Figure 49: Photo generation efficiency as a function of irradiation time for 20 µg L⁻¹ Se - 1,7 mol L⁻¹ HCOOH.

Increasing irradiation time leads to lower generation efficiencies, probably due to the prevalence of the volatile species decomposition.

4.2.3.1.3 Influence of the analyte concentration

As a high concentration of Se has been reported to form microscopic aggregates when irradiated, triplicates of solutions of 40 and 200 µg L⁻¹ Se in 1,7 y 4,6 mol L⁻¹ HCOOH were assayed. At high selenium concentration efficiency decreased (Table 24).

HCOOH	Se (µg L ⁻¹)	Efficiency (%)
1,7 mol L ⁻¹	40	57
	200	37
4,6 mol L ⁻¹	40	58
	200	39

Table 24: Generation efficiency for low and high levels of selenium in 1,7 and 4,6 mol L⁻¹ HCOOH.

After evaluating the variables: acid concentration, irradiation time and Se concentration, quintuplicate replications samples of 1,7 and 4,6 mol L⁻¹ formic acid 20 µg L⁻¹ Se were irradiated during 30 s. For each concentration of formic acid, the generation efficiency was 60 % with a precision better than 5 %.

Working conditions for the determination by ETAAS are presented in Table 25:

stage	T (°C)		t (s)	ramp (°C s ⁻¹)	Ar (L min ⁻¹)
	1,7 mol L ⁻¹ HCOOH	4,6 mol L ⁻¹ HCOOH			
drying	100	100	30	10	0,2
pyrolysis	1200	900	70	150	0,2
atomisation	2300	2300	3	0	0
cleaning	2500	2500	3	1	0,2
chemical modifier: Pd 1,5 µg – Mg 0,6 µg per firing					

Table 25: Temperature programme of the graphite furnace for Se in 1,7 mol L⁻¹ and 4,6 mol L⁻¹ HCOOH

Photo generation of selenium derivatives has been confirmed and the best generation conditions established; its direct determination is now to be sought.

4.2.3.2 Introduction

Head space single drop micro extraction is a pre concentration technique. Analyte is distributed among three phases: the solution from where the new formed gaseous phase is removed, the head space of the solution and a liquid phase where the gaseous compound is soluble. The last consists on a tiny drop hanging from the tip of a micro syringe.

The overall performance of the extraction method depends on the rate of analyte transference to the gaseous phase, and the transference from the gas phase to the liquid drop; even if the agitation of the solution may induce convection in the head space, the last is done by diffusion as the drop can be considered stagnant. Vigorous stirring of the solution contributes; as the drop is not in contact with the solution, it does not disturb drop stability.

Once reaching the drop, the volatile species transference towards the liquid phase is favoured by the decomposition to a soluble compound, this last process is irreversible and as no other compound but the sorbent is present, it is also interference free (Liu & Dasgupta, 1996) (Mogaddam, Mohebbi, Pazhohan, Khodadadeian, & Farajzadeh, 2018) (Xu, Basheer, & Lee, 2007) (Theis, Waldack, Hansen, & Jeannot, 2001).

The mechanism of caption of the hydrides in the palladium drop is as follows: when hydrides are generated by sodium tetrahydroborate, hydrogen evolves from solution, reaches the drop and reduces ionic palladium:



Hydrides decompose in the metallic palladium (Gil, de Loos-Vollebregt, & Bendicho, 2009). When formic acid is the LMWOC used for the photo generation, there is also a hydrogen evolution. It is assumed volatile species other than hydride are absorbed in the same way.

A scheme of the device is depicted in Figure 50.

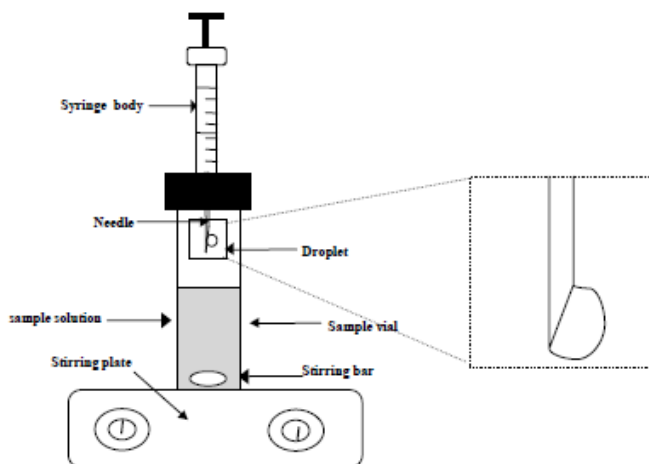


Figure 50: Scheme of the SDME device, extracted from V. Colombini et al. / Talanta 63 (2004) 555–560

Coupling this preconcentration technique with graphite furnace (ETAAS) for the determination allow achieving sensitive measurements. Moreover electrothermal analysis handles with sample volume generally no larger than 50 μL hence, the drop can be manually introduced to the graphite tube and directly analysed (Pena-Pereira, Lavilla, & Bendicho, 2010) (Figuroa, García, Lavilla, & Bendicho, 2005).

4.2.3.3 Experimental section

Photo generated selenium volatiles species were preconcentrated by head space – single drop micro extraction (HS-SDME) and determined by ETAAS.

4.2.3.4 Instrumentation

The **4.2.1 Continuous flow UV reactor** was used for the photo generation. Flow system was fed by the peristaltic pump. Determination of the volatile species absorbed were performed in a Thermo Scientific (Waltham, MA, USA) iCE 3500 AAS Spectrometer with GFS35Z Graphite Furnace fitted with a selenium hollow cathode lamp (Thermo Scientific), Zeeman background correction and pyrolytic coated graphite tubes. The determination was achieved at 196,0 nm. Working conditions were optimised by means of atomisation and pyrolysis curves. Peak area was the analytical signal.

For SDME a 100 μL GC syringe (Hamilton 710, cemented needle) fitted with a 0,8 i.d. PTFE tube pressed at the end of the needle was used in order to prevent its contact with the extractive solution. Tube

protruding from the bottom of the needle could house up to 30 μL of solution; it ended in a bevelled edge so as to hold the drop.

4.2.3.5 Reagents and solutions

Diluted solutions were prepared with deionised water (ASTM type I) obtained from a Millipore (São Paulo, Brazil) Direct-Q 5 water purifier. Se(IV) 1000 mg L^{-1} standard solution was prepared from sodium selenite (Aldrich, 99 %). Selenium working solutions were prepared daily by dilution of the Se(IV) 1000 mg L^{-1} standard solution in 1 mol L^{-1} HCl.

Palladium absorbent solution (35 mg L^{-1}) was prepared by dilution with 0,1% v/v HNO_3 of palladium Chemical Modifier (Merck, matrix modifier for graphite furnace, 10 g L^{-1}). Analytical reagent grade formic acid was used.

Standard N_2 , was obtained from Air Liquide Uruguay S.A. .

4.2.3.6 Procedure

The lamp was warmed up 60 min Then it was turned off while loading 1,5 mL sample (Se(IV) solution + 1,5 % v/v HCOOH). After 30 s of irradiation it was turned off again and sample eluted to a 4 mL vial provided with a septum in the cap and a 2 mm magnetic bar. The vial containing the solution was gently closed without tighten it.

The syringe was loaded first with a 2 - 3 μL bubble, then 8 μL of the palladium solution and another little bubble. The syringe was introduced through the septum, kept vertical by a holder and the drop was let to hang in the PTFE tube (Figure 51).

After 15 min of vigorous agitation drop was retaken and injected manually to the graphite tube of the graphite furnace for selenium determination.

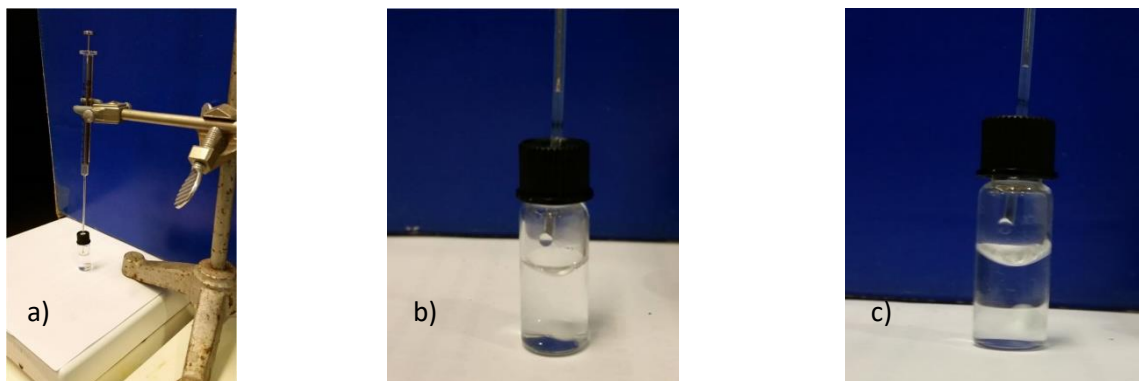


Figure 51: a) HD – SDME device b) without stirring c) with stirring

4.2.3.7 Results and discussion

Different solutions were used as sorbents for the volatile species generated. The ones of first choice were those already used for trapping hydrides when using graphite furnace as atomiser, for example the mixture Ce(IV)/I₂ in different ratios and palladium solutions in different concentrations. They also act as a chemical modifier for the ETAAS determination (Mandjukov & Tsalev, 1990).

Other parameters optimised were drop size and extraction time; the bigger the drop the more prone to break off while stirring.

Before achieving the determination, optimum drying, pyrolysis and atomisation temperatures were studied for each sorbent by pyrolysis and atomisation curves. A solution of the sorbent and a suitable amount of selenium in the same conditions of the extraction was used.

Table 26 shows the furnace temperature programme for the sorbent chosen (35 mg L⁻¹ Pd).

stage	T (°C)	t (s)	ramp (°C s ⁻¹)	Ar (L min ⁻¹)
drying	100	30	10	0,2
pyrolysis	1000	20	150	0,2
atomisation	2200	3	0	0
cleaning	2500	3	1	0,2

Table 26: Graphite furnace temperature program for selenium determination after HS – SDME.

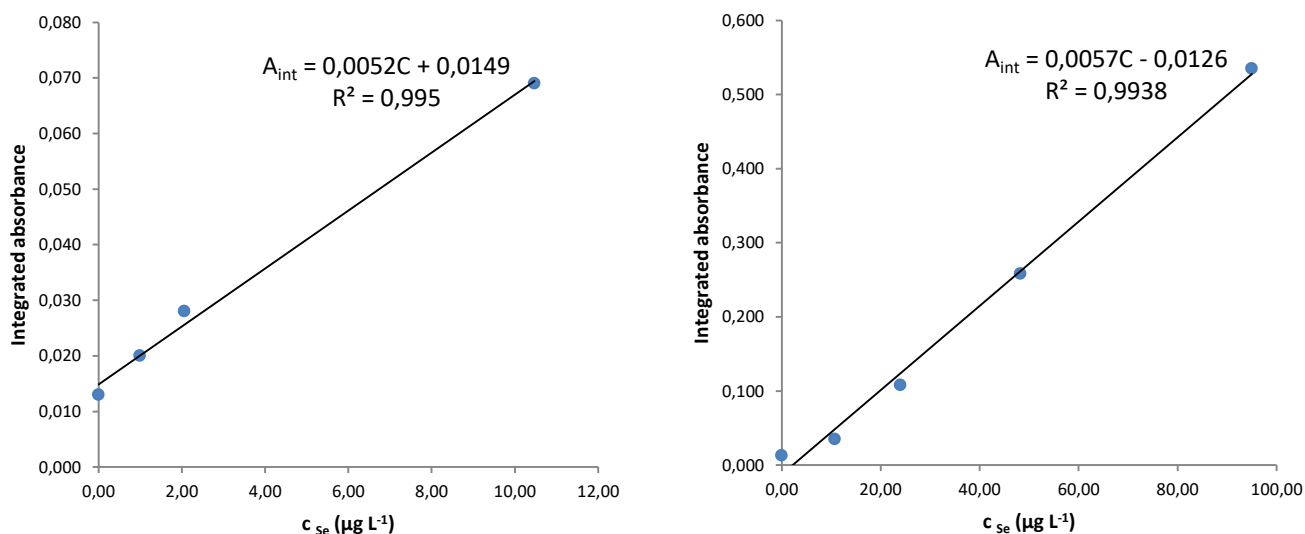


Figure 52: Calibration curves for Se determination by PVG-HS-SDME-ETAAS at low and high concentration ranges. A_{int} : integrated absorbance, C: Se concentration ($\mu\text{g L}^{-1}$)

Figure 52 shows the calibration curves obtained in different concentration ranges, and, as can be seen, a linear response was found up to $100 \mu\text{g L}^{-1}$.

Increasing signals for increased concentration levels is not trivial in this experience; an isolated signal could have been considered an occasional carryover of the solution towards the drop due to turbulences of the stirring, but, facing the tendency yet at low concentrations there is no doubt there is a gaseous selenium compound evolving from the solution. The methodology has its limitations and if intended to be applied, needs improvements especially in terms of dispersion control.

The evolution of the drop since it starts to get out the tube until it stays still hanging needs a careful oversight of the strength applied to the syringe plunger: the surface exposed to the head space must be the same for each determination as it conditions the amount of volatile species transferred from the gas phase to the sorbent. A syringe pump would be ideal as it can deliver precise volumes of sorbent almost with none risk of the drop to fall.

However, the limitation is in the way the volatile species are being determined. It is necessary to increase the handled sample volumes in order to increase the effective amount of gaseous compound reaching the detector so as to avoid the pre concentration stage.

4.2.3.8 Conclusions

Results obtained for selenium by means of PVG – HS – SDME – ETAAS were the first actual evidence of the success of the photo generation; signals were generated by the volatile species themselves. Efforts to continue improving the system as a whole is worthwhile.

4.2.3.9 Other attempts of PVG-HS-SDME-AAS

PVG-HS-SDME-AAS was also performed for lead and nickel. As lead tetrahydride can be absorbed in 1 mg mL^{-1} Ce(IV) – $0,8 \text{ mg mL}^{-1}$ KI (Dedina & Tsalev, Hydride Generation Atomic Absorption Spectrometry, 1995, p. 300), it was also tried as a sorbent in addition to palladium. No previous experience of absorbents for nickel volatile derivatives was available, thus both were tried. Optimum pyrolysis and atomisation temperatures in the absorbent solutions for each analyte are presented in Table 27.

Analyte	Absorbent / Chemical modifier per firing	T _p (°C)	T _a (°C)
Ni	0,60 µg Pd	1100	2800
	8 µg Ce(IV) – 6,4 µg KI	1100	2600
Pb	0,60 µg Pd	900	1700
	0,28 µg Pd	900	1700
	8 µg Ce(IV) – 6,4 µg KI/ 30 µg Pd – 3 µg Mg	900	1800

Table 27: Graphite furnace working conditions for the different analytes. Except for Pb in Ce(IV)/KI, sorbent acted as chemical modifier. T_p: pyrolysis temperature (°C); T_a: atomisation temperature (°C).

Palladium absorbent solutions (35 mg L^{-1} and 75 mg L^{-1}) were prepared by dilution with 0,1% v/v HNO₃ of palladium chemical modifier (Merck, matrix modifier for graphite furnace, 10 g L^{-1}). Ce(NH₄)₂(NO₃)₆ and KI were of analytical reagent grade.

4.2.3.9.1 PVG-HS-SDME-AAS: lead

Solutions (0 – 12 – 24 – 50 – 72) µg L⁻¹ Pb – 10 % v/v CH₃CH₂OH were sequentially irradiated for 30 s. Each of them was collected in 4-mL vial provided with a septum in the cap and a 2 mm magnetic bar. The vial containing the solution was gently closed without tightening it.

The syringe was loaded first with a 2 - 3 µL bubble, then with 8 µL of the Ce(IV) / KI solution and another little bubble. The syringe was introduced through the septum, kept vertical by a holder and the drop was let to hang in the PTFE tube pressed in the syringe needle.

After 15 min of vigorous agitation the drop was retaken and injected manually into the graphite tube of the graphite furnace. 30 µg Pd – 3 µg Mg chemical modifier was added and lead determined by ETAAS.

The analytical signals from the solutions containing lead were not consistent with their concentrations (Table 28).

c ($\mu\text{g L}^{-1}$)	A _{int} (s)
0	0,027
12	0,038
24	0,067
50	0,062
72	0,041

Table 28: Analytical signal for different concentrations of Pb by PVG-HS-SDME-AAS.

c ($\mu\text{g L}^{-1}$): concentration of the lead solutions; A_{int}: integrated absorbance (s).

Due to the variability of the results for the same solution and the lack of correlation between the signals and the concentration, the net signal could have different explanations:

Photochemical generation was being achieved but the transference of the volatile species to the absorbing solution was not suitable and thus needed to be optimised in terms of extraction time and / or absorbent concentration.

Photochemical generation was not taking place and the net signal was due to a carryover to the absorbent solution as the result of a too vigorous stir. This fact could have been confirmed by stirring a lead non irradiated solution (not done).

When instead of using Ce(IV) / KI as absorbent solution, 35 mg L⁻¹ and 75 mg L⁻¹ Pd solutions were used, there was no significant differences between the drop signal of the lead solutions and the blank. Again, possible explanations could be:

Photochemical generation was being achieved but the transference of the volatile species to the absorbing solution was not taking place thus the absorbent was not suitable.

Photochemical vapour generation is not taking place. As the agitation rate was the same as with the other absorbent, this fact can discard the possibility of solution carryover previously suggested.

With the experiences performed and the results obtained no conclusions about the photochemical generation of lead volatile species can be drawn.

4.2.3.9.2 PVG-HS-SDME-AAS: nickel

Volatile species generation of nickel were attempted in 5 % v/v HCOOH. Pd and Ce(IV) / KI were tried as absorbent solutions. The dispersion between replicates could not be handled. For the sake of exemplifying, some results are presented in Table 29:

	A _{int} 1	A _{int} 2	A _{int} 3	A _{int} 4
20 µg L ⁻¹ Ni	0,102	0,046	0,058	0,223
blank	0,023	0,019	0,016	0,017

Table 29: Analytical signal for different replicates of Ni in 5 % HCOOH by PVG-HS-SDME-AAS and their corresponding blank signals using 75 mg L⁻¹ Pd as absorbent solution. A_{int}: integrated absorbance (s).

Contamination of the graphite furnace was of concern. Frequent instances of cleaning with 0,1 % HNO₃ heating programs had to be performed mainly when direct injections of standard solutions for peak control were accomplished.

As for the case of lead, no conclusions could be drawn about photochemical volatile species generation of nickel.

Chapter IV

In-house reactor

Scientific Production

Foto-generación de derivados volátiles de selenio*Mollo, Alicia; Knochen, Moisés*

Química Analítica, Facultad de Química, Universidad de la República

La generación de especies volátiles para la determinación de elementos a nivel de concentración traza reviste gran importancia en Química Analítica ya que a la vez que se separa la fase gaseosa del resto de la muestra, aumenta la sensibilidad del análisis y disminuye la interacción con la misma mejorando el control de las interferencias.

Generalmente, el selenio es determinado a partir de Se (IV) en medio ácido con tetrahidrobórato de sodio por espectrometría de absorción atómica mediante generación de hidruros [1].

Recientemente, se ha propuesto la formación de derivados volátiles metálicos de ácidos de cadena corta que se forman al irradiar la solución que los contiene con radiación ultravioleta. De esta forma, se evita el empleo de tetrahidrobórato de sodio, reactivo de alto costo, ecotoxicidad y baja estabilidad así como también los medios fuertemente ácidos [2].

En el presente trabajo se foto-generaron especies volátiles de selenio en solución de ácido fórmico 4,6 M. Para eso, se construyó un reactor UV en flujo al cual se introdujeron las soluciones de medida mediante una bomba peristáltica y se irradiaron durante 30 segundos.

En primera instancia, se verificó la formación de la especie volátil determinando el selenio en las soluciones de estudio antes y después de ser irradiadas, mediante espectrometría de absorción atómica electroterma de horno de grafito (GF-AAS). Se observó una disminución en la señal del 75%.

Para la determinación, se recogieron las muestras a la salida del reactor en viales cerrados con septo. A través de éste se suspendió una gota de solución ácida de paladio, que se expuso a los vapores de la solución [3]. Se determinó el selenio extraído en la gota mediante GF-AAS. La solución de paladio cumple la doble función de ser la solución de extracción de la especie gaseosa y el modificador químico para la determinación de selenio mediante GF-AAS. Se optimizaron las condiciones de la determinación mediante curvas de pirólisis y atomización en esas condiciones.

Se realizó la foto-generación y micro extracción para soluciones de 10 a 100 $\mu\text{g L}^{-1}$. Se evaluó el área de pico en función de la concentración encontrándose una relación lineal, $A_p = 0,006.C - 0,020$ (A_p = área de pico, C concentración en mg L^{-1}), $r^2 = 0,9999$.

La generación fotoquímica de especies volátiles de selenio con micro extracción en gota de paladio y determinación por GF-AAS, es una promisoriosa alternativa a la generación de hidruros convencional.

[1] Dedina, J.; Tsalev, D.L., Hydride generation Atomic Absorption Spectrometry. Chichester: John Wiley & Sons Ltd, 1995, 127, 308.

[2] Guo, X.; Sturgeon, R.E.; Mester, Z.; Gardner, G. J., Vapor generation by UV irradiation for sample introduction with Atomic Spectrometry. Anal Chem; 2004; 76; 2401-2405.

[3] Fragueiro, S.; Lavilla, I.; Bendicho, C. Hydride generation-headspace single-drop microextraction-electrothermal atomic absorption spectrometry method for determination of selenium in waters after photoassisted prerelution. Talanta; 2006; 68; 1096-1101.

Chapter IV

Commercial reactor: Continuous flow and flow injection manifolds

This section contents a general description of the manifolds used for the photochemical generation with a commercial reactor, both continuous flow and flow injection. A brief comment of their component is also included. Likewise, the first attempts in photo generation are described.

4.3 Experiences achieved with the commercial reactor

4.3.1 Reactor description

A commercial flow through photo reactor was purchased at Beijing Titan Instrument Co. Ltd, Beijing, China.

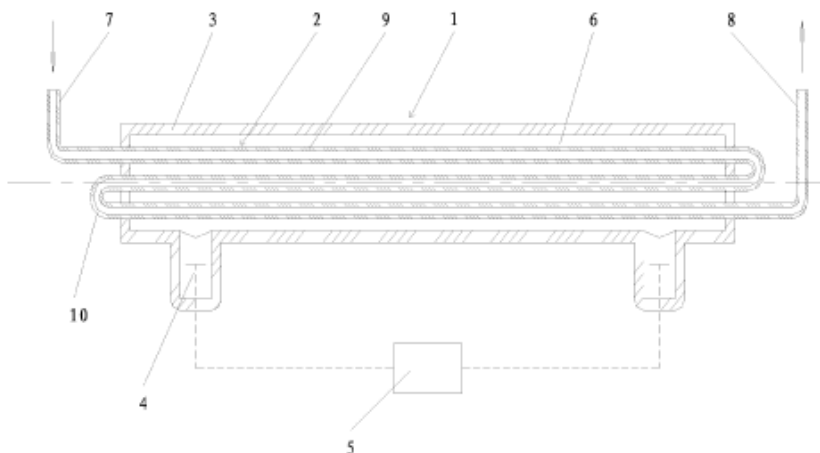


Figure 53: Diagram of the UV reactor 1: low pressure mercury lamp; 2: sample quartz tube; 3: lamp quartz tube; 4: tungsten electrodes; 5: power source; 6: sealed gas chamber between inner lamp tube and outer sample quartz tube; 7: sample inlet; 8: sample outlet; 9: straight line section of the sample quartz tube; 10: bending section of the sample quartz tube that communicate both parallel straight sections of the sample quartz tube.

Figure 53 shows its diagram. It is a 19W low pressure mercury lamp with a 720 μL reaction tube (1019 mm in length \times 0.30 mm i.d.⁷) inserted into the gas chamber itself, preventing the photons to be absorbed by the molecules of oxygen and nitrogen of the air. The design of the reactor and the high transmissivity of the sample quartz tube allow maximum irradiation efficiency, as sample is irradiated from multiple directions with high intensity.

⁷ These are the dimensions given by the supplier company; however, they do not match for that volume (72 μL should be expected). The inner volume was calculated timing a known flow through it and 720 μL is dependable; its length is also coincident. Apparently the wrong data is the tube's inner diameter, that should be 0,95 mm most similar to what with a naked eye seems.

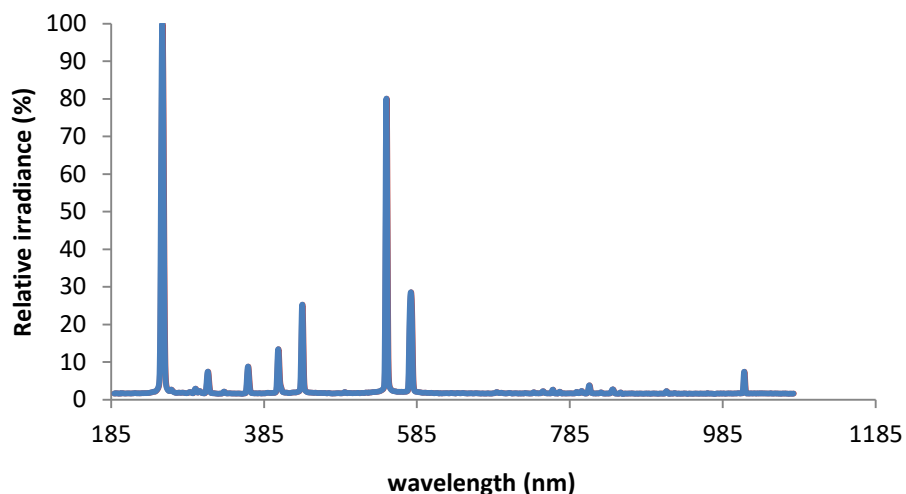


Figure 54: Spectrum of the UV reactor's lamp.

The emission spectra of the low pressure mercury lamp used was obtained with a concave grating spectrometer (StellarNet BLACK-Comet-SR) and is displayed in Figure 54 plotting the relative irradiance as a function of the wavelength. The maximum emission was measured at 252,5 and was taken as the reference (100 %).

As shown in Figure 55, for the operator's protection the reactor was mounted in an inner aluminium covered plastic box. The thermal irradiation from the lamp is quite important, so, a PC fan (Figure 56) and four vents (Figure 57) were installed for the lamp refrigeration. The whole system was assembled in the Faculty of Chemistry's Tools and equipment workshop.

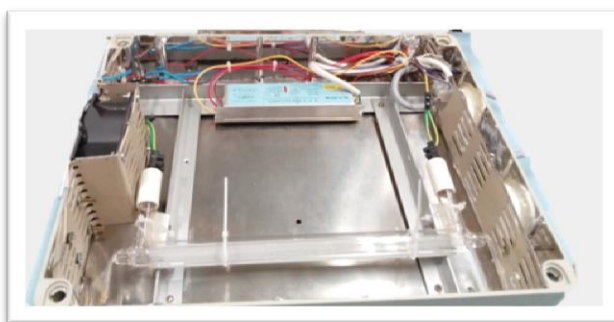


Figure 55: UV reactor holder. Internal view.



Figure 56: Lateral external view of the reactor from the fan side outlet **Figure 57:** Lateral external view of the reactor from the airing outlet

The reactor was mounted in both a continuous flow and a flow injection system. The first served as a screening tool for the evaluation of the feasibility of the photo generation process for the elements tried. Once confirmed, the second was mounted for the working condition's optimisation.

4.3.2 Continuous flow manifold

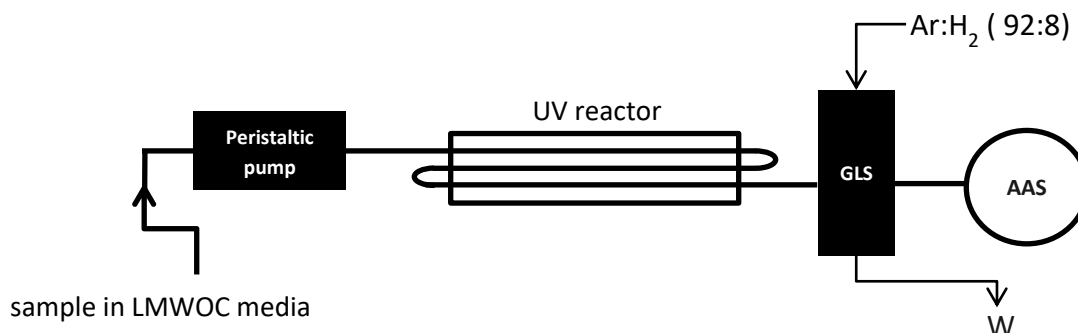


Figure 58: Continuous flow manifold. LMWOC: low molecular weight organic compound; GLS: forced outlet gas liquid separator; AAS: atomic absorption quartz detection cell; W: waste

The continuous flow analyser described in Figure 58 consists on a single line system composed by a peristaltic pump, the UV reactor, a forced outlet gas-liquid separator, and a gas stream that let the volatile species reach the absorption cell mounted in an atomic absorbance spectrometer (Thermo Scientific iCE 3500) provided by a hollow cathode lamp and deuterium background correction. For elements other than mercury an electrically heated quartz cell was used. The determination is achieved by atomic absorption spectrometry. An absorbance continuous signal is obtained whose magnitude at the steady state serves as the analytical signal.

Sample (analyte already mixed with the derivatising agent) is taken by the peristaltic pump and pushed towards the UV reactor. There, radiation is absorbed and the volatile species are generated. The irradiation time, which means the time sample last inside the reactor, is determined by the pump speed and the inner diameter of the tube. Once leaving the reactor, the solution enters the forced outlet gas-liquid separator where a mixture of argon and hydrogen sweep the volatile species away up to a quartz atomisation cell. The gas at the gas-liquid separator in addition to its transport function promotes the atomisation in the cell when hydrogen is necessary in this step.

4.3.3 Flow injection manifold

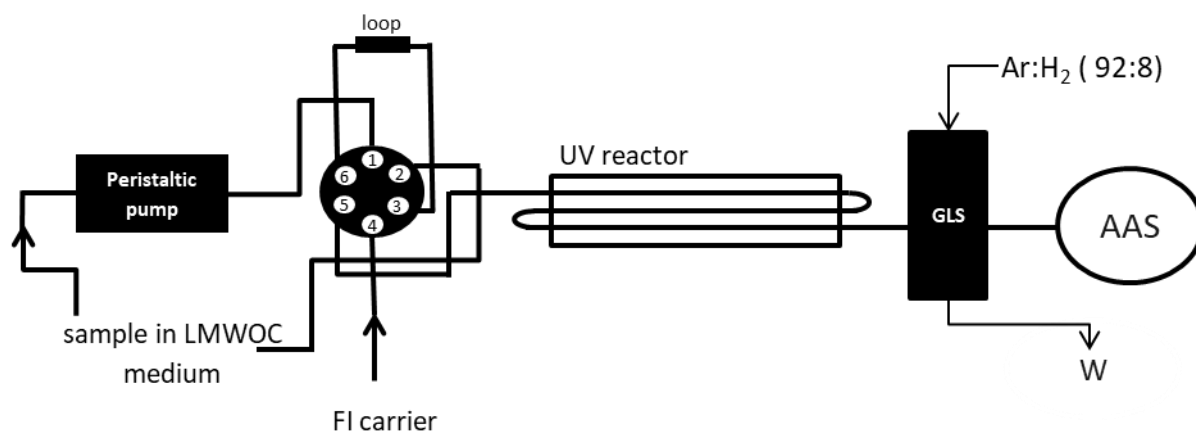


Figure 59: Flow injection manifold: LMWOC: low molecular weight organic compound; FI carrier: flow injection carrier; IV: injection valve; GLS: gas-liquid separator; AAS: atomic absorption quartz detection cell; W: waste

As depicted in Figure 59, the photochemical generation system consists on a single line flow injection system provided by a six-port injection valve. As will be explained later, the FI carrier is air or nitrogen. When sample is injected, air or nitrogen fills the loop. Whenever the valve is let to the reload position again, loop fills pushing gas through the waste. Sample inlet and sample waste are both connected to the same sample flask in a closed circle as there is no risk of sample dilution.

0,15 – 0,6 – 1,0 and 2,0 mL loops were made of 0,8 mm inner diameter PTFE tubes.

A transitory absorbance signal is obtained which area (integrated absorbance) serves as the analytical signal.

4.3.4 Atomic absorption cells

4.3.4.1 Absorption cell (mercury)

A 15 cm long, 0,7 cm inner diameter absorption cell was used. As can be seen in Figure 60, it is a closed cell fitted with two quartz windows. It has an inner and outlet arm at 0,5 cm from the extremes so as gas phase from the gas-liquid separator can enter and leave the absorption volume. Considering the safety hazards of gaseous atomic mercury, the outlet arm is connected to a waste flask, where the outgoing gas bubbles in an acidic permanganate solution where mercury is fixed as ionic mercury (II) (Figure 61).

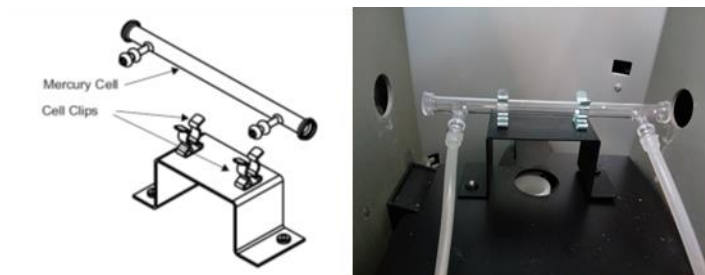


Figure 60: Mercury absorption cell.



Figure 61: Mercury absorption cell: inlet connected from the gas-liquid separator, outlet connected to the waste flask.

4.3.4.2 Atomisation cell

For the elements other than mercury, an atomisation cell (Figure 62) is used, consisting in a silica T-shaped open ended cell, 12 cm long and 0,8 cm of internal diameter. The cell is heated in an electrical device, protruding 0,7 cm from each side of it and connected to the gas-liquid separator by a 0,8 cm outer diameter Tygon tubing.

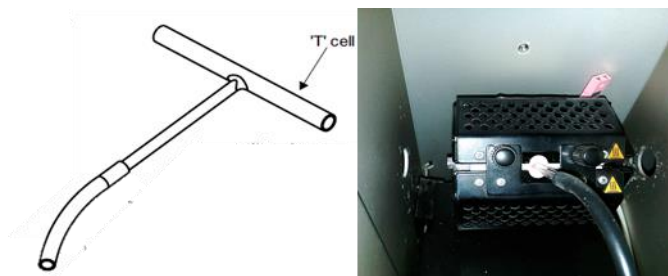


Figure 62: Atomisation cell and atomisation cell in heating device

The heating device is aligned in the sample compartment of the spectrometer; its temperature range is from ambient to 1000 °C in 1 °C steps. It has a 220V, 50 Hz power supply.

4.3.5 Peristaltic pumps

Peristaltic pumps were used for sample introduction to the system and to force the sample out of the gas-liquid separator. In the continuous flow system pump speed and tube diameter determines the irradiation time, so pump flow is relevant.

When using continuous system, the reactor was mounted in a card box with the inlet and outlet sample tubes extending beyond the irradiation zone so, just the inner lamp tube was exposed to UV. In that condition, irradiation time could be calculated with the flow of the sample and the inner volume of the quartz tube (720 µL).

Pump flow rate was determined for the Tygon tubes in use as follows: water was propelled by the pump and weighed for a timed number of seconds. The corresponding mass was transformed to volume considering the density of water 1,0 g mL⁻¹. The determination was repeated three times for each pump speed. Once the flow rate was determined, the time lasting for the flow to go across the 720 µL was calculated. In order to find the mathematical relation between them, a plot of instrument indication vs irradiation time was drawn. Two peristaltic pumps were used: Rainin, Dynamax RP-1 (Figure 63) and Thermo Scientific VP100 (Figure 64 and Figure 65).

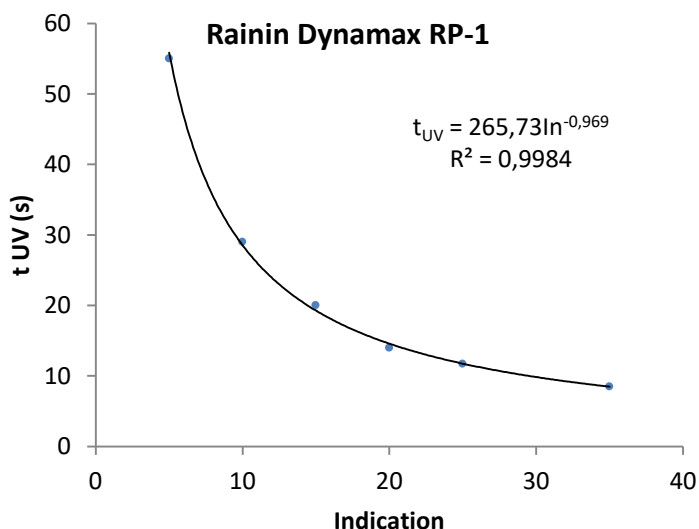


Figure 63: Correlation between pump speed instrument indication and irradiation time (s) for the Rainin, Dynamax RP-1 peristaltic pump fitted with a 1,52 mm inner diameter Tygon tube. t_{UV} : irradiation time (s); In: indication

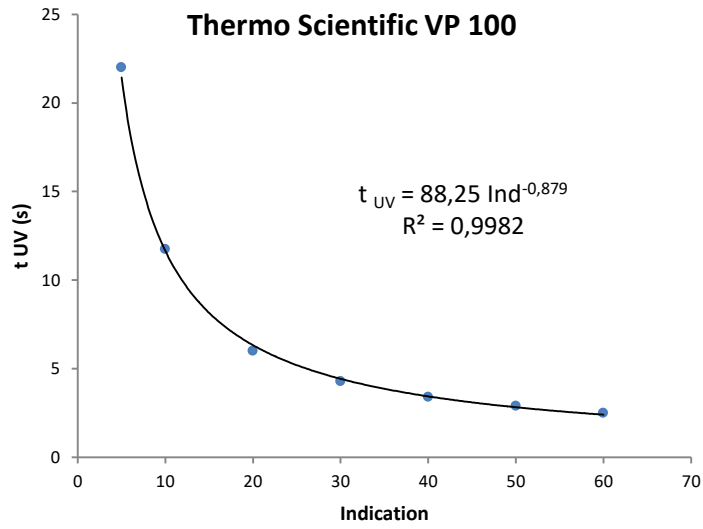


Figure 64: Correlation between pump speed instrument indication and irradiation time (s) for theThermo Scientific VP100 peristaltic pump fitted with a 3,16 mm inner diameter Tygon tube. t_{UV} : irradiation time; Ind: indication.

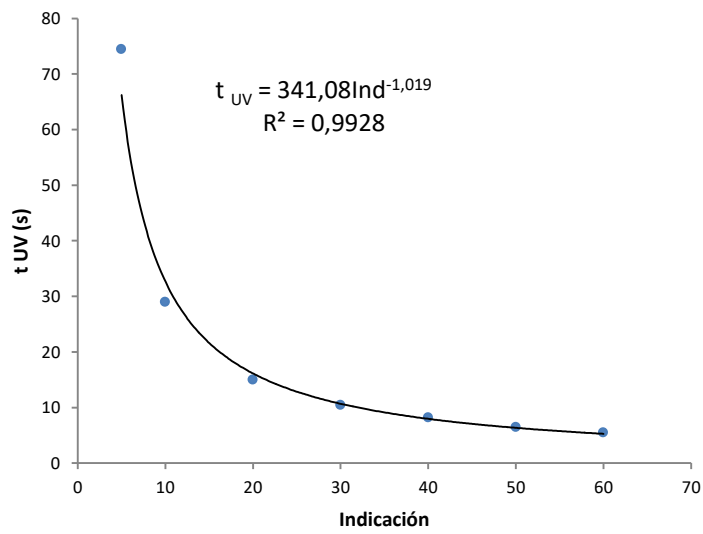


Figure 65: Correlation between pump speed instrument indication and irradiation time (s) for theThermo Scientific VP100 peristaltic pump fitted with a 1,52 mm inner diameter Tygon tube. t_{UV} : irradiation time; Ind: indication.

The irradiation time was verified for some indications with a chronometer, measuring the time from solution entering and leaving the reactor, finding the same results as previously calculated.

By reading the pump display, with the formula calculated, the irradiation time is known. In some instances stopped-flow was also tried but larger times are prone to solution evaporation caused by the lamp heat; the irradiation times reached within both tubes from 2,5 up to 74,5 s let avoid that drawback.

4.3.6 Gas-liquid separator

A forced outlet gas-liquid separator provided by the Thermo Scientific VP100 was used (Figure 66). It has an approximate 4 cm³ volume reaction zone where the solution is mixed with the gas (argon hydrogen mixture in this work) so as to the volatile species be pushed out of the solution. It is filled with 4mm glass beads for improving both phases blending and diminishing the dead volume. The hydrophobic membranes fitted in the base of the expansion volume let the volatile species pass through but prevents the evaporation and carryover of water and it condensation in the tube which connects the cell and the cell itself.

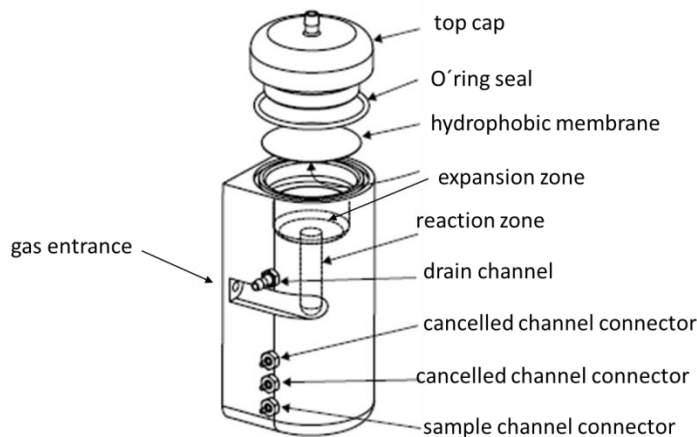


Figure 66: Forced outlet gas-liquid separator

As it is a commercial device for HG-AAS, it has foreseen three inlets (sample, carrier and reductant) and one outlet (drain channel) for the remaining solution. Pump pushes the solutions inside the GLS and they rise along a narrow path until they reach the reaction zone. In this case, as only the solution emerging from the UV reactor reaches the GLS, the others two channels have been cancelled.

Even though the manufacturer's recommendations are not to let beads in the floor of the expansion volume, for certain working conditions, best results were found filling the expansion volume with glass beads. For selenium determination, there is a remarkable difference between the signals with the expansion zone empty or filled (Figure 67).

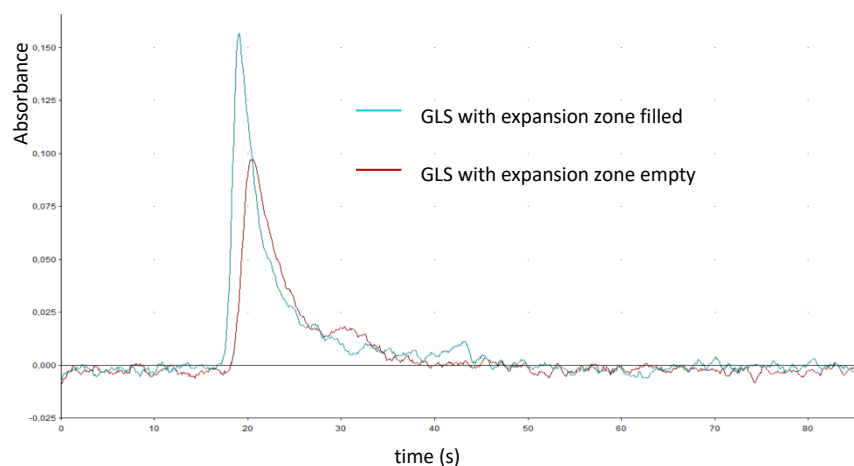


Figure 67: Selenium signal using the gas liquid separator empty or filled with glass beads.

The incidence is only noticed in the case of selenium; for mercury determination, the GLS filling is not relevant, as peak shape and calibration's curve slope are not affected. It cannot be ascertained if it is inherent to the volatile species generated or to the respective flow system.

4.3.7 Data acquisition software

Data acquisition was achieved by the SOLAAR software for Thermo Scientific iCE 3000 Spectrometers. According to the system used, continuous or transient signal parameters can be obtained. For the last, the program records both absorbance and integrated absorbance at the time; as soon as the sample is manually injected, the program is run and the absorbance in function of the time is displayed. The maximum reading time is 100 s and the program has the possibility of integrating within an assigned range of time. With this last option peak area is more accurately calculated improving the reproducibility of the measurements.

The software displays the signal of the background, the signal of the analyte and the corrected one. Aiming to make clear the visualisation, whenever signals are presented they correspond to the background corrected one.

4.3.8 First attempts in photochemical vapour generation

4.3.8.1 Experimental section

The first studies driven with the commercial reactor were focused in finding working conditions where photo generation could be evidenced in order to proceed afterwards with the optimisation stage. Conditions similar to those most frequently tested in the literature were the first tried.

4.3.8.2 Instrumentation

The continuous flow system shown in **4.3.2 Continuous flow manifold** was used. The detection system uses, depending on the analyte, the absorption cell (4.3.4.1) or the atomisation cell (4.3.4.2) mounted in the iCE3000 Thermo Scientific Spectrometer (Waltham, MA, USA) fitted with the appropriate hollow cathode lamp (Thermo Scientific).

4.3.8.3 Reagents and solutions

Diluted solutions were prepared with deionised water (ASTM type I) obtained from a Millipore (São Paulo, Brazil) Direct-Q 5 water purifier. Antimony, arsenic, cadmium, lead, mercury and tin working solutions were prepared daily by dilution of their corresponding 1000 mg L⁻¹ atomic absorption standard solution. Selenite solutions were prepared daily from sodium selenite (Aldrich, 99 %) dissolution in 1 mol L⁻¹ HCl.

Acetic, formic and hydrochloric acid (36% w/w), and ethylic alcohol were of analytical reagent grade. High purity, mixture of Ar: H₂ (92:8) was obtained from Air Liquide Uruguay S.A..

4.3.8.4 Procedure

Table 30 shows for the element tried in the media mentioned. In each case, different irradiation time and argon hydrogen flow rate were tried.

	HCOOH 5 mol L ⁻¹	CH ₃ COOH 0.8 % HCl 0.01 %	CH ₃ CH ₂ OH 10 %	CH ₃ CH ₂ OH 10 % HCl 0.01 %
As (µg L ⁻¹)	274	100	100	
Cd (µg L ⁻¹)	540			
Pb (µg L ⁻¹)	280	130 ^(*)	150	
Sn (µg L ⁻¹)		150	150	120
Hg (µg L ⁻¹)			15 ^(*)	100
Sb (µg L ⁻¹)	100		100	180
Se (µg L ⁻¹)	100	150 ^(*)	100	100

Table 30: Concentration of the analytes assayed at different media. The signal found for the working conditions marked with (*) are shown in Figure 68, Figure 69, and Figure 70.

4.3.8.5 Results and discussion

The first evidences of photo generation found are shown in

Figure 68, Figure 69 and Figure 70 :

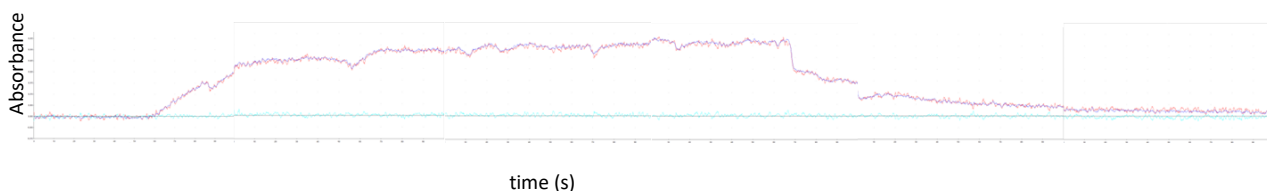


Figure 68: Pb ($130 \mu\text{g L}^{-1}$), in 0,01% w/wHCl, 0.8% w/w CH_3COOH ; irradiation time 14 s; Ar:H₂ 200 mL min⁻¹; atomisation temperature: 900°C. The decrease in the signal corresponds to the replacement of the lead solution by water (*).

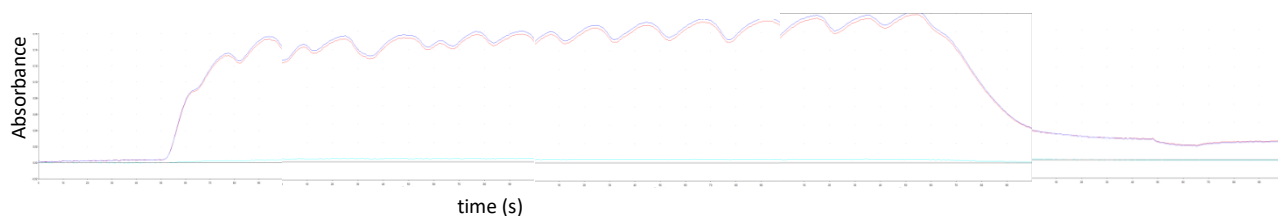


Figure 69: Hg ($15 \mu\text{g L}^{-1}$) in $\text{CH}_3\text{CH}_2\text{OH}$ 10%; irradiation time: 14 s, Ar:H₂: 200 mL min⁻¹. The decrease of the signal corresponds to the replacement of the mercury solution by water (*).

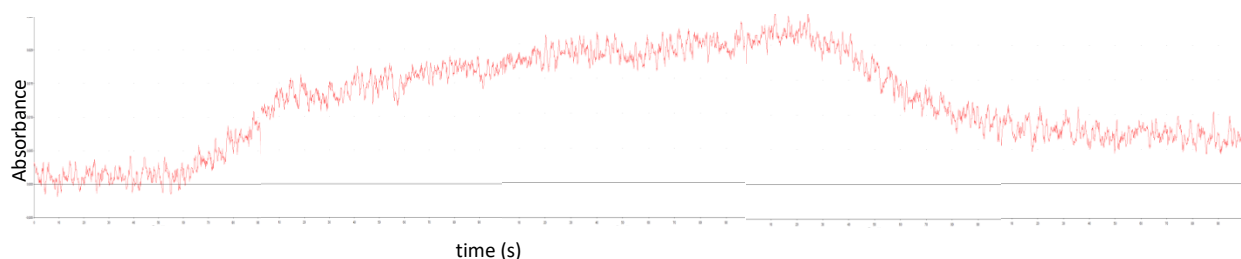


Figure 70: Se ($150 \mu\text{g L}^{-1}$), in 0.01% w/wHCl, 0.8% w/w CH_3COOH ; irradiation time 14 s; Ar:H₂ 100 mL min⁻¹; atomisation temperature: 900°C. The decrease in the signal corresponds to the replacement of the selenium solution by water. (*)

Tin led to negative and erratic signals and for the other analytes there was no signal at all.

4.3.8.6 Conclusions

In view of the results, mercury was chosen as the analyte to work on at first in order to get experience with the reactor and with the whole process of the photochemical generation.

Chapter IV

Photochemical generation of mercury

This section regards mercury as a tool for learning the technique. In the beginning of the work it was generated in continuous flow but afterwards experience was made in flow injection also. The different variables influencing the response were evaluated and the methodology for its determination partially characterised.

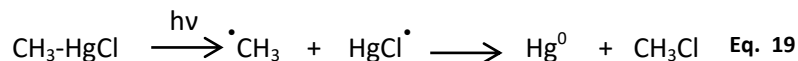
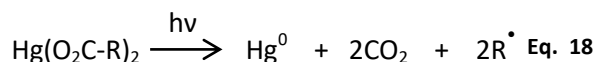
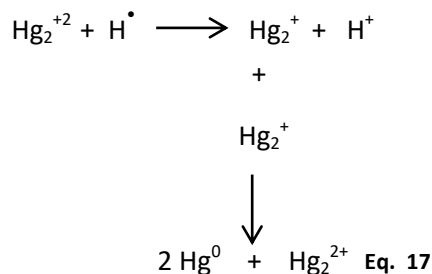
4.4 Photochemical generation of mercury

4.4.1 Introduction

The cold vapour atomic absorption spectrometry technique allows mercury determination at very low levels. Due to its high vapour pressure, 1600 Pa at 20°C, free mercury atoms are formed at room temperature once mercury is reduced without the need of an atomisation step. Strong reducing agents like stannous chloride or sodium tetrahydroborate are the most frequent reagents used for that purpose (Welz & Sperling, 1999).

Mercury was one of the first elements studied for the photo generation process. Photo reduction of mercury can be achieved in the presence of low molecular weight alcohols, aldehydes and carboxylic acids. Best results in terms of generation efficiency were found with formic acid, probably due to its higher absorption and consequent improved generation of reducing species (Han, Zheng, Wang, Cheng, Lv, & Hou, 2007) (López-Rouco, Stanisz, Matusiewicz, Lavilla, & Bendicho, 2008) (Sturgeon R., 2017).

Cold vapour generation in the presence of LMWOC and UV irradiation, depending on the mercury species found in solution, could be achieved (Leonori & Sturgeon, 2019) as presented in Eq. 19:



In the presence of formic acid, both methyl mercury and mercuric ion can be reduced to elemental mercury by 253,7 nm irradiation. Nevertheless, Hg^{+2} can be even reduced with visible light. In order to produce elemental mercury, mercury ion must be first reduced and, in the case of organo mercury compounds the cleavage of the C-Hg bond must first happen. For such break, the appropriate energy (in terms of photon wavelength and intensity) must reach the solution. Photons of both 253,7 and 365,0 nm lines are able to excise the organic substituent, but the latter is less transmitted and needs more time to get the bond broken. This fact was used for speciation purposes (Chen, Lai, Mei, Liu, & Mao, 2017) (Zheng, Li, He, Ma, & Hou, 2005) (Mo, Li, Guo, Zhang, & Wang, 2017).

Sample digestion is of concern as inorganic acid, nitric in particular, can interfere in the photo generation. Thus, alternatives digestion procedures have been tried as, for example, tetramethylammonium hydroxide (TMAH) and even formic acid as tissue solubiliser, in many cases helped by ultrasound assistance.

Vieira *et al* found that TMAH was involved in the photogeneration as well as in the tissue digestion; for clear mercury solutions besides, they found it acted also as a reductant without the need of irradiation (Vieira , Ribeiro, Curtius , & Sturgeon, 2007).

4.4.2 Continuous flow photochemical cold vapour generation (CF-PCVG)

4.4.2.1 Experimental section

Once the mercury photo generation was evidenced, aiming to develop a methodology for its determination, the correlation between the concentration and the magnitude of the signal was sought. For the irradiation time previously found, the argon hydrogen flow was varied as the signal did not reach a plateau in the steady state but a slightly wave shaped continuous signal, probably originated by the pulses of the peristaltic pump.

4.4.2.2 Instrumentation

The **4.3.2 Continuous flow manifold** was used with the 4.3.4.1 Absorption cell (mercury) fitted in the iCE 3000 spectrometer provided by a mercury hollow cathode lamp (Thermo Fisher Scientific (Shanghai) Instrument Co Ltd China). The determination was achieved at 253,7 nm using a deuterium background correction. Rainin, Dynamax RP-1 peristaltic introduced the sample at a flow rate leading 14 s of irradiation, and the argon hydrogen flow was of 100 mL min⁻¹. Deuterium background correction was used and absorbance in the steady state was the analytical signal.

4.4.2.3 Reagents and solutions

Diluted solutions were prepared with deionised water (ASTM type I) obtained from a Millipore (São Paulo, Brazil) Direct-Q 5 water purifier. Mercury working solutions was prepared daily by dilution of the 1000 mg L⁻¹ atomic absorption standard solution.

Ethyl alcohol was of analytical reagent grade.

High purity, mixture of Ar: H₂ (92:8) was obtained from Air Liquide Uruguay S.A..

4.4.2.4 Procedure

Working solutions of (0,0 – 0,10 – 0,5 – 1,0 – 3,0 – 5,0 – 10,0 – 30,0 – 50,0 – 75,0 – 95,0) µg L⁻¹ in 10% w/V CH₃CH₂OH were prepared and triplicates of each solutions read in order to examine if there was a range where linearity could be assessed.

4.4.2.5 Results and discussion

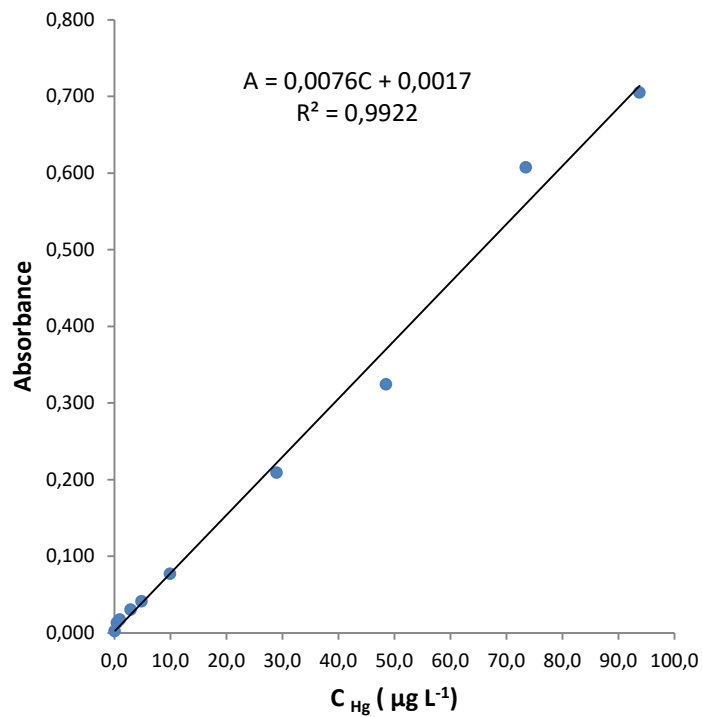


Figure 71: Mercury calibration curve in the continuous flow mode. A: absorbance; C: mercury concentration in $\mu\text{g L}^{-1}$.

As can be seen in Figure 71, the calibration function resulted linear for all the studied range.

4.4.2.6 Conclusions

After the results obtained, the flow injection manifold can be assayed with mercury so as to get transient signals which will be more useful to understand how the different variables of the system affect the response.

4.4.3 Flow injection photochemical cold vapour generation (FI-PCVG)

4.4.3.1 Experimental section

With the aim of learning about how the variables of influence of the photochemical system (type and concentration of LMWOC, irradiation time and transport ratio), impact in the response, a flow injection manifold was built for mercury determination. Thus, the analytical signal is transient, depending on the atom supply to the atomiser and its removal from the atomisation cell.

4.4.3.2 Instrumentation

The flow injection system shown in **4.3.3 Flow injection manifold** was used. The detection system uses, the absorption cell (4.3.4.1) mounted in the iCE3000 Thermo Scientific Spectrometer (Waltham, MA, USA) fitted with mercury hollow cathode lamp (Thermo Scientific). The determination was achieved at 253,7 nm using a deuterium background correction. Flow system was fed by both the Rainin, Dynamax RP-1 and the VP100 peristaltic pumps. The analytical signal was absorbance in the optimisation stage and integrated absorbance for quantification purpose.

4.4.3.3 Reagents and solutions

Diluted solutions were prepared with deionised water (ASTM type I) obtained from a Millipore (São Paulo, Brazil) Direct-Q 5 water purifier. Mercury working solutions were prepared daily by dilution of the 1000 mg L⁻¹ atomic absorption standard solution.

Ethyl alcohol and, formic and acetic acids were of analytical reagent grade.

High purity, mixture of Ar: H₂ (92:8) was obtained from Air Liquide Uruguay S.A..

4.4.3.4 Procedure

Each variable was optimised at a time. When evaluating the LMWOC concentration and the flow injection carrier composition, signals for the same concentration of mercury were compared. For the irradiation time, flow ratio of the gas mixture and generation efficiency, the same working solution was used in each instance.

For calculating the efficiency of the photochemical generation, the continuous flow system **4.3.2 Continuous flow manifold** was mounted. A mercury solution of an intermediate concentration of mercury was passed through the reactor; its absorbance was recorded. After leaving the gas-liquid separator, the remaining solution was collected and again exposed to the UV irradiation; its absorbance was recorded. Generation efficiency was calculated by the signal decrease between successive irradiations:

$$\text{Efficiency (\%)} = \left(1 - \frac{A_2}{A_1}\right) \times 100 \quad \text{Eq. 20}$$

A_1 is the absorbance of the solution when first irradiated and A_2 is the absorbance of the same solution when irradiated the second time. The experiment was run for the three reductant medias (ethanol, formic and acetic acid) in each optimum working condition in what refers to concentration of the LMWOC, irradiation time and gas mixture flow.

4.4.3.5 Results and discussions

When selecting the LMWOC, the FI carrier was the LMWOC itself. Both, the FI carrier flow rate (determining the irradiation time) and the mixture gas flow rate (determining the analyte's rate towards the absorption cell) were varied until finding working conditions where well-shaped peaks were obtained. In that condition, different LMWOC concentrations were tried.

Then, for each LMWOC at the optimum working conditions, some figures of merit characterising the methodology were sought. Aiming not to be reiterative, each variable of the photochemical generation system will be presented at the same time for everyone.

4.4.3.5.1 Low molecular weight organic compound and LMWOC's concentration:

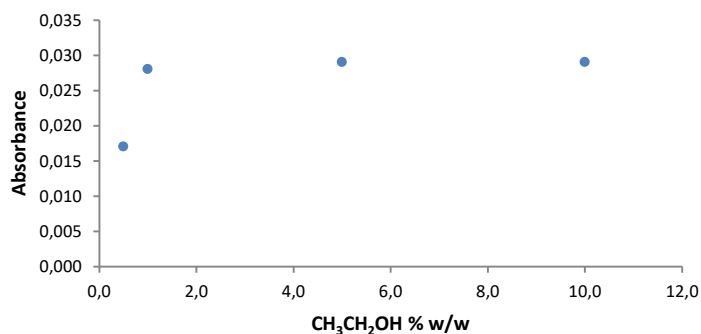


Figure 72: Variation of mercury signal (Absorbance) with ethanol concentration. $50 \mu\text{g L}^{-1}\text{Hg}$; sample volume: 0,15 mL; irradiation time: 6 s; Ar:H₂ flow rate: 200 mL min^{-1}

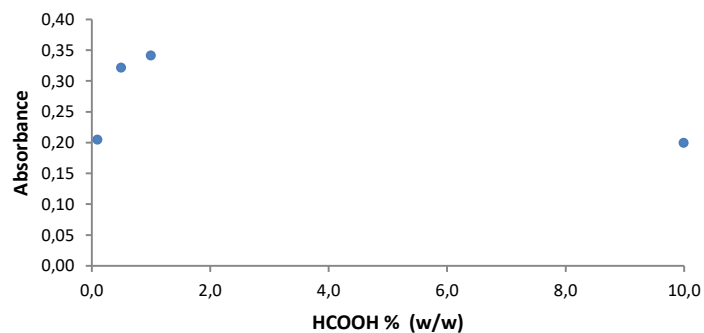


Figure 73: Variation of the mercury signal (Absorbance) with formic acid concentration. $50 \mu\text{g L}^{-1}$ Hg; sample volume: 0,15 mL; irradiation time: 6 s; Ar:H₂ flow rate: 200 mL min⁻¹

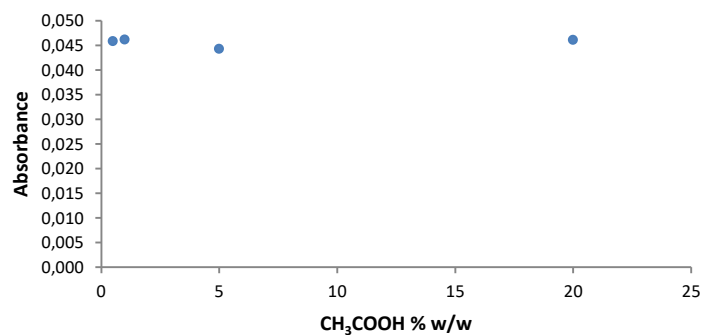


Figure 74: Variation of the mercury signal (Absorbance) with acetic acid concentration. $50 \mu\text{g L}^{-1}$ Hg; sample volume: 1,0 mL; irradiation time: 3,5 s; Ar:H₂ flow rate: 500 mL min⁻¹

Figure 72 to Figure 74 show the variation of the signal at different LMWOC concentrations. As can be seen, for all of them, there is no need of high concentrations for the photo generation to be accomplished, thus, the lowest concentration leading to suitable signal were chosen.

4.4.3.5.2 Carrier composition of the FI system

Air, water and 1,0% CH₃CH₂OH were tried as the carriers of the FI system.

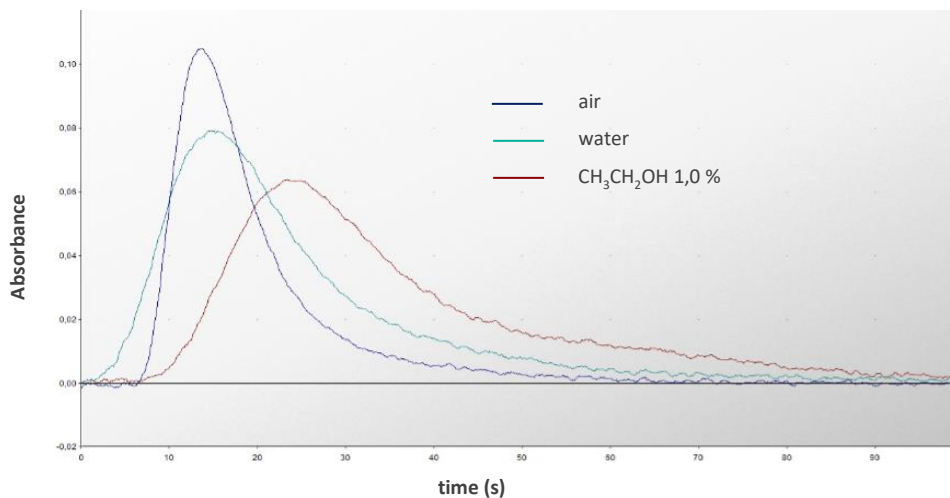


Figure 75: Mercury signal for air, water and 1,0% CH₃CH₂OH as FI carriers. 50 µg L⁻¹ Hg; 1,0% CH₃CH₂OH; Sample volume: 0,15 mL; irradiation time: 6 s; Ar:H₂ flow rate: 200 mL min⁻¹

As can be seen in Figure 75, peaks get slimmer as the flow injection carrier changes from ethanol to water and air. The gaseous phase helped to release the vapour generated from solution. The air supply was provided by a channel of the peristaltic pump (Figure 76). Due to the simplicity of the system and as there is neither sample dilution nor wastes of carrier solution generated, air was taken as the carrier for every LMWOC used. Sample can recirculate in the same flask after each injection.

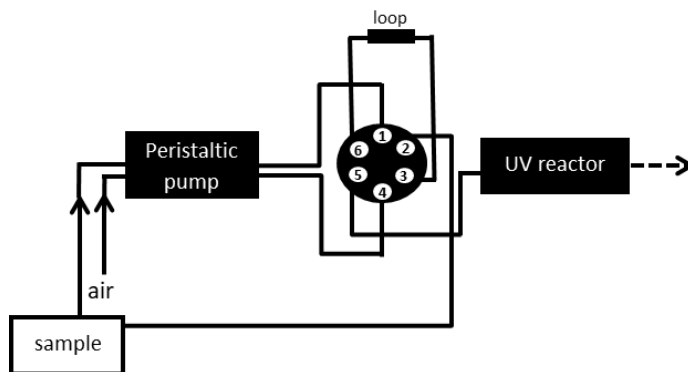


Figure 76: FI system using air as the carrier

4.4.3.5.3 Irradiation time

The irradiation time is the time the sample remains exposed to the UV irradiation passing within the reactor. For each LMWOC, sample was passed through the reactor at different carrier speed (peristaltic pump speed for a given Tygon tube) and peak height measured. The optimum irradiation time was considered as the one whose signal was the highest without much dispersion.

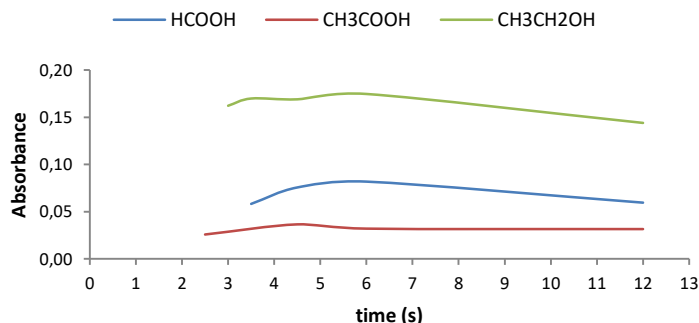


Figure 77: Variation of mercury signal (peak height) for different irradiation times for formic acid, acetic acid and ethylic alcohol respectively.

Figure 77 shows the average of peak height for at least three replicates at different irradiation time. At first sight, there are no considerable variation between the measured times; formic acid and ethanol have a slight maximum between four and seven seconds followed by a barely perceptible decay. For each LMWOC the same solution were measured, but were of different mercury concentration within them. In order to choose the irradiation time, peak shape was visual inspected. Examples are shown in Figure 78 for ethanol and in Figure 79 for formic acid.

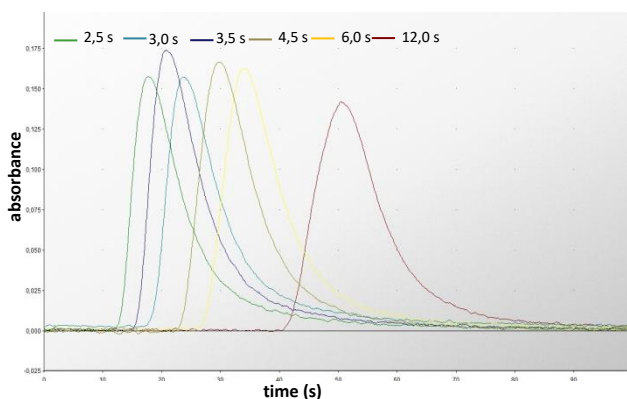


Figure 78: Mercury signal for different irradiation times $60 \mu\text{g Kg}^{-1} \text{Hg}^{+2}$; 1,0% $\text{CH}_3\text{CH}_2\text{OH}$; 0,6 mL sample; Ar:H_2 500 mL min^{-1} .

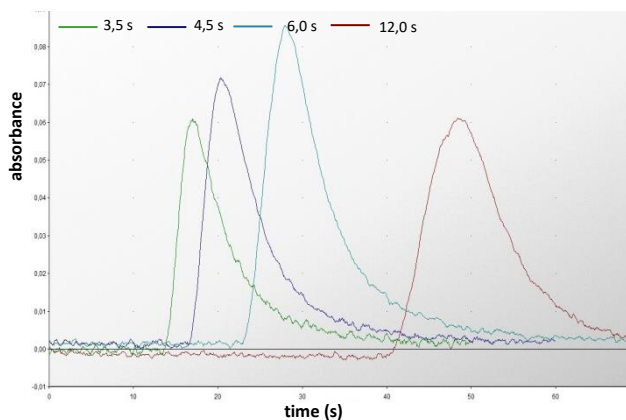


Figure 79: Mercury signal for different irradiation times $60 \mu\text{g Kg}^{-1} \text{Hg}^{+2}$; 0,5% HCOOH ; 0,6 mL sample; Ar:H_2 500 mL min^{-1} .

4.4.3.5.4 Argon : hydrogen (92:8) flow

The gas mixture transports the elemental mercury formed towards the absorption cell. Low flow rates delay the entrance of the bolus of gaseous mercury to the absorption cell leading to short and wide peaks. If too high, sample dilution occurs, the optimum gas flow rates gives balanced peaks in height and width.

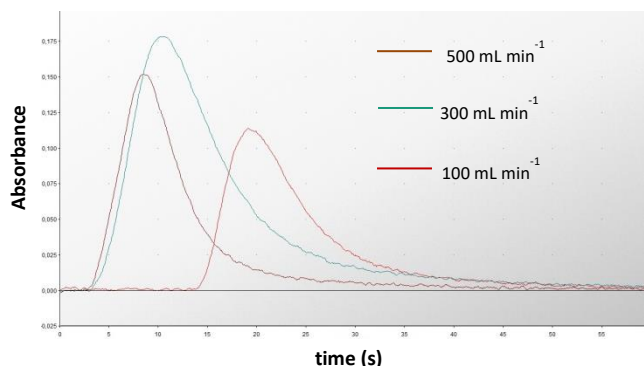


Figure 80: Mercury signal for different Ar : H₂ flow 60 µg kg⁻¹ Hg⁺² ; 1,0% CH₃CH₂OH; 0,6 mL sample

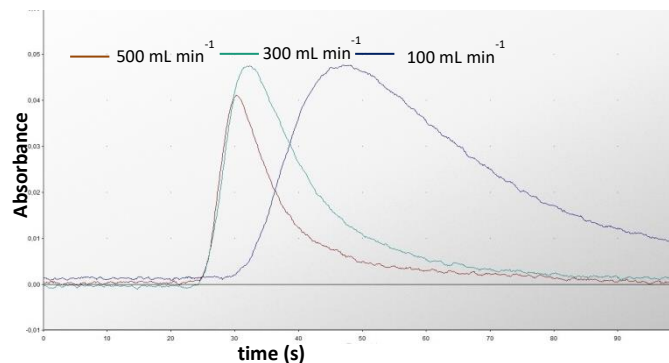


Figure 81: Mercury signal for different Ar : H₂ flow 60 µg kg⁻¹ Hg⁺² ; 0,5% HCOOH; 0,6 mL sample

In both ethanol and formic acid generation media, (Figure 80 and Figure 81), although the highest gas flow decreases a bit the signal, it makes the peak more narrow and thus more suitable for forthcoming quantification purposes. Acetic acid gave the same results. Signals are obtained in the same way for every flow rate, as expected, for each media, the higher the rate, the sooner the peak appears.

As in this case gaseous atomic mercury is the volatile species photo generated, there is no need of hydrogen in the absorption cell. High purity argon was assayed as the carrier gas of the gas-liquid separator but no difference within both types of gases was found (Figure 82). For the sake of operative simplicity the gas mixture remained connected to the manifold for further applications and was used for mercury determination.

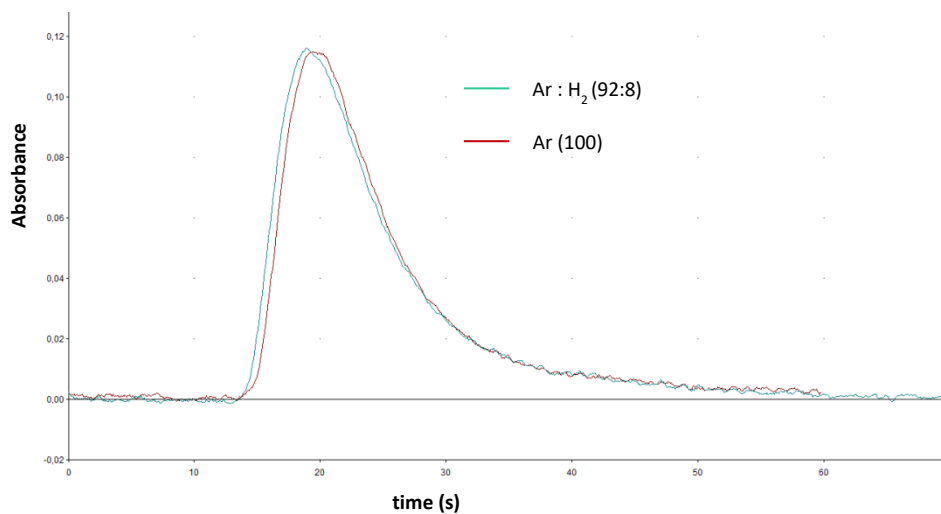


Figure 82: Mercury signal using the mixture Ar:H₂ (92:8) and Ar as the carrier gas in the gas liquid separator

4.4.3.5.5 Sample volume

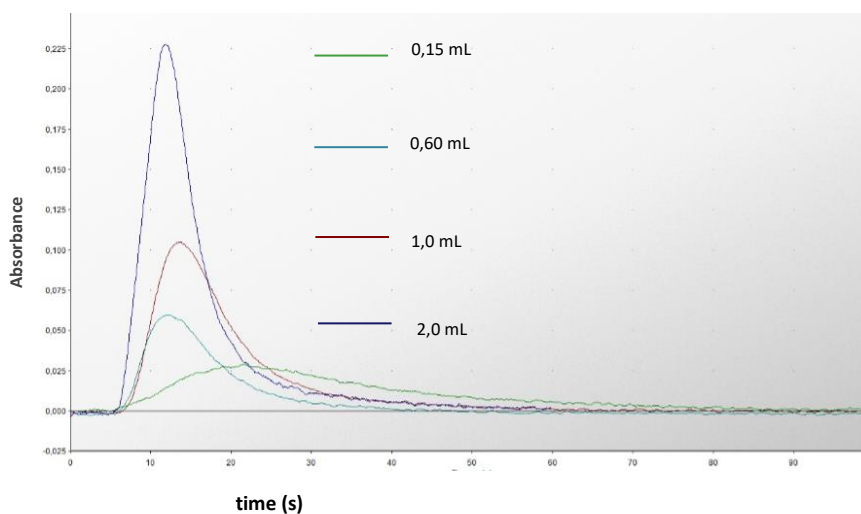


Figure 83: Mercury signal for different amount of sample (different loops). 60 $\mu\text{g kg}^{-1}$ Hg⁺²; 1,0% CH₃CH₂OH; Ar : H₂ 500 mL min⁻¹.

The amount of gaseous atoms of mercury reaching the absorption cell depends on the volume of sample injected thus samples amounts of 0,15 – 0,6 – 1,0 and 2,0 mL were evaluated. As shown in Figure 83, increasing the volume of sample leads to higher and narrower peaks. No larger loops were tried for sample saving.

4.4.3.5.6 Efficiency

The efficiency of the photochemical generation applies to the fraction of the analyte that can be removed from solution and determined in the whole process. It was evaluated as the signal decay for the same solution after being irradiated. Before the collection of the remaining solution after its first passage through the reactor, the entire manifold was exhaustively rinsed with the solution so as not to dilute it and be able to attribute the signal decay to the previous photo generation.

The selection of the continuous flow system instead of the flow injection one was in order to ensure a reliable measure of the waste solution (the one that was already passed through the UV reactor). If generation efficiency was too high, analyte concentration in the waste solution would be very small, so the transient signal would have been more affected of error. With continuous flow, signal increases until a steady state is reach where the supply of volatile species to the absorption cell is constant, even if low, the amount atoms in the absorption cell would always be large enough so as to give a confident signal.

Table 31 shows that the photo generation process elapses in a suitable extend for every LMWOC tried. In order to characterise the method some figures of merit were determined.

Efficiency (%)	CH ₃ COOH	CH ₃ CH ₂ OH	HCOOH
	68	82	91

Table 31: Photochemical mercury vapour generation efficiency in 0,5 % w/w CH₃COOH, 1 % w/w CH₃CH₂OH and 0,5 % w/w HCOOH.

4.4.3.5.7 Some parameters for characterising the method for each LMWOC.

In order to learn about the potential applications this methodology could have, parameters as linear range evaluation, signal dispersion between replicates, and limit of detection and quantification were assessed.

Even as whenever the methodology could be applied, integrated absorbance would be the analytical signal of choice as a transient signal is obtained, parameters deriving from peak height (absorbance) were considered of interest at this stage as it brings more information about the system.

Photochemical generation in formic acid gave the best generation efficiency, thus, the application of the methodology for the determination of mercury in dogfish liver Certified Reference Material was intended. Nevertheless results were not satisfactory; at first instance it could not be attributed to the

methodology failure but to an incomplete process of extraction of the analyte from the matrix; full discussion will be presented in 4.4.3.5.7.5 Attempt to method application.

4.4.3.5.7.1 Evaluation of the linear range and calibration function

Mercury solutions at different concentration were prepared and measured at the optimum working conditions for every LMWOC. Several instrumental replicates were performed for each one. Both absorbance and integrated absorbance were used to evaluate the calibration function.

4.4.3.5.7.1.1 1,0 % w/w ethyl alcohol:

Ethyl alcohol was the first LMWOC tried, so in order to evaluate the calibration function a nine points calibration curve was prepared in 0,5 % w/w $\text{CH}_3\text{CH}_2\text{OH}$ up to $250 \mu\text{g kg}^{-1} \text{Hg}^{+2}$.

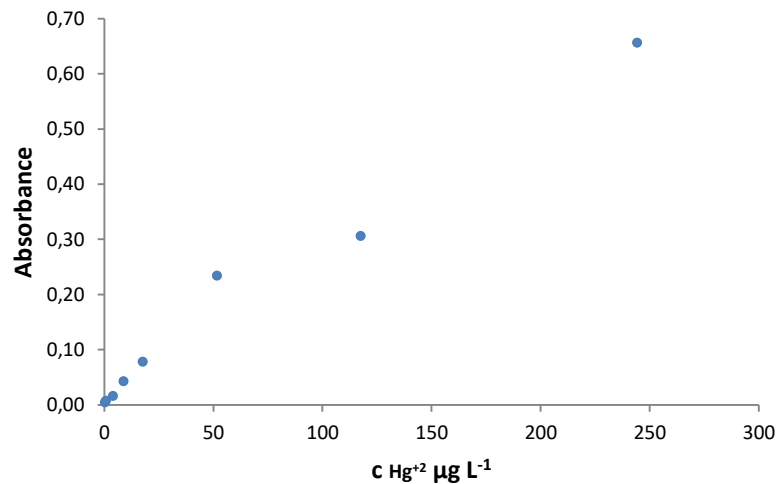


Figure 84: Evaluation of the calibration function for mercury in 1,0 % w/w $\text{CH}_3\text{CH}_2\text{OH}$

Figure 84 shows that in the concentration range evaluated a linear function cannot be assessed; linear response probably goes up to $50 \mu\text{g kg}^{-1} \text{Hg}^{+2}$.

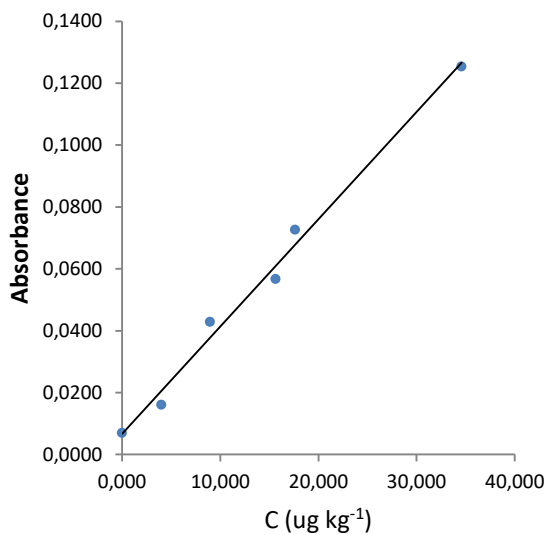


Figure 85: Peak height as a function of the concentration

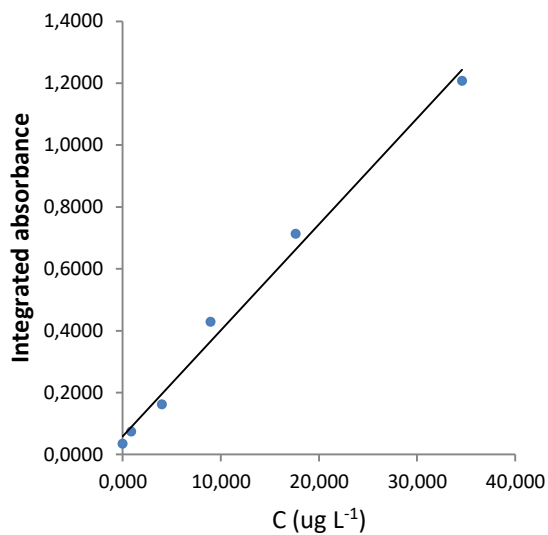


Figure 86: Peak area as a function of the Concentration.

4.4.3.5.7.1.2 0,5 % w/w formic acid:

The evaluation of the calibration function was performed up to 100 $\mu\text{g kg}^{-1} \text{Hg}^{+2}$, throughout the entire range it could be considered linear.

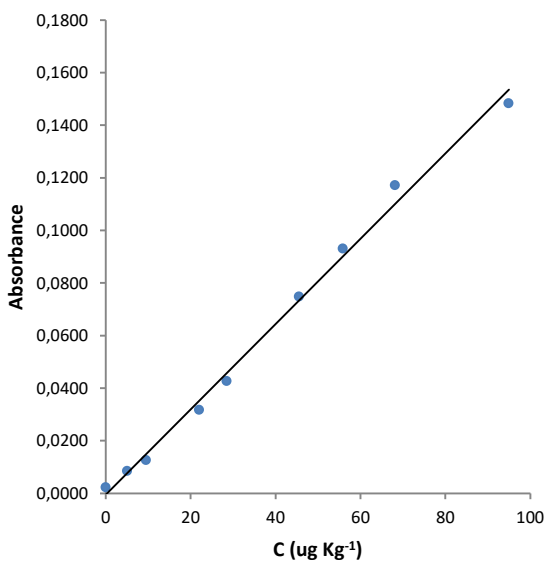


Figure 87: Peak height as a function of the concentration.

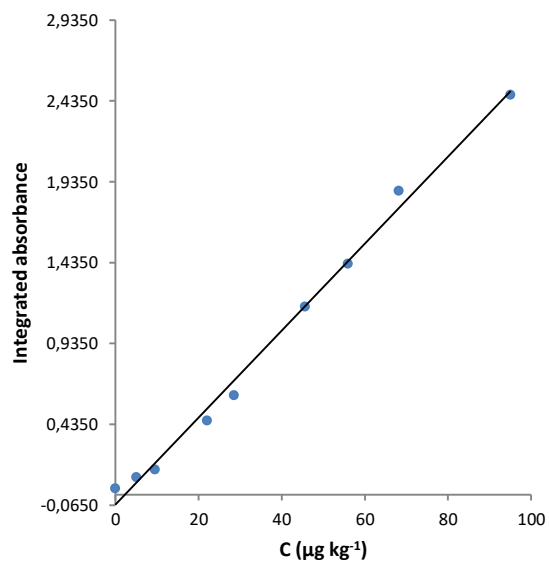


Figure 88: Peak area as a function of the concentration.

4.4.3.5.7.1.3 0,5 % w/w acetic acid:

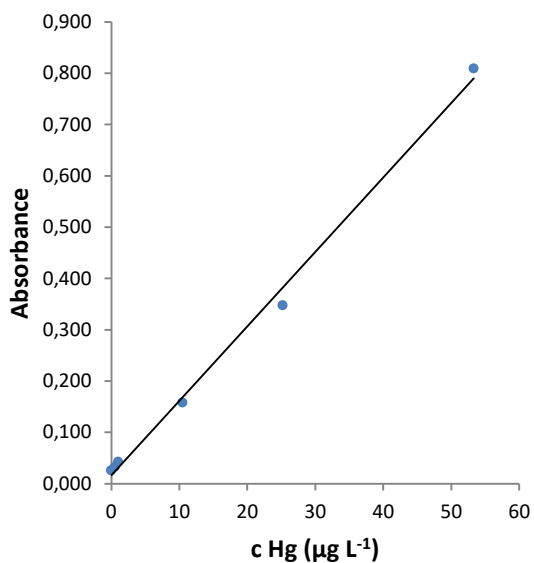


Figure 89: Peak height as a function of the concentration.

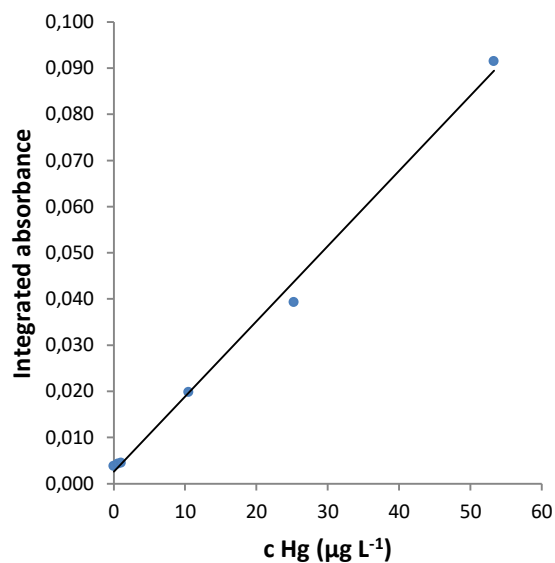


Figure 90: Peak area as a function of the concentration.

The evaluation of the calibration function was performed up to $50 \mu\text{g kg}^{-1} \text{Hg}^{+2}$, throughout the entire range it could be considered linear.

4.4.3.5.7.2 Signal dispersion between replicates

4.4.3.5.7.2.1 1,0 % w/w ethyl alcohol:

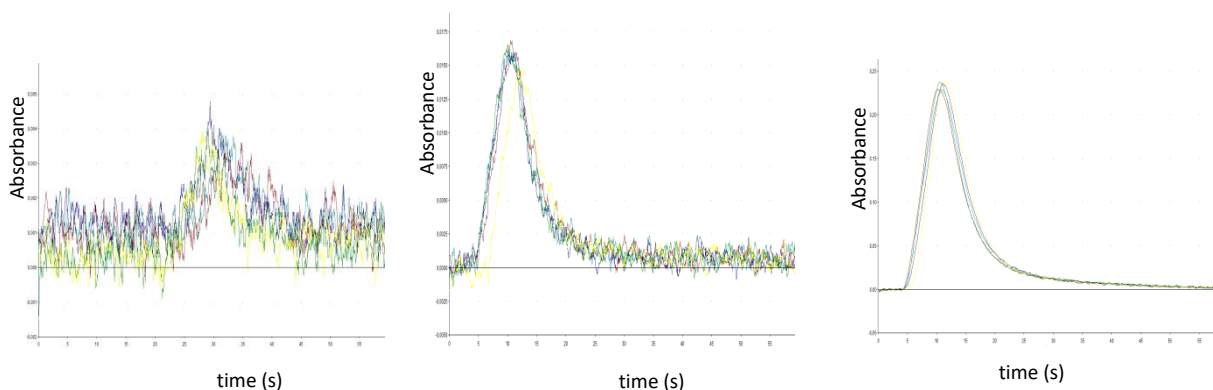


Figure 91: Signal replicates for blank, 5 $\mu\text{g kg}^{-1}$ – Hg and 50 $\mu\text{g kg}^{-1}$ – Hg respectively

Instrumental precision (repeatability, n= 5), s_r (%)		
Concentration level ($\mu\text{g kg}^{-1}$)	Peak height	Peak area
0	1,0	10,3
5	4,5	3,8
15	1,9	3,3
35	6,1	2,7

Table 32: Instrumental precision at different concentration levels of mercury in 1,0 % w/w ethyl alcohol.

4.4.3.5.7.2.2 0,5 % w/w formic acid:

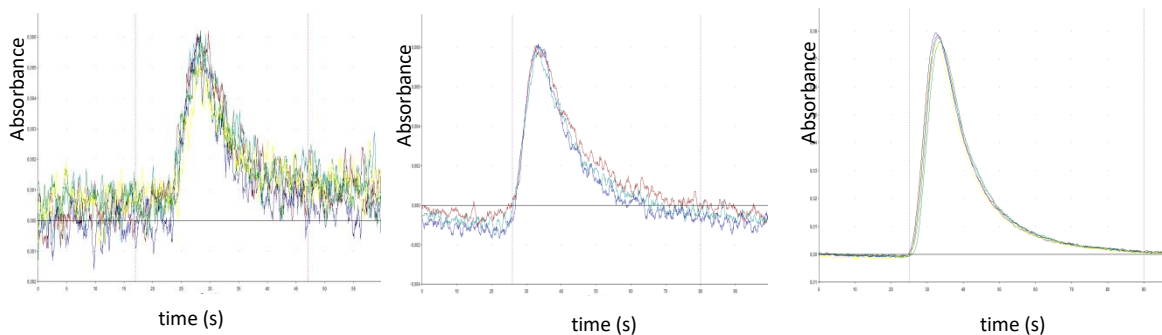


Figure 92: Signal replicates for blank, 5 $\mu\text{g kg}^{-1}$ – Hg and 50 $\mu\text{g kg}^{-1}$ – Hg respectively

In Figure 92 can be seen five replicates at different concentrations levels of mercury.

Instrumental precision (repeatability, n= 5), s_r (%)		
Concentration level ($\mu\text{g kg}^{-1}$)	Peak height	Peak area
0	7,1	5,4
5	4,1	4,1
20	5,1	3,2
50	0,7	3,2
100	3,2	3,6

Table 33: Instrumental precision at different concentration levels of mercury in 0,5 % w/w formic acid.

4.4.3.5.7.2.3 0,5 % w/w acetic acid:

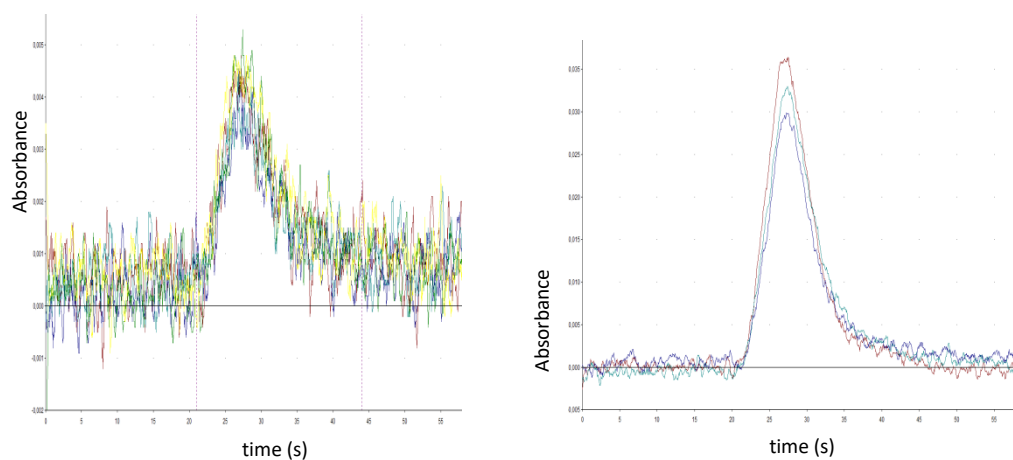


Figure 93: Signal replicates for blank and $50 \mu\text{g kg}^{-1}$ – Hg respectively

Instrumental precision (repeatability, n= 5), s_r (%)		
Concentration level ($\mu\text{g kg}^{-1}$)	Peak height	Peak area
0	1,8	12,8
50	3,4	9,6

Table 34: Instrumental precision at different concentration levels of mercury in 0,5 % w/w acetic acid.

4.4.3.5.7.3 Limit of detection and quantification

As shown in Figure 91 through Figure 93, every solution of LMWOC studied has a definite blank signal. This probably arises from a mercury contamination in the reagents. Zheng et al (Zheng, Li, He, Ma , & Hou, 2005) already demonstrated that Hg^{+2} can be reduced by visible irradiation, this was confirmed passing the solution with the lamp turned off. A signal, even if not too pronounced, can be appreciated. It was not done, but mercury contamination could have been eliminated from the reagents just by letting them exposed to visible light previous to using them (all of them where stored in amber flasks).

As blank solutions had a definite signal that clearly distinguishes form the baseline, its dispersion was used for calculating the limits of detection and quantification.

Limits were calculated as follows: $LOD = \frac{3s}{m}$ and $LOQ = \frac{10s}{m}$ were s is the standard deviation of ten signal replicates (absorbance or integrated absorbance, as appropriate) of the blank and m the slope of the corresponding calibration function.

4.4.3.5.7.3.1 1,0 % w/w ethyl alcohol:

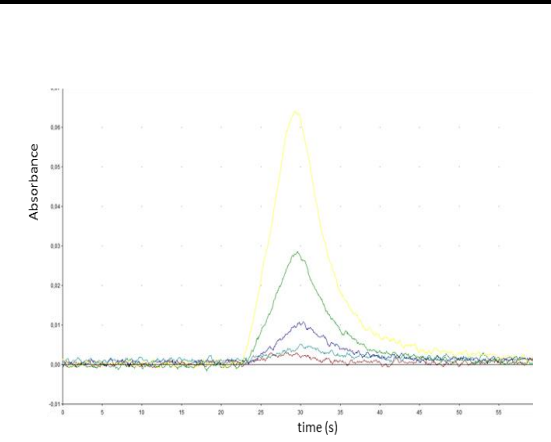
	Calibration function	Peak height	
	$A = 0,00108C + 0,00024$ $R^2 = 0,9904$	LOD ($\mu\text{g kg}^{-1}$)	LOQ ($\mu\text{g kg}^{-1}$)
		0,91	3,0
	Calibration function	Peak area	
$A_{\text{int}} = 0,0100C + 0,0179$ $R^2 = 0,9903$	LOD ($\mu\text{g kg}^{-1}$)	LOQ ($\mu\text{g kg}^{-1}$)	
	0,81	2,7	

Table 35: Calibration function and limit of detection (LOD) and limit of quantification (LOQ) for the photochemical generation of mercury in 1,0 % w/w ethyl alcohol. A: absorbance; A_{int} : integrated absorbance (s); C: mercury concentration ($\mu\text{g kg}^{-1}$).

4.4.3.5.7.3.2 0,5 % w/w formic acid:

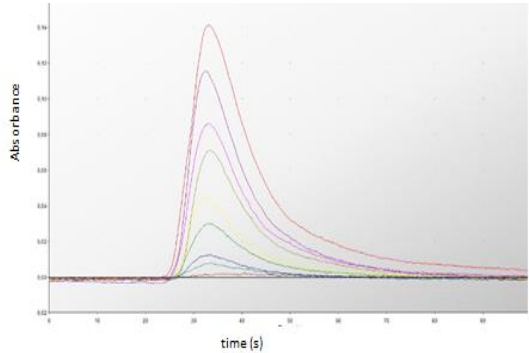
	Calibration function		Peak height	
	$A = 0,00162C - 0,0005$ $R^2 = 0,9943$		LOD ($\mu\text{g kg}^{-1}$)	LOQ ($\mu\text{g kg}^{-1}$)
			0,34	1,1
	Calibration function		Peak area	
$A_{\text{int}} = 0,02690C - 0,0615$ $R^2 = 0,9936$		LOD ($\mu\text{g kg}^{-1}$)	LOQ ($\mu\text{g kg}^{-1}$)	
		0,54	1,8	

Table 36: Calibration function and limit of detection (LOD) and limit of quantification (LOQ) for the photochemical generation of mercury in 0,5 % w/w formic acid. A: absorbance; A_{int} : integrated absorbance (s); C: mercury concentration ($\mu\text{g kg}^{-1}$).

4.4.3.5.7.3.3 0,5 % w/w acetic acid:

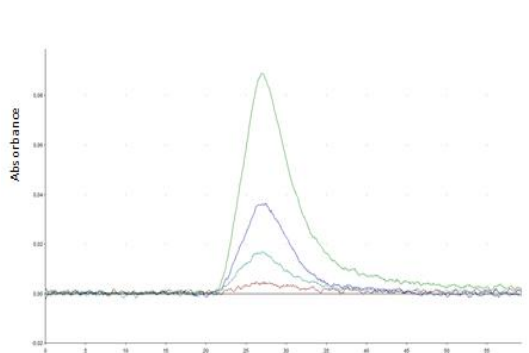
	Calibration function		Peak height	
	$A = 0,00162C - 0,0023$ $R^2 = 0,9920$		LOD ($\mu\text{g kg}^{-1}$)	LOQ ($\mu\text{g kg}^{-1}$)
			0,51	1,7
	Calibration function		Peak area	
$A_{\text{int}} = 0,0146C - 0,0288$ $R^2 = 0,9960$		LOD ($\mu\text{g kg}^{-1}$)	LOQ ($\mu\text{g kg}^{-1}$)	
		1,4	4,5	

Table 37: Calibration function and limit of detection (LOD) and limit of quantification (LOQ) for the photochemical generation of mercury in 0,5 % w/w acetic acid. A: absorbance; A_{int} : integrated absorbance (s); C: mercury concentration ($\mu\text{g kg}^{-1}$).

Within the LMWOC tried, acetic acid was the one with less reliable results. Dispersion of the signal was of relevance especially the integrated absorbance; peak height was less variable.

Ethyl alcohol gave satisfactory results but in terms of sensitivity and dispersion, formic acid had the best performance. It was the one chosen for the evaluation of the accuracy of the method.

4.4.3.5.7.4 Summary of the working conditions and performance of the photochemical vapour generation of mercury

Ethyl alcohol – CH₃CH₂OH						<i>Optimum</i>	
<i>Concentration % (w/w)</i>	0,5	1,0	5,0	10		1,0	
<i>t_{UV} (s)</i>	2,5	3,0	3,5	4,5	6,0	12	3,5
<i>Sample volume (mL)</i>	0,15	0,60	1,00	2,00			2,00
<i>LOD (µg kg⁻¹)</i>	0,81	<i>LOQ (µg kg⁻¹)</i>	2,7	<i>PVG efficiency</i>			82 %
Formic acid – HCOOH						<i>Optimum</i>	
<i>Concentration % (w/w)</i>	0,1	0,5	1,0	10			0,5
<i>t_{UV} (s)</i>	3,5	4,5	6,0	12			6
<i>Sample volume (mL)</i>	0,6	1,0	2,0				0,6
<i>LOD (µg kg⁻¹)</i>	0,54	<i>LOQ (µg kg⁻¹)</i>	1,8	<i>PVG efficiency</i>			91 %
Acetic acid – CH₃COOH						<i>Optimum</i>	
<i>Concentration % (w/w)</i>	0,5	1,0	5,0	20			0,5
<i>t_{UV} (s)</i>	2,5	4,5	6,0	12			6
<i>Sample volume (mL)</i>	0,6	1,0	2,0				2,0
<i>LOD (µg kg⁻¹)</i>	1,6	<i>LOQ (µg kg⁻¹)</i>	3,6	<i>PVG efficiency</i>			68 %

Table 38: Summary of the variables affecting mercury signal studied and the optimum conditions found. For every experience, the flow rate of the Ar: H₂ mixture was 500 mL min⁻¹.

4.4.3.5.7.5 Attempt to method application

Once the photochemical cold vapour generation method is characterised, the study of its applicability is mandatory. In the most of the cases, an acid digestion precedes the determination. Nitric acid is a limiting concomitant for the photo generation process. In order to avoid that drawback, an alkaline digestion proposed by Tao *et al.* (Tao, Willie, & Sturgeon, 1998) was assayed. It consists on the addition of 4 mL of tetramethylammonium hydroxide (TMAH) to 0,25 g of sample, let it react for 5 min and bring to 25 mL with deionised water. It is intended to be used in biological tissue, in particular it was applied to dogfish flesh and dogfish liver CRMs.

Dogfish liver Certified Reference Material declaring 3,37 µg g⁻¹ inorganic mercury content and 1,59 µg g⁻¹ methyl mercury content was used.

4 mL of TMAH (ACROS Organics, 25 % w/w in methanol) were added to 0,1 g of sample. After 5 minutes it had a dark colour and was not dissolved at all. It was then let stand for two hours; it was neutralised, added with formic acid so as to get a final concentration of 0,5 % w/w in it. The total volume was approximately 25 mL a brownish suspension; afterwards, it was filtered by a nylon membrane (Simplepure, 0,45 µm). If mercury was completely extracted from samples, the resulting solution would be 20 µg kg⁻¹ Hg approximately. Triplicates of sample and a blank were run and measured against a seven-point external standard calibration curve.

The digestion is expected to extract both inorganic and methyl mercury in its original species. The mentioned literature states that for CVG, the slopes for the organic mercury compounds are different to the slope for the inorganic mercury. However, Vieira *et al* found no differences between them (Vieira , Ribeiro, Curtius , & Sturgeon, 2007). The last could not be confirmed for PVG in this work as there was no methyl mercury standard available in the laboratory.

The mercury concentration found in solution was about a 50 %.

Any conclusion can be run as:

- The recommended sample amount of CRM is 0,25 g, but as available amount is very few, about 0,1 g were taken for each aliquot losing representativeness.
- For the same reason, the TMAH digestion procedure was not optimised for this sample, so there is no evidence that the full extraction was achieved.
- The number of replicates was very little; for the last experience only one replicate developed a signal.

Either, quintuplicates of mercury standard were digested with nitric acid and formaldehyde (the explanation of this procedure will be done in 4.5.3 Nitric acid interference abatement study, but it was proved to ensure the elimination of the nitric acid interference). If this experiment would have been successful, the remaining sample could have been digested with nitric acid and the matrix completely digested. Nevertheless, the result of the experiment evidenced that mercury is unstable in those conditions, no recovery was found in none of the replicates.

Thereby, the steps that should be followed after the acquisition of new mercury CRM would be:

- Optimisation of the digestion procedure: as nitrate is a known interfering oxidant of the PVG efforts for achieving properly the TMAH digestion are worthwhile. Its effectiveness can be traced by CVG. Once optimised, the resulting suspension should be neutralised and added by formic acid.
- Independent standard of inorganic and methyl mercury, and the mixture in the same ratio as in the CRM should be run simultaneously in order to assess if there are the difference between the slopes for PCVG determination in this working conditions.
- Once the digestion process is optimised and the effect of the methyl mercury in the mercury signal evaluated, replicates of the digested CRM should be analysed by PCVG-AAS.

Results found are promising as there are signals for mercury in the analysed solutions, no conclusion about the accuracy of the methodology can be derived until the previous studies proposed are accomplished.

The detection and quantification limits obtained by PVG of mercury restricts its application in the monitoring of the quantities of mercury in some human consumption products like drinking water as the

regulatory levels allowed ($1 \mu\text{g L}^{-1}$) are low (Uruguay, 1994). Nonetheless, in consumption products in general, the threshold is $0,05 \text{ mg kg}^{-1}$ (Uruguay, 1994). Sea products are undoubtedly one of most concern. Considering an average amount of water content in fish of 70% (Nations), the threshold for dry fish is $0,17 \text{ mg kg}^{-1}$. Following the sample preparation suggested by (Tao, Willie , & Sturgeon, 1998), the resulting solution will be near the LOQ ($1,7 \mu\text{g L}^{-1}$), so some adjustment in the total volume (15 mL) or in the mass of sample (0,45 g) should be done in order to provide dependable results (measurement solution approx. $3 \mu\text{g L}^{-1}$).

4.4.3.6 Conclusions

A photochemical cold vapour generation system was mounted for mercury atomic absorption determination. The different variables affecting the response were studied for three low molecular weight organic compound and some figures of merit like linear range and limits of detection and quantification determined.

The application of this methodology is a mandatory continuation of this work especially what refers to interferences that certainly will arose after acidic sample digestion. Even if results were not concluding, they were encouraging for envisaging alkaline digestions methods for its achievement.

Chapter IV

Photochemical generation of mercury

Scientific Production



STUDY OF THE VARIABLES AFFECTING A FIA-CV-AAS SYSTEM FOR MERCURY DETERMINATION BY PHOTOCHEMICAL GENERATION

Alicia Mollo[†], Moisés Knochen

Universidad de la República, Facultad de Química.
Av. Gral. Flores 2124. 11800 Montevideo, Uruguay
[†]amollo@fq.edu.uy

Photochemical vapor generation is an alternative to chemical reduction in cold vapor generation for the analytical determination of mercury. Gaseous mercury atoms are formed by UV irradiation in the presence of low molecular weight organic compounds (LMWOC) like organics acids and alcohols, and transferred by means of an inert gas to an atomic absorption cell for its determination (1).

The aim of this work was to study the different variables affecting the AAS response when photochemical generation is used for cold vapor generation of mercury. For that purpose a single line FIA system was mounted in order to obtain a transient signal. Air was used as the stream propelling the sample injected by the injection valve to the UV reactor and subsequently to the gas liquid separator. The gas phase was transferred to the atomic absorption cell by an argon stream. The UV reactor was a commercial device, consisting of a 720- μ L tubular reactor inside a 19-W low pressure mercury discharge lamp. For the cold-vapor photochemical generation, ethanol, formic and acetic acids were tried. For each of them, the variables considered were: LMWOC concentration, irradiation time, FIA carrier, argon flow rate and sample volume. The criterion for optimum conditions was to maximize the ratio S/s , S being the average signal (peak height) and s the estimation of the standard deviation of five replicates. Low LMWOC concentrations were found more suitable, acetic acid being the only one for which peak height was independent from its concentration. As FIA carriers, LMWOC solutions (at the tested concentrations), deionized water and air were tried, finding best results with air. Parameters that most influenced peak shape were irradiation time, that determined its rise portion, and the argon flow rate, that, in the rates assayed, only conditioned its width. As expected, sample volume affected the linear range and repeatability of the response. As air was used as carrier, efficiency could be calculated by signal attenuation in the waste solution from the gas liquid separator. Once the optimum conditions for the different variables were found, a calibration plot up to 50 $\mu\text{g L}^{-1}$ -Hg was constructed and the limits of detection and quantification calculated. In terms of optimum S/s ratio, efficiency, and method performance characteristics, formic acid gave the best results. Further investigation will be focused on attempting to improve the analytical variables of influence by reducing the volume of the atomic absorption cell.

Reference: 1 He Y, Hou X, Zheng Ch, Sturgeon RE, Anal Bioanal Chem, 338, 2007, 769

Introduction

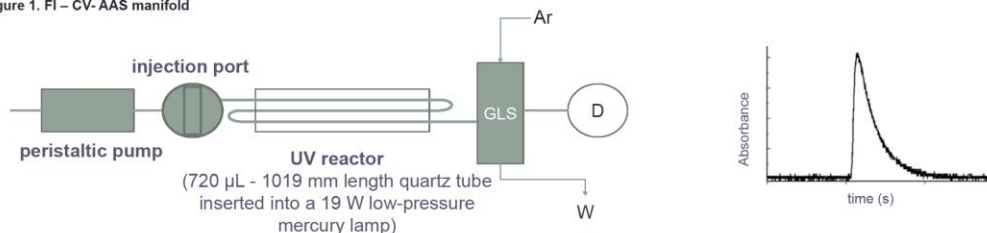
Photochemical vapour generation (PVG) is a sample introduction method for AAS combining the attributes of the vapour generation (enhancement of transport efficiency, high selectivity, reduction of interferences and improved limits of detection and quantification), with the advantages of a greener reaction medium, minimising potential interferences.

UV irradiation of aqueous solutions of metal ions containing low molecular weight organic compounds (LMWOC) as organic acids or alcohols, yield to its excision and later formation of the volatile ion specie, which can be in turn strip out of the solution by an inert gas and transferred to an atomic absorption cell for its determination.

The aim of this work was to study the different variables affecting the AAS response when photochemical generation is used for cold vapor generation of mercury.

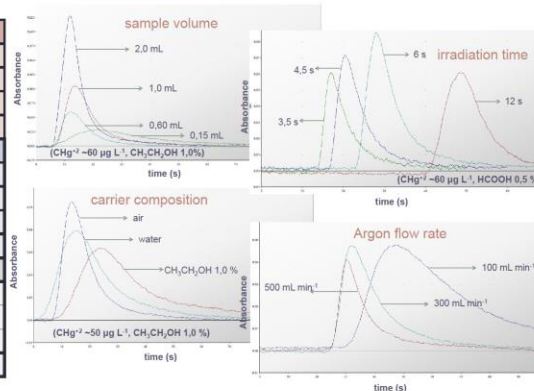
FI - CV - AAS manifold

Figure 1. FI - CV - AAS manifold



Variables affecting the FI-CV-AAS system

Low weight organic compound: ETHANOL					Optimum		
Concentration (% _{w/w})	0.5	1.0	5.0	10	1.0		
t _{UV} (s)	2.5	3	3.5	4.5	6	12	3.5
Sample volume (mL)	0.15	0.60	1.00	2.00	2.00		
LOD (µg L ⁻¹)	0.36		LOQ (µg L ⁻¹)	1.21			PVG efficiency 82 %
Low weight organic compound: FORMIC ACID					Optimum		
Concentration (% _{w/w})	0.1	0.5	1.0	10	0.5		
t _{UV} (s)	3.5	4.5	6	12	6		
Sample volume (mL)	0.60		1.00	2.00	0.60		
LOD (µg L ⁻¹)	0.33		LOQ (µg L ⁻¹)	1.11			PVG efficiency 91 %
Low weight organic compound: ACETIC ACID					Optimum		
Concentration (% _{w/w})	0.5	1.0	5.0	20	0.5		
t _{UV} (s)	2.5	4.5	6	12	6		
Sample volume (mL)	0.60		1.00	2.00	2.00		
LOD (µg L ⁻¹)	0.54		LOQ (µg L ⁻¹)	1.79			PVG efficiency 68 %



Discussion and conclusions

For the LMWOC assayed, concentrations above the selected as optimum did not change reduction efficiency. Irradiation time determined the rise portion of the signal, requiring time enough for analyte reduction but not too long to decompose and decrease response. Argon flow rate influenced peak width. At 500 mL min⁻¹ a slight dilution effect was noticed. As expected, sample volume affected the linear range and repeatability of the response. The criterion for optimum conditions was to maximize the ratio S/s, S being the average signal (peak height) and s the estimation of the standard deviation of five replicates. For each LMWOC in the optimum conditions, a calibration plot up to 100 µg L⁻¹-Hg was constructed and the limits of detection and quantification calculated. Atomic absorption cell's volume and shape was also varied not founding significant differences between the method performance characteristics. In terms of optimum S/s ratio, efficiency, and method performance characteristics, formic acid gave the best results

Acknowledgements

Authors wish to thank CSIC and PEDECIBA Química for financial support and Mariana Da Luz Potes for refer us the reactor

9

Chapter IV

Volatile selenium derivatives

In this section, a flow injection system for selenium (IV) and total selenium is presented. The section is divided in two parts, first the optimisation stage where the study of the parameters is discussed, and second, an exhaustive interference abatement study. The methodology achieved has been applied to the analysis of total selenium in a water certified reference material and a spiked digest of rice flour.

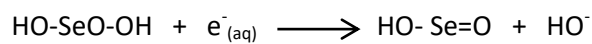
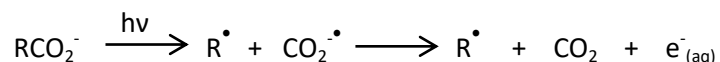
4.5 Photochemical generation of volatile selenium compounds

4.5.1 Introduction

In the first stages of the photochemical vapour generation, the technique was presented by Sturgeon & Guo (Guo, Sturgeon, Mester, & Gardner, UV Vapor Generation for Determination of Selenium by Heated Quartz Tube Atomic Absorption Spectrometry, 2003) introducing a novel methodology for the determination of selenium in aqueous solutions. The reactor consisted on a PTFE tube wrapped around a low pressure mercury lamp. The LMWOC used were formic, acetic, propionic and malonic acid with a 2 min irradiation time for all of them except for malonic acid that was shorter (between 17 and 40 s). For quantification purposes, solution leaving the reactor entered a gas-liquid separator and the gaseous phase was transported by a He stream towards a 900°C quartz tube atomiser for its determination. They found the variables (LMWOC type and concentration and irradiation time) were interrelated, depending on the concentration of the LMWOC, the irradiation time could be adjusted.

In order to identify the volatile species, when leaving the gas-liquid separator, the gaseous phase was condensed in a cryogenic trap, then eluted and characterised by GC-MS and GC-ICP-MS. Using formic acid (HCOOH) as the generating media, the volatile species formed were H₂Se (60 – 70 %) and SeCO (40 – 30 %). For both acetic (CH₃COOH) and malonic acid (CH₂(COOH)₂) dimethyl selenide (CH₃)₂Se was the sole reaction product; for propionic acid just diethyl selenide (CH₃CH₂)₂Se.

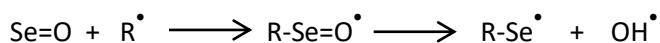
One of the possible reaction mechanisms is (Sturgeon & Grinberg, 2012) (Leonori & Sturgeon, 2019):



+



Eq. 21



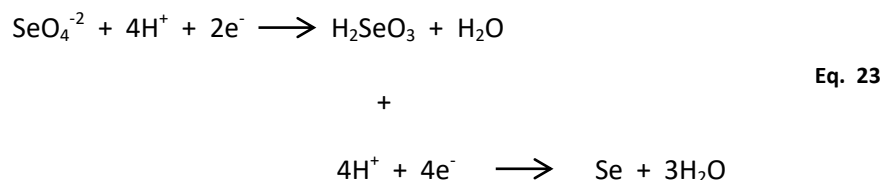
+



Eq. 22

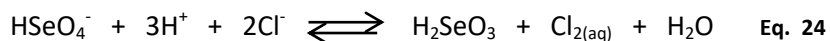
Se(VI) oxidation state is not able to yield volatile species neither by CVG (Dedina & Tsalev, Hydride Generation Atomic Absorption Spectrometry, 1995) (Welz & Sperling, 1999) nor by PVG (Sturgeon R. , 2017). In this sense, there are also two ways of facing the reduction step: by a chemical or by a photochemical approach. Even if in this work the first was the option undertaken, it is worthwhile to look out at the photo reduction as it was one of the first photochemical processes studied in PVG.

TiO₂ was used as a heterogeneous photo catalyst for the reduction of selenate to selenite. The TiO₂ surface absorbs the photons promoting the electron from the valence band to the conduction band where the selenate is reduced yielding amorphous elemental selenium:



Then, elemental selenium is reduced to the hydride in the surface of the TiO₂ as well as formic acid or other LMWOC is oxidised. Selenite reduction up to the volatile species does not need the heterogeneous photo catalyst, just the UV irradiation and the LMWOC are enough (Kikuchi & Sakamoto, 2000) (Leonori & Sturgeon, 2019).

The most commonly used method for chemical reduction of Se(VI) to Se(IV) is by hot hydrochloric acid. The reduction rate has been found strongly depending on the temperature and hydrochloric acid concentration; at higher acid concentration, lowest temperatures are needed.



Boiling is not recommended as selenium can be lost as SeCl₄ or SeOCl₂ (Pettersson & Olin, The Rate of Reduction of Selenium (VI) to Selenium (IV) in hydrochloric Acid, 1991) (Bye, Critical Examination of Some Common reagents for Reducing Selenium Species in Chemical Analysis, 1983).

4.5.2 PVG working conditions optimisation

4.5.2.1 *Experimental section*

In the optimisation stage, different organic acids and alcohols were tried. Formic acid was the one which led to best results in terms of sensitivity. The other parameters were optimised based on its performance.

4.5.2.1.1 *Instrumentation*

The flow injection system shown in **4.3.3 Flow injection manifold** was used. The detection system uses, the externally heated atomization cell (4.3.4.2) mounted in the iCE3000 Thermo Scientific Spectrometer (Waltham, MA, USA) fitted with a selenium hollow cathode lamp (Thermo Scientific). The determination was achieved at 196,0 nm using a deuterium background correction. Flow system was fed by the VP100 peristaltic pump. Working conditions chosen were those leading to a well-shaped peak signal (sharp and high peaks) and when relevant, the ones which maximize the ratio average signal (peak height) over the signal dispersion (estimated as the standard deviation of five replicates). For quantification purposes, peak area was chosen as the analytical signal.

4.5.2.1.2 *Reagents and solutions*

Diluted solutions were prepared with deionised water (ASTM type I) obtained from a Millipore (São Paulo, Brazil) Direct-Q 5 water purifier. Selenite solutions were prepared from sodium selenite (Aldrich, 99%). Selenium working solutions were prepared daily by dilution of the Se (IV) 1000 mg L⁻¹ standard solution in 1 mol L⁻¹ HCl.

Methyl and ethyl alcohols, acetic, formic, sulfamic and 36% w/w hydrochloric acids were of analytical reagent grade.

High purity, mixture of Ar: H₂ (92:8) and N₂, were obtained from Air Liquide Uruguay S.A. .

Whenever mentioned gravimetric dilutions of hydrochloric acid, they refer to 36 % w/w HCl.

4.5.2.1.3 *Procedure*

As previously explained, Se(IV) is the only oxidation state of selenium able to form volatile species. For the sake of simplicity, Se(IV) solutions were used for these studies at a concentration high enough in order to ensure a well-defined peak signal. The variables of influence affecting the photochemical vapour generation were evaluated in univariant way keeping the others constant, ordered by relevance in the following sequence: low molecular weight organic compound at different concentration and irradiation

times, carrier composition of the FIA system, argon: hydrogen flow rate in the gas-liquid separator and the sample volume.

4.5.2.2 Results and discussion

4.5.2.2.1 Low molecular weight organic compound and LMWOC's concentration:

The low molecular weight organic compounds assayed were: methanol, ethanol, formic and acetic acid. The alcohols were tried at 1,0, 5,0 and 10% v/v. Up to 1% methanol achieved photo generation but with very low efficiency as there were needed high concentrations of selenium for visualizing a signal. Ethanol did not evidence photo generation at any concentration level.

Acids had a much better performance. Results are shown in Table 39. Acetic acid was tried at 0,5 – 3,0 - 10 and 20% w/w. Defined peaks appeared at every acid concentration founding the best relation signal-to-noise for 10 and 20%. However, as shown in Figure 94, formic acid attained improved sensitivity at lower acid concentration, with the highest signal to noise ratio between 1,5 and 3,0 % w/w.

LMWOC	CH ₃ COOH				HCOOH				
C _{LMWOC} (%) _{w/w}	0.5	3.0	10	20	1.5	3.0	4.5	6.0	7.5
Peak height	0.0245	0.061	0.078	0.074	0,26	0.26	0,22	0,19	0.15
s _r (%)	7.2	5.1	4.2	3.8	4.9	6.0	2.2	15	6.8
Se (µg L ⁻¹)	60				30				

Table 39: Selection of type and concentration of the LMWOC.

Photolysis of acetic and formic acid leads to the formation of strong reducing CO₂^{-•} radicals (Leonori & Sturgeon, 2019). The latter are able to reduce Se(IV) to Se(0). When the acid concentration gets higher, so does the reducing radical amount and there is no longer Se(IV) available for the formation of the volatile species.

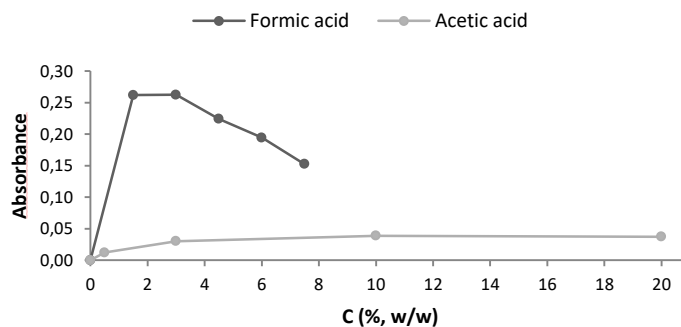


Figure 94: Variation of selenium signal (peak absorbance) for acetic and formic acid at different concentration levels (C_{Se} = 30 µg L⁻¹)

Formic acid optimum concentration for the photo generation was found to be strongly dependent on the acidic concentration of the media.

Figure 95 evinces the variation in selenium response at different acidic concentrations. Results are expressed as signal percentage for the same concentration of selenium. 50 µg L⁻¹ Se(IV) and 5 % HCOOH solutions at increasing acidic concentration were prepared. A portion of each of them was directly measured and the other previously added with formic acid up to 10 % w/w. Considering the dilution of the latter, all signals were normalized to the same concentration of selenium and then the corresponding to 1 % HCl – 5% HCOOH taken as the reference (its peak area was considered 100 %). For the same formic acid concentration, signal decreases as long as acidity increases.

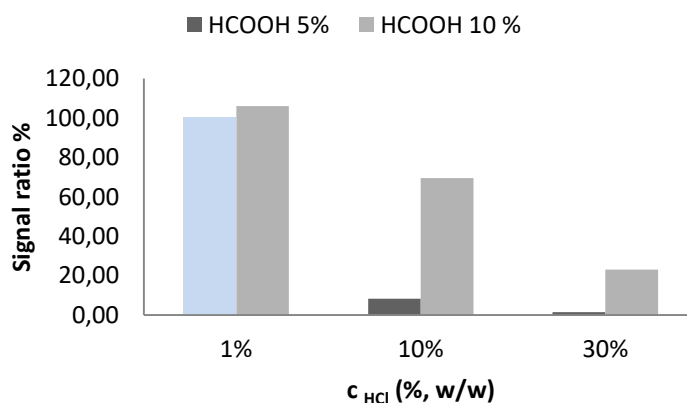


Figure 95: Selenium signal ratio for different acidic concentration in 5 % and 10 % formic acid. Light blue column corresponds to the reference.

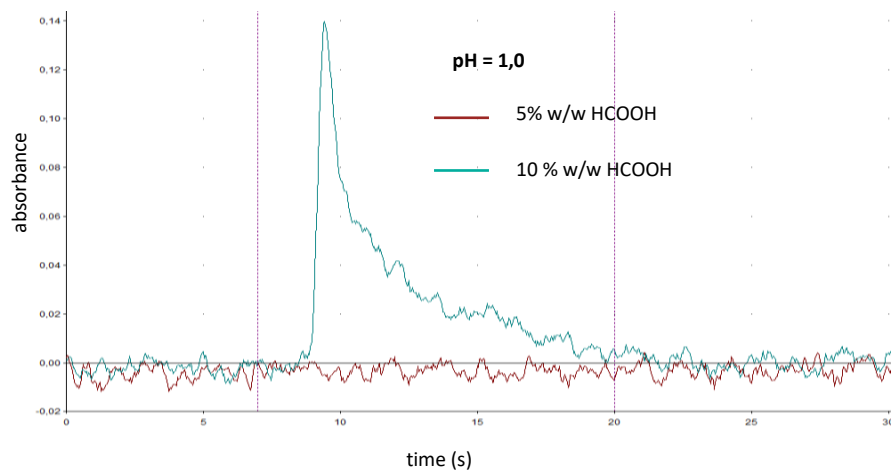


Figure 96: Variation of selenium signal with the addition of formic acid according to the acidic media

Figure 96 exemplifies the importance of the pH of the media in PVG; selenium at pH = 1,0 when added with formic acid (5 % HCOOH resulting solution) yielded no signal. In the same solution 10 % HCOOH let attain a well – defined selenium signal. The pH adjustment was done with hydrochloric acid.

The same experiment was carried out at chloride concentration close to those present in the acid (given by NaCl) and 1% w/w hydronium so as to ensure results depend only on the acid concentration and not on the counter ion (chloride). Solutions containing increasing amounts of chloride were prepared at 1,0 – 12,3 – 32,7 and 63,7 % w/w HCl and 3,8 – 16,0 and 32,3 % w/w NaCl.

Intending to simplify the interpretation, Figure 97 shows the variation in the signal ratio when increasing chloride concentration; full line when only hydrochloric acid was the chloride source and in dots when chloride was given by 1 % w/w HCl and sodium chloride. A possible interpretation is that acidity was the variable that precluded the photo generation, not chloride.

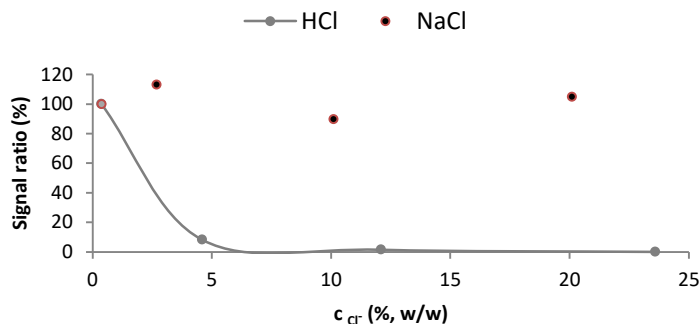


Figure 97: Selenium signal variation according to the variation of chloride given either by HCl or NaCl.

Envisaging the application in samples where the reduction step is unavoidable, after hydrochloric acid evaporation the acid concentration remaining is variable. In order to ensure a reproducible rate of photo generation, solutions were neutralized up to a pH between 7,0 and 7,5 before setting up the formic acid concentration.

4.5.2.2.2 Carrier composition of the FIA system

Carrier pushes the sample bolus through its way from the loop towards the reactor and unto the gas-liquid separator. As it interacts directly with the sample, it conditions the stability of the nascent gas phase. Two potential options could fit the purpose: a liquid phase (1,5% w/w formic acid and aqueous solution of sodium chloride were tried) or a gaseous phase (argon – hydrogen mixture and nitrogen were tried). The same selenium solution was measured with each carrier.

The PVG medium, 1,5 % w/w formic acid provides LMWOC in the neighbouring of the sample zone ensuring an excess of formate radicals to promote the photo reduction of selenite and the derivatisation reaction, leading to the volatile species formation. Sodium chloride solution would lead to a salting-out effect that could enhance the gas removal from the solution.

The use of gas as a carrier helps to extract the volatile species. The mixture of argon:hydrogen injected to the gas-liquid separator was also tried as a carrier as the hydrogen in the UV reactor would possibly promote the hydride generation. Nonetheless, there was no signal at all; perhaps hydrogen large excess enhanced the radical decomposition of the species generated, defeating the searched reaction.

Nitrogen as the carrier was doubtlessly the option that impacted most in the results. As shown in Figure 98, the signal is almost three times the one of the solutions. At the same time it moved the sample through the system, it extracted the nascent gas phase, limiting its interaction with the aqueous solution where the volatile species tend to decompose. Air was also tried as a carrier; it was taken from the environment by a channel of the peristaltic pump and then connected to the injection port of the carrier in the valve. Its diameter and the pump speed determined its flow rate. As can be seen in Figure 99 the

signal was much noisier. Certainly it was not a problem of the type of gas but of its supply; thus, if pump pulses were eliminated, probably results would have been similar to those of nitrogen. Nitrogen was connected directly from the gas bottle to the flow meter and the last to the inlet port of the carrier in the injection valve of the FIA system. Schemes of the FIA system for each gas are depicted in Figure 100 and Figure 101.

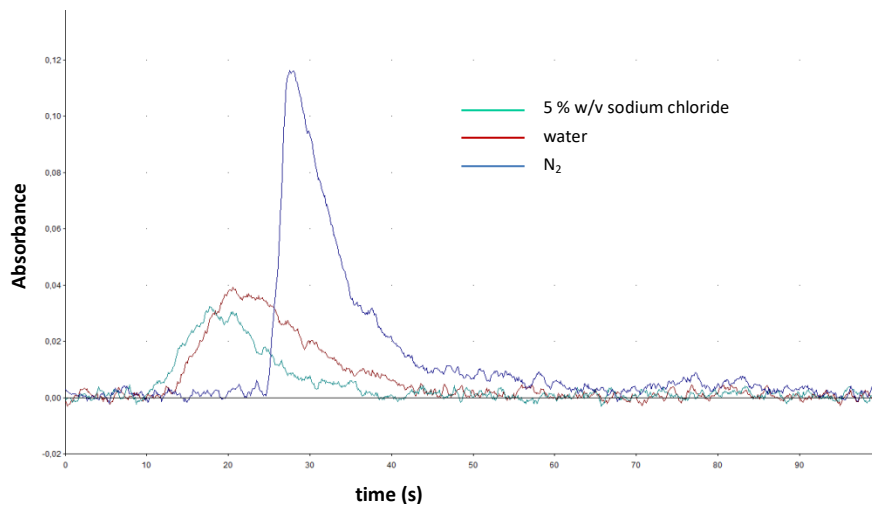


Figure 98: Selenium signal for 5 % sodium chloride, water and nitrogen as carriers of the flow injection system.

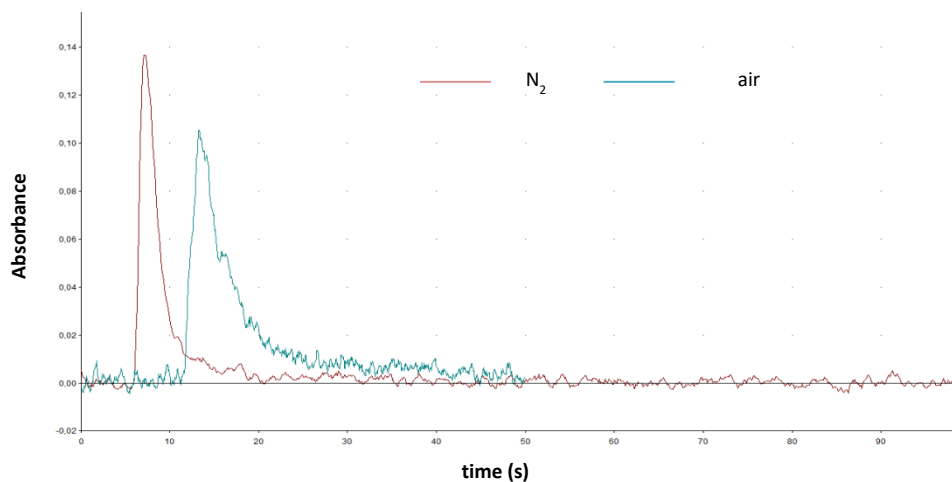


Figure 99: Selenium signal using nitrogen and air as carriers

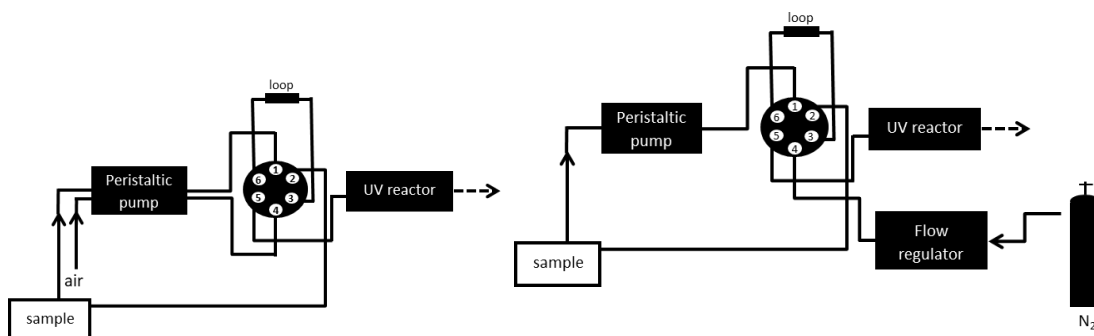


Figure 100: FI system when using air as a carrier.

Figure 101: FI system when nitrogen used as a carrier.

In both cases, as the carrier phase is gaseous, the sample waste injection port can be connected to the same flask where the sample is collected; there is no sample dilution by the carrier, so sample consumption reduces just to the one needed for the first tube rinsing and the injections.

4.5.2.2.3 Irradiation time

The irradiation time is the residence time of the solution inside the UV reactor and it was determined by the carrier gas flow rate. Different gas flow rates were tried between 10 and 84 mL min⁻¹. Figure 102 shows how the signal of a selenium solution varies as long as the nitrogen flow rate of the FI system is increased. Higher nitrogen flow rates (less time of irradiation exposure), gave better shaped signals. The best conditions were found between 56 and 72 mL min⁻¹, choosing the latter which corresponds to 3 s of sample exposure to the UV irradiation. The irradiation time was measured with a chronometer since sample entered the reactor and until it left it for the selected nitrogen's flow rate.

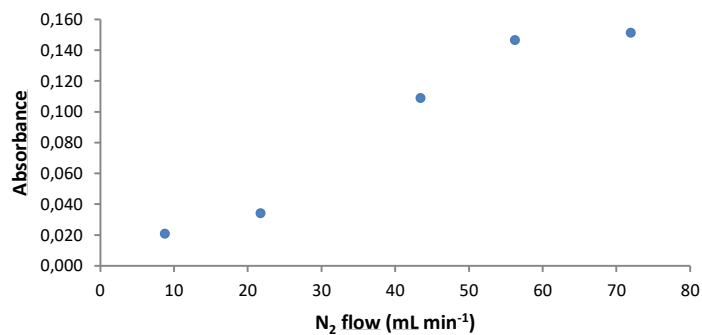


Figure 102: Variation of the peak height of selenium signal according to the carrier flow rate variation of the FIA system.

4.5.2.2.4 Argon : hydrogen (92:8) flow rate

A mixture of argon and hydrogen (92:8) fed the gas-liquid separator, removing from solution the volatile species photo generated and transporting it to the atomisation cell. It must be slow enough so as not to disperse and dilute the bolus of gas phase generated but sufficient to supply an appropriate amount of hydrogen for the atomisation process.

Argon : hydrogen flow rates from 100 to 500 mL min⁻¹ were tried, finding the best results between 250 and 350 mL min⁻¹. At 300 mL min⁻¹ the signal aroused and reached the baseline leading to high and narrow peak. When increasing the flow rate, peaks got taller and narrower (Figure 103) until reaching its optimum where dilution prevails and even if narrower, signal height decreases.

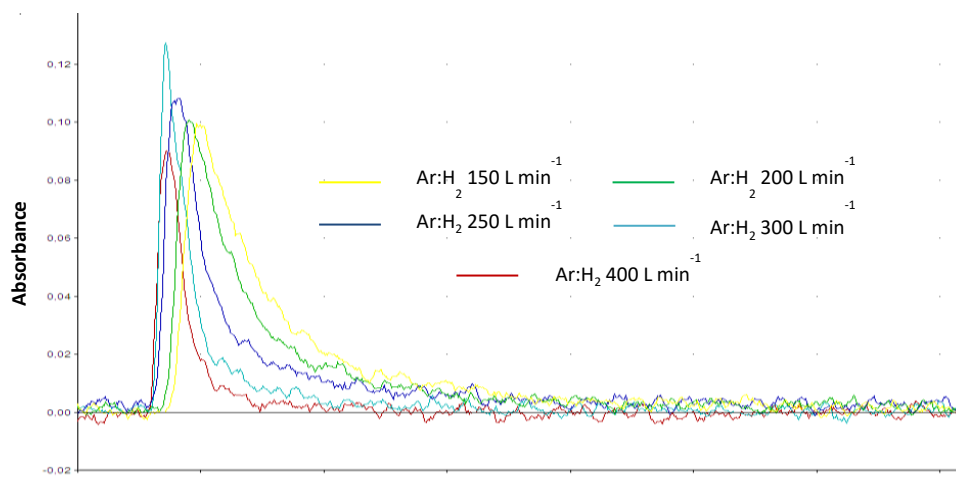


Figure 103: Selenium signal for different Ar:H₂ flows in the gas liquid separator

4.5.2.2.5 Sample volume

The volume of sample injected to the UV reactor was changed by varying the loop size. As expected, it determined the peak shape as it conditioned the size of the bolus of sample reaching the gas-liquid separator. As shown in Table 40, if too short, fewer amounts of volatile species were generated and the analytical signal decreased. If too large, even if more selenium was generated, its decay was slowed down and peaks became short and wide.

Sample volume (μL)	1000	600	375
Peak height	0.030	0.040	0.010
S_r (%)	7.0	5.5	11

Table 40: Volume of sample injected to the UV reactor.

4.5.2.2.6 Efficiency

The efficiency of the photo generation of selenium in 1,5 w/w % HCOOH was performed as in **4.4.3.5.6 Efficiency** for a $50 \mu\text{g kg}^{-1}$ Se solution. It was found to be 76 %.

4.5.2.2.7 Summary of the working conditions for the photochemical vapour generation of selenium derivatives

From the study of the results found for each variable, optimum working conditions are shown in Table 41:

LMWOC	FIA carrier	irradiation time	Ar:H ₂ flow rate	Sample volume
1,5 % w/w HCOOH	N ₂ 72 mL min ⁻¹	3 s	300 mL min ⁻¹	600 μL

Table 41: Summary of the working conditions

4.5.2.2.8 Influence of HCOOH in the atomisation cell

Tašev *et al* (Tasev, Karadjova, & Stafilov, 2005) found that ethanol interferes in the atomisation of the arsine depleting its signal in the quartz atomic cell after hydride generation. Karadjova *et al* (Karadjova, Lampugnani, Dedina, D'Ulivo, Onor, & Tsalev, 2006) studied the effect of organic solvents on arsine atomisation for different solvents in a miniature diffusion flame and a flame-in-flame atomiser at

different working conditions; one of the conclusions drawn was that the more carbon the chain, the greater the incidence in the atomisation cell depressing the signal.

Yuan *et al* (Yuan, Guo, & Tong, 1998) (only the abstract could be accessed) abated nickel interference on selenium determination by hydride generation using among others, formic acid; it can then be considered that formic acid does not interfere in the chemical hydride generation. Incidence of formic acid in dihydrogenselenide atomisation was studied using chemical hydride generation.

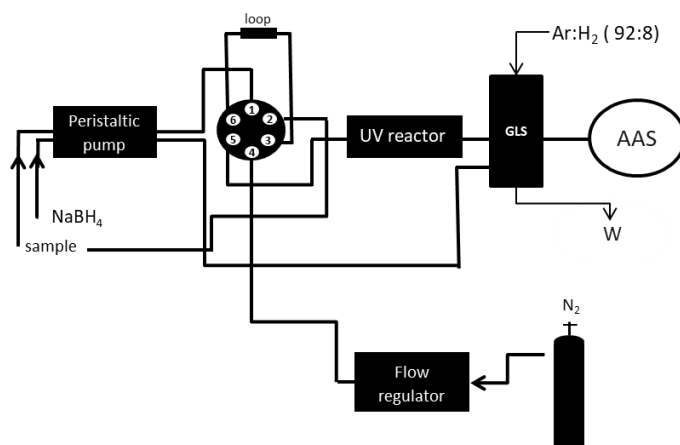


Figure 104: Flow injection manifold for the chemical hydride generation of dihydrogenselenide. GLS: gas-liquid separator; W: waste; AAS: electrically heated quartz cell for AAS.

The flow injection system used is shown in Figure 104. It was built keeping whenever possible the same features as the photochemical one, the chemical reductant, 0,5 % w/v NaBH₄ in 1,0 % w/v NaOH was introduced by the peristaltic pump directly to the GLS. After the sample was injected it was pushed towards the GLS passing through the UV reactor off.

The efficiency of the chemical generation is determined by the mixing rate of the sample and reductant's solutions so each of their flow was optimised as well as the flow of the gas in the GLS. A 50 µg kg⁻¹ Se – 1,5 % w/w HCOOH solution was used for that purpose.

Optimum conditions for 600 µL of sample were: sample flow rate: 56,3 mL min⁻¹, NaBH₄ flow rate 3,2 mL min⁻¹, Ar:H₂ flow rate: 500 mL min⁻¹.

In order to study the potential interference of formic acid in selenium derivatives atomisation, the experimental design posed was to construct the calibration curve for both the standards solutions with and without the addition of formic acid and compare its slopes. In the case of the standard solutions with no formic acid added, the same pH was attempted with hydrochloric acid in order to get similar generation conditions.

Surprisingly, solutions without formic acid lead to no selenium signal. When these solutions were spiked with formic acid the recovery was quite good, between 80 and 125%.

4.5.3 Nitric acid interference abatement study

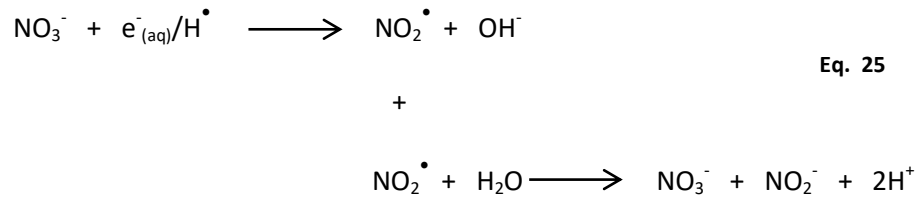
4.5.3.1 Introduction

Transition metals are known chemical interferent when using sodium tetrahydroborate as they reduce to the metal and prevent hydride formation and/or release. As in PVG reductant species formed are in many cases not able to reduce transition metals, this kind of interference (except for copper) is more controlled (Guo, Sturgeon, Mester, & Gardner, UV Vapor Generation for Determination of Selenium by Heated Quartz Tube Atomic Absorption Spectrometry, 2003) (Sturgeon R. , 2017).

Nevertheless, the presence of oxidant species in solution still remains of concern for PVG. Nitrate is one of the most frequent interfering substance found as nitric acid is deliberately added to samples for wet digestion or for its preservation.

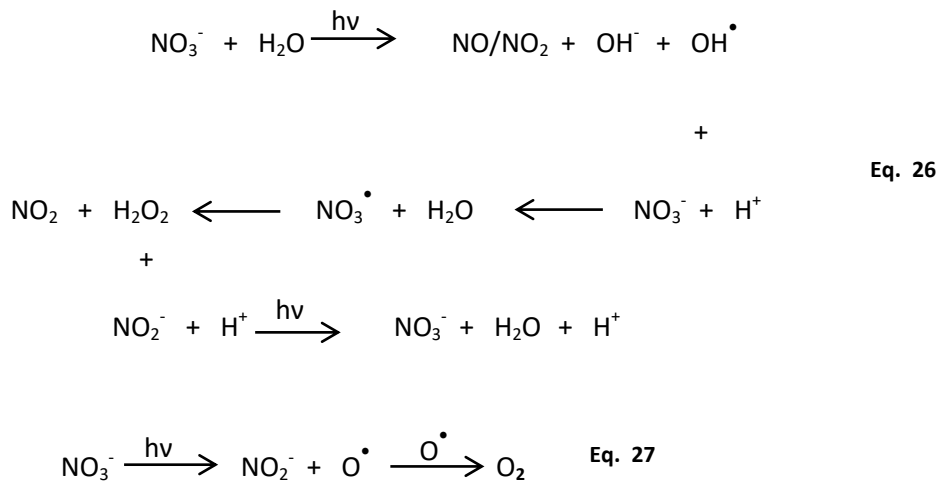
Nitrate reacts with reducing species (hydrated electrons, reductant and hydrogen radicals) decreasing its availability and yielding oxidising ones, consequently, the medium is no longer reductant and the formation of the volatile species is absolutely quenched.

Nitrate reaction with the reductant species of the media is showed in Eq. 25:



Lopes *et al* (Lopes, Sturgeon, Grinberg, & Pagliano, 2017) found the same selenium signal decay for much lower concentrations of nitrite than nitrate proving nitrite is a more severe interfering than nitrate.

Besides, nitrate and nitrite photolysis yields oxidising species:



Eq. 25 shows the decay of the reducing species population while Eq. 26 and Eq. 27 show the increment of the oxidising one. The radical cascade needed for reducing and derivatising the analyte is prevented, thus there is no volatile selenium formed (Motomizu & Sanada, 1995) (Mack & Bolton, 1999) (Lopes, Sturgeon, Grinberg, & Pagliano, 2017).

Among the possible reductants for nitrate, formaldehyde in hot solution was chosen in this work as its possible oxidising reactions of prevalence, depending on nitric acid concentration upon a study made by T.V. Healy (Healy, 1958) are:

For HNO₃ concentration above 7 mol L⁻¹:



For HNO₃ concentration between 1 and 7 mol L⁻¹:

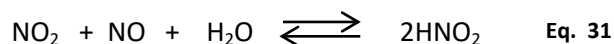


And for HNO₃ concentration below 1 mol L⁻¹:



If reaction of Eq. 30 occurs, the reaction product is formic acid, not foreign to the solution as it is added afterwards for the photo generation or, if it elapses until carbon dioxide is formed (Eq. 28 and Eq. 29), no product reaction will remain in solution as it is removed from solution by evaporation.

The permanence in the solution of the nitrogen oxides formed must be taken in consideration as they can hydrolyse in aqueous solution yielding nitrous acid which in turn will be an interfering for the hydride formation (Eq. 31) (Park & Lee, 1988).



The last can be removed by the addition of sulfamic acid in acidic media (Brasted, 1952) (Dzelzkalns & Ronner, 1978) (Mahfud, Ronze, Wehrer, & Zoulalian, 1998) (Granger & Sigman, 2009).



Lopes *et al* found this methodology prone to selenium losses and non effective in the absence of metal catalysers, high temperature and pressure (Lopes, Sturgeon, Grinberg, & Pagliano, 2017).

4.5.3.2 Experimental section

The interference abatement was first intended to be done on-line, as, once optimised, together with the nitrate elimination, selenium determination can be accomplished, in the same run, saving time and handling troubles. The reductant was added to the nitric solution altogether with the derivatising reagent.

However, in view of the results, an off line strategy had to be built. The elimination process was done previously so that the solution entering the FI-PVG-AAS system was already free from nitrate. Selenium stable species in nitric acid is Se(VI), so, for volatile species generation, the hydrochloric pre reduction step is mandatory. The possibility of nitrate elimination within that stage was also evaluated. Two situations were studied according to nitric acid concentration:

- 1) simultaneous elimination of nitrate and reduction of Se(VI)
- 2) nitrate elimination in stronger conditions

4.5.3.2.1 Instrumentation

The flow injection system is the same used in **4.5.2.1.1 Instrumentation**. As previously mentioned, the “on-line” and “off line” refers to the treatment of the interference; the difference between both situations is the composition of the solution that gets into the system, not the physical part of the system itself. The off line treatment was accomplished by evaporation on hot plates in extraction hood.

For the pH solutions adjustment, a Thermo Fisher Scientific Orion Versa Star Pro bench top meter fitted with a glass body pH electrode was used.

4.5.3.2.2 Reagents and solutions

Diluted solutions were prepared with deionised water (ASTM type I) obtained from a Millipore (São Paulo, Brazil) Direct-Q 5 water purifier. Working and calibration solutions were prepared by dilution of stock solutions of Se(VI) 1000 mg L⁻¹ standard atomic solution Carlo Erba E497625. Selenite solutions were prepared from sodium selenite (Aldrich, 99 %).

Ascorbic, formic, sulfamic, 36 % w/w hydrochloric and 65% w/w nitric acid, 35% w/w ammonia and 40 % w/w formaldehyde were of analytical reagent grade.

pH 4,01 and pH 7,00 buffer capsules (Hydrion® - Micro Essential Laboratory, Brooklyn, New York) were used for pH meter adjustment.

High purity, mixture of Ar: H₂ (92:8) and N₂, were obtained from Air Liquide Uruguay S.A..

4.5.3.2.3 Procedure

For the nitric acid interference study, increasing nitric acid concentration solutions were prepared at a fixed concentration of selenium within the linear range of the calibration curve. Then, the proposed sample treatment was achieved and the resulting solutions measured by FI-PVG-AAS. Peak area for each solution was recorded and compared with the one of a nitric acid free solution of the same selenium concentration.

Nitric acid interference was considered to be abated when the relative coincidence between the signals arising from the interfered solution overlapped about 80 – 120 % the interference free one. As solutions were gravimetrically prepared, concentration between them was close but not exactly the same, so, each peak area was normalised to the same concentration formerly to the comparison. For each experience, blank and interference free solutions were run.

At the first stages of the work efficient evidence of photo generation was found working on 1,0 % w/w HCl – 5,0 % w/w HCOOH media, afterwards it was found that the hydrochloric acid addition was unnecessary working at lower concentration of formic acid (1,5 % w/w). Working conditions for every experiment are detailed.

4.5.3.2.3.1 *On-line interference abatement*

The reagent intended to reduce the nitric acid of the medium, was added directly to the measurement solution as well as the derivatising agent. The aim was to find a reductant which could reduce nitrate beyond nitrite.

For that purpose, selenium solutions of 0.5 – 1.0 and 2.0 % w/w HNO₃ were added with formic, sulfamic and ascorbic acid in addition to the formic acid needed for the photo generation of the volatile species.

4.5.3.2.3.2 *Off-line interference abatement*

4.5.3.2.3.2.1 *Se(VI) reduction to Se(IV)*

Sample : 37 % HCl (2:1) was gently boiled on a hot plate under fumes extraction until the volume left was half the original. This procedure was carried out for standards and samples after nitrate elimination stage.

4.5.3.2.3.2.2 *Simultaneous elimination of nitrate and reduction of Se(VI)*

Once the reduction formerly mentioned was finished, 0,5 – 0,6 g of HSO₃NH₂ were added and then gently boiled for a few seconds. The resulting solution was neutralised and added with formic acid up to 1,5 % w/w HCOOH.

4.5.3.2.3.2.3 Nitrate elimination under stronger conditions

Formaldehyde was employed for nitric acid reduction; sample was added with formaldehyde, heated in a hot plate almost to dryness and retaken to its original volume with water. Then the proceeding was as in 4.5.3.2.3.2.1 and 4.5.3.2.3.2.2.

4.5.3.4 Results and discussion

4.5.3.4.1 On-line interference abatement

Even at low concentration, (below 0,5 %), nitric acid suppresses selenium signal. As previously mentioned, 0,5 – 1,0 and 2,0 % w/w HNO₃ were tried. For 1,0 and 2,0 % w/w HNO₃ no evidence of nitrate elimination was found, so, for every study mentioned later only reference to 0,5 % concentration will be done.

4.5.3.4.1.1 Formic acid:

A 0,5% w/w HNO₃ – 1,0 % w/w HCl – 5,0 % w/w HCOOH – 25 µg kg⁻¹ Se solution was added at 5 – 10 – 15 and 20 % w/w HCOOH. As seen in Figure 105, there is a slight peak formation as HCOOH concentration increases, probably because as there is no much nitric present. Formic amount is enough for reacting completely with it, but, the volatile species is not properly generated. As previously discussed, the photo generation needs a careful choice of the acidic conditions that are out of control in this situation.

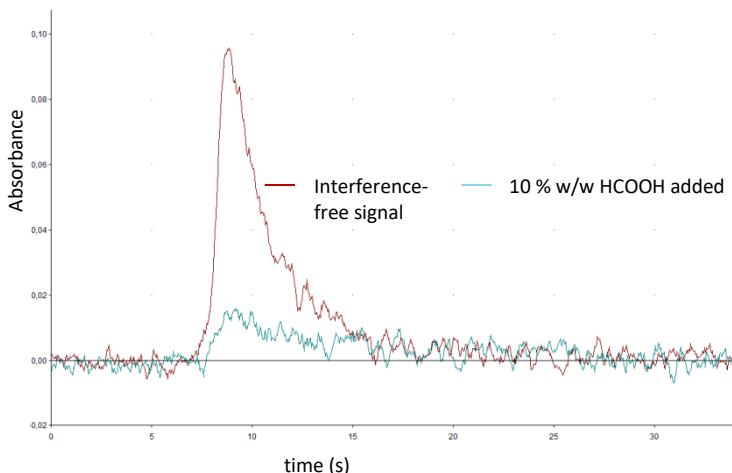


Figure 105: Selenium signal for a 0.5% w/w HNO₃ – 1,0 % w/w HCl – 5,0 % w/w HCOOH - 25 µg kg⁻¹ Se solution added with 10 % w/w HCOOH.

Signals were not better for higher additions of HCOOH as it started to decrease due to the high concentration of HCOOH in the generating media.

4.5.3.4.1.2 Sulfamic acid:

A 0,5% w/w HNO_3 – 1,0 % w/w HCl – 5 % HCOOH – $25 \mu\text{g kg}^{-1}$ Se solution was added at increasing concentrations of sulfamic acid evidencing no signal until it reached 30 g L^{-1} concentration. Sulfamic acid solubility in water is reported as $175,7 \text{ g L}^{-1}$ at 20°C (Ullmann, 2007).

A 0,5 % w/w HNO_3 – 1 % w/w HCl – 5 % HCOOH – $25 \mu\text{g kg}^{-1}$ Se solution was added with sulfamic acid up to 50 – 100 and 150 g L^{-1} HSO_3NH_2 . Figure 106 shows how the addition of sulfamic acid allows the photo generation. However, generation efficiency is too low, as compared with the expected signal. Interference is apparently abated, but the generation process is not being properly fulfilled, probably, because sulfamic acid leads to an acid concentration in which more formic acid is needed. When the last is added so as to get a final concentration close to 10 % w/w, there is a signal increment but the recovery is not enough yet.

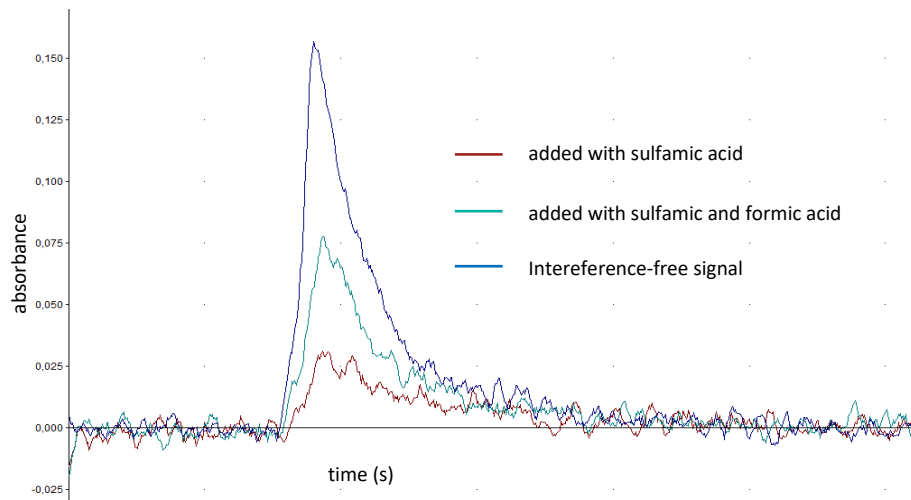


Figure 106: Selenium signal in 0,5 % w/w HNO_3 solution after the addition of sulfamic acid and sulfamic and formic acid.

Formic acid in the nitric solution was increased (from the previous experiment, 8 – 9 % w/w HCOOH leads to suitable signal) as well as the sulfamic acid one, in order to find the optimum ratio between the reagents that abate the interference in suitable photo generation conditions.

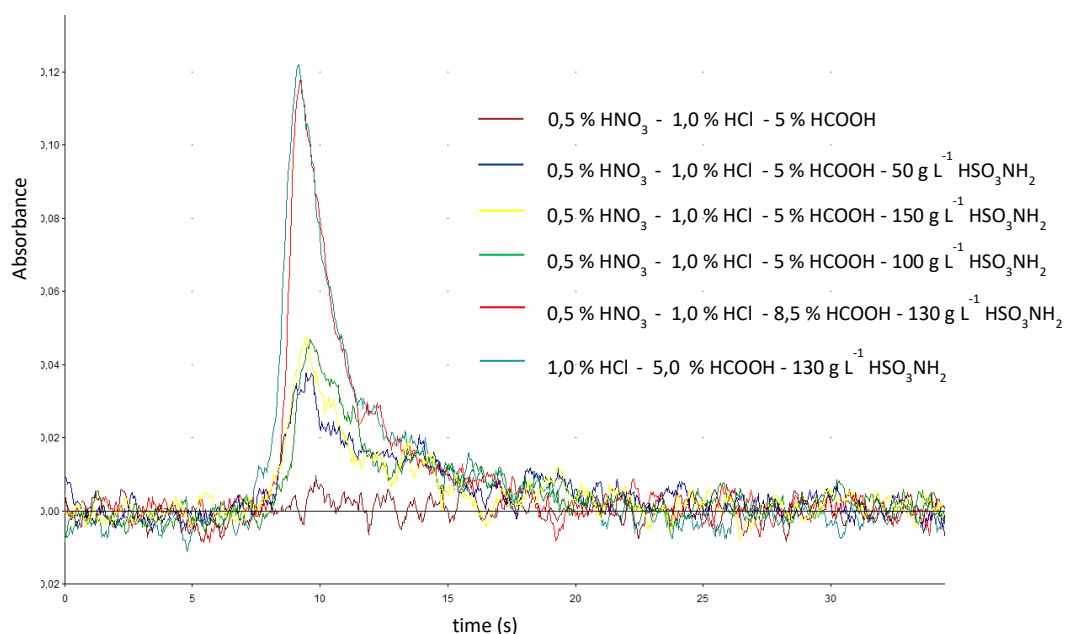


Figure 107: Selenium signal for solutions containing different amounts of formic and sulfamic acid.

Taking as reference a 1 % w/w HCl – 5 % HCOOH solution, similar results were found with 1 % w/w HCl – 8,5 % w/w HCOOH – 130 g L⁻¹ HSO₃NH₂ for solutions up to 0.5 % w/w HNO₃ with a 115,2 % recovery of selenium signal (Figure 107).

4.5.3.4.1.3 Ascorbic acid

A 0.5% w/w HNO₃ – 1,0 % w/w HCl – 5 % HCOOH – 25 µg kg⁻¹ Se solution was added by 3,5 % w/w ascorbic acid, There was no evidence of photo generation. A brownish solid precipitated in the solution. Evidently irradiation accelerates the reaction between nitric and ascorbic acid as the solution (under no exposure) gets brown after some hours. Ascorbic reduction is not complete, the intermediate products precipitate inside the reactor adhering to the reactors inner walls preventing the irradiation to reach the solution and increasing the risk of irreversible damage of the reactor. Efforts to find appropriate conditions were left aside.

To sum up, only sulfamic acid in the previously specified conditions was able to abate the interference produced by 0,5 % w/w HNO₃ interference on-line. Acidic media of this range of concentration are not frequent in solutions were inorganic analyses is to be performed. It is necessary to find a method relevant to selenium determination in a wider range of nitric acid concentration.

4.5.3.4.2 Off-line interference abatement

From all above discussed, the methodology concerning the nitrate interference should consider both the same media acidity (for a constant amount of formic acid) and an efficient reduction of Se(VI) to Se(IV) (upmost volatile generation efficiency) so as to assess reproducible results.

4.5.3.4.2.1 Simultaneous reduction of Se(VI) to Se(IV) and nitrate elimination:

Procedures 4.5.3.2.3.2.1 Se(VI) reduction to Se(IV) and 4.5.3.2.3.2.2 Simultaneous elimination of nitrate and reduction of Se(VI) were carried out in solutions from 0 to 7.0 % w/w HNO₃ at the same selenium concentration.

Interference was considered to be abated when: $80\% < \frac{A_{\text{int}}^{\text{interfered solution}}}{A_{\text{int}}^{\text{interference free solution}}} \times 100 < 120\%$, A_{int} is the integrated absorbance, both areas correspond to the same concentration of selenium. Results are shown in Figure 108. The shaded area corresponds to the acceptance criteria zone.

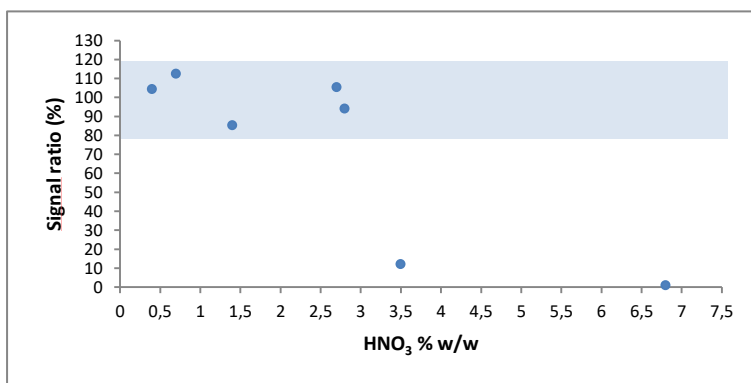


Figure 108: Elimination of nitric acid's interference in the selenium (VI) reduction step. Nitric acid concentration refers to % w/w of 65% HNO₃.

Up to 3.0 % HNO₃, nitrate interference could be defeated simultaneously within the reduction process.

For higher concentrations of nitric acid, stronger conditions must be used.

4.5.3.4.2.2 Nitrate elimination in stronger reductant conditions.

Formaldehyde was the reductant chosen for the elimination of nitrate as its potential products of oxidation are formic acid (the photochemical reagent) and carbon dioxide (which does not remain in solution).

Several experiments at different nitric acid concentration, within the range 0,5 – 21 % w/w HNO₃ were tried at 10, 20, 40 and 60 % w/w H₂CO. Figure 109 shows some of the experiments achieved when optimising the concentration of formaldehyde. Blue area corresponds to the amounts of nitric acid; it

was chosen between the common concentrations found for sample preservation or after a wet sample digestion. The orange zone shows for each nitric acid concentration, the formaldehyde amount added to the samples. The green one corresponds to the recovery of selenium attained.

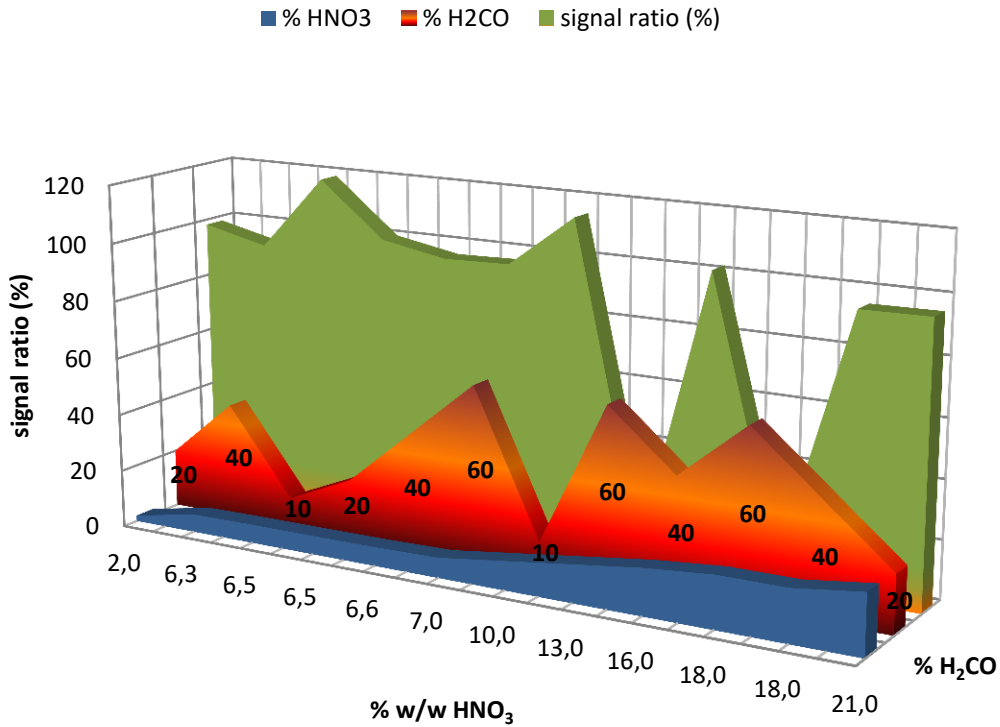


Figure 109: Signal ratio for the elimination of different amounts of nitrate with different reductant (H₂CO) concentrations.

The signal absence both at high nitric acid and formaldehyde even if not concluding is explained in “Elucidation of the lack of signal after nitrate elimination” (page 225).

20 and 40 % w/w H₂CO threw suitable recovery all nitric range long; 40% was chosen in order to ensure its efficiency whenever a sample could have another oxidant.

Results are shown in Figure 110. The shaded area corresponds to the acceptance criteria zone.

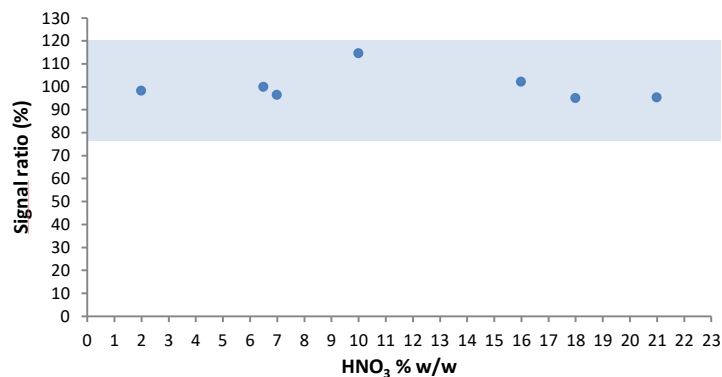


Figure 110: Elimination of nitric acid interference by 40% w/w H₂CO.
Nitric acid concentration refers to % w/w of 65% HNO₃.

Nitrate elimination was ensured in solutions up to 21 % w/w HNO₃ which is, generally the maximum acid concentration of samples after a wet digestion. No higher acid concentration was tried.

4.5.4 Method characterization/method evaluation

4.5.4.1 Experimental section

In order to evaluate the applicability of the method, some performance characteristics such as limit of detection and quantification, linear range, precision (repeatability) and trueness were assessed. Up to now, nitrate elimination was performed in standards solutions; the aim was to ensure that it can be efficiently removed for selenium to be determined in different matrix. Hence, for assessing trueness, two samples at low and high, both selenium and nitric acid concentration were chosen: a water sample reference material (2% v/v HNO₃ – 2,8% w/w HNO₃ approx., 24,3 Se - µg L⁻¹) and a spiked solution of a rice flour acid digestion (18,5 % w/w HNO₃ approx., 103,1 Se - µg L⁻¹ after spiking).

4.5.4.2 Instrumentation

The flow injection system is the same used in **4.5.2.1.1 Instrumentation**.

For sample digestion (rice flour) an acid wet digestion was achieved in a Mars 6, CEM Corporation, Matthews, NC, USA microwave oven.

Sample nitrate elimination and Se(VI) reduction was accomplished by evaporation on hot plates inside an extraction hood.

For the pH solutions adjustment and potentiometric measures, a Thermo Fisher Scientific Orion Versa Star Pro bench top meter fitted with a glass body pH electrode was used.

4.5.4.3 Reagents and solutions

Diluted solutions were prepared with deionised water (ASTM type I) obtained from a Millipore (São Paulo, Brazil) Direct-Q 5 water purifier. Working and calibration solutions were prepared by dilution of stock solutions of Se (VI) 1000 mg L⁻¹ standard atomic solution Carlo Erba E497625.

Formic, sulfamic, 36 % w/w hydrochloric acid, 35% w/w ammonia and 40 % w/w formaldehyde were of analytical reagent grade.

Certified reference material, MRC.INO.101 Trace elements in water, was obtained from Laboratorio Tecnológico del Uruguay (LATU).

pH 4,01 and pH 7,00 buffer capsules (Hydrion® - Micro Essential Laboratory, Brooklyn, New York) were used for pH meter adjustment.

High purity, mixture of Ar: H₂ (92:8) and N₂, were obtained from Air Liquide Uruguay S.A..

4.5.4.4 Procedure

The blank signal obtained did not differ from the baseline, so, the estimation of the limit of detection and the limit of quantification were calculated from the standard deviation of ten replicates of the signal of a solution of the blank reagent spiked at a low concentration of Se(VI) and reduced with hydrochloric acid.

The linear range was evaluated up to 100 µg L⁻¹ with a seven point external standards calibration curve. The standard solutions were prepared from Se(VI) atomic absorption standard, diluted with deionised water and reduced with hydrochloric acid.

The spiked solution of the rice flour acid digestion was prepared as follows: 0,5 g of sample was treated with 8 mL of HNO₃ 1:1, let stand for 10 minutes and wet digested with microwave assistance. The heating programme consisted on a 20 min ramp up to 120 °C, holding at that temperature along 20 minutes, followed by a 20 min ramp from 120 °C up to 170 °C and 15 minutes at this last temperature. After digestion, samples were diluted with ultrapure water to 30 g. Five portions of sample were digested altogether with two blanks solutions. The digests were brought together, mixed and separated in two portions. One of them was spiked with Se(VI) and analysed by quintuplicate. The other, analysed without spiking to verify the absence of selenium in it. Blank digests were also analysed.

Trace element in water CRM needed no sample preparation step; it was analysed by quintuplicate.

Precision of repeatability was assessed at 20 Se - µg L⁻¹ level and at 100 Se - µg L⁻¹ level as the relative standard deviation of the results of the five replicates of water CRM and spiked digest of rice flour respectively.

4.5.4.5 Results and discussion

4.5.4.5.1 Evaluation of the linear range and calibration function

The calibration function was found linear within the whole range studied. The analytical signal was peak area (integrated absorbance).

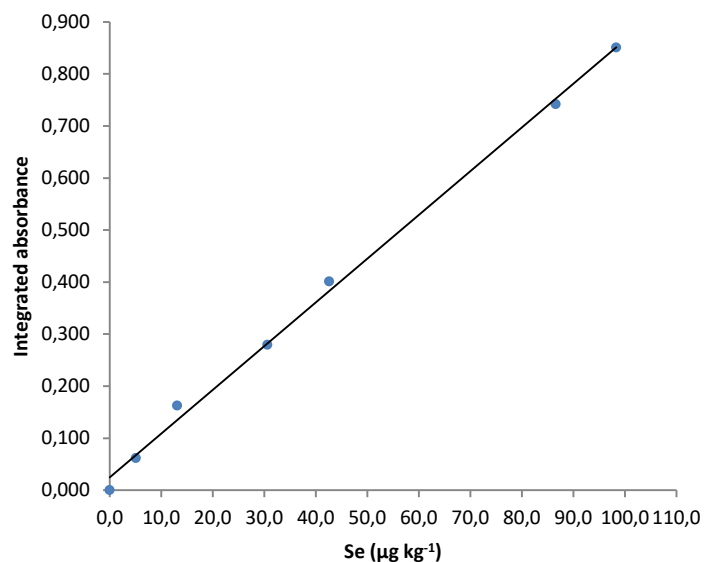


Figure 111: Calibration function: Peak area as a function of the concentration.

4.5.4.5.2 Signal dispersion between replicates

The signal was recorded from the moment of the injection to 40 s. For each signal the area was integrated within the limits of the peak (the interval of time in which it leaves and reaches again the baseline). The blank signals, as there is no peak, correspond to the integration of the baseline between the time limits of the lowest calibration standard signal.

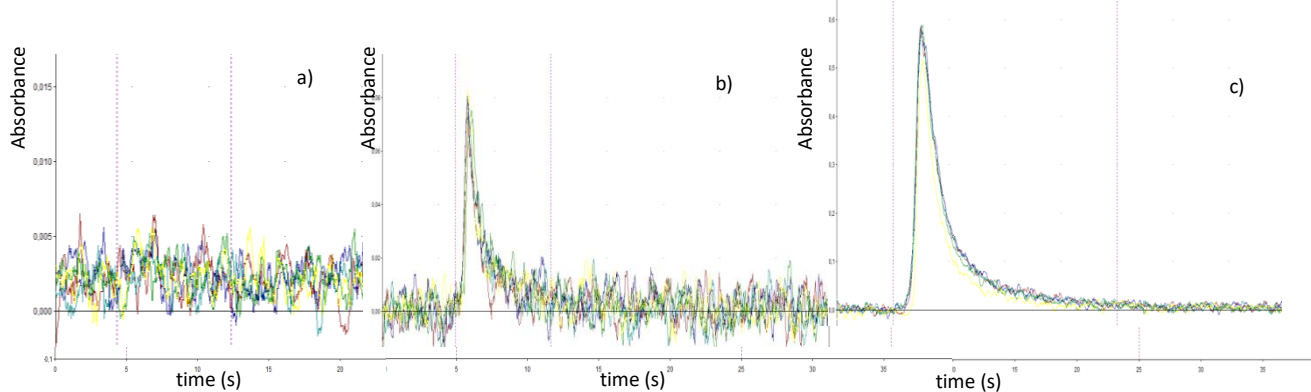


Figure 112: Signal replicates for a) blank; b) $10 \mu\text{g kg}^{-1}$ – Se; c) $100 \mu\text{g kg}^{-1}$ – Se

Instrumental precision (repeatability, n = 5)	
Concentration level ($\mu\text{g kg}^{-1}$)	s_r (%)
0	5,1
5	4,3
10	2,8
20	1,3
30	2,3
40	2,6
50	4,3
100	6,4

Table 42: Instrumental precision at different concentration levels of selenium in 1,5 % w/w formic acid.

As presented in Table 42 the repeatability of the signals is below the 5 % in the most of the concentration levels, suitable for quantification purposes.

4.5.4.5.3 Summary of the performance of the photochemical vapour generation of selenium derivatives in 1,5 % w/w HCOOH.

A summary of some parameters used for the characterisation of the method are presented in Table 43.

Limits of detection and quantification were calculated as follows: $LOD = \frac{3s}{m}$ and $LOQ = \frac{10s}{m}$ where s is the standard deviation of ten signal replicates (integrated absorbance) of the spiked blank and m the slope of the calibration function.

As expected the precision of repeatability was high at low levels of selenium, even though, considering all the manipulation that is involved for the low amount of selenium it is acceptable.

Recovery of selenium found in both samples confirms the nitrate abatement was attained.

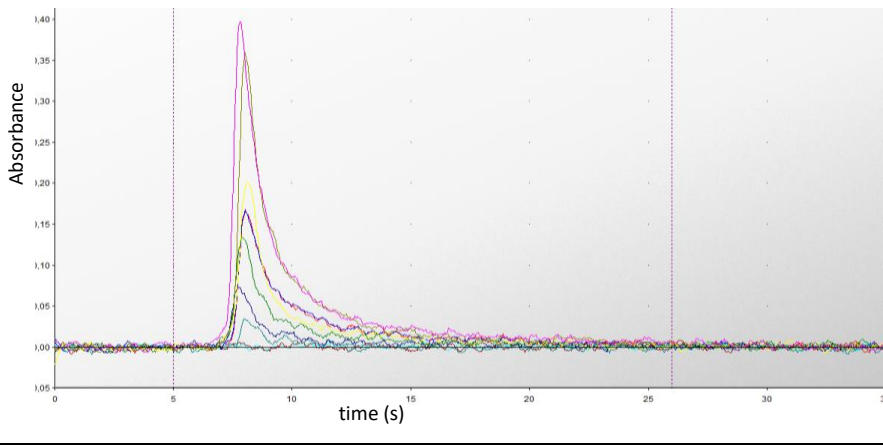
				Calibration function	
				$A_{int} = 0,0166C - 0,0883$	
				$R^2 = 0,9900$	
				LOD ($\mu\text{g kg}^{-1}$)	LOQ ($\mu\text{g kg}^{-1}$)
				0,98	3,3
Precision (repeatability), n = 5					
$20 \mu\text{g L}^{-1}$	s_r (%) : 20,2	$100 \mu\text{g L}^{-1}$	s_r (%) : 5,2		
Trueness (%), n = 5					
Trace element in water CRM (2 % v/v HNO_3)	100,3	Spiked flour digest (18 % w/w HNO_3)	85,0		

Table 43: Method characterisation. A_{int} : integrated absorbance (s); C: concentration ($\mu\text{g kg}^{-1}$); LOD: limit of detection; LOQ: limit of quantification; s_r (%): relative standard deviation; n: number of replicates. Trace Element in Water CRM: $24,3 \mu\text{g L}^{-1}$ - Se; Spiked rice flour digest: $103,1 \mu\text{g L}^{-1}$ - Se.

The methodology developed is able for nitrate interference abatement and, even if it was intended for selenium determination in the first instance, it could be extended for other elements as it aims to the interfering substance and not to the analyte.

It cannot be disregarded that the manipulation involved is time consuming as, for selenium determination there are two evaporation steps. The first one, where the oxidation of formaldehyde takes place, is fast and can be accomplished with a vigorous boiling without inconvenient. Nevertheless, the second one, the Se(VI) reduction step in solutions where nitrate has been eliminated, must be done softly, in gentle boiling just to allow the evaporation, to avoid and volatile selenium chloride formation; besides solution is very prone to project. In the first stage, solution turns brownish, probably because incomplete nitrous intermediate compounds still remain in the solution and now get out of it because they are reduced by the hydrochloric acid added. In the very first minutes, until their appearance, solution must be gently shaken periodically so as gas cavities do not create and project in their expansion. The risk of projection decreases once the solution gets uncoloured again.

The ideal situation would be to accomplish all the determination on-line, but, even if a reductant was found, the pH control for the photo generation stage is unavoidable.

If photo generation is intended to be used, the proposed methodology ensures a reliable way of eliminating nitrate interference and obtaining suitable results, fit for trace analyses.

4.5.5 Elucidation of the lack of signal after nitrate elimination

For the same working conditions, after nitrate elimination, some solutions developed a signal and others did not. Different hypothesis were made:

- 1) Nitrate was not eliminated
- 2) Increased levels of formic acid (oxidation of formaldehyde)
- 3) Formaldehyde treatment causes selenium losses.
- 4) Reduction step was not properly accomplished so selenium is as Se(VI) and no volatile species is generated. The reduction step is no reproducible and needs to be optimized.

Different strategies were implemented so as to find the true reason.

4.5.5.1 Nitrate was not eliminated

If nitrate is not eliminated from solution, the radical cascade is quenched and the photo generation is suppressed. As some replicates did present measurable recoveries, probably the elimination step is no reproducible and needs to be optimised.

Se(IV) was spiked to five different solutions in which selenium signal was absent and determined by PVG. If nitrate was present in that solution, no signal is expected. Se(IV) and not Se(VI) was added to avoid the reduction step and not vary the nitrate concentration (during the reduction stage) if it was not already eliminated.

Recoveries were 78,3 , 90,2 , 94,2 , 95,8 and 113,9 %.

Hence it was concluded that there is no nitrate present in the solutions; the elimination step is running properly, there is no need of further optimisation.

4.5.5.2 Increased levels of formic acid

Depending on nitric acid concentration and the temperature, formaldehyde can be partially converted to formic acid (Healy, 1958). The product of the reaction depends on the working conditions. Considering the reaction described by Healy, at 100°C (gentle boiling in this work), two moles of formic acid would be formed per mole of nitrate eliminated once the acidity of the media is decreased. However, assuming nitrate complete reaction in these conditions, for a known amount of nitric acid, the number of moles of H₂CO converted to HCOOH may be calculated and so the latter final concentration: 0,23 g HCOOH are formed in solution per gram of 65% w/w HNO₃ eliminated. A 10 % w/w HNO₃ solution when decomposed by formaldehyde almost duplicates the amount of formic acid in the generation media. As was previously studied, if the final concentration of formic acid in solution is higher than the optimal, signal would be depressed. So, it would be of relevance knowing the amount of formic acid left after the

interference elimination. Again, as not every solution presented the same behaviour probably the evaporation was not running properly and had to be optimised.

To those solutions which gave no selenium signal, the amount of formic acid was potentiometrically determined by an acid-base back titration. The different species of formic acid upon the steps of the process:

- i. Nitrate elimination (formaldehyde oxidation), formic acid is produced:



- ii. Selenium reduction: HCOOH formed remains under this chemical species

- iii. Neutralisation (formic acid turns to formate):



- iv. Addition of HCOOH for the photochemical generation (HCOOH added partially dissociates, mixture HCOOH/HCOO⁻).

If reaction i) occurs, the measured solution (the one which gave no selenium signal) is composed by a mixture of HCOO⁻/HCOOH. The acid base titration of this solution by the addition of NaOH, makes only the HCOOH react; so, the titration of this solution gives the amount of formic acid added.

To determine the amount of formate in that solution (which comes from the oxidation of the formaldehyde), a known amount of hydrochloric acid can be added:



The acid base titration of this solution by the addition of NaOH, reacts first with the excess of HCl remaining in the solution and then with all the formic acid present in solution, the formed by the addition of the hydrochloric acid and the one added for the photochemical reaction; so, the titration of this solution gives the total amount of formic acid.

In brief:

The direct titration of the solution gives information about the formic acid added. The back titration of the known amount of hydrochloric acid added gives information about the total amount of formate/formic acid in solution.

If the latter is too high, the possible cause of the lack of selenium signal in solution is the excess of formate/formic acid.

Thus, to an aliquot of a solution that gave no selenium signal after the treatment, a potentiometric acid base titration was performed and the amount of formic acid added calculated.

To another aliquot of the same solution, a known amount of hydrochloric acid was added so as to convert the formate to formic acid. The resulting solution is a mixture of formic and hydrochloric acid. This titration would have two end points, the first corresponding to the titration of the excess of hydrochloric acid and the second corresponding to the back titration of the formate transformed to formic plus the formic added to the photo generation.

The known amount of hydrochloric acid added is determined by titrating an aliquot of it. The acid base titration was performed with $0,10 \text{ mol L}^{-1}$ NaOH as the titrant.

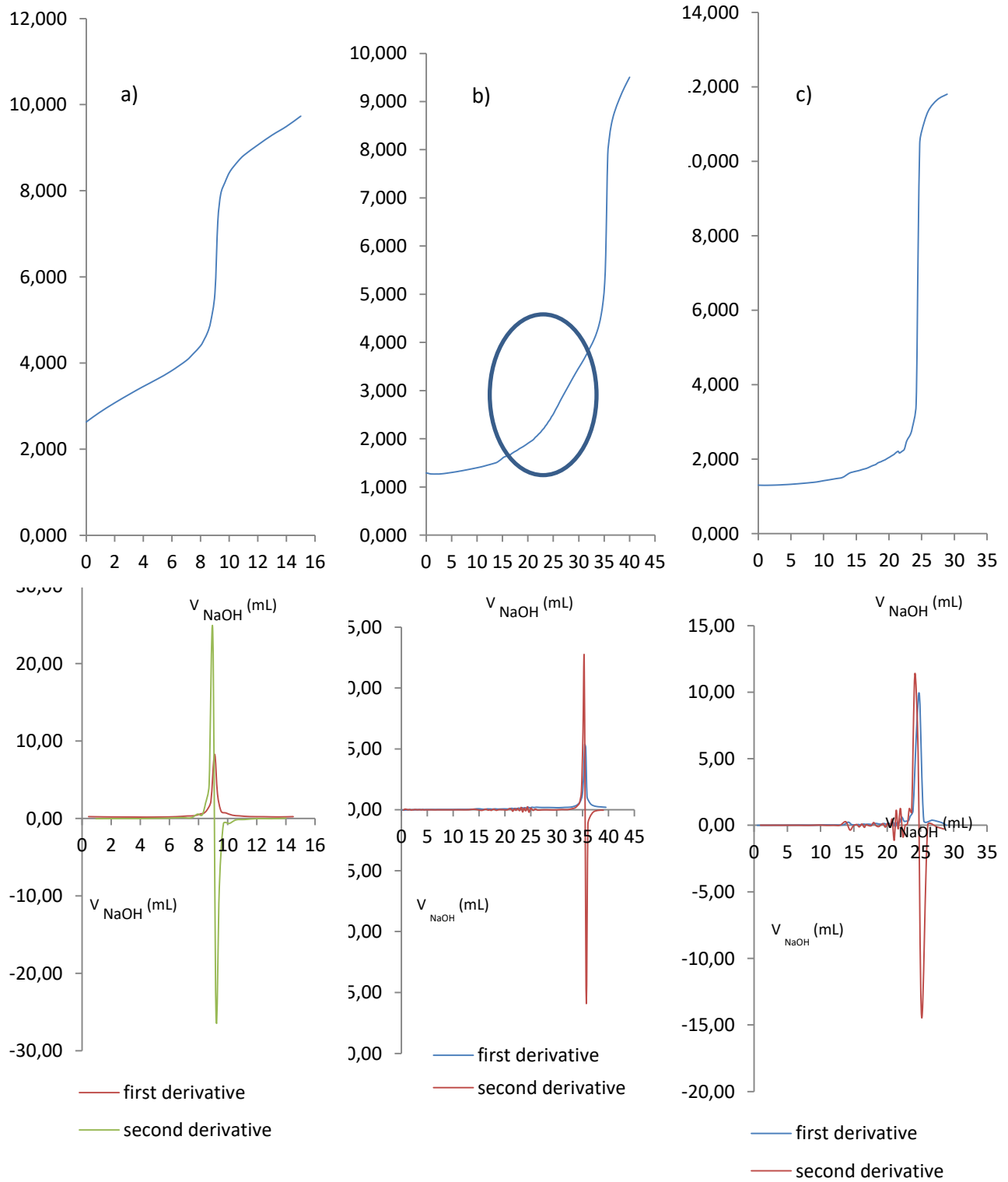


Figure 113: Titration curves and its first and second derivative. a) titration of formic acid added, b) titration of total formic/formate, c) titration of HCl.

Figure 113 shows the titration curves for a), the measured solution (in which peak was absent), b) the same solution added with hydrochloric acid so as to back titrate the formate and formic added and the c) hydrochloric acid added in the previous one. To each of them the first and second derivative were plotted so as to calculate the end point.

Curve a) was obtained as follows: for the amount of formic acid expected and its acid dissociation constant ($k_a=1,8 \times 10^{-4}$), 0,6 g of solution were taken, diluted to approx. 20 mL and titrated with 0,10 mol L⁻¹ NaOH. A glass electrode measured the cell potential after each titrant addition and the curve pH vs volume of titrant added was plotted. The sharp end point corresponds to the titration of the formic acid added to the solution as derivatising agent for the photochemical reaction.

The end point is determined by the second derivative function crossing the abscise axis. The measured solution is 0,0014 mol g⁻¹ in HCOOH.

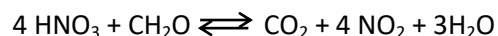
Curve b) was obtained as well. In turn, the titrated solution is another similar aliquot of the same solution, added with hydrochloric acid. Now the titration corresponds to the mixture of the strong acid (hydrochloric acid excess, firstly titrated) and the whole formic acid (the protonated formate and the formic acid added). The first end point is expected at the pH of acid dissociation of formic acid (formate neutralised plus formic added), for the concentration expected is about pH = 2,6 (actually similar with the one found in the previous aliquot), a solvent buffered zone, thus it was not surprising that it was almost imperceptible as it is remarked in the curve. It is noticeably that accurate results cannot be waited from this experiment. However, it can give an idea if formate is increased in a relevant amount so as to completely suppress selenium signal.

Curve c) is the titration of the hydrochloric acid, so, it enables to calculate the exact amount added: 0,0065 mol g⁻¹.

The second derivative of b) is very noisy near the first end point, but it defines a close interval where the end point may be. Considering the extremes of this interval, total formic concentration lies within 7,6 and 10,0 % w/w. As verified in the optimisation studies, even if these amounts were present in solution, selenium signal would be undoubtedly lowest but would have never been suppressed.

Furthermore, all the elimination process was achieved skipping the addition of formic acid. No selenium signal arose from these solutions.

Consequently, there is no extra formate amount in the measuring solutions. Apparently in the working conditions formaldehyde is completely oxidised to carbon dioxide, possibly:



There is not formate in excess that could explain the lack of selenium signal.

4.5.5.3 Formaldehyde treatment causes selenium losses

During nitrate elimination sample is vaporised almost to dryness maybe causing losses of selenium. The excess of formaldehyde can reduce selenate to selenite and selenite to elemental selenium, thus, no volatile species is generated.

The same procedure as for interference abatement was accomplished but in the absence of nitric acid. Recoveries of 107,1 – 115,5 % were found. The first stated is not taking place in the working conditions, so, there are no selenium losses.

4.5.5.4 Reduction step was not properly accomplished

If selenium is under whatever species other than Se(IV) no volatilisation will take place.

4.5.3.4.1 Se(IV) determination by CVG

In those solutions where selenium gave little or no signal, it was determined by chemical vapour generation so that to confirm the presence of Se(IV).

Se(IV) was determined by HG-MIPOES: the hydride was chemically generated by sodium tetrahydroborate and determined by atomic emission in a microwave induced plasma. Working conditions were first optimised: pump speed 30 rpm (together with tubes diameter determines the ratio between the reductant and the sample), stabilisation time 15 s (is the time the reaction takes place in the chamber before the reading stage starts), read time 10 s, viewing position – 80 (relative height of the torch indicating the greater population of exited atoms) and nitrogen flow 0,9 L min⁻¹ (sweeps the hydride from the reaction chamber to the plasma). Selenium was determined at 196,026 nm with 2,0 % w/v NaBH₄ – 1,0% w/v NaOH as the chemical reductant.

Results from the alternative method are consistent with those found by photo generation: solutions that gave no selenium signal by PVG either by CVG gave, and those which gave a signal lower than expected differed between both methods about a 20 %. The reduction step is out of control and needs optimisation.

From all the previous results, it can be concluded that the photo generation is working properly: nitric acid is eliminated, no excessive additional formic acid is formed and no losses of selenium are detected in the first evaporation step; thus, the absence of signal in some of the solutions may be due to a non-efficient reduction of Se(VI) to Se(IV).

Reproducible reduction conditions are imperative.

The nitrate elimination stage was accomplished to six replicates of a nitric selenium solution. Then, for the reduction step, three were evaporated just to half the original volume and the other three almost

to dryness (taking care not to dry at all). The rest of the procedure was accomplished as usual and solutions measured by PVG.

A nitrate free reference solution was run altogether. Normalised areas were compared.

For those solutions which were taken almost to dryness, signal kept away between 27 and 19 % below the expected value, probably due to volatiles selenium chlorides volatilisation. The ones which were evaporated to half its volume fell between -1,6 and 3,8 % the expected value.

Summarizing, the steps to follow for nitric acid samples are:

- i. sample : 40 % H_2CO (5:2), evaporation almost to dryness
- ii. retaken to original volume with water
- iii. sample : 37 % HCl (2:1), evaporation to half its volume
- iv. addition of 0,5 – 0,6 g HSO_3NH_2 and gentle boiling for a few seconds
- v. neutralisation
- vi. addition of HCOOH to 1,5 % w/w HCOOH

For samples up to 3,0 % w/w HNO_3 steps i and ii can be avoided.

Compared to classic chemical vapour generation (hydride generation), the main advantage of the photochemical vapour is undoubtedly the media where the reaction takes place. Tetrahydroborate is avoided, working conditions are milder as not concentrated hydrochloric acid is needed, reagents employed are cheaper and easy to find in any analytical lab and all the system operates friendly. The performance found is within the expected for gaseous sample introduction techniques.

However, as in CVG, the impact of the nitrate derivatives interference is of greater importance; nitrite among its reduction products rather than nitrate is a more relevant interferent (Pierce & Brown, 1976) (Brown, Fry, Moyers, Northway, Denton, & Wilson, 1981). The last authors discuss for CVG that in clean nitrate systems the interference is not manifested but it becomes important when nitrate was added for a sample treatment as by-products of the reaction are present. In the case of photochemical reactions, these intermediates are formed by nitrate photolysis, so their presence is unavoidable whenever nitrate is in solution.

The nitrate elimination step is labouring and time consuming as was discussed in **4.5.4.5.3**, but, is unavoidable whenever volatile species are involved, no matter how they are generated. So, these inconvenient are beyond the scope of the photochemical generation itself.

4.5.6 Conclusions

The variables of influence of a flow injection photochemical vapour generation atomic absorption spectrometry system were studied and optimized for selenium determination. The elimination of nitrate's interference with hot 40 % w/w formaldehyde prior the photo generation resulted successful up to 21% w/w nitric acid media. The strategy was verified for the determination of selenium in CRM and a spiked sample; even though, it can be extended whenever photochemical vapour generation is chosen as the sample introduction technique for atomic absorption spectrometry.

Chapter IV

Volatile selenium derivatives

Scientific production



O OTR 01

Radicales reductores y ácido nítrico: avances en la principal limitante de la aplicación de la fotogeneración de derivados volátiles

Mollo, Alicia; Knochen, Moisés

Química Analítica, Facultad de Química, UdelaR
amololo@fq.edu.uy

La generación fotoquímica de compuestos volátiles es una técnica de introducción de muestra para espectrometría de absorción atómica que ha cobrado importancia en los últimos años. Consiste en la generación de derivados volátiles a partir de precursores metálicos iónicos y moléculas de compuestos orgánicos de bajo peso molecular por irradiación ultravioleta. Los fotones escinden las moléculas orgánicas generando radicales que reducen y sustituyen al ion formando compuestos gaseosos que se liberan de la solución y son arrastrados hacia una celda de atomización para su determinación por espectrometría de absorción atómica.

A pesar de las ventajas inherentes a la generación de especies volátiles, como son la preconcentración del analito con la consecuente mejora de los límites de detección y cuantificación, la generación fotoquímica tiene como principal desventaja la inestabilidad de los radicales reductores formados en presencia de agentes oxidantes en el medio de reacción que disminuye la eficiencia de la fotogeneración o la elimina completamente. Esto implica una limitación que se torna imperativa de solucionar al pretender aplicar la técnica en el análisis de la mayoría de las muestras ya que la presencia de ácido nítrico es de esperarse por requerir la muestra de digestión ácida para su disolución y/o eliminación de materia orgánica o simplemente porque se lo agrega como estabilizante para su conservación.

El presente trabajo es parte de la validación de la generación fotoquímica de derivados volátiles de selenio. Las condiciones óptimas encontradas para la fotogeneración, es el medio ácido clorhídrico al 1% m/m, empleando ácido fórmico al 5% m/m como ácido orgánico e irradiando la muestra con radiación ultravioleta durante 6s.

En la evaluación de la aplicabilidad de la técnica a muestras diversas se ensayaron posibles estrategias para la eliminación del ácido nítrico: dado que la generación del derivado volátil transcurre exclusivamente para el estado de oxidación (4) del selenio, es necesario reducirlo previamente a esa especie mediante el tratamiento térmico en HCl al tercio. Se verificó que es posible realizar la fotogeneración sin más pretratamiento que la reducción química con posterior eliminación de los productos de reacción intermedios con ácido sulfámico al 10% m/m en soluciones de hasta 1% m/m en HNO₃. Se ensayó también el formaldehído como reductor. Para soluciones con HNO₃ al 2% m/m, se ensayaron distintas proporciones lográndose vencer también la interferencia mediante el agregado de una masa de formaldehído correspondiente al 10% m/m de la masa total de la solución. Se está trabajando en la determinación de una proporción óptima entre HNO₃ y H₂CO que permita ampliar el rango de aplicabilidad del tratamiento a soluciones más concentradas en ácido nítrico de forma de poder determinar el selenio mediante fotogeneración a cualquier digesto de muestra.

Lopes G.S., Sturgeon E.R, Grinberg P., Pagliano E. Evaluation of approaches to the abatement of nitrate interfere with photochemical vapor generation. J. Anal. At. Spectrom., 2017,32, 2378-2390

Towards the abatement of nitrate interference in selenium determination by photochemical vapour generation (PVG)

Alicia Mollo ^{*}, Moisés Knochen ^{*}

^{*} Facultad de Química, Universidad de la República, Montevideo, Uruguay
amolloy@fq.edu.uy

Keywords: photochemical vapour generation, interference study, atomic absorption spectrometry

Vapour generation is a well-established sample introduction technique for atomic absorption spectrometry, reaching low limits of detection and quantification and minimizing matrix interaction with the analyte. The element volatile specie is generated by reduction with sodium tetrahydroborate in strong acid medium and swept away by a gaseous carrier up to the atomisation cell. Photochemical vapour generation expand its advantages working in milder conditions. It consists in a radical based reaction between the metal ion and a low molecular weight carboxylic acid (LMWCA) when irradiated by a UV source, leading to the generation of the gaseous compound. Despite its benefits, the presence of oxidants such as nitrate, limits its applicability as it suppresses the photogeneration. The use of nitric acid for sample pre-treatment is practically unavoidable so, the abatement of the interference is mandatory¹.

This work presents a methodology for nitrate elimination in digested samples for selenium determination by photochemical vapour generation in formic acid medium.

In order to remove nitrate, formaldehyde was added and the solution heated up to its half of volume. Selenium volatiles species are exclusively generated from Se IV, subsequently a reduction step is achieved with hot hydrochloric acid. Ultimately, sulfamic acid was incorporated. The resulting solution is nitrate free and with selenium in the adequate oxidation state. It is then neutralized and made up to the concentration of formic acid suitable for the photo generation.

For the photo generation, a single line flow injection manifold was built: a peristaltic pump propelled the sample (interference free solution of Se IV and the LMWCA) to a six port injection valve. When injected the sample is carried through a commercial flow through UV reactor using nitrogen as carrier. The irradiated solution is driven to a forced outlet gas liquid separator where the volatile specie was carried by a mixture of argon and hydrogen to a heated atomisation cell. Optimum working conditions were: 0,6 mL of sample, HCOOH 6,5% (m/m), 3s of irradiation, and Ar:H₂ (90:10) 400 mL min⁻¹ for the gas liquid separator.

The success of the interference abatement was evaluated by means of recovery percentage for known amounts of selenium (80 - 120 %). Nitrate was eliminated with H₂CO 40%-10% w/w for nitric acid solutions up to 10% w/w. Digests of rice flour and wheat flour in HNO₃ 18 % w/w gave recoveries no better than 60%. The same solutions were measured by hydride generation microwave induced plasma emission atomic spectrometry (HG-MIPOES) founding similar results as PVG. Besides, after spiking them with Se IV the recoveries by PVG were acceptable. Consequently, the interference was undoubtedly abated. Selenium reduction was the limiting step of the process, being its improvement the focus of the work in these days.

Acknowledges:

Authors wish to thank Mariela Pistón, Javier Silva, Florencia Cora Jofré and Marianela Savio for their contribution for HG-MIPOES measurements.

References:

- [1] G. S. Lopes, R. E. Sturgeon, P. Grinber, E. Pagliano, Evaluation of approaches to the abatement of nitrate interference with photochemical vapour generation, *J. At. Spectrom.* 32 (2017) 2378-2390.
DOI: 10.1039/c7ja00311k.

Chapter V

Construction of an electrically heated volatile species atomiser

This chapter describes the different stages of the construction of an electrically heated atomiser and different tests carried out to evaluate its performance.

Chapter 5: Abbreviations

CVG: Chemical Vapour Generation

ECVG: Electrochemical Vapour Generation

EHQTA: Externally Heated Quartz Tube Atomiser

LMWOC: Low Molecular Weight Organic Compound

PID: Proportional Integral Derivative

PVG: Photochemical Vapour Generation

SSR: Solid State Relay

THB: Tetrahydroborate

5 Construction of an electrically heated volatile species atomiser

5.1 Background

In the first stages of the work, atomisation of the volatiles species was expected to be achieved in an EHQTA mounted on a 10 cm burner and heated with an air-acetylene flame.

As previously mentioned, for volatile species atomisation (other than mercury), hydrogen is needed in order to provide a hydrogen radical cloud to achieve the atomisation.

In CVG, hydrogen evolving from the THB decomposition is enough for that purpose and, in ECVG, hydrogen is generated as the result of the cathodic reduction of the hydron ions.

In the case of PVG, the sole LMWOC leading to hydrogen is formic acid, and in very low amount thus hydrogen must be provided.

Whatever the option of the volatile species generation chosen, external flame heating of the atomisation device for high amounts of hydrogen, can lead to hydrogen ignition at the extremes of the atomisation cell resulting in nonspecific absorption, difficult to correct and which would impact on the repeatability of the measurement.

With an electrically heated heating device the temperature can be controlled. Hatfield (Hatfield, 1987), introduced the ends of the quartz cell optical tube into a coiled high resistant to corrosion nichrome wire for attaining the atomisation temperature.

The first purpose of this work was simply to heat the quartz tube with a wire resistor, isolating it from the contact of the air just to not get ignited and safeguarding its surroundings in the optical path of the spectrometer. Then, in sight of the good performance attempted a more robust appliance was sought. Finally, thanks to the enthusiastic participation of Ricardo Mosquera, a teacher of the Mechanical Industrial Technology career (CETP -UTU - UdelaR – UTEC) the first precarious attempts turned into a quasi-commercial device.

The sequence of different arranges of heating and insulating materials leading to the final atomiser as well as some results of its performance are presented.

5.2 Atomiser evolution

5.2.1 Nichrome wire and ceramic fibre tape

The T-shaped cell (Precision Glassblowing, Centennial, CO, USA) was heated by a nichrome wire (0,40 mm diameter – $8,674 \Omega \text{ m}^{-1}$ at 20°C) wrapped around it.

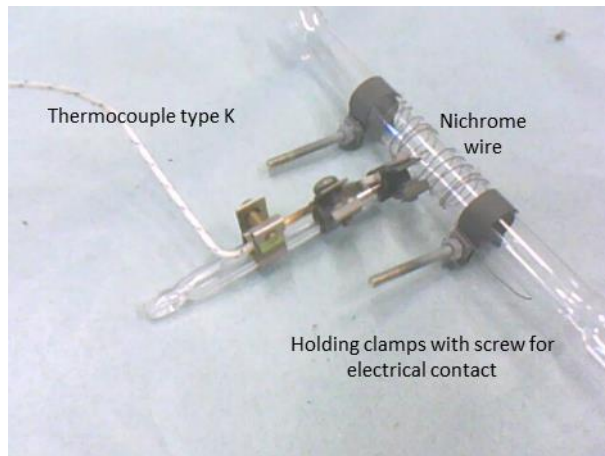


Figure 114: EHQTA cell heated by nichrome wire.

The wire was tightened to the cell by clamps which at a time served as electrical contact for the power supply (Figure 114). The screws needed to be long enough so as to protrude the insulating material (a ceramic tape made of aluminosilicate fibrous wool)

Ceramic tape is build up with resin binder which carbonises at high temperatures so the direct contact with the wire would burn it; as the carbon residues have conductive properties it could short-circuit the resistance. In this way, the tape was cooked before using it.



Figure 115: Calcination of the tape.

First it was burned on a burner and then ashed at 500°C until the carbon residue disappeared (30 min approx.) (Figure 115). The heating process did not change the tape's tissue firmness. The cell was wrapped with the tape and connected to a 0 -30 V / 0 - 5 A power supply.

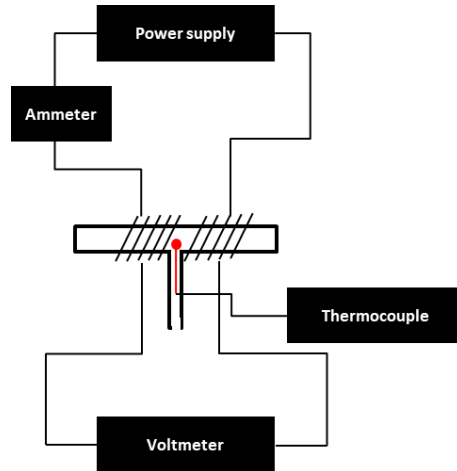


Figure 116: Electrical assembly of the EHQTA.

The power supply was operated at constant current; an ammeter and a voltmeter monitored the current and the voltage respectively. At first, the resistance of the cell was about 6 Ω. A type K thermocouple (nickel /chrome – nickel / aluminium) was installed in the outside wall of the T cell in the junction of the perpendicular tubes as showed in Figure 116.

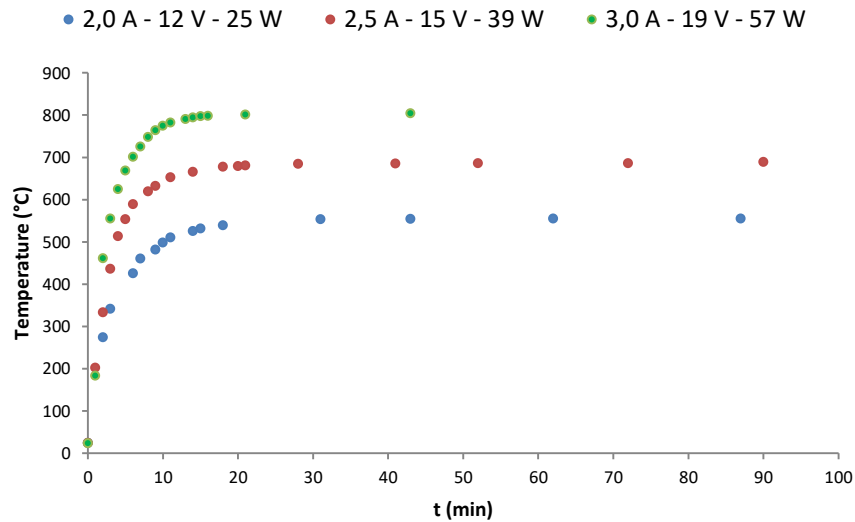


Figure 117: Temperature at the surface of the cell at increasing times for different constant currents supplied.

Figure 117 shows the variation of the temperature with the supply of different constant currents. The values of voltage presented are the approximation of the average in the whole time range. As well, the power was calculated at each time and the approximation of the average presented.

After approximately 20 minutes operation, temperature reached a plateau, extremely convenient for atomisation purposes. Temperatures close to 550, 680 and 800°C were reached at 2,0 - 2,5 and 3,0 A respectively. From those results it seemed that currents between 3,5 and 4,0 A could lead to the desired temperature (900 – 1000°C). Unfortunately, the power supply got broken.

A new power supply had to be tried which limitations were of 24 V and 6 A, being voltage the parameter to be adjusted. Whenever the desired temperature (900 – 1000 °C) could not be reached within these parameters, a change in the resistance (the wrapped wire) had to be done.

Nichrome 0,4 mm at 22 V attained 800 °C but got easily broken. Nichrome 0,8 – 0,6 mm and 0,4 mm rolled in a double strand were tried. Nichrome 0,8 already at 10 V developed a current close to the maximum but the temperature was still too low. Nichrome 0,6 at the threshold of voltage attained 800°C. Best results were found with Nichrome 0,4 rolled in a double strand as showed in Figure 118.

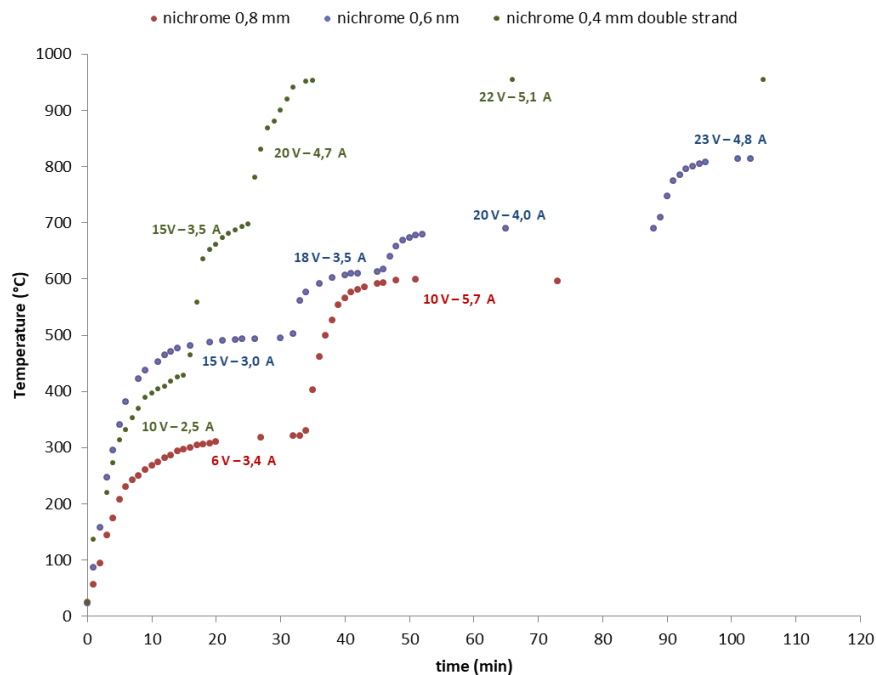


Figure 118: Temperature rise according to the voltage supplied for different resistances.

Even if the voltage increase is shown stepwise, it can be seen that high temperatures can be obtained pretty fast.

A second thermocouple was placed inside the optical arm of the cell, in the inner junction of both tubes of the T with a nitrogen flow of 760 mL min^{-1} .

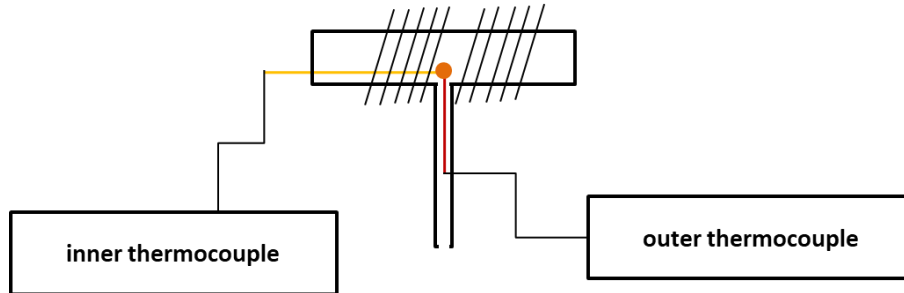


Figure 119: Type K inner and outer thermocouples for monitoring temperature as voltage increases.

The idea was to emulate the atomisation conditions in order to have an approach of the temperature at the place of the cell where atomisation is to be expected. Figure 119 shows a diagram of the system mounted: in yellow the inner thermocouple and in red the outer. The orange point represents the thermocouples arranged in the same tube junction but at both sides of the cell surface.

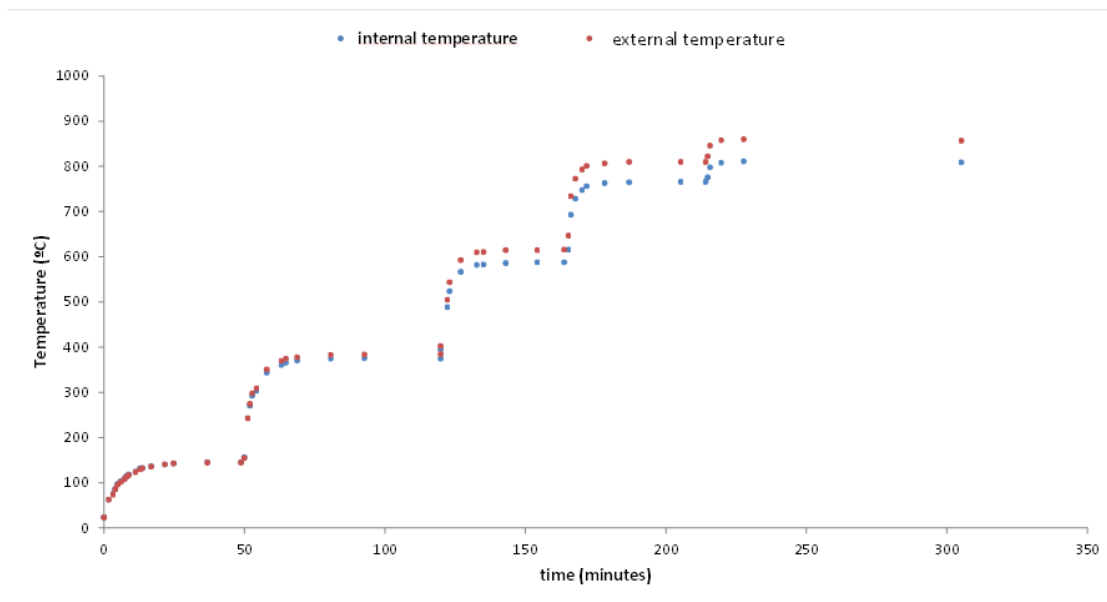


Figure 120: Internal and external cell temperature at increasing voltages

It can be seen in Figure 120 that for every temperature reached, the difference of temperature between the surface and the inner of the cell close to the physical place where the atomisation is expected to occur is not of significant difference, hence, the temperature measured at the external surface is a good approximation of the atomisation temperature. From now on, whenever mentioned the atomisation temperature, it is referred to the temperature taken by the thermocouple at the external surface of the junction of the T cell (Figure 116).

5.2.1.1 Atomiser performance

The atomiser performance was assayed by CVG of trihydridoantimony in the batch mode and when relevant, compared with the results obtained by atomising in the flame heated device.

5.2.1.1.1 Instrumentation

The manifold used is shown in Figure 121, hydrides were generated in a manual hydride generator (MHS 15, Perkin Elmer). A cell holder adapter for mounting the atomiser in the optical pass of the spectrometer (AAAnalyst 200, Perkin Elmer) was constructed in a local turnery. The spectrometer was fitted with an antimony electrodeless discharge lamp (217,6 nm) and deuterium background correction.

The atomiser was operated by adjustment of the voltage with a home-made power supply. Parameters control was performed by an ammeter connected in series and a voltmeter in parallel; the temperature was monitored by a K type thermocouple. The heating device was nichrome 0,4 mm rolled in double strand (not visible in the picture).

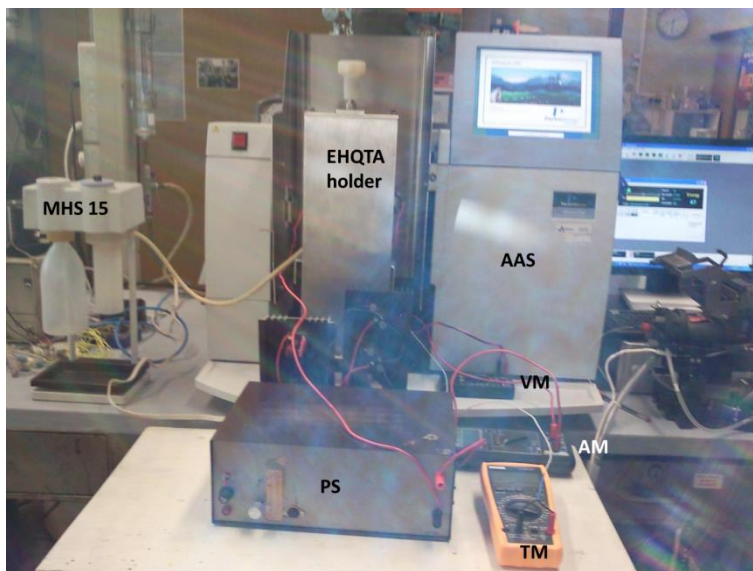


Figure 121: Manifold for the atomisation of antimony in the electrically heated EHQTA. MHS 15: hydride generation system; EHQTA: externally heated quartz tube atomiser; AAS: atomic absorption spectrometer; VM: voltmeter; AM: ammeter; TM: thermocouple multimeter; PS: power supply.

For the flame operated mode, the EHQTA holder was removed and replaced by the air-acetylene burner with its cell holder.

5.2.1.1.2 Reagents and solutions

De-ionised water (ASTM type I) was obtained from a Millipore (São Paulo, Brazil) Direct-Q 5 water purifier. Antimony stock standard solution was prepared from potassium antimonyl tartrate hemihydrate ($K(SbO)C_4H_4O_6 \cdot \frac{1}{2}H_2O$) dissolved in water. Working standard solutions were prepared daily by dilution of the stock solution with 1,5 % HCl. Sodium tetrahydroborate solution 3,0 % w/v in sodium hydroxide 1,0 % was prepared from sodium tetrahydroborate (Hydride-Generation grade, Fluka).

All reagents used were of analytical reagent grade unless otherwise specified.

Standard nitrogen and acetylene were supplied by Linde Uruguay.

5.2.1.1.3 Procedure

Solutions of increasing amount of antimony in 1,5 % HCl were prepared and measured in the same spectrometer by CVG in the MHS 15 with the electrically heated EHQTA and the flame EHQTA. The quartz cell differed only in the way of being heated. The voltage of the electrical assembly was set in 21 V so as to reach 1000°C in the atomiser.

5.2.1.1.4 Results and discussion

The decision of taking as the atomisation temperature 1000°C arose from the study of the variability and magnitude of the response at different temperatures.

100 ng of antimony were atomised by quintuplicate at 850 – 900 – 950 – 1000 and 1050°C. The relative standard deviation was calculated for each temperature; the one leading to highest ration signal/noise was selected.

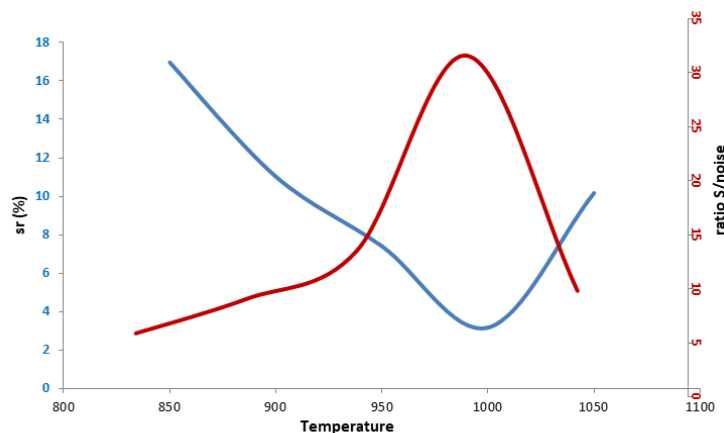


Figure 122: Relative standard deviation of antimony integrated absorbance (blue) and ratio signal to noise (red) at different atomisation temperatures.

The same increasing amounts of antimony were atomised in both heating devices; the analytical signal was integrated absorbance (A_{int}).

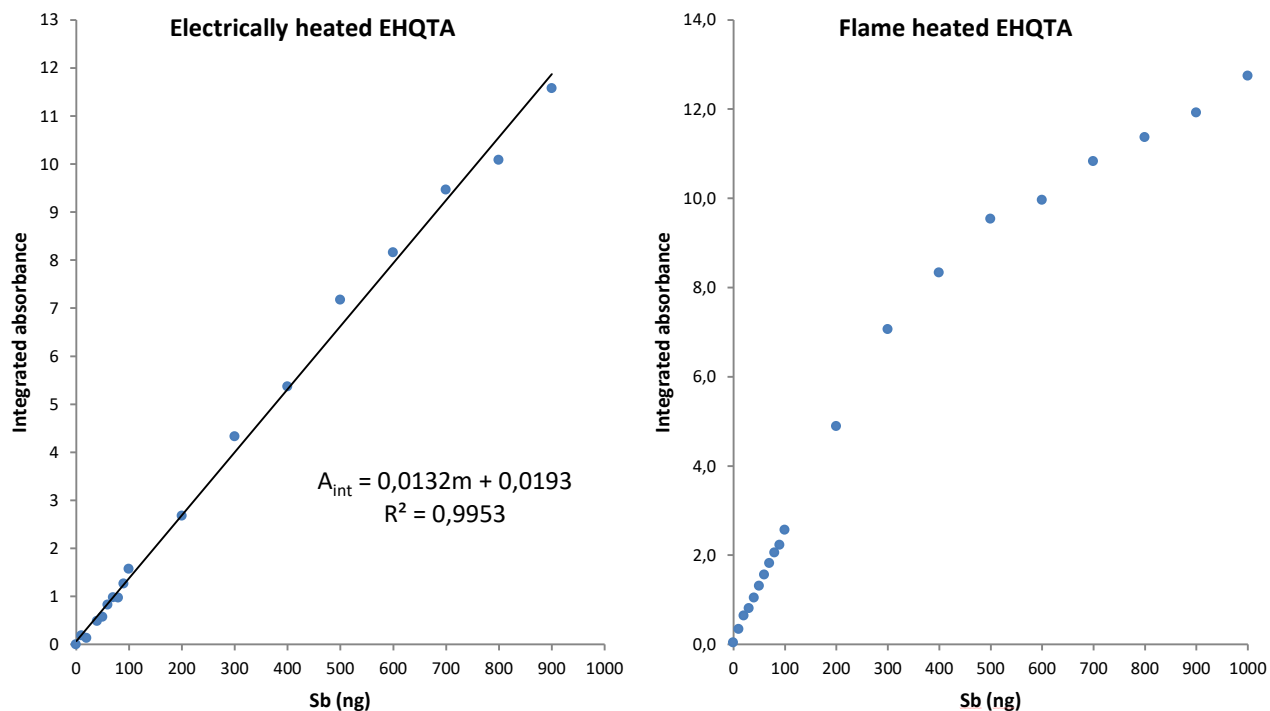


Figure 123: Signal variation (integrated absorbance, A_{int} , s) for increasing amounts of antimony (m, ng), for the electrically heated EHQTA (left) and the flame heated EHTQA (right).

As shown in Figure 123, the flame heated device exhibits a narrower linear range (up to around 300 ng) while is almost 1000 ng for the electrically heated one. At low amounts of antimony, electrically heated EHQTA yields acute peaks enabling an easier visualisation.

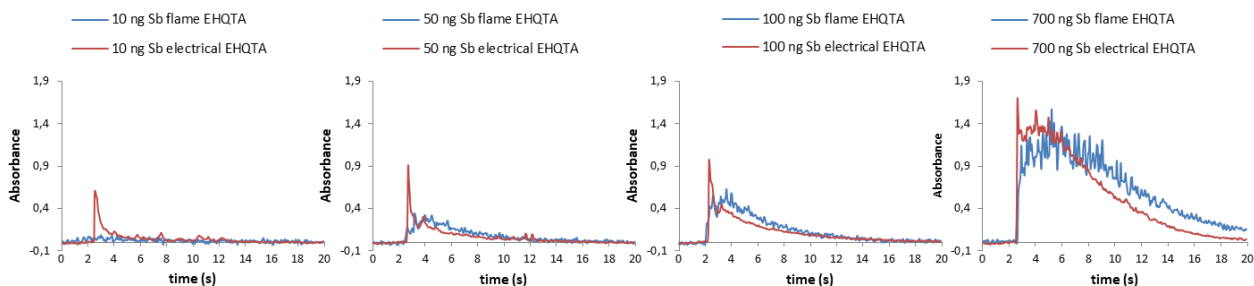


Figure 124: Comparison of the response for different amounts of antimony of the flame EHQTA and the electrically heated EHQTA.

Figure 124 overlaps the signals of both atomisers for the same amount of antimony. Up to 100 ng, even if less sensitive (as can be seen in Figure 123), peaks are better defined. They start sharply from the baseline and decay increasing the height from where the tail begins as the mass of atomised antimony rises (Figure 125).

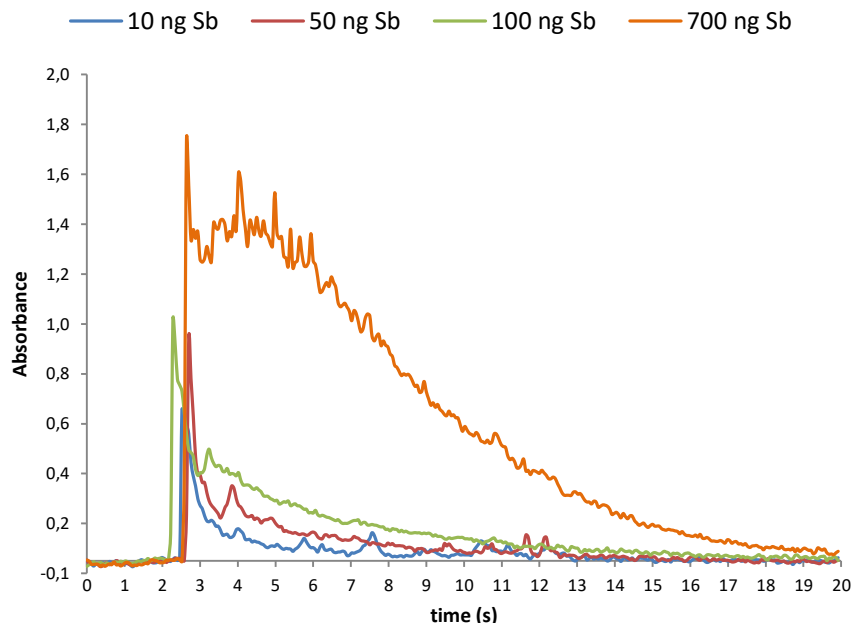


Figure 125: Antimony peak shape in the electrically heated atomiser.

For high amounts of antimony peak shape gets distorted as shown, but as linearity is kept, for a particular application, trueness at that concentration level has to be assessed in order to conclude whether it is an actual limitation or not.

Related to peak shape, what really concerned was its integrated absorbance variability at low concentrations. The signal was unambiguously detected as previously shown because of its height but its area was not reproducible.

Results are presented in Table 44:

10 ng ($1 \mu\text{g L}^{-1}$ Sb)				100 ng ($10 \mu\text{g L}^{-1}$ Sb)			
s_r (%) Flame EHQTA		s_r (%) Electrically heated EHQTA		s_r (%) Flame EHQTA		s_r (%) Electrically heated EHQTA	
height	area	height	area	height	area	height	area
5,5	4,2	6,5	17,0	3,5	3,0	6,4	3,2

Table 44: Relative standard deviation (s_r , %, $n = 10$) for peak height and peak area for both atomisation devices.

For the atomisation of 100 ng of Sb the variability attained with the electrically heated device is suitable and comparable with the results obtained when using the flame for heating the cell.

At low concentrations, flame achieves suitable precision, thus, as the only difference between both results is the way of heating the cell, the causes of the dispersion may be due to the variation of the

temperature during the process: the voltage applied to the cell is always the same; the temperature is determined by the voltage and the gas flow rate inside it.

When the hydride is generated, the system is closed; nitrogen enters the MHS 15 system and goes to the atomisation cell. As it is a batch system, each time the hydride is generated the sample needs to be renewed. In that moment, the system is opened, no nitrogen circulates within the cell and thus the temperature rises.

Between each determination, temperature constancy needs to be attained; this temperature variation is easy controllable as is just enough to wait until the temperature goes back to its value.

While the hydride is being generated, hydrogen evolves from the reactor due to THB decomposition; it also promotes a temperature variation of about 6 degrees which cannot be controlled. The temperature is given by the thermocouple supported against the external surface of the cell. The time elapsed within the measurement are 20 s, thus due to the inertia of the heat transference it is probable that the temperature variation in the atomisation enclosure is higher than the one perceived by the instrument. Hence, temperature control should be improved.

5.2.1.1.5 Conclusions

The atomiser so constructed is able to attain atomisation temperatures up to 1000 – 1050 °C and keep it constant while the gas flow rate within the cell remains unchanged.

At low amounts of analyte, dispersion is higher than what can be expected if compared with the flame heated cell atomiser. The temperature control is provided by the voltage set at the power supply. A more accurate temperature control has to be sought.

5.2.2 Proportional – Integral – Derivative (PID) temperature controller

5.2.2.1 Introduction

The temperature controller is a feedback system. The thermocouple gives the input signal of the actual temperature to the system which compares it with the one set and provides an output to the controlling element, a solid state relay in this case.

While the temperature is far from the set point the power supply is on; it decreases in average when approaching or increases it when moving away. There is a proportional band around the set point (a percentage of the desired temperature) where the heating rate is varied; this is the proportional control of the temperature. The aim is not to get too far from the desired temperature within a preset interval by supplying a fraction of the total power.

The proportional derivative control considers the speed at which the temperature varies; if the temperature is under the set point but increasing so fast that it would be exceeded, the control decreases the power of the heating device. By the contrary, if the temperature is already above the preset but decreasing abruptly, some power will be supply in order to prevent it. This type of control allows a very stable temperature.

The temperature gets stabilised close to the set point, the narrower the proportional band, the smaller the difference between them, but, the system can become too oscillating. Thus, the proportional integral control considers and corrects the amount of bias in a certain time.

The overall action of the proportional integral derivative control is to provide a stable temperature. The proportional band, the integration and derivative constants have to be optimised for each particular device.

5.2.2.2 Instrumentation

The temperature of the atomiser was controlled by a temperature controller (Novus N 1200) fitted with a type K thermocouple and a solid state relay, and an alternating current power supply (24 V) (Figure 126).

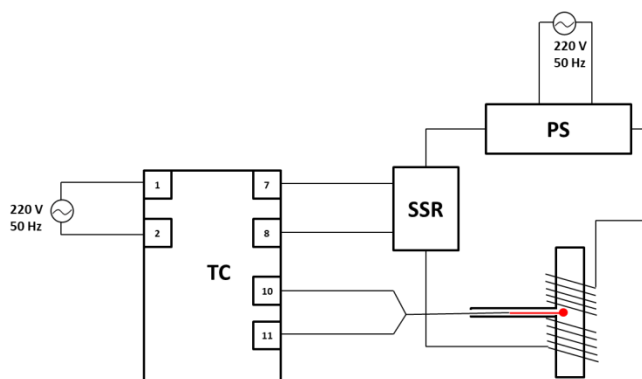


Figure 126: Atomiser electrical assembly. TC: temperature controller; SSR: solid state relay; PS: power supply.

5.2.2.3 Procedure

The new electrical assembly was connected to the atomiser. The temperature controller displayed both the actual and the set temperature of the system.

Different combinations of the PID parameters were tried in order to get acquainted and take advantage of the capabilities of the controller.

5.2.2.4 Results and discussions

Figure 127 shows the temperature variation in time without PID control. After reaching the setpoint (1050°C) temperature varies within 1038 and 1055 °C.

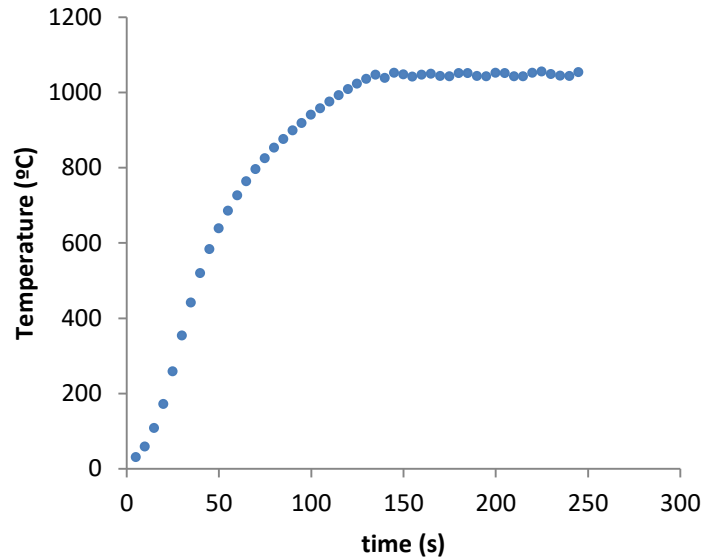


Figure 127: Temperature variation without PID control. Set temperature: 1050 °C

It is not shown in the figure but the system can operate hours (3 hours was the maximum it was left on) without evidencing any damage.

Results shown in Figure 128 were obtain setting two ramps in the system, one at 600°C and the other at 950°C. In the first ramp at 600 °C it appears a kind of overshoot and then temperature stabilises. At 950°C the temperature is attained and kept constant. When the overshoot was prevented, the second ramp turned too large and it took a long time to reach the final temperature.

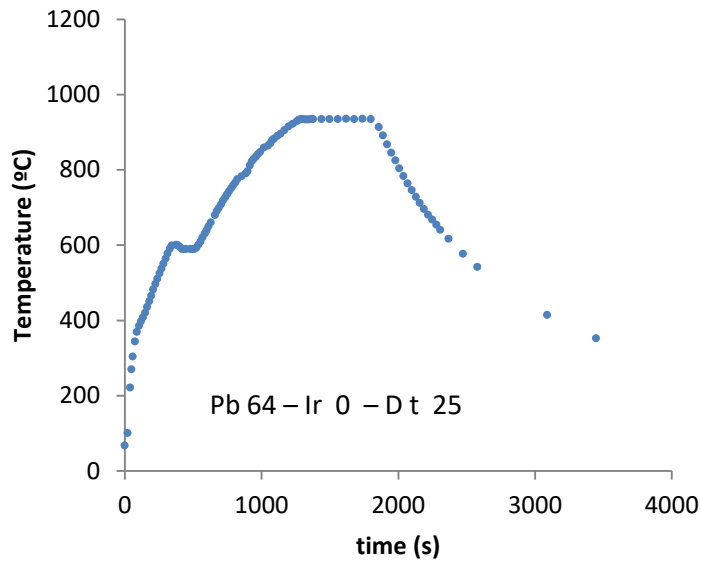


Figure 128: Temperature variation with PID control. Setpoints: 600 and 950°C. Pb: proportional band; Ir: integral rate; Dt: derivative time. The plateaus were reached in a reasonable time.

For the 600°C plateau, temperature reached was 589°C and remained unchanged, for the 950°C plateau the temperature reached was 934°C and the variation was within 933 and 935°C.

The actual way to eliminate or minimise the bias is setting a value of Ir (in this experiment it was set at zero). So was done, the temperature fixed at 600°C was between 598 and 604°C but the temperature set at 1050°C was not reached in a reasonable time. Figure 129 exemplifies this situation.

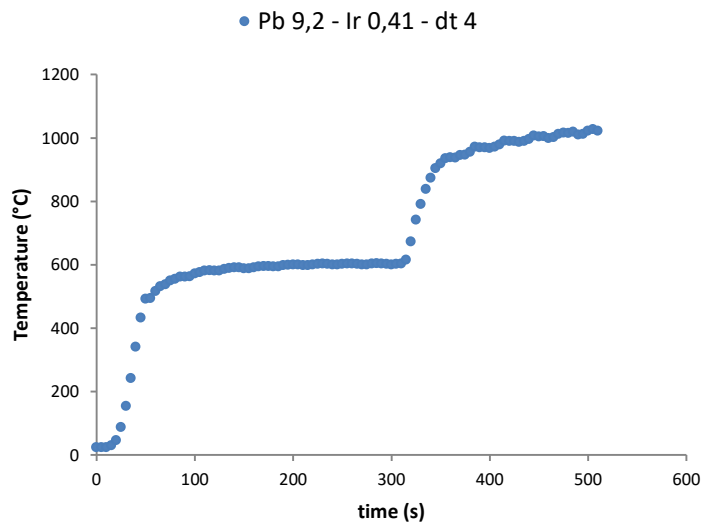


Figure 129: Temperature variation setting a Ir value. Pb: proportional band; Ir: integral rate; Dt: derivative time

After combining varied sets of PID parameters better responses than the one showed could not be found. The difference between the setpoint and the actual temperature can be easily offset by increasing the setpoint a few degrees.

Thus, setting a PD control (proportional derivative) was the choice of working with the temperature controller, reaching very stable temperatures.

5.2.3 Nichrome tape

Being strict, the plots above already shown correspond to the resistances of the final version of the atomiser presented in 5.3. At first the same studies were performed with the nichrome 0,4 mm rolled in double strand finding similar results. For the sake of brevity and due to their resemblance, only the ones of the final heating element were presented. Long exposure of the wire to the heat made it more fragile and got broken frequently, thus alternatives to the wire were sought.

Instead of the wire, a 2,5 mm width nichrome tape was used. First it was interwoven in the ceramic tape and then also wrapped around the cell. Different length were tried. Temperature did not rise above 700°C (Figure 130 and Figure 131).



Figure 130: Nichrome tape as heating element (interwoven in the ceramic tape).



Figure 131: Nichrome tape as heating element (wrapped around the cell).

5.3 Final version of the atomiser

The main drawback of the resistances used was their fragility. The nichrome 0,4 mm rolled in double strand was replaced by two iron-chromium-aluminium alloy (Kanthal) resistances rolled up around the T-cell but not in direct contact as the nichrome wire was (Figure 132).



Figure 132: Resistance (Fe Cr Al) as heating device.

The T-cell was mounted on a stainless steel box. The electrical assembly included in the same body the power supply and the temperature controller, its diagram is depicted in Figure 133:

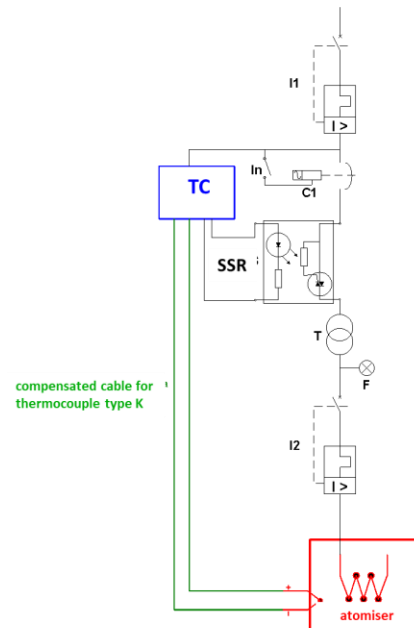


Figure 133: Electrical connection. TC: PID temperature controller; I1: 10A bipolar thermomagnetic switch; In: bipolar switch; C1: 220 V coil contactor; SSR: solid state relay; T: 220/24 V single phase transformer; F: Indicator light; 25A bipolar thermomagnetic switch (Device and diagram constructed by R. Mosquera).

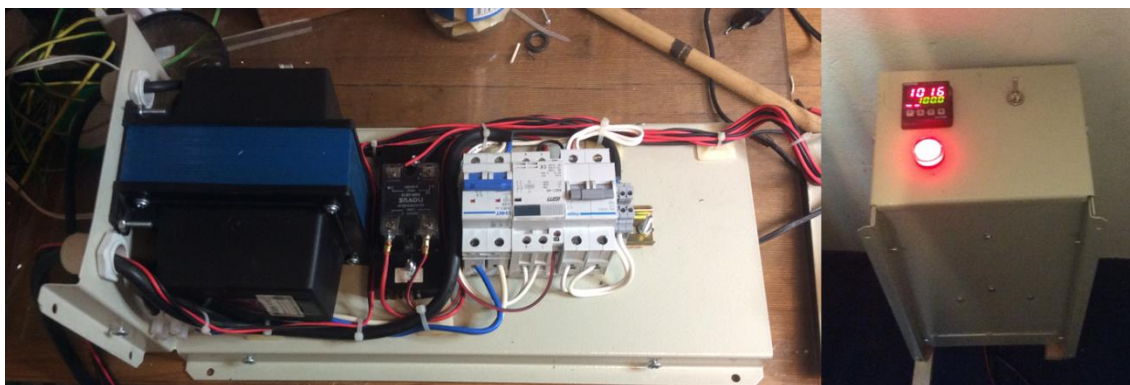


Figure 134: Left: internal view of the electrical control of the atomiser. Right: external view.

5.4 Conclusions

Combining the thicker resistors with the PID controller a robust device with very accurate temperature control was achieved. It attained long lasting working periods at constant temperatures. Due to its feedback system, subtle changes in the gas flow rate could be fast and easy compensated.

Chapter V

Construction of an electrically heated volatile
species atomiser

Scientific production

CONSTRUCCIÓN DE UN ATOMIZADOR ELÉCTRICO PARA ESPECTROMETRÍA DE ABSORCIÓN ATÓMICA

Alicia Mollo, Ricardo Mosquera*, Moisés Knochen
Química Analítica, Departamento Estrella Campos, Facultad de Química, Udelar
* Bachiller en Ciencias de Ingeniería
amolloy@fq.edu.uy

La atomización de especies volátiles de metales y semi metales para su determinación por espectrometría atómica transcurre mediante un mecanismo radicalario que requiere la presencia de hidrógeno para iniciarse. En la generación convencional de especies volátiles, el hidrógeno es un subproducto de la reacción y es suficiente para que la atomización se realice cuando se calienta la celda de atomización mediante llama acetileno – aire. Cuando la reacción no libera hidrógeno (por ejemplo en la generación fotoquímica), es necesario suministrarlo tornándose necesario cambiar la llama por calentamiento eléctrico. Se construye un atomizador eléctrico que se fue modificando en función de los resultados obtenidos.



Chapter VI

General conclusions and perspectives

6 General conclusions and perspectives

The work achieved up to now allowed covering different aspects of the generation of volatile species as a sample introduction technique. Encompassing the chemical, electrochemical and photochemical generation enabled a deeper understanding of the process involved.

Chemical generation of selenium by SI-HG-AAS was the first approach to the technique and let focus the main variables of influence of the hydride generation.

Lead tetrahydride generation in turn, helped to highlight the relevance of the knowledge of the mechanism of the reaction of tetrahydroborate and its interaction with the additives in order to face the optimisation of the working conditions. Some work has been done but further studies with on-line pre-mixing of the reagents are likely to be achieved. Although results found are promising, especially because MIP OES as the detection system for the lead tetrahydride is not very extended in use, maybe an additional improvement of the limits of detection and quantification can be accomplished. Application to samples with a much lower content of lead is also need to be tried.

The electrochemical hydride generation needs a second approach; the drawback in accomplishing the generation lies undoubtedly in a bad choice of the cell design. The problems faced were not related to the technique but to the physical disability of operating the cell as the leakages could not be controlled. The volumes handled and the electrical contacts are of utmost importance to be improved as well as the electrodes shape and dimensions. However, the work done served to point out parameters of caring; it was a starting point as there is much to learn and understand about the electrolytic process as a whole.

Photochemical vapour generation was a great challenge. At first sight it seemed a very simple technique; in fact it is easy to achieve but it requires a deep study of the variables in order to control them. The reactor design played the most important role in the generation success. Sample irradiance of the in-house reactor was attenuated both by the lamp glass cover and the PTFE tubing restricting the applicability. Among the elements tried, selenium was the only to which the volatile species generation could be confirmed. Changing to the commercial reactor opened a new field of possibilities. One of the most impacting findings was the dramatic change in the magnitude of the signal according to a pH variation; of course literature warned of that fact but certainly it was not expected to be of such relevance. This makes necessary to formulate again the tests performed to which no response was found.

The sole limitation of the reactor is the short amount of sample that can handle; the manufacturer would modify the design only if buying a hundred of units, thus, the way of increasing sample volume up to now is to add another reactor and so is planned to be done. It was also found a quartz manufacturer in Argentina which can roll up a quartz tube so as to replace the PTFE one of the in-house reactor. It is not the best situation as low wavelength irradiations are prevented by the lamp cover but is another alternative to be tried.

The construction of the atomiser started to meet a need but it turned out venturing in an unknown field. In the meantime the commercial device was bought but its finalisation was achieved anyway as it is an alternative to be used in the other spectrometer available in our laboratory.

Finally, working with reagents other than chemical was a fruitful experience which brought knowledge to our area; there is still too much work to be done but there is now a way forward.

Chapter VII

Bibliography

7 Bibliography

- Barnett, N. (1987). Further experience with a miniature hydride generation device used in conjunction with microwave induced plasma-atomic emission spectrometry (MIP-AES) for the determination of antimony, arsenic, lead and tin. *Spectrochimica Acta B*, 42, 859-864.
- Brasted, R. (1952). Reaction of Sodium Nitrite and Sulfamic Acid - Indirect Gravimetric Determination of Nitrites. *Analytical Chemistry*, 24(7), 1111-1114.
- Brockmann, A., Nonn, C., & Golloch, A. (1993). New Concept for Hydride Generation Technique: Electrochemical Hydride Generation. *Journal of Analytical Atomic Spectrometry*, 8, 397 - 401.
- Brown, R., Fry, R., Moyers, J., Northway, S., Denton, M., & Wilson, G. (1981). Interference by Volatile Nitrogen Oxides and Transition-Metal Catalysis in the Preconcentration of Arsenic and selenium as Hydrides. *Anal. Chem.*(53), 1560 - 1566.
- Bureau, C. C. (2011). *Norma CIE S017/E:2011 International Lighting Vocabulary – Versión en español*. Retrieved 07 09, 2019, from https://www.ceisp.com/fileadmin/pdf/Downloads/ILV_Vocabulario_Internacional_Iluminacion_04-2013v2.pdf
- Buxton, G., & Sellers, R. (1977). The radiation chemistry of metal ions in aqueous solution. *Coordination Chemistry Reviews*(22), 195-274.
- Bye, R. (1983). Critical Examination of Some Common reagents for Reducing Selenium Species in Chemical Analysis. *Talanta*, 30(12), 993 - 996.
- Bye, R., & Lund, W. (1988). Optimal conditions for the reduction of selenate to selenite by hydrochloric acid. *Fresenius Z Anal Chem*(332), 242-244.
- C. Ferreira , S., dos Santo, W., Quintella, C., Neto, B., & Bosque-Sendra, J. (2004). Doehlert matrix: a chemometric tool for analytical chemistry—review. *Talanta*, 63 , 1061–1067.
- Castillo, J., Mir, J., Martínez, C., Val, J., & Colón, M. (1985). Influence of Oxidising Agents in Lead Determination by Hydride Generation Direct Flame Atomic Absorption Spectroscopy. *Mikrochimica Acta*(1985 I), 253 - 263.
- Chen, G., Lai, B., Mei, N., Liu, J., & Mao, X. (2017). Mercury speciation by differential photochemical vaporgeneration at UV-B vs. UV-C wavelength. *Spectrochimica Acta Part B*(137), 1-7.
- Clesceri, L., Greenberg , A., & Eaton, A. (1998). Arsenic and Selenium by Hydride Generation/Atomic. In *Standard Methods for the Examination of Water and Wastewater* (pp. 3-32 - 3-36). Washington DC: American Public Health Association.

- D'Ulivo, A. (2004). Chemical vapor generation by tetrahydroborate(III) and other borane complexes in aqueous media A critical discussion of fundamental processes and mechanisms involved in reagent decomposition and hydride formation. *Spectrochimica Acta Part B*, 59, 793 - 852.
- D'Ulivo, A. (2010). Mechanism of generation of volatile species by aqueous boranes Towards the clarification of most controversial aspects. *Spectrochimica Acta Part B*(65), 360 - 375.
- D'Ulivo, A. (2016). Mechanisms of chemical vapor generation by aqueous tetrahydridoborate. Recent developments toward the definition of a more general reaction model. *Spectrochimica Acta Part B*(119), 91 - 107.
- D'Ulivo, A., Baiocchi, C., Pitzalis, E., Onor, M., & Zamboni, R. (2004). *Spectrochimica Acta Part B*(59), 471 - 486.
- D'Ulivo, A., Onor, M., & Pitzalis, E. (2004). Role of Hydroboron Intermediates in the Mechanism of Chemical Vapor Generation in strongly acidic media. *Analytical Chemistry*(76), 6432 - 6352.
- Dedina, J. (2007). Atomisation of volatile compounds for atomic absorption and atomic fluorescent spectrometry: On the way towards the ideal atomiser. *Spectrochimica Acta Part B*(62), 846 - 872.
- Dedina, J., & Rubeska, I. (1980). Hydride atomization in a cool hydrogen-oxygen flame burning in quartz tube atomizer. *Spectrochimica Acta*, 35B, 119 - 128.
- Dedina, J., & Tsalev, D. (1995). *Hydride Generation Atomic Absorption Spectrometry*. Chichester: Wiley.
- Denkhaus, E., Beck, F., Bueschler, P., Gerhard, R., & Golloch, A. (2001). Electrolytic hydride generation atomic absorption spectrometry for the determination of antimony, arsenic, selenium, and tin – mechanistic aspects and figures of merit. *Fresenius J Anal Chem*, 370, 735 - 743.
- D'Ulivo, A., Onor, M., Spiniello, R., & Pitzalis, E. (2008). Mechanisms involved in chemical vapor generation by aqueous tetrahydroborate(III) derivatization Role of hexacyanoferrate(III) in plumbane generation. *Spectrochimica Acta Part B*(63), 835–842.
- D'Ulivo, A. (2019). The contribution of chemical vapor generation coupled with atomic or mass spectrometry to the comprehension of the chemistry of aqueous boranes. *J. Anal. At. Spectrom.*
- Dvořák, P., Talába, M., Kratzer, J., & Dědina, J. (2019). Radical theory of hydride atomization confirmed after four decades – determination of H radicals in the quartz hydride atomizer by two-photon absorption laser-induced fluorescence. *Chemical Science*.
- Dzelzkalns, L., & Ronner, F. (1978). Reaction between Nitric and Sulfamic Acids in aqueous solution. *Inorganic Chemistry*, 17(12), 3710-3711.
- Figueroa, R., García, M., Lavilla, I., & Bendicho, C. (2005). Photoassisted vapor generation in the presence of organic acids for ultrasensitive determination of Se by electrothermal-atomic absorption

- spectrometry following headspace single-drop microextraction. *Spectrochimica Acta Part B*, 60 , 1556 – 1563.
- Gil, S., de Loos-Vollebregt, M., & Bendicho, C. (2009). Optimization of a single-drop microextraction method for multielemental determination by electrothermal vaporization inductively coupled plasma mass spectrometry following in situ vapor generation. *Spectrochimica Acta Part B*(64), 208–214.
- Golimowski, J., & Golimowska, K. (1996). UV photooxidation as pretreatment step in inorganic analysis of environmental samples. *Analytica Chimica Acta*(325), 111-133.
- Goncalves, D., McSweeney, T., & Donati, G. (2016). Characteristics of a resonant iris microwave-induced nitrogen plasma. *Journal of Analytical Atomic Spectrometry*(31), 1097 - 1104.
- Granger, J., & Sigman, D. (2009). Removal of nitrite with sulfamic acid for nitrate N and O isotope analysis with the denitrifier method. *Rapid Communications in Mass Spectrometry*(23), 3753 - 3762.
- Guo, X., Sturgeon, R., Mester, Z., & Gardner, G. (2003). Photochemical Alkylation of Inorganic Selenium in the Presence of Low Molecular Weight Organic Acids. *Environ. Sci. Technol.*(37), 5645 5650.
- Guo, X., Sturgeon, R., Mester, Z., & Gardner, G. (2003). UV Vapor Generation for Determination of Selenium by Heated Quartz Tube Atomic Absorption Spectrometry. *Anal. Chem.*, 75(9), 2092-2098.
- Guo, X., Sturgeon, R., Mester, Z., & Gardner, G. (2004). Vapor Generation by UV Irradiation for Sample Introduction with Atomic Spectrometry. *Anal. Chem.*(76), 2401-2405.
- Hammer, M. (2008). A magnetically excited microwave plasma source for atomic emission spectroscopy with performance approaching that of the inductively coupled plasma. *Spectrochimica Acta Part B*, 63 , 456–464.
- Han, C., Zheng, C., Wang, J., Cheng, G., Lv, Y., & Hou, X. (2007). Photo-induced cold vapor generation with low molecular weight alcohol, aldehyde, or carboxylic acid for atomic fluorescence spectrometric determination of mercury. *Anal Bioanal Chem*(388), 825-830.
- Hatfield, D. (1987). Electrically Heated Quartz Atomization Cell for Hydride Generation-Atomic Absorption Spectrophotometry. *Analytical Chemistry*(59), 1887 - 1888.
- He, Y., Hou, X., Zheng, C., & Sturgeon, R. (2007). Critical evaluation of the application of photochemical vapor generation in analytical atomic spectrometry. *Anal Bioanal Chem*, 388, 769-774.
- Healy, T. (1958). The reaction of nitric acid with formaldehyde and with formic acid and its application to the removal of nitric acid from mixtures. *J. appl. chem.*(8), 553-561.

- Karadjova, I., Lampugnani, L., Dedina, J., D'Ulivo, A., Onor, M., & Tsalev, D. (2006). Organic solvents as interferences in arsenic determination by hydride generation atomic absorption spectrometry with flame atomization. *Spectrochimica Acta Part B*(61), 525–531.
- Kikuchi, E., & Sakamoto, H. (2000). Kinetics of the Reduction Reaction of Selenate Ions by TiO₂ Photocatalyst. *Journal of The Electrochemical Society*, 147(12), 4589 - 4593.
- Laborda, F., Bolea, E., & Castillo, J. (2007). Electrochemical hydride generation as a sample introduction technique in atomic spectrometry: Fundamentals, interferences, and applications. *Anal. Bioanal. Chem.*(388), 743 - 751.
- Leonori, D., & Sturgeon, R. (2019). A unified approach to mechanistic aspects of photochemical vapor generation. *J. Anal. At. Spectrom.*
- Liu, H., & Dasgupta, P. (1996). Analytical Chemistry in a drop. Solvent extraction in a microdrop. *Analytical Chemistry*(68), 1817 - 1821.
- Lopes, G., Sturgeon, R., Grinberg, P., & Pagliano, E. (2017). Evaluation of approaches to the abatement of nitrate interference with photochemical vapor generation. *J. Anal. At. Spectrom.*, 32(12), 2378-2390.
- López-Rouco, A., Stanisiz, E., Matusiewicz, H., Lavilla, I., & Bendicho, C. (2008). UV reduction with ultrasound-assisted gas–liquid separation for the determination of mercury in biotissues by atomic absorption spectrometry. *Journal of Analytical Atomic Spectrometry*(23), 1026 - 1029.
- Mack, J., & Bolton, J. (1999). Photochemistry of nitrite and nitrate in aqueous solution: a review. *Journal of Photochemistry and Photobiology A: Chemistry*(128), 1-13.
- Mahfud, L., Ronze, D., Wehrer, A., & Zoulalian, A. (1998). Reduction de l'acide nitreux par une solution aqueuse d'urée ou d'acide sulfamique en vue du traitement des NO_x, d'un effluent gazeux. *Chemical Engineering Journal*(70), 85 - 92.
- Mandel, J., & Lining, F. J. (1957). Study of Accuracy in Chemical Analysis Using Linear Calibration Curves. *Analytical Chemistry*, 29(5), 743 - 749.
- Mandjukov, P., & Tsalev, D. (1990). Study of Cerium (IV) and Cerium (IV)-Palladium (II) as Chemical Modifiers in Electrothermal Atomization-Atomic Absorption Spectrometry. *Microchemical Journal*(42), 339 - 348.
- Massart, D., Vandeginste, B., Buydens, L., De Jong, S., Lewi, P., & Smeyers-Verbeke, J. (1997). *Handbook of Chemometrics and Qualimetrics: Part A*. Amsterdam, The Netherlands: Elsevier.
- Mesquita, R., & Rangel, A. (2009). A review on sequential injection methods for water analysis. *Analytica Chimica Acta*(648), 7 - 22.

- Miller, J., & Miller, J. (2010). *Statistics and Chemometrics for Analytical Chemistry* (Sixth ed.). Harlow, England: Pearson.
- Mittal, L., Mittal, J., & Hayon, E. (n.d.). Photo-I nduced Decarboxylation of Aliphatic Acids and Esters in Solution. Dependence upon State of Protonation of the Carboxyl Group. *The Journal of Physical Chemistry*, 77(12), 1482-1487.
- Mo, J., Li, Q., Guo, X., Zhang, G., & Wang, Z. (2017). Flow Injection Photochemical Vapor Generation Coupled with Miniaturized Solution-Cathode Glow Discharge Atomic Emission Spectrometry for Determination and Speciation Analysis of Mercury. *Analytical Chemistry*, 89(19), 10353-10360.
- Mogaddam, M., Mohebbi, A., Pazhohan, A., Khodadadeian, F., & Farajzadeh, M. (2018). Headspace mode of liquid phase microextraction: A review. *Trends in Analytical Chemistry*.
- Motomizu, S., & Sanada, M. (1995). Photo-induced reduction of nitrate to nitrite and its application to the sensitive determination of nitrate in natural waters. *Analytica Chimica Acta*(308), 406-412.
- Nations, U. (n.d.). *The composition of fish - FAO*. Retrieved 06 25, 2019, from The composition of fish - FAO: <http://www.fao.org/3/x5916e01.htm>
- Nerin, C., Olavide, S., Cacho, J., & Garnica, A. (1989). Determination of lead in airborne particulate by Hydride Generation. *Water, Air, and Soil Pollution*(44), 339-345.
- Park, J.-Y., & Lee, Y.-N. (1988). Solubility and Decomposition Kinetics of Nitrous Acid in Aqueous Solution. *J. Phys. Chem.*(92), 6294 - 6302.
- Pena-Pereira, F., Lavilla, I., & Bendicho, C. (2010). Liquid-phase microextraction approaches combined with atomic detection: A critical review. *Analytica Chimica Acta*(669), 1–16.
- Pettersson, J., & Olin, A. (1991). The rate of reduction of selenium (VI) to selenium (IV) in hydrochloric acid. *Talanta*, 38(4), 413-417.
- Pettersson, J., & Olin, A. (1991). The Rate of Reduction of Selenium (VI) to Selenium (IV) in hydrochloric Acid. *Talanta*, 38(4), 413 - 417.
- Pierce, F., & Brown, H. (1976). Inorganic Interference Study of Automated Arsenic and Selenium Determination with Atomic Absorption Spectrometry. *Analytical Chemistry*, 48(4), 693 - 695.
- Qin , D., Gaob, F., Zhang, Z., Zhao , L., Liua, J., Ye, J., et al. (2013). Ultraviolet vapor generation atomic fluorescence spectrometric determination of mercury in natural water with enrichment by on-line solid phase extraction. *Spectrochimica Acta Part B*(88), 10 - 14.
- Reuther, A., Laubereau, A., & Nikogosyan, D. (1996). Primary Photochemical Processes in Water. *J. Phys. Chem.* (100), 16794-16800.
- Ruzicka, J., & Marshall, G. (1990). Sequential injection: a new concept for chemical sensors, process analysis and laboratory assays. *Analytica Chimica Acta*(237), 329 - 343.

- Salzberg, H., & Goldschmidt, B. (1960). Arsine Evolution and Water Reduction at an Arsenic Cathode. *Journal of the Electrochemical Society*, 107(4), 348 - 352.
- Sima, J., Rychlovsky, P., & Dedina, J. (2004). The efficiency of the electrochemical generation of volatile hydrides studied by radiometry and atomic absorption spectrometry. *Spectrochimica Acta Part B*(59), 125–133.
- Sima, J., & Rychlovsky, P. (2003). Electrochemical selenium hydride generation with in situ trapping in graphite tube atomizers. *Spectrochimica Acta Part B*(58), 919–930.
- Smichowski, P., & Farías, S. (2000). Advantages and analytical applications of chloride generation. A review on vapor generation methods in atomic spectrometry. *Microchemical Journal*(67), 147 - 155.
- Stripeikis, J., Costa, P., Tudino, M., & Troccoli, O. (2000). Flow injection hydride generation atomic absorption spectrometric determination of Se(VI) and Se(IV): utility of a conventionally heated water bath for the on-line reduction of Se(VI). *Anal. Chim. Acta*, 1-2(408), 191 - 197.
- Sturgeon, R. (2017). Photochemical vapor generation: a radical approach to analyte introduction for atomic spectrometry. *J. Anal. At. Spectrom.*, 32(12), 2319-2340.
- Sturgeon, R., & Grinberg, P. (2012). Some speculations on the mechanisms of photochemical vapor generation. *J. Anal. At. Spectrom.*, 222-231.
- Tao, G., Willie, S., & Sturgeon, R. (1998). Determination of total mercury in biological tissues by flow injection cold vapour generation atomic absorption spectrometry following tetramethylammonium hydroxide digestion. *Analyst*, 123, 1215–1218.
- Tasev, K., Karadjova, I., & Stafilov, T. (2005). Determination of Inorganic and Total Arsenic in Wines by Hydride Generation Atomic Absorption Spectrometry. *Microchimica Acta*, 149(1-2), 55 - 60.
- Theis, A., Waldack, A., Hansen, S., & Jeannot, M. (2001). Headspace Solvent Microextraction. *Anal. Chem.*(73), 5651-5654.
- Thomsen, C., Madsen, D., Keiding, S., & Thogersen, J. (1997). Two-photon dissociation and ionization of liquid water studied by femtosecond transient absorption spectroscopy. *Journal of chemical physics*, 110(7), 3453 - 3462.
- Ullmann, F. (2007). *Ullmann's Encyclopedia of Industrial Chemistry* (Vol. 12). Weinheim: Willey - VHC.
- Uruguay. (1994, 07 05). *Reglamento Bromatológico del Uruguay*. Retrieved 06 25, 2019, from Reglamento Bromatológico del Uruguay: <http://extwprlegs1.fao.org/docs/pdf/uru3268anx.pdf>
- Vieira, M., Ribeiro, A., Curtius, A., & Sturgeon, R. (2007). Determination of total mercury and methylmercury in biological samples by photochemical vapor generation. *Anal Bioanal Chem*(388), 837 - 847.

- Wardle, B. (2009). *Principles and Applications of Photochemistry*. Manchester, United Kingdom: John Wiley & Sons Ltd.
- Welz, B., & Sperling, M. (1999). *Atomic Absorption Spectrometry* (3rd ed.). Weinheim: Wiley-VCH.
- Xu, L., Basheer, C., & Lee, H. (2007). Developments in single-drop microextraction. *Journal of Chromatography A*, *1152*, 184–192.
- Yin, Y., Liu, J., & Jiang, G. (2011). Photo-induced chemical - vapor generation for sample introduction in atomic spectrometry. *Trends in Analytical Chemistry*, *30*(10), 1672 - 1684.
- Yuan, Y., Guo, X., & Tong, K. (1998). Interference of high concentration of nickel on the determination of selenium and its elimination in hydride generation-atomic fluorescence spectrometry. *Fenxi Huaxue*, *26*(3), 262.
- Zechner, J., & Getoff, N. (1974). Photoproduction of hydrated electrons from formate ions at 184,9 nm. *Int. J. Radiat. Phys. Chem.*, *6*, 215 - 218.
- Zheng, C., Li, Y., He, Y., Ma, Q., & Hou, X. (2005). Photo-induced chemical vapor generation with formic acid for ultrasensitive atomic fluorescence spectrometric determination of mercury: potential application to mercury speciation in water. *J. Anal. At. Spectrom*(20), 746-750.
- Zheng, C., Ma, Q., Wu, L., Hou, X., & Sturgeon, R. (2010). UV photochemical vapor generation–atomic fluorescence spectrometric determination of conventional hydride generation elements. *Microchemical Journal*, *95*, 32-37.